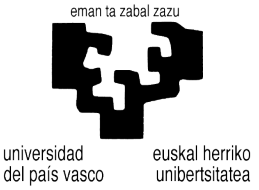

"Exploring new labelling strategies for boronated compounds: towards fast development and efficient assessment of BNCT drug candidates"

A Dissertation Submitted to the Department of Organic Chemistry
Of University of the Basque Country (UPV/EHU),
For the Degree of DOCTOR OF PHILOSOPHY

by

Kiran Babu Gona

Thesis supervisor: Dr. Jordi Llop Roig

Donostia-San Sebastian, Spain

2015

Contents

Acknowledgements

First of all, I would like to express my thanks to Professor Manuel Martín Lomas and Professor Luis Liz Marzán, former and current scientific directors of CIC biomaGUNE, respectively, for giving me the opportunity to develop the experimental work of this PhD in the outstanding facilities of the Centre. Thanks for the precious opportunity to get familiar with such an amount of diverse equipment in a multi-disciplinary, multi-cultural environment.

I express my deep sense of gratitude to my research supervisor Dr. Jordi Llop, for giving me the opportunity to carry out PhD thesis under his supervision, teaching me many things about this fascinating field and for being very supportive throughout these years. I consider myself very fortunate to have an advisor like him, who directed me in the right path while giving the freedom to explore on my own. Jordi "You will be my role model and I wish in future if I need to advice students, I would love to be as good as you. Thanks a ton for your support"

I am especially grateful to Dr. Vanessa Gomez for her invaluable support from the day one of my stay here. She is the reason for the professionalism inside the group, her deadline settings and email alerts are the working fuels for us. Vanessa "I don't remember a single moment where you said no whenever I asked for any help, Thank you very much for everything"

I take this moment to shower my words of gratitude to all my past and present colleagues in the group, Zurine, Carlos, Maria, Enrique, Vijay, Borja, Mikel Errasti, Mikel Gonzalez, Aitor, Larraitz, Beatriz, Sameer, Eunice, Unai, Xabier and Luis, It's a pleasure for me meeting you all here. The past four years I spent here, are certainly the best days in my life, I never felt away from home and each & every one of you is the reason for that, Thank you all.

I owe my sincere thanks all the platform managers, who gave their continuous support for getting my job done. I thank Dani for his help in NMR studies, Javi for his support in mass spectrometry, Bogdan for imaging, Irantzu for spectroscopy and Eneko for his help in PMOD training.

I would like to thank Prof. Clara Viñas and Prof. Francesc Teixidor for their collaborative work on COSAN.

A special thanks to people of animal lab, Ainhoa and Ander for their support during animal studies. I would also like to thank Abraham for his support during collaborative work.

It's my pleasure to thank all the people at CIC biomaGUNE for their great hospitality during my stay here.

I would also like to thank all the people of administration, maintenance and other supporting departments.

I also take this opportunity to thank my entire Indian friend that I met here in Donostia. Mohan-Shanthi, Lakshmi-Leela, Anand-Sara, Sudam-Pallavi, Arul-Geetha, Ravi-Garima, Kiranpala-Swetha, Ram, Musthafa, Ameen, Sallel, and Eithiraj. I feel very fortunate to meet them all here.

This is the time thank my Indian friends, who supported me throughout these days from India, Sivaji, Jeeva, Puli, Sarat, Vinay, Pawan and all my PG friends.

Here I take the opportunity to thank all my family in India, Nanna-Amma, Mamayya-Attha, Anna-Vadina, babu, Jeshwi and manya. Many Special thanks to my brother, because of whom I stand here today.

Many special thanks to my wife Jaya, for her continuous support in every moment of my life after marriage. It's her dream more than me to get this degree, Jaya "I am very fortunate to have you in my life, Thank you for everything". A special hug and lots of love to my son Aasrith.

Thanks to almighty.

Summary

Cancer is described as abnormal mass growth of cells that do not undergo the programmed cell death called apoptosis, and is considered to be one of the leading causes of morbidity and mortality worldwide. Despite the recent advances in the early diagnosis and treatment, cancer still accounts for 14 million new cases and 8.2 million cancer-related deaths worldwide in the year 2012, and for some types of cancer (e.g., pancreatic ductal adenocarcinoma) incidence equals to mortality. Existing cancer therapies like chemotherapy have benefits, but the side-effects can be traumatic as a reason of off-target toxicity, whereas targeted drugs can reduce collateral damage. So the development of binary therapies is urgently required in order to increase the therapeutic efficacy against the harm caused by side effects. Among few binary therapies like Boron Neutron Capture Therapy (BNCT), Photodynamic Therapy (PDT) and Photothermal Therapy (PTT), BNCT looks very promising.

Boron neutron capture therapy (BNCT) is a binary approach to cancer therapy which relies in the selective or preferential accumulation of ^{10}B atoms in the tumor; local irradiation with non ionizing thermal neutrons yields ^{4}He and ^{7}Li ions which, due to their high linear energy transfer, are able to damage tumor cells. Even though this therapy looks very promising, its clinical application has been historically restricted, mainly due to: (i) the lack of compounds able to selectively deliver boron atoms in sufficient quantity in the tumor, and (ii) the lack of techniques able to determine, *in vivo* and on real time, the accumulation of boron compounds in the tumor and surrounding tissue. In this context, appropriately targeted carboranes or metallacarboranes might serve as suitable boron carrier drugs due to their high boron content, their high thermal and chemical stability and their solubility in physiologic conditions. On the other hand, nuclear imaging techniques such as Positron Emission Tomography (PET) and Single Photon Emission Computed Tomography (SPECT) in combination with Computerized Tomography (CT) are valuable tools for the assessment of pharmacokinetic properties of new chemical entities; they are thus anticipated to be suitable for the determination of the accumulation of boron-rich compounds in the tumor and surrounding tissues.

The main aim of my PhD thesis was the development of strategies for the incorporation of radioactive isotopes (mainly positron and gamma emitters) in boron rich structures (carborane clusters), to enable the subsequent preparation of a library of potential BNCT drug candidates and their evaluation using nuclear imaging techniques such as PET and SPECT in combination with anatomical techniques such as CT. With that aim, the most widely used carborane clusters, namely dicarba-*closo*-dodecaboranes and cobalt-*bis*-dicarbiollide (COSAN), were selected and strategies to radiolabel them with different isotopes such as ^{11}C, ^{18}F, ^{124}I, ^{125}I and ^{131}I were developed.

In **chapter 4**, radiolabelling of carborane was discussed. Carboranes are initial attractions for BNCT agents because of their high boron content and stability to catabolism. Carboranes in pharmaceuticals increase the hydrophobic interactions with the receptors to increase the *in vivo* stability and hence bioavailability. In the context of nuclear imaging, Fluorine-18 with sufficiently long half-life and short positron range is a very useful radionuclide. Up to date there is no report of the ^{18}F-fluorination of *o*-carborane. We developed a novel strategy for the preparation of mono-F-18 labelled carborane, which was further functionalized with targeting vectors on cluster carbon atoms. In another work included in the same chapter, radiolabelling of decaborane, a precursor for the preparation of many functionalized *o*-carboranes, was developed using ^{125}I and ^{131}I. Different carborane analogues were subsequently prepared by reaction with different acetylenes.

In **chapter 5**, radiolabelling of cobalt-*bis*-dicarbollide, commonly known as COSAN, is described. As recently demonstrated, COSAN can cross through synthetic lipid membranes without disrupting membrane integrity and accumulates *in vitro* within living cells. Additionally, it can be readily multi-decorated by incorporation of functional groups in the different vertexes. These properties, together with its high boron content, its chemical stability and its solubility in physiologic conditions, turn COSAN into a suitable building block for the preparation of boron carrier drugs. In this chapter, the synthesis of a new bi-functional COSAN derivative and its unprecedented radiolabelling with either ^{125}I (gamma emitter) or ^{124}I (positron emitter) via palladium catalyzed isotopic exchange reaction is reported. Biodistribution information after intravenous administration in rodents was obtained by using dissection/gamma counting and PET-CT, respectively.

In **chapter 6**, the synthesis of two analogues of 2-(4-aminophenyl)benzothiazole (a compound that was found to elicit pronounced inhibitory effects against certain breast cancer cell lines in vitro) in which the

phenyl ring has been substituted by *m*-carborane and their radiolabelling with Carbon-11 using [^{11}C]CH_3OTf are reported.

Finally, in **chapter 7**, a method to synthesize *m*-carboranyl amides via the one-pot one-step carbonylation reaction of 1-I-mcarborane with primary and secondary amines in the presence of a palladium catalyst and under carbon monoxide atmosphere (Heck reaction) is presented. Different catalysts, ligands, bases, and experimental conditions have been evaluated and the results in terms of yield and formation of by-products are discussed. This strategy should be suitable for the preparation of ^{11}C-labelled carboranyl amides using [^{11}C]CO as labeling agent for further in vivo evaluation using PET.

Resumen

La terapia por captura de neutrones (BNCT o Boron Neutron Capture Therapy), fue descrita por primera vez por Locher en 1936 y es una modalidad terapéutica binaria para el tratamiento del cáncer que se basa en la captura de neutrones térmicos por medio de átomos de ^{10}B, previamente acumulados en las células tumorales. La captura del neutrón térmico resulta en la formación de un núcleo de ^{11}B, que fisiona para generar dos iones altamente energéticos: $^{4}He^{2+}$ y $^{7}Li^{3+}$. El daño y la posterior muerte celular se producen por la ionización que provocan estas partículas en su recorrido, antes de perder completamente su energía. El desarrollo histórico de la BNCT se ha centrado en el tratamiento de tumores cerebrales malignos, cuya extirpación resulta arriesgada y el tratamiento mediante técnicas como la radioterapia o la quimioterapia provocan daños importantes en el tejido sano circundante. Se estima que se requieren aproximadamente entre 10 y 30 μg de ^{10}B por gramo de tumor para obtener resultados terapéuticos relevantes, aunque esta cantidad puede reducirse considerablemente si la acumulación se localiza cerca del núcleo celular.

De lo expuesto anteriormente se deduce que resulta de elevada importancia el diseño de moléculas que posean un gran número de átomos de ^{10}B en su estructura y que presenten elevada afinidad/especificidad por las células tumorales. Los heteroboranos poliédricos representan una estructura química altamente recurrida para su aplicación en la BNCT. Este hecho se debe, por un lado, a la alta acumulación de átomos de boro en una misma molécula y, por otro lado, a su elevada versatilidad química. Entre los heteroboranos poliédricos se encuentran los dicarba-*closo*-dodecaboranos (también llamados carbaboranos o carboranos, de fórmula empírica general $C_2B_{10}H_{12}$), que presentan geometría prácticamente icosaédrica, de modo que cada átomo de carbono y/o boro están hexacoordinados. Existen en las formas isoméricas orto, meta y para, que difieren entre sí en la posición relativa de los átomos de carbono del clúster; sus características físico-químicas más relevantes son su elevada versatilidad y su elevada estabilidad térmica y fotoquímica en el rango UV-visible. Debido a estas características únicas, los carboranos se han utilizado históricamente para preparar catalizadores, polímeros, compuestos de coordinación y radiofármacos, aunque una de sus principales aplicaciones

radica en la preparación de compuestos aptos para su utilización en la BNCT; durante las últimas décadas, muchos grupos de investigación han desarrollado nuevas estructuras incorporando heteroboranos poliédricos en general y carboranos en particular con potencial aplicación en la BNCT.

Una de las estrategias más utilizadas consiste en incorporar una molécula de *orto*-carborano a diferentes carbohidratos, ya que estos últimos presentan no sólo baja toxicidad, sino que poseen cierta afinidad hacia determinados receptores específicos que se encuentran en la superficie tumoral y compensan la elevada hidrofobicidad inherente al clúster de carborano, que podría provocar unión inespecífica indeseada o acumulación en el hígado. Estrategias alternativas proponen la síntesis de aminoácidos, porfirinas, poliaminas, o nucleósidos (o derivados de éstos) que contienen carboranos como grupos sustituyentes, o de liposomas que contienen en su interior heteroboranos poliédricos que se liberan en los tumores aprovechando la vasculatura inmadura que se encuentra en las inmediaciones de los tumores que proliferan rápidamente.

Estudios pre-clínicos efectuados sobre algunos de los compuestos anteriormente citados han demostrado claramente la eficacia terapéutica en muchos modelos tumorales (especialmente en tumores cerebrales), e incluso algunos ensayos clínicos han demostrado que la BNCT puede implementarse de forma segura a nivel clínico. Sin embargo, la eficacia terapéutica sólo está garantizada en el caso en que el fármaco se encuentre en el interior de las células tumorales y, a ser posible, cerca del núcleo. Es por lo tanto crucial disponer de una herramienta capaz de monitorizar el comportamiento fisiológico y farmacológico de los átomos de ^{10}B (o del fármaco portador) dentro del paciente. Dicha herramienta debería permitir (idealmente) determinar de manera no invasiva la concentración de ^{10}B en tejido, sangre y orina, así como la distribución espacial microscópica a nivel celular y sub-celular.

En la actualidad, la comunidad científica dispone de varios métodos que permiten determinar la concentración de ^{10}B en muestras, tanto a nivel macroscópico como microscópico. Uno de los más utilizados históricamente es la Espectroscopia de Rayos Gamma Prompt (PGRA) que permite medir el contenido medio de ^{10}B en muestras macroscópicas. Otras técnicas comúnmente utilizadas (de forma aislada o en combinación con otras) son la Espectroscopia de Emisión por Plasma de Acoplamiento Inductivo (ICP-EOS), Autorradiografía Alfa de Alta Resolución, Radiografía por Captura de Neutrones (NCR) y Espectroscopía Electrónica de Pérdidas de Energía (EELS).

Todas las técnicas citadas anteriormente tienen en común que son invasivas (aunque no necesariamente destructivas) y que determinan directamente la cantidad de boro. Una alternativa a dichas técnicas consiste en determinar la concentración de fármaco portador de boro y no directamente la cantidad de ^{10}B, y es en este escenario donde cobran importancia las técnicas de imagen molecular, en especial las técnicas nucleares de imagen, entre las que se encuentran la Tomografía por Emisión de Fotón Único (SPECT) y la Tomografía por Emisión de Positrones (PET). Ambas técnicas (PET y SPECT) permiten obtener imágenes tridimensionales *in vivo* y a tiempo real, que ofrecen información acerca de la distribución espacio-temporal de un radiotrazador administrado a un sujeto, siendo el radiotrazador cualquier especie química marcada con un radioisótopo emisor de fotones gamma (SPECT) o de positrones (PET). Durante los últimos años las técnicas nucleares se han postulado como una herramienta fundamental no sólo en el entorno diagnóstico, sino también para el estudio farmacocinético y farmacodinámico de nuevas entidades químicas. En el supuesto que se marcara isotópicamente un fármaco con potencial aplicación en la BNCT, las técnicas de imagen nuclear permitirían conocer, en cada momento y para cada parte del organismo, la concentración de fármaco una vez éste se hubiera administrado a un sujeto.

A pesar del potencial teórico que presentan las técnicas de imagen nuclear, la principal dificultad en su aplicación radica en la necesidad de marcar radiactivamente todos y cada uno de los fármacos potencialmente activos. Este hecho, unido al corto período de semidesintegración de los isótopos más comúnmente empleados (que obliga a desarrollar procesos de marcaje rápidos, efectivos y automatizables) ha provocado que hasta la fecha tan sólo se haya marcado un candidato (L-para-boronofenilalanina, BPA) con Flúor-18 (isótopo emisor de positrones). Los ensayos realizados con este compuesto (en los que se combina la PET con técnicas de imagen anatómicas, concretamente Tomografía Computerizada o CT) permitieron determinar la farmacocinética, el metabolismo y la acumulación en tejido del radiotrazador (^{18}F-BPA). La acumulación del radiotrazador en tumor determinada mediante las técnicas de imagen correspondía con la acumulación de fármaco (BPA) determinada mediante técnicas ex vivo.

Es evidente, pues, que las técnicas de imagen nuclear, especialmente la PET (que a diferencia de la SPECT permite una cuantificación absoluta de la distribución espacio-temporal del radiotrazador) pueden desarrollar un papel fundamental en el salto hacia la aplicación clínica de la BNCT como modalidad terapéutica rutinaria en el entorno hospitalario. Para ello es imprescindible, sin embargo, diseñar estrategias para la incorporación de isótopos radiactivos

(emisores de positrones o emisores gamma) a moléculas ricas en boro. Esta es precisamente la temática que se aborda en la presente tesis doctoral.

En el **capítulo 4** se presentan dos estrategias diferentes para la incorporación de isótopos radiactivos en carboranos funcionalizados. La primera estrategia se basa en la mono-[^{18}F]fluoración del *o*-carborano mediante sustitución nucleofílica, utilizando el anión [^{18}F]F^{-} producido mediante irradiación de agua enriquecida en oxígeno-18 con protones acelerados, y una sal de arilyodonio del carborano. Una vez producido el marcaje, se plantea la funcionalización del carborano marcado radiactivamente mediante formación de la sal litiada y posterior reacción con aldehídos. La segunda estrategia se basa en la preparación de decaborano radio-yodado mediante intercambio isotópico, y subsiguiente reacción con acetilenos sustituidos en acetonitrilo (que actúa simultáneamente como base de Lewis y como disolvente) bajo calentamiento con microondas, rindiendo derivados del *o*-carborano funcionalizados con diferentes sustituyentes. Ambas estrategias poseen un elevado valor sintético ya que permiten la preparación de una amplia variedad de carboranos marcados radiactivamente. Fruto del trabajo expuesto en este capítulo han resultado dos publicaciones científicas en revistas internacionales:

1- Gona KB, Gómez-Vallejo V, Padro D, Llop J; [^{18}F]Fluorination of *o*-carborane via nucleophilic substitution: towards a versatile platform for the preparation of ^{18}F-labelled BNCT drug candidates. *Chemical Communications*, **2013**. 49(98): 11491-11493.

2- Gona KB, Lakshmi VPN Thota J, Baz Z, Gómez-Vallejo V, Llop J, Straightforward synthesis of radioiodinated Cc-substituted o-carboranes: towards a versatile platform to enable in vivo assessment of BNCT drug candidates. *Dalton Transactions*. **2015**. 44: 9915-9920.

Actualmente se está preparando una tercera publicación.

En el **capítulo 5** se presentan estrategias para el marcaje de derivados del anión cobalto-bis-dicarballuro (COSAN). Para ello, se utilizan reacciones de intercambio isotópico catalizadas por paladio utilizando dos isótopos radiactivos: ^{125}I (emisor gamma de baja energía) y ^{124}I (emisor de positrones). Los derivados marcados con ^{125}I se utilizaron para determinar el patrón de biodistribución en roedores utilizando disección y contaje de órganos, mientras que los análogos marcados con ^{124}I se utilizaron para determinar el patrón de biodistribución mediante PET-CT, utilizando para ello tanto animales sanos como diferentes modelos tumorales. Cabe destacar que este trabajo se realizó en estrecha colaboración con el grupo de investigación liderado por los

Profesores Francesc Teixidor y Clara Viñas, del Institut de Ciència de Materials de Barcelona (ICMAB-CSIC). Dicho grupo de investigación llevó a cabo la síntesis de los precursores para el marcaje y participó activamente en el análisis de los resultados obtenidos y presentados en este capítulo. Fruto del trabajo realizado, ha resultado una publicación científica en una revista internacional:

3- Gona KB, Zaulet A, Gómez-Vallejo V, Teixidor F, Llop J, Viñas C; COSAN as a molecular imaging platform: synthesis and "in vivo" imaging. *Chemical Communications*. **2014**. 50: 11415-11417.

Actualmente se está preparando una segunda publicación.

Los capítulos 6 y 7 de esta tesis doctoral se han focalizado en la preparación de análogos de carboranos marcados con Carbono-11.

En el **capítulo 6** se describe la preparación de dos análogos del 2-(4-aminofenil) benzotiazol en los que el anillo bencénico se sustituye por una unidad *m*-carborano. Posteriormente, se procede a la incorporación del isótopo radiactivo mediante metilación. Para ello, se genera en primera instancia el precursor radiactivo $[^{11}C]CH_3I$, que es transformado en $[^{11}C]CH_3OTf$ para llevar a cabo la correspondiente reacción de metilación. Este trabajo resultó en la publicación de un artículo científico:

4- Gona KB, Lakshmi VPN Thota J, Baz Z, Gómez-Vallejo V, Llop J, Synthesis and ^{11}C-radiolabelling of 2-carboranyl benzothiazoles. *Molecules*. **2015**. 20: 7495-7508.

Por último, en el **capítulo 7** se describe un método novedoso para la preparación de amidas en un solo paso, mediante carbonilación catalítica de 1-iodo-1,7-dicarba-*closo*-dodecaborano utilizando monóxido de carbono. Esta reacción, si bien no se ha ensayado en condiciones de radiactividad, sería fácilmente trasladable a la preparación de compuestos marcados con carbono-11, ya que el $[^{11}C]CO$ es un sintón ampliamente utilizado en el contexto de la radioquímica. Con el fin de proceder en un futuro a la preparación de amidas marcadas radiactivamente incorporando un clúster de carborano, en el contexto de esta tesis doctoral se ha puesto a punto un método para producir rutinariamente la especie radiactiva $[^{11}C]CO$ a partir de $[^{11}C]CO_2$ producido en el ciclotrón. Asimismo, se ha diseñado e implementado un módulo automático para la producción de esta especie radiactiva. Fruto del trabajo realizado, ha resultado una publicación científica:

5- Gona KB, Gómez-Vallejo V, Llop J; Synthesis of m-carboranyl amides via palladium-catalyzed carbonylation. *Tetrahedron Letters*, **2013**. 54(8): 941-944.

A parte del trabajo descrito anteriormente (incluido en la presente tesis doctoral) cabe remarcar que durante la ejecución de la tesis doctoral he tenido la oportunidad de participar en diferentes proyectos científicos, que si bien no están reflejados en este manuscrito, han contribuido a obtener una formación integral y amplia en el área de la radioquímica y la imagen molecular. Fruto de mi implicación en estos proyectos, han resultado diferentes publicaciones científicas en las cuales estoy reflejado como coautor.

6- Soria FN, Pérez-Samartín A, Martin A, Gona KG, Llop J, Szczupak B, Chara JC, Matute C, Domercq M; Extrasynaptic glutamate release through cystine/glutamate antiporter contributes to ischemic damage. *The Journal of Clinical Investigation*. **2014**. 124: 3645-3655.

7- Gómez-Vallejo V, Vázquez N, Gona KB, Puigivila M, González M, San Sebastián E, Martin A, Llop J, Synthesis and *in vivo* evaluation of ^{11}C-labeled (1,7-dicarba-closo-dodecaboran-1-yl)-*N*-{[(2S)-1-ethylpirrolidin-2-yl]methyl}amide. *Journal of labeled compounds and radiopharmaceuticals*. **2014**. 57: 209-214. DOI: 10.1002/jlcr.3159

8- Gómez-Vallejo V, Gaja V, Gona KB, Llop J; Nitrogen-13: Historical review and future perspectives; *Journal of labeled compounds and radiopharmaceuticals*. **2014**. 57: 244-254.

1. INTRODUCTION (I): BORON NEUTRON CAPTURE THERAPY

1.1. Cancer: A general public health problem

Despite recent advances, cancer remains a pressing public health concern. There were 14.1 million new cancer cases worldwide in 2012, and the global cancer burden is expected to nearly double to 21.4 million cases and 13.5 million deaths by 2030. Advances in the early diagnosis and treatment of cancer have raised the 5-year relative survival rate for all cancers from 50% (1974) to 68% (2007) [1]; however, cancer still accounted for 8.2 million deaths worldwide in 2012 [2], and for some types of cancer (e.g., pancreatic ductal adenocarcinoma) incidence equals mortality [3]. The development of new treatments and therapies is therefore urgently required, but since many cytotoxic therapies are highly toxic to the patient, therapeutic efficacy needs to be carefully balanced against the harm caused by side effects.

1.2. Boron Neutron Capture Therapy (BNCT)

1.2.1. Binary approaches to cancer therapy: The Principle behind BNCT

Binary approaches to cancer therapy, in which two non- or low-toxicity components of the treatment require co-localization in the tumour to become effective, are promising strategies to improve patient outcomes and reduce side effects. Photodynamic therapy (PDT) and photothermal therapy (PTT) are binary therapies based on the injection of an intrinsically non-toxic photosensitising agent, followed by specific irradiation of the treated area with visible or near-infrared (IR) laser light. The process by which cancer cells are killed by these two modalities is different: in PDT, cancer cell toxicity is mediated by an oxidative process caused by highly toxic singlet oxygen [4], while in PTT photons are absorbed and rapidly decay back to the ground state, which converts light energy into thermal energy and induces a temperature spike that initiates tumour necrosis. However, both PDT and PTT are limited by the low penetration of visible or near-IR light into tissue, limiting their application to the treatment of superficial tumours.

Boron Neutron Capture Therapy (BNCT) is an alternative binary approach to cancer therapy based on the ability of the non-radioactive nuclide boron-10

[1] National Cancer Institute at the National Institute of Health. Available online: http://www.cancer.gov/cancertopics/factsheet/cancer-advances-in-focus/cancer (accessed on 14th May 2014)
[2] International Agency for Research on Cancer. GLOBOCAN 2012: http://globocan.iarc.fr/Pages/fact_sheets_cancer.aspx (accessed on 14 May 2014)..
[3] D. Hariharan, et al., *HPB*. **2008**, *10*, 58.
[4] B. H. Henderson, *et al.*, *Photochem. Photobiol.* **1992**, *55*, 145.

(^{10}B) to capture thermal neutrons, which results in the rapid nuclear reaction ^{10}B(n, α, γ)^{7}Li. Alpha particles and ^{7}Li recoil ions have high linear energy transfer (LET) properties (150keV μm^{-1} and 175keV μm^{-1}, respectively) and path lengths in the range of 4 to 10 μm. Hence, their energy deposition is limited to the diameter of a single cell. The concept behind BNCT is thus relatively intuitive: if cancer cells selectively take up a sufficient amount of ^{10}B and are irradiated with thermal neutrons, the ions produced as a consequence of the ^{10}B(n, α, γ)^{7}Li nuclear reaction result in cellular damage and trigger cell death, while sparing healthy surrounding tissue and decreasing unwanted off-target side effects (Figures 1.1 and 1.2).

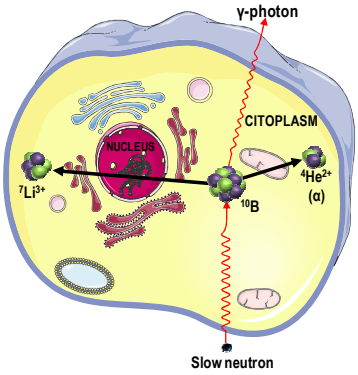

Figure 1.1. Schematic representation of the nuclear reaction that takes place inside the cell during irradiation with slow neutrons.

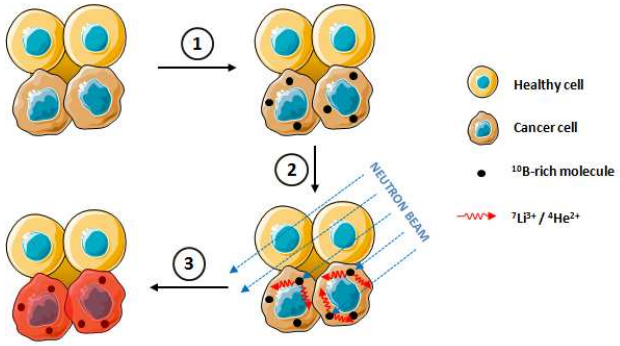

Figure 1.2. Schematic representation of the principle behind BNCT: ^{10}B atoms preferentially accumulate in cancer cells (1). Neutron irradiation (2) produces the rapid nuclear reaction ^{10}B(n, α, γ)^{7}Li. Alpha particles and ^{7}Li ions have high linear energy transfer, triggering cell damage and death (3) while sparing healthy surrounding cells.

Despite the simplicity of the concept and the fact that it was proposed almost 80 years ago by Locher [5], the successful application of BNCT has been thwarted by a number of problems, not least the unease around conducting clinical irradiations in nuclear research reactors. Apart from this, the main limitation of BNCT is the need to develop drugs that are able to deposit a sufficient number of ^{10}B atoms specifically in tumour cells or tissues. Two main parameters need to be considered during development of new BNCT drug candidates: first, the boron concentration in the tumour should be >20-35 μg ^{10}B/g (natural abundance of ^{10}B 19.9%), although lower amounts might be sufficient if the boron nuclei are specifically localised to the target cells and are close to the nucleus. Second, tumour-to-normal tissue and tumour-to-blood ratios should be greater than five to prevent damage to healthy tissue in the path of the neutron beam [6].

1.2.2. Boron-rich derivatives as therapeutic drugs in BNCT

Abnormal metabolism and the over-expression of certain membrane receptors have previously been exploited to design boron-rich compounds capable to accumulate ^{10}B nuclei in cancer cells. In this context, small boron molecules (e.g., boronic acid and polyhedral heteroboranes) have been used to prepare carbohydrate [7], amino acid (Figure 1.3), peptide [8], and nucleic acid derivatives [9] (Figure 1.4). The main idea behind all these compounds is simple: To try to design a molecule or system with two differentiated functionalities. One part of the system provides the biological properties and enhances selective or preferential accumulation in tumour cells; the second part of the molecule acts as a boron source.

Antibodies (Abs), which demonstrate exceedingly high antigen specificity, have also been also proposed as vectors to accumulate ^{10}B atoms in the tumour. It is estimated that a boronated Ab should contain 10^3 ^{10}B atoms to provide a therapeutic dose to the tumour [10], but the incorporation of such a large

[5] G. L. Locher, *Am. J. Roentgenol. Radium Ther.* **1936**, *36*, 1.
[6] R. F. Barth, et al., Cancer 1992, 70, 2995.
[7](a) J.L. Maurer, *et al., Organometallics*, **1988**, *7*, 2519; (b) W. Tjarks, *et al.*, *J. Med. Chem.* **1992**, *35*, 1628; (c) G.B. Giovenzana, *et al.*, *Tetrahedron*, **1999**, *55*, 14123; (d) S. Ronchi, *et al.*, *Tetrahedron Asymmet.* **2005**, *16*, 39.
[8](a) M. Y. Stognyi, *et al., Polyhedron* **2013**, *55*, 117; (b) A. Semioshkin, *et al.*, *J. Organometallic Chem.* **2007**, *692*, 4020.
[9](a) W. Tjarks, *J. Organomet. Chem.* **2000**, *614-615*, 37; (b) S. Hasabelnaby, *et al.*, *Eur. J. Med. Chem.* **2012**, *55*, 325; (d) A. Semioshkin, *et al.*, *Tetrahedron* **2013**, *37*, 8034.

[10] F. Alam, *et al., Antibody Immunoconjugates Radiopharm.* **1989**, *2*, 145.

amount of boron may result in a significant loss of immunoreactivity. Strategies to incorporate boronated macromolecules (e.g., polymers and dendrimers) containing a large number of boron atoms via linkers have also been explored, with moderate success [11].

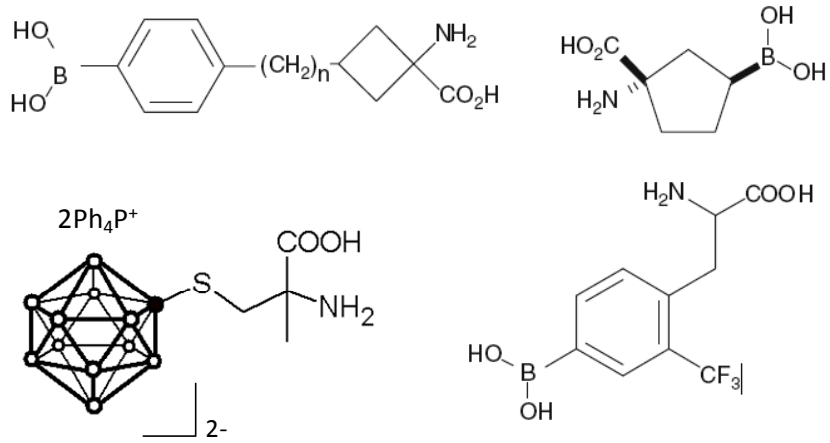

Figure 1.3. Structures of boron-containing amino acids. In the cluster, white dots stand for B-H; black dot stands for B.

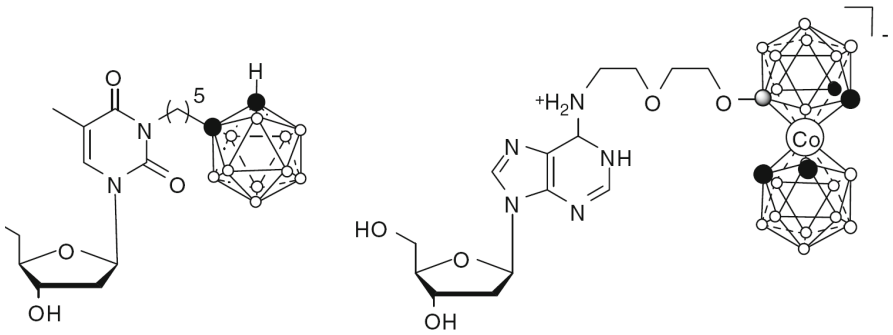

Figure 1.4. Structures of boron-containing nucleic acids. In the cluster, white dots stand for B-H; black dots stand for C (left) or C-H (right); grey dot stands for B.

[11] (a) F. Alam, *et al., J. Med. Chem.* **1989**, *32*, 2326; (b) R. F. Barth, *et al.*, *Bioconjugate Chem.* **1994**, *5*, 58; S. Shukla, *et al.*, *Bioconjugate Chem.* **2003**, *14*, 158.

More recently, and with the emergence of nanotechnology, drug delivery systems such as liposomes have gained attention [12], since when appropriately designed they have a long circulating half-life and preferentially accumulate in cancer tissues due to the leaky neovasculature and immature lymphatic network that characterise tumour tissues. This passive uptake - the so-called enhanced permeability and retention (EPR) effect - can be improved further by attaching ligands that target tumour-specific receptors. The same rationale has been applied to the preparation of side-wall functionalised targeted single wall carbon nanotubes (SWCNTs) [13] (Figure 1.5) and boron nitride nanotubes [14], among others.

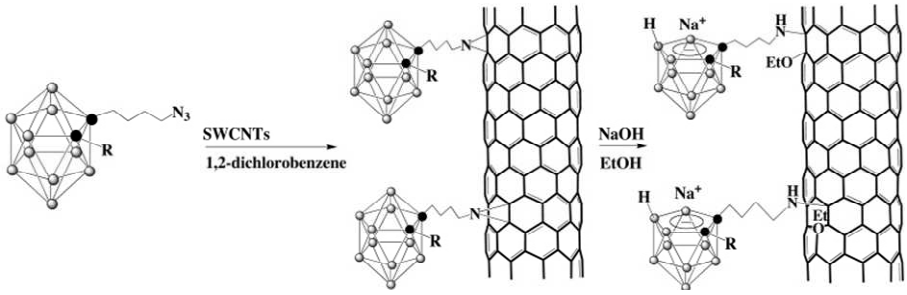

Figure 1.5. Syntheses of Substituted Carborane-Appended single wall carbon nanotubes (SWCNTs). In the clusters, white dots stand for B-H; black dots stand for C. Adapted from reference [13].

1.2.3. Determination of boron accumulation in the tumour

As mentioned above, one of the main problems for the clinical application of BNCT is the development of boron-rich molecules capable to accumulate in cancer cells after systemic administration. However, there is a second major drawback that is probably underestimated; this second drawback relates to the need to determine, *in vivo* and in a non invasive way, the accumulation of boron in the tumour and surrounding tissue as a function of time, in order to define the optimal time-window for the application of neutron irradiation, for the therapeutic effect to be optimal, while minimizing side effects and destruction of the surrounding tissue. This is schematized in Figure 1.6.

[12] D. A. Feakes, *et al.*, *Proc Natl Acad Sci USA* **1994**, *91*, 3029; (b) K. Maruyama, *et al.*, *J. Control. Release* **2004**, *98*, 195; (c) M. Ueno, *et al.*, *Bioorg. Med. Chem.* **2010**, *18(9)*, 3059.
[13] Y. H. Zhu, *et al.*, *J. Am. Chem. Soc.* **2005**, *127*, 9875.
[14] G. Ciofani, *et al.*, *Nanoscale Res. Lett.* **2009**, *4*, 113.

Currently, different alternatives are available to determine the concentration of boron in tissues, although most of them are invasive and do not provide real-time information. These methods are summarized below:

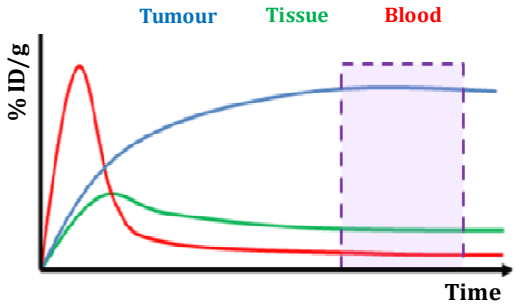

Figure 1.6. Fictitious time-activity-curves (percentage of injected dose per gram of tissue) in the tumour, surrounding tissue and blood, after administration of a boron-rich drug candidate. Determination of these curves permits the identification of the optimal time-window for the application of neutron irradiation, when the concentration in the tumour is maximum and the concentration both in blood and surrounding tissue are low.

1.2.3.1. Prompt Gamma-ray Spectroscopy

Prompt Gamma-ray is a fast method to determine the average ^{10}B-content in a macroscopic sample [15]. The technique is based on gamma-ray spectroscopy following neutron capture in ^{10}B. The resulting ^{7}Li-nuclei from the nuclear reaction decays to the ground state by emitting gamma rays with an energy of 478 keV. The number of photons emitted is proportional to the neutron capture reaction, and hence to the boron concentration in the sample. The source of neutrons is usually a nuclear reactor, and different filters are applied to achieve neutrons with the desired quality. To use this technique, appropriate calibration against ^{10}B-reference samples is mandatory to prevent systematic errors, but preparation of the sample is quite simple. The main advantage of this technique is that it opens the possibility to perform *in vivo* gamma-ray spectroscopy of the patient during treatment [16]. Information about boron concentration in volumes of a few cm^3 with a temporal resolution of a few

[15] Kobayashi T, et al., *Nucl Instrum Methods Phys Res* **1983**, 204, 525–31.
[16] (a) Munck af Rosenschold PM, et al., *Med Phys* **2001**, *28*, 787–95. (b) Verbakel WF, et al., *Int J Radiat Oncol Biol Phys* **2003**, *55*, 743–56

minutes can be obtained, although improvement of the method is required before routine application in the clinical setting.

1.2.3.2. Inductively Coupled Plasma Spectroscopy

Inductively Coupled Plasma-Atomic Emission Spectroscopy (ICP-AES), uses a plasma to produce excited atoms that emit electromagnetic radiation at a wavelength characteristic of a particular element. Because each element emits energy at specific wavelengths, the nature of the atom can be determined. The intensity of the energy emitted at a pre-determined wavelength is proportional to the concentration of that element.

Inductively Coupled Plasma Mass Spectrometry (ICP-MS) is based on coupling together inductively coupled plasma as a method of producing ions (ionization) with a mass spectrometer to separate and identify the ions. ICP-MS methods have been developed to determine parts per billion (ppb) levels in different biological fluids and tissues, with the advantage that both isotopes can be quantified individually. One of the main problems in the application of ICP-MS to the determination of boron contents in samples is the memory effect, due to the tendency to absorb onto glass. Hence, carefully validated methods have to be used. On the other hand, ICP-MS has the advantages of a very high sensitivity and the above mentioned possibility to determine both boron isotopes in one run.

1.2.3.3. High Resolution Alpha Autoradiography

The principle behind high resolution alpha autoradiography is the following: Small tissue samples to be analyzed, usually surgically removed from the patient or experimental animal, are frozen and cut into 1-2μm thick slices. These are mounted on Ixan and Lexan films, adhered on quartz glass slides. The quartz slide/tissue/Ixan/Lexan units are packed with dry ice and irradiated with thermal neutrons. After irradiation, the sections are stained using hematoxilin–eosin staining. During neutron irradiation the interaction of the alpha and ^{7}Li charged particles with the Lexan film causes molecular weakening of the Lexan along the paths of these particles. The samples are then analyzed with digital microphotographs, and correlation of the distribution of tracks with the anatomical features of the tissue provides maps of ^{10}B-distribution in the tissue. Appropriate calibration is required to obtain quantitative data. Importantly, one of the main drawbacks of this method is its

invasive character, derived from the need to get a surgical removal of a tissue sample.

1.2.3.4. Neutron Capture Radiography

In neutron capture radiography, the boron concentration in a tissue section (a few millimetre thickness) is determined in an area of approximately 0.5 cm^2 using the spectroscopy of charged particles emitted in the boron neutron capture reaction, and is then spatially correlated with stained tissue sections. The slice is laid flat on a nuclear detection film and is irradiated with thermal neutrons. In those areas of the tissue where ^{10}B is present, the alpha particles or ^{7}Li ions resulting from neutron capture are emitted and cause damage to the nuclear detection film. The tissue sample is finally removed from the film and the image of the ^{10}B-distribution is obtained by chemical etching [17].

Besides the above mentioned methods, other techniques for the determination of boron concentration and distribution in tissues or samples have been developed, including Laser post-ionization Secondary Neutral Mass Spectrometry (laser-SNMS) and Electron Energy Loss Spectroscopy (EELS). The detailed description is out of the scope of this PhD thesis, and an excellent revision can be found elsewhere [18].

Importantly, all the above mentioned techniques (with exception of Prompt Gamma-ray Spectroscopy) can be only applied in tissue samples or sections, and hence they cannot be considered *in vivo* techniques. It would be very convenient for the evaluation of newly-developed boron-rich compounds to have access to a technique able to determine the concentration of boron in organs and tissues on real time, *in vivo* and in a minimally invasive way. This can be achieved by using nuclear imaging techniques, such as Positron Emission Tomography (PET) and Single Photon Emission Computerized Tomography (SPECT), which are described in Chapter 2 of this thesis. Of note, the use of these techniques requires the incorporation of a positron or gamma emitter in the molecule under investigation. This, together with the low availability of the technology required, has historically hampered the utilization of *in vivo* imaging in the context of BNCT.

[17] Enge W, et al., *NIM A* **1974**, *115*, 263–70.
[18] Wittig, A., et al., *Critical Reviews in Oncology/Hematology* **2008**, *68*, 66–90.

2. INTRODUCTION (II): NUCLEAR IMAGING

2.1. Molecular imaging: General aspects

Molecular imaging can be defined as a set of techniques that allow the non invasive visualization of cell function and the monitoring of molecular processes in living organisms. They differ from traditional imaging techniques because biomarkers (which interact with the surrounding, being the resulting image a representation of the molecular changes taking place) are used. Molecular imaging has paved the way to explore biological, physiological and medical processes which cannot be studied using other techniques. Positron emission tomography (PET), single photon emission computerized tomography (SPECT), optical/fluoresce imaging, and magnetic resonance spectroscopy (MRS) are considered molecular imaging techniques.

Molecular imaging techniques usually offer poor anatomical information. Thus, such techniques are often combined with other modalities able to provide accurate anatomical/morphological information. The combination of the resulting images offers information at anatomical and molecular level; this approach is known as multi-modal imaging. Anatomical modalities include mainly magnetic resonance imaging (MRI), ultra-sound imaging (US), X-ray imaging and computed tomography (CT).

It is worth mentioning that each imaging modality has strengths and limitations. Thus, while nuclear imaging techniques such as PET and SPECT offer unparalleled sensitivity, their resolution is in the range of 1 mm in the preclinical setting and a few mm in the clinical systems. On the other hand, MRI can offer high resolution (up to a few micrometers) while its sensitivity is low. As a consequence, the application of one modality or another will depend on the problem under investigation and often the combination of two or more modalities will provide the most accurate data.

In this chapter, only an introduction to the imaging modalities used in the current work (PET, SPECT and CT) will be provided.

2.2. Nuclear Imaging techniques

Nuclear imaging techniques rely on the administration of trace amounts of a radiotracer. A radiotracer can be defined as a compound labelled with a radioactive isotope to enable external, non-invasive detection. Gamma ray-emitters are appropriate radioisotopes because high-energy gamma rays can travel though biological tissues without suffering significant scatter or

attenuation. Gamma rays (or photons) can be detected using specific instrumentation, and the original concentration of radiotracer can be accurately quantified using tomographic reconstruction algorithms. As a result, a series of tomographic images conveying information on absolute radioisotope concentration can be obtained over time, *in vivo* and in a non invasive way. Positron emission tomography, single photon emission computed tomography and scintigraphy are nuclear imaging techniques. The latter will not be described because it has not been used in the context of this PhD thesis.

2.2.1. Positron Emission Tomography

2.2.1.1. General aspects

Positron emission tomography (PET) is an ultra-sensitive imaging technique, which enables the determination of the spatiotemporal distribution of a radiotracer labelled with a positron emitter after administration into a living organism. Typical positron emitters used in the biomedical arena include Fluorine-18, Carbon-11, Nitrogen-13, Oxygen-15, Galium-68, Copper-64, Zirconium-89 and Iodine-124 (see Table 2.1 for physical properties).

Table 2.1. Physical characteristics of Fluorine-18, Carbon-11, Nitrogen-13, Oxygen-15, Galium-68, Copper-64, Zirconium-89 and Iodine-124.

Isotope	Half-Life	β^+_{max} Energy (β^+ fraction)
^{18}F	109.8 min	0.63 MeV (0.97)
^{11}C	20.4 min	0.96 MeV (1.00)
^{13}N	9.97 min	1.20 MeV (1.00)
^{15}O	122 sec	1.73 MeV (1.00)
^{68}Ga	67.7 min	1.89 MeV (0.89)
^{64}Cu	12.7 hours	0.66 MeV (0.18)
^{89}Zr	78.4 h	0.90 MeV (0.23)
^{124}I	4.18 days	2.14 MeV (0.23)

The radioactive decay of a positron emitter, process that takes place spontaneously, produces a positron, which after travelling a certain distance (positron range) annihilates with the electron of a surrounding atom; as a result, two photons emitted in opposite directions and with energy of 511 keV each are emitted. These high-energy gamma rays have a high penetration power, and can escape from the body without suffering significant attenuation or scattering effects. Hence, they can be detected with a ring of detectors placed around the organism under investigation. The detection of hundreds of

thousands of photons permits the reconstruction of a 3D image that contains information about the spatiotemporal distribution of the radiolabelled tracer within the organism (Figure 2.1).

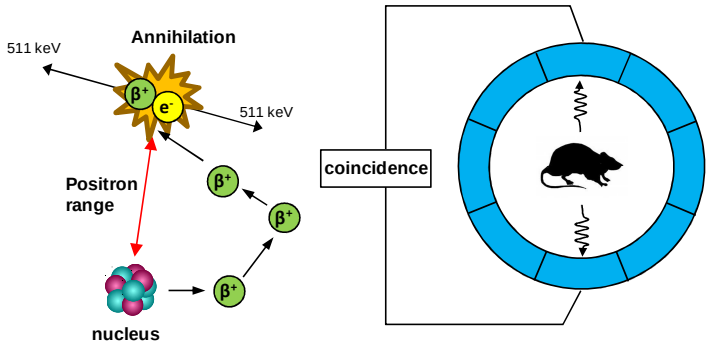

Figure 2.1. Schematic representation of the annihilation process and the detection of photons using PET.

2.2.1.2. PET isotopes and labelling agents

Only a few positron emitters have the adequate physical properties for the preparation of radiotracers. Mainly four radioisotopes have been historically exploited, namely: Carbon-11, Nitrogen-13, Fluorine-18 and Oxygen-15. There are a number of reasons for the wide use of the above mentioned radioisotopes. First, all of them can be produced in biomedical cyclotrons with relatively high yield; second, they can be easily introduced in a biomolecule without altering the properties of the original compound, as the stable isotopes (and this is strictly true in the case of Nitrogen, Oxygen and Carbon) are present in the vast majority of organic molecules. Additionally, their decay mode is close to 100% positron emission (table 2.1).

Very recently, other positron emitters have been incorporated in the toolbox of radiochemists. These are mainly Copper-64, Gallium-68, Zirconium-89 and Iodine-124.

^{68}Ga (t1/2 = 67.7 minutes) was one of the first radionuclides to be used for non-invasive nuclear imaging in scanning applications [1]. It can be obtained from the parent radionuclide ^{68}Germanium (^{68}Ge, $t_{1/2}$ =270.8 days). This radioisotope decays via electronic capture to ^{68}Ga, which subsequently decays to the stable

[1] Brownell GL, et al., *Nucleonics*, **1953**, *11*, 40–45.

isotope ^{68}Zn (Figure 2.2). With 89% positron branching, low photon emission, and a half-life matching the pharmacokinetics of many small biomolecules such as peptides, ^{68}Ga has recently become a very interesting tool for the preparation of a wide range of labelled species. The increased use of ^{68}Ga can be partially attributed to the development of ^{68}Ge-^{68}Ga generators, which allow daily production of ^{68}Ga in ionic form without the need for an on-site cyclotron [2].

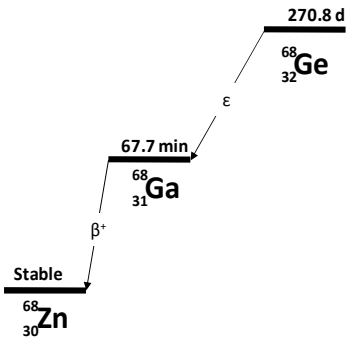

Figure 2.2. Principal decay scheme for ^{68}Ge; ε: electronic capture

The radioactive radionuclide ^{64}Cu exhibits a "triangular" decay scheme (Figure 2.3) [3]: It can undergo electron capture (ε, 43.8%), β^+ emission to ^{64}Ni (17.8%), and β^- emission to ^{64}Zn (38.4%). The positron-branch and its relatively long half-life (12.7 hours) make it a useful candidate for diagnostic imaging, while the beta-minus branch along with the emission of Auger electrons following electron-capture decay make it an attractive candidate also for therapy. Copper-64 can be effectively produced by both reactor-based and accelerator-based methods. Reactor-based methods usually entail the irradiation of materials with thermal or fast neutrons. Thermal neutrons have relatively low energy; in low energy neutron irradiation processes, the target (irradiated) material is of the same element as the product radionuclide; therefore, low-specific activity radionuclides are obtained. For the production of high-specific activity ^{64}Cu, fast neutrons can be used. Unlike a thermal neutron, a highly energetic neutron has sufficient energy to eject a particle from the target nucleus, and the irradiated material can undergo (n,p) reactions. Thus, ^{64}Cu can

[2] Riss PJ, et al., *Bioorg Med Chem Lett,* **2008**, *18*, 5364-5367.
[3] Bé MM, et al., *Appl Radiat Isot*, **2012**, *70(9)*, 1894–1899.

be efficiently produced from ^{64}Zn *via* the ^{64}Zn(n,p)^{64}Cu nuclear reaction [4]. The main drawback of this methodology arises from the fact that fast neutron reactions using reactor neutrons are always accompanied by thermal neutron reactions, which may produce significant quantities of undesirable impurities, such as ^{65}Zn ($T_{1/2}$ = 243.7 d). Alternatively to reactor methods, ^{64}Cu can be also produced using biomedical cyclotrons via the ^{64}Ni(p,n)^{64}Cu nuclear reaction. This methodology was firstly proposed by Szelecsenyi *et al.* [5], and has been continuously improved.

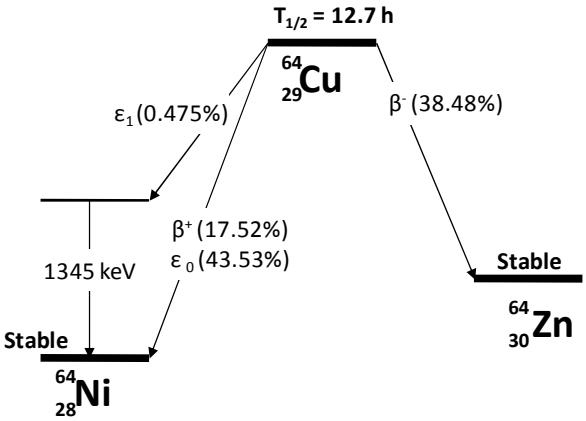

Figure 2.3. Principal decay scheme for ^{64}Cu; ε: electronic capture.

The radioactive radionuclide ^{89}Zr exhibits a decay scheme as shown in Figure 2.4. It has 23% positron branching and emits a low-energy positron ($E_{\beta+,max}$ = 0.897 MeV), which is favourable for high spatial resolution in imaging studies. Its relatively long half-life (78.4 hours) makes it a useful candidate for diagnostic imaging. Unfortunately, ^{89}Zr also emits a high energy gamma ray with a high branching ratio (99.0%). Thus, ^{89}Zr has a high gamma factor, meaning that the dose rate for this isotope is significant [6].

Zirconium-89 can be effectively produced by using the ^{89}Y(p,n)^{89}Zr nuclear reaction. Despite radioactive impurities can be formed during irradiation of natural yttrium, high radionucleidic purity can be achieved using ~15 MeV

[4] Zinn KR, et al., *Cancer,* **1994**, *73(3)*, 774-778.
[5] Szelecsényi F, et al., *Appl Radiat Isot*, **1993**, *44(3)*, 575-580.
[6] Lake Wooten A, et al., *Appl Sci*, **2013**, 3, 593-613.

protons [7]. After irradiation, ^{89}Zr atoms must be chemically extracted to yield a solution of $^{89}Zr^{4+}$ suitable for radiolabelling. The separation of ^{89}Zr from other metals (mainly yttrium) has been performed with different techniques [8].

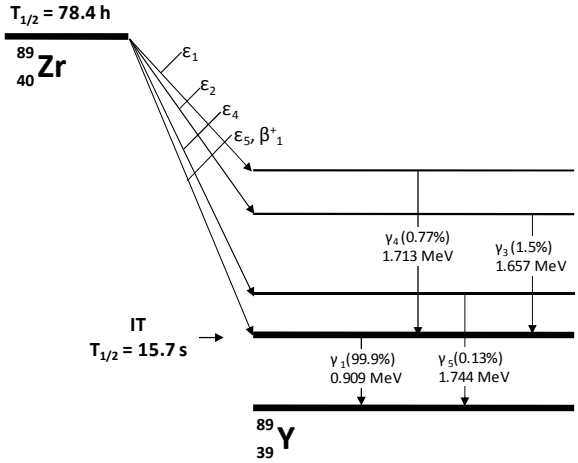

Figure 2.4. ^{89}Zr decay scheme; ε: electronic capture; IT: Internal transition

In the context of this PhD thesis, three PET isotopes have been used: ^{18}F, ^{11}C and ^{124}I. All of them can be produced in biomedical cyclotrons. However, the technology for the production and purification of ^{124}I is not established in our lab, and it was purchased from commercial suppliers. ^{18}F and ^{11}C were produced in our lab using the cyclotron available. A more detailed explanation of the main principles behind the cyclotron operation and the production of ^{18}F and ^{11}C are included in this introductory chapter. The production of ^{124}I is also briefly explained; finally, an introduction to the main labelling strategies using these three isotopes is included.

The cyclotron

A cyclotron (See Figures 2.5 and 2.6 for general schematics) is a particle accelerator in which an electric field is used to accelerate ions, such as H^- or D^-, which are guided with a magnetic field. The electric field is generated by the application of an electric potential between two electrodes (do called "dees" and "counter-dees"), connected to an alternating current source.

[7] National Nuclear Data Center (NNDC). http://www.nndc.bnl.gov (accessed on 4 July 2013).
[8] Fadeeva VI, et al., *Anal Chim Acta*, **1989**, 219, 201-212, and references therein; (b) Holland JP, et al., *Nucl Med Biol*, **2005**, *36*, 729–739

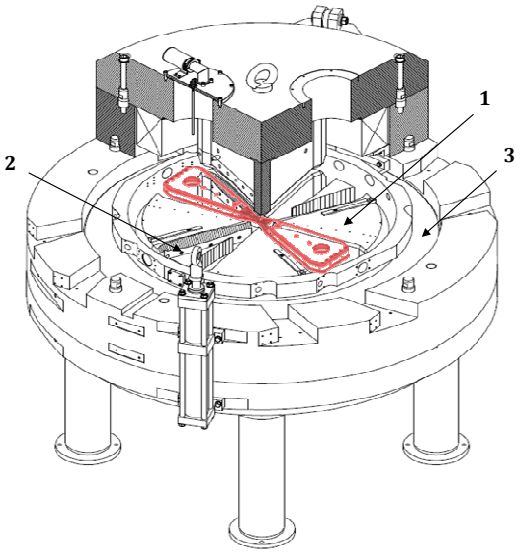

Figure 2.5: General view of the main body of an IBA Cyclone 18/9 cyclotron. Some parts have been removed from the drawing for clarity. The electrical current passing through the coils (3) that surround the four wedge-shaped steel sectors (1) creates the magnetic field. "Dees" (highlighted in red) are placed between the steel sectors and "counter dees" (not shown in the drawing) are placed on the edges of the four steel sectors close to the "dees". For dual particle cyclotrons (acceleration of H^- and D^-), small steel sectors called flaps (2) can be introduced or removed to modulate the magnetic field when particle is changed from H- to D-. The drawing has been adapted from the PhD Thesis of Vanessa Gómez-Vallejo.

Negative ions are generated in the ion source (placed in the centre of the cyclotron) by applying a high voltage to hydrogen or deuterium gas. When the "dee" is positively charged, the "counter-dee" is negatively charged, and vice-versa. When the "dee" is positively charged, the negative ions, which are extracted from the ion source using an electric field, are accelerated towards the "dee" by the electric field. Due to the presence of the magnetic field, the charged particles describe a curved trajectory. When the ion leaves the "dee", the polarity on the "dees"/"counter dees" is reversed, and the ion is accelerated again towards the "counter dee". The same process is repeated, and the orbit radius becomes larger as the speed of the ion is higher. The ion describes a spiralling outward trajectory towards the border of the magnetic field, and when the radius is sufficient, the two electrons of the accelerated particle are removed with a carbon foil (named stripper). The accelerated particle becomes

positively charged, and the direction of rotation is inversed. As a result, the accelerated ion escapes from the cyclotron and impacts in one of the targets, which are situated in the periphery of the cyclotron. In the target, a stable material is irradiated to produce the nuclear reaction and generate the radioisotopes.

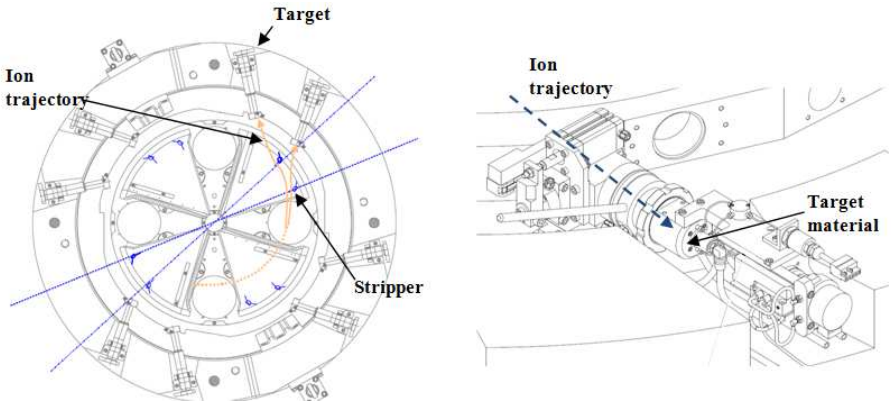

Figure 2.6: Left: Negative ions are accelerated until they hit a stripping foil (stripper), which removes the electrons. The ion charge, now positive, experiences the same force in the same direction but with opposite sense. As a result, the charged particle escapes from the cyclotron and hits the selected target; right: disposition of a target in an IBA Cyclone 18/9 cyclotron. Positive ions deflected by the stripper collision with the target material to produce the radioisotope. The figure has been adapted from the PhD Thesis of Vanessa Gómez-Vallejo.

Fluorine-18

Fluorine-18 can be generated in biomedical cyclotrons in two chemical forms ($[^{18}F]F^-$ and $[^{18}F]F_2$) by using different nuclear reactions (see Table 2.2).

Table 2.2. Nuclear reactions for the production of ^{18}F.

Nuclear reaction	Energy range (MeV)	Natural abundance
$^{18}O(p,n)^{18}F$	4 - 14	0.2
$^{16}O(^3He,p)^{18}F$	1 - 15	99.7
$^{16}O(^4He,np)^{18}F$	20 - 40	99.7
$^{16}O(^4He,2n)\ ^{18}Ne: {}^{18}F$	10-52	99.7
$^{20}Ne(d, \alpha)\ ^{18}F$	0-15	90.5
$^{20}Ne(p,2pn)\ ^{18}F$	30-40	90.5
$^{20}Ne(^3He, \alpha p)\ ^{18}F$	10-40	90.5

Among them, mainly the $^{18}O(p,n)^{18}F$ and $^{20}Ne(d,\alpha)^{18}F$ reactions are currently used. The first reaction is used to produce both $[^{18}F]F^-$ and $[^{18}F]F_2$, while the latter is commonly applied to the production of $[^{18}F]F_2$. In the present PhD, only $[^{18}F]F^-$ has been used, and hence no details will be provided for the production of $[^{18}F]F_2$.

The production of $[^{18}F]F^-$ is usually achieved by irradiation of ^{18}O-enriched water (95-98%) with protons in the energy range 8-18 MeV. The enriched water is introduced in the target body (see Figure 2.7 for scheme of the target), which is made of a chemically inert material. The irradiated material is physically separated from the cyclotron main chamber using metal foils with high mechanical resistance and good thermal conductivity (windows). After finishing the irradiation, the enriched water containing $^{18}F^-$ is transferred to a shielded hot cell and processed.

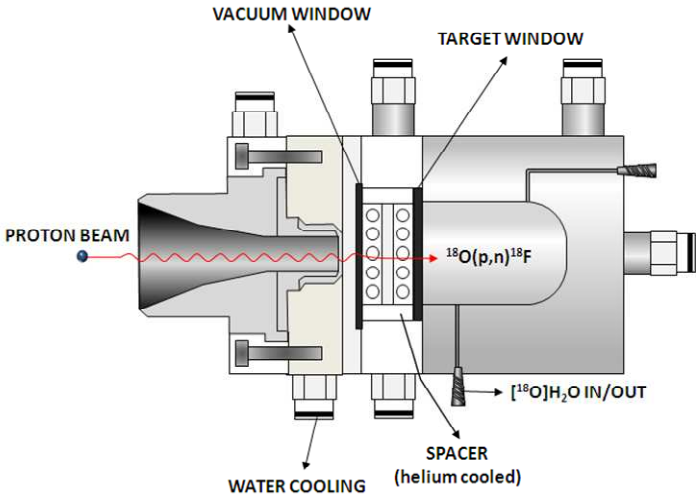

Figure 2.7. Schematic representation of the target used for the production of $[^{18}F]F^-$ via the $^{18}O(p,n)^{18}F$ nuclear reaction; drawing is based on the target commercialized by Ion Beam Applications (IBA).

^{18}F can be directly applied to the radiolabelling of molecules. In this scenario, the labelling process relies in a nucleophilic substitution reaction using a precursor bearing a good leaving group. As the nucleophilic properties of the $^{18}F^-$ anion are compromised in the presence of water, a pre-purification step is required. This step consists of retaining $^{18}F^-$ in an anion exchange column,

elution with a solution of a non-nucleophilic base in water using a cryptand as phase transfer catalyst followed by azeotropic evaporation to yield water-free $^{18}F^-$, which is ready to conduct nucleophilic substitution reactions on substrates bearing a good leaving group.

Direct fluorination of molecules usually requires harsh conditions (high temperature). For the radiolabelling of temperature-sensitive molecules or macromolecules, the preparation of labelled prosthetic groups for further reaction with reactive sites at the molecule to be labelled has also been widely exploited. This reaction of the prosthetic group with the molecule to be labelled usually occurs under mild conditions, and hence this strategy is appropriate for the preparation of labelled proteins, antibodies or peptides. For an extensive review on ^{18}F radiochemistry, please refer to [9].

Carbon-11

^{11}C can be generated using different nuclear reactions (see table 2.3). Among these reactions, $^{14}N(p,\alpha)^{11}C$ is the most convenient and the most commonly used nowadays. This reaction, which relies in the irradiation of N_2 gas, produces carbon-11 with high yields. With the addition of small amounts of oxygen, carbon-11 is obtained as $[^{11}C]CO_2$; alternatively, if hydrogen is added to the irradiated gas instead of oxygen, $[^{11}C]CH_4$ can be produced. $[^{11}C]CO_2$ and $[^{11}C]CH_4$ are the most commonly used primary labelling agents in the preparation of ^{11}C-labelled compounds.

Table 2.3. Nuclear reactions for the production of ^{11}C.

Nuclear reaction	Energy range (MeV)	Natural abundance
$^{11}B(p,n)^{11}C$	5-20	80.1
$^{10}B(d,n)^{11}C$	3-12	19.9
$^{12}C(p,pn)^{11}C$	20-50	98.9
$^{14}N(p,\alpha)^{11}C$	7-15	99.6
$^{14}N(d,n\ \alpha)^{11}C$	10-15	99.6
$^{12}C(^{3}He,\ \alpha)^{11}C$	7-15	98.9

The stopping power of gases is low, and consequently the penetration of the incident protons in the irradiated material is higher in gas targets than in liquid targets. Gas targets are thus larger (irradiated volume of a few tens of mL,

[9] Dollé, F., et al., *Fluorine and Health*, **2008**, Pages 3-65.

versus a few mL in liquid targets) and the gas is pressurized before irradiation (c.a. 20 bar). A typical gas target is schematized in Figure 2.8.

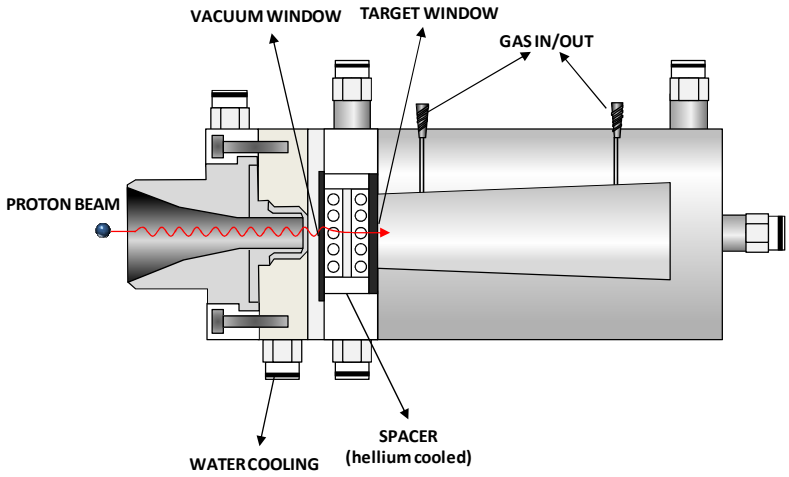

Figure 2.8. Schematic representation of the target used for the production of $[^{11}C]CO_2$ and $[^{11}C]CH_4$ via the $^{14}N(p,\alpha)^{11}C$ nuclear reaction; drawing is based on the target commercialized by Ion Beam Applications (IBA).

One of the simplest labelling strategies for the incorporation of ^{11}C into molecules consists of performing Grignard-type reactions by using $[^{11}C]CO_2$. However, primary labelling agents produced in the cyclotron have very limited applications and consequently, these radioactive species (either $[^{11}C]CO_2$ or $[^{11}C]CH_4$) are chemically transformed into other more convenient labelling agents (Figure 2.9).

The most widely used ^{11}C-labelling agent is $[^{11}C]CH_3I$, which enables execution of methylation reactions. $[^{11}C]CH_3I$ can be prepared by using two different alternative strategies: the "wet" method [10] or by the "gas-phase" reaction [11]. The "wet" method consists of reducing $[^{11}C]CO_2$ in the presence of $LiAlH_4$ (solution in diethyl ether or tetrahydrofuran, THF) to produce $[^{11}C]CH_3OH$, followed by evaporation of the solvent, iodination with hydriodic acid and distillation of $[^{11}C]CH_3I$. The gas phase method consists of performing a gas-solid iodination reaction of $[^{11}C]CH_4$ with I_2 in a quartz tube at high temperature (720°C) to yield $[^{11}C]CH_3I$. The disadvantage of this methodology

[10]Langstrom, B, et al., *Int J Appl Radiat Isot*, **1976**, 27: 357-363.
[11] Larse, P., et al., *Appl Radiat Isot*, **1997**, *48(2)*: 153-157

is the low efficiency in the reaction; as a consequence, the gas must be recirculated several times to obtain acceptable yields.

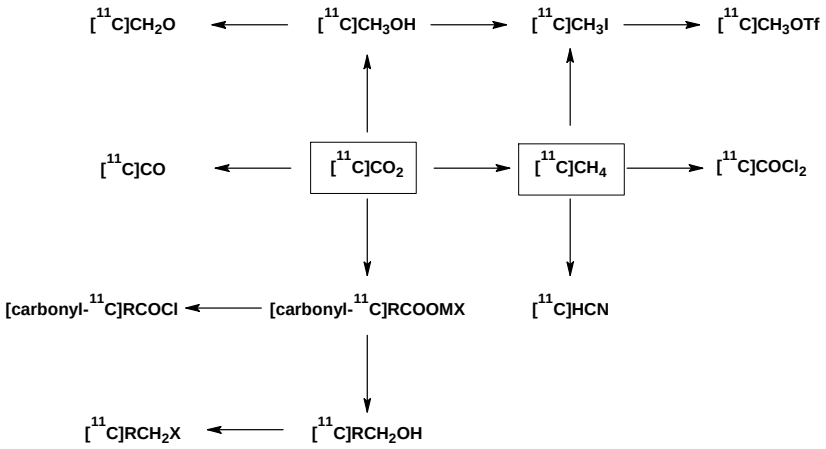

Figure 2.9: Most important ^{11}C precursors used in the synthesis of ^{11}C-labeled compounds produced from either $[^{11}C]CO_2$ or $[^{11}C]CH_4$.

The methylating agent $[^{11}C]CH_3I$ can be further processed to obtain $[^{11}C]$methyl triflate, which is a stronger methylating agent. $[^{11}C]$methyl triflate is prepared by passing gaseous $[^{11}C]$methyl iodide (either prepared by the "wet" or the "gas phase" methods) through a silver triflate column at high temperature [12]. This alkylating agent has been used in this PhD for the preparation of ^{11}C-labelled carboranes (chapter 6). Other alkylating agents have been developed, such as $[^{11}C]$ethyl iodide, $[^{11}C]$propyl iodide, $[^{11}C]$butyl iodide and $[^{11}C]$benzyl iodide [13], although reactions are usually slower due to steric hindrance.

Apart from methylation, other chemical reactions using the different labelling agents depicted in Figure 2.9 have been developed. For example, a large number of reaction strategies for the formation of C-C, C-O and C-N bonds via Palladium-catalyzed reactions have been described in the literature. Among them, carbonylation reactions using $[^{11}C]CO$ have had a significant impact in the literature. The interest in labelling molecules with $[^{11}C]CO$ is due to two main reasons: (i) the wide variety of carbonyl-containing biologically molecules which can be synthesized through carbonylation reactions and (ii) the possibility to obtain $[^{11}C]CO$ through the reduction of $[^{11}C]CO_2$ over zinc or

[12] Jewett, D.M; *Appl Radiat Isot*, **1992**, *43(11)*: 1383-1385
[13] Langstrom, B., et al; *Appl Radiat Isot,* **1986**, *37(11)*: 1141-1145

molybdenum in an on-line process. The most widely used method is the palladium-mediated [^{11}C]carbonylation process [14]. Carboxylic acids [15], esters [16], amides [17] and imides [18]are some of the products which can be synthesized via palladium-mediated carbonylation of olefins, alkynes and organic halides using carbon monoxide at atmospheric pressure.

The limited use of [^{11}C]CO as a radioactive precursor in the insertion of carbon-11 is due to the poor reactivity of carbon monoxide as a result of its low solubility in organic solvents at low CO pressures. Recently, different strategies to improve [^{11}C]CO trapping have been developed with promising results [19].

Iodine-124

^{124}I is a positron emitter with a long half-life (4.17 days) and a complex decay scheme [20] (See Figure 2.10), with many high energy γ-emissions (0.603 MeV, 63.0% abundance) and high energy positron emission ($E_{\beta max}$ = 2.14 MeV, 23% abundance).

^{124}I can be produced using different nuclear reactions. The most widely used strategy in the past consisted of the irradiation of enriched ^{124}Te via the ^{124}Te(d,2n)^{124}I nuclear reaction [21]. More recently, the nuclear reaction ^{124}Te(p,n)^{124}I has been increasingly used [22]. Both methods have been recently compared [23]; proton-induced reaction on enriched ^{124}Te should be the method of choice for cyclotrons with energies <16 MeV, due to lower formation of long-lived by-products.

^{124}I is produced in solid targets, consisting of elemental tellurium or tellurium oxide [24]. After irradiation, recovering of ^{124}I is usually achieved by liberation

[14] Kihlberg, T., et al., International pattent application, PCT/IB2005/001939, **2005**.
[15] Itsenko, O., et al., *Nature Protocols*, **2006**, *1*, 798-802.
[16] Itsenko, O., et al., *Eur. J. Org. Chem.*, **2005**, 17: 3830-3834.
[17] Rahman, O., et al.,*J. Org. Chem.*, **2003**, *68(9)*, 3558–3562.
[18] Karimi, F., et al., *J. Chem. Soc., Perkin Trans.* **2001**, *1*, 1528–1531.
[19] (a) Kealey, S., et al., *J. Label. Compd. Radiopharm.*, **2009**, *52*, (S1): S5; (b) J. Eriksson, et al., J. Label. Compds. Radiopharm. 2012, 55, 223.
[20] Preylowski V et al., *PLoS ONE 8(8)*, e71729.
[21] Clem RG, er al., *Nucl Instrum Methods: Phys Res Sect A—Accel Spectrom Detectors Assoc Equip*, **1991**, *303*, 115–118.
[22] Scholten B, et al., *Appl Radiat Isot*, **1995**, *46*, 255–259.
[23] Aslam MN, et al., *Appl Radiat Isot*, **2010**, 68, 1760–1773.
[24] (a) Stevenson NR, et al., *Proceedings of the sixth workshop on Targetry and Target Chemistry*, **1995**, *TRIUMF, Vancouver,* 82–83; (b) Qaim SM, *Nucl Instrum Methods Phys Res A*, **1989**, *282*, 289–295.

of iodine by heat, achieved by submitting the target material to heating (750°C) in a quartz tube under a gas flow [25]. Alternatively, the irradiated target is dissolved in an oxidizing alkaline medium, followed by reduction of tellurium and iodine. The iodine is finally purified by cation exchange chromatography and enriched tellurium can be recovered for further use.

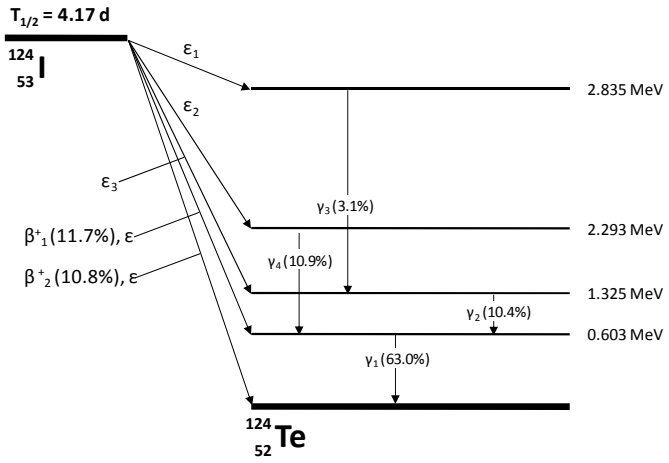

Figure 2.10: Simplified decay scheme of ^{124}I. ε: Electron capture. Adapted from Preylowski V et al., *PLoS ONE 8(8)*, e71729.

In the context of the current PhD, as mentioned above, ^{124}I was purchased from commercial suppliers and received as a solution in aqueous NaOH.

Radioiodine, usually received from commercial suppliers (or produced on site) as basic solution of NaI in NaOH, can be directly incorporated into molecules by *in situ* oxidation of the anionic species (I^-) using an oxidizing agent in solution, such as chloramine-T [26], and subsequent electrophilic substitution on an activated aromatic ring (typically, an aromatic ring containing electron-donors in the *ortho*- or *para*- positions). Because this strategy has been widely applied to the radiolabelling of proteins and peptides, and in order to achieve milder oxidizing conditions to prevent protein/peptide decomposition, other oxidizing agents have been developed. One example is 1,3,4,6-tetrachloro-3α,6α-diphenyl glycoluril or Iodogen [27], a commercially available water-insoluble oxidizing

[25] Weinreich R, et al., *J Radioanal Nucl Chem—Lett*, **1996**, *213*, 253-261
[26] Hunter WM, et al., *Nature* **1962**, *194*, 495-496.
[27] Fraker PJ, et al., *Biochem Bioph Res Co* 1978, *80*, 849-857.

agent which can be dissolved in an organic solvent and coated on the walls of the glass reaction tube. When Iodogen is used, the reaction can be terminated at any time by removal of the crude from the reaction tube.

Alternatively to direct incorporation of radioiodine, indirect methods can be also applied. These consists of covalent attachment of a pre-labelled group to a reactive group present in the molecule to be labeled; the most widely used conjugation reagent is radioiodinated *N*-succinimidyl 3-(4-hydroxyphenyl)propionate (Bolton–Hunter reagent) [28]. If the molecule under investigation already contains one or more iodine atoms, isotopic exchange under catalytic conditions can be conducted [29]. In this PhD, direct incorporation using electrophylic substitution and isotopic exchange have been used. Experimental details will be provided in the corresponding chapters.

2.2.2. Single Photon Emission Computerised Tomography

2.2.2.1. General aspects

Similar to PET, single photon emission computerised tomography (SPECT), is an ultra-sensitive imaging technique, which enables the determination of the spatiotemporal distribution of a radiotracer labelled with a gamma emitter after administration into a living organism. Typical gamma emitters used in the biomedical arena include Technetium-99 metastable, Iodine-123, Indium-111, Galium-67 and Iodine-131 (see Table 2.4 for physical properties).

Table 2.4. Typical Single photon emitters (with half-life and energy).

Isotope	Half-life	γ Energy (γ Fraction)
^{99m}Tc	6.02 h	141 KeV (89%)
^{123}I	13.22 d	159 KeV (83%)
^{111}In	2.80 d	171 (91%), 245 KeV (94%)
^{67}Ga	3.26 d	93 (39%), 185 (21%), 300 (17%), 394 (5%)
^{131}I	8.02 d	364 KeV (82%)

Gamma emitters emit directly gamma rays. The gamma rays resulting from spontaneous radioactive decay are directly detected with a ring of detectors placed around the organism under investigation. Because the photons are

[28] Bolton AE, et al., *Biochemical J* **1979**, *111*, 529-539.
[29] Breslav M, et al. *Anal Biochem* **1996**, *239*, 213–217.

detected individually and not in pairs, physical collimators are required. These are usually placed in front of the detectors (Figure 2.11).

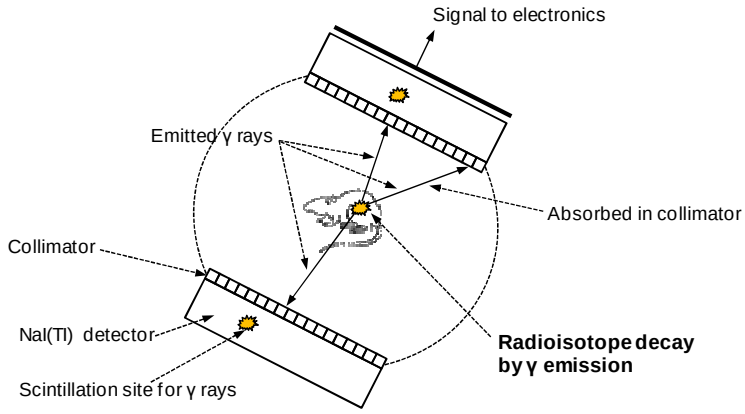

Figure 2.11. Schematic representation of the detection of photons using SPECT.

2.2.2.2. SPECT isotopes and labelling agents

There is a large collection of gamma emitters that can be used. However, only a few of them are routinely used in the clinical setting.

Technetium-99 metastable (^{99m}Tc) is the "workhorse" for radiopharmaceutical imaging, because nearly 80% of nuclear medicine imaging procedures are currently performed with ^{99m}Tc-labelled compounds. It has an emission γ-energy of 141 keV, a suitable half-life of 6.02 h, and well-known coordination chemistry. Additionally, it can easily be obtained as $^{99m}TcO_4^-$ in aqueous buffer from ^{99}Mo/^{99m}Tc generators, which are commercially available.

^{99m}Tc is produced from the decay of ^{99}Mo (see Figure 2.12 for decay scheme) using ^{99}Mo/^{99m}Tc generators. Such generators consist of a mother–daughter pair (^{99}Mo-^{99m}Tc). The component with the longer half-life (^{99}Mo: $t_{1/2}$ = 67 hours) is reliably held as $^{99}MoO_4^{2-}$ on a small bed of acidic alumina or similar. The ^{99}Mo decay process leads to the formation of ^{99m}Tc ($^{99m}TcO_4^-$), which can be eluted on a periodic basis in a pure form and in high radioactive concentration. A schematic representation of a standard ^{99}Mo/^{99m}Tc generator is shown in Figure 2.13.

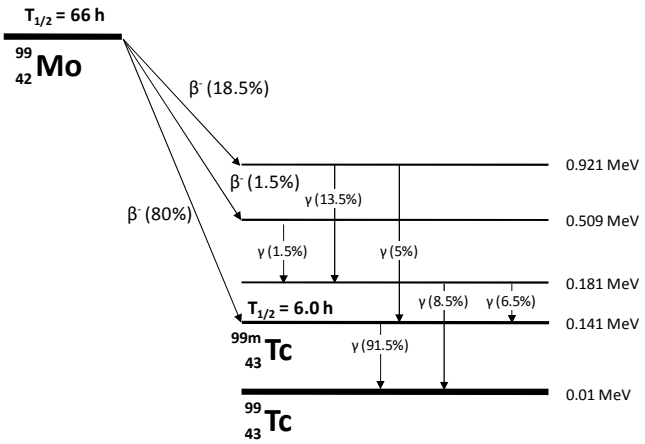

Figure 2.12. Principal decay scheme for ^{99}Mo and ^{99m}Tc.

^{99}Mo is usually produced by irradiation of highly enriched uranium (HEU) with neutrons. This nuclear reaction yields a small fraction of ^{99}Mo, which is purified and shipped to manufacturers for the fabrication of ^{99}Mo/^{99m}Tc generators. The reactors producing ^{99}Mo have been in operation for a considerable time and need decommissioning or refurbishment [30].

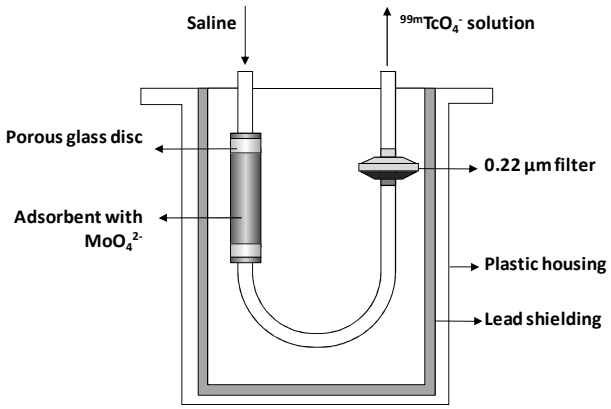

Figure 2.13. General scheme of a ^{99}Mo/^{99m}Tc generator. ^{99}Mo is reliably hold as $^{99}MoO_4^{2-}$ on a small bed of acidic alumina or similar. ^{99}Mo decay process leads to the formation of ^{99m}Tc. The decay product ($^{99m}TcO_4^-$) can be eluted on a periodic basis in a pure form and in high radioactive concentration.

[30] Tárkányi F, et al., *Appl Radiat Isotopes*, **2011**, *69*, 18–25.

In addition, a transition from using HEU to low enriched uranium (LEU) is being implemented to minimize potential proliferation issues [31]. This may create a shortage of ^{99}Mo worldwide; as a consequence, reactor- and accelerator-based alternative strategies are currently being explored. These alternative methods have been recently reviewed and discussed [32]. In the medium term and as a complement or alternative to irradiation of HEU targets, direct production of ^{99m}Tc *via* the ^{100}Mo(p,2n)^{99m}Tc nuclear reaction in cyclotrons may be the most feasible option.

^{67}Ga is a gamma emitter with a long half-life (3.26 days), it decays to stable Zn by electron capture and has no β emission. ^{67}Ga can be produced in particle accelerators using different nuclear reactions, including ^{67}Zn(p,n)^{67}Ga, ^{68}Zn(p,2n)^{67}Ga [33], ^{66}Zn(d,n)^{67}Ga and ^{67}Zn(d,2n)^{67}Ga [34].^{67}Ga is usually separated from the irradiated material by ion exchange chromatography [35] or by liquid extraction [36]. Due to its long half life, the radioisotope is usually supplied to end users at reasonable cost in citrate solution, which is widely used in the clinical setting.

In the context of this PhD thesis, two gamma emitters have been used: ^{125}I and ^{131}I. ^{125}I has a low gamma energy emission and hence it is not very appropriate for *in* vivo imaging in large animals or humans. However, it is a very convenient radioisotope to set up synthetic conditions or to conduct *ex* vivo experiments. Hence, we include here an explanation of the production process for ^{125}I and ^{131}I. A brief introduction to ^{123}I, a more convenient radioisotope for SPECT imaging, is also provided.

^{125}I has a half-life of nearly 59 days and decays by electron capture to an excited state of ^{125}Te, which decays immediately by gamma rays emission with a maximum energy of 35.5 keV. Due to its long half-life and low gamma energy, this radioisotope is especially relevant for *in vitro* and *ex vivo* applications, while *in vivo* imaging (especially in large species or eventually humans) might be challenging.

[31]Bonet H, et al., 9th International Topical Meeting on Research Reactor Fuel Management (RRFM), **2005,** Hungary. Available at: http://www.euronuclaer. org/pdf/RRFM2005.Session1.pdf.
[32] Pillai MRA, et al., *J Nucl Med*, **2013**, *54(2)*, 313-323.
[33] Lee Y-K, et al., *J Nucl Med*, **2012**, 53, 1462–1470.
[34] Steyn J, et al., *Int J appl Radiat Isotopes*, **1973**, *24*, 369-372.
[35] Helus F, et al., *J Labelled Compd Rad*, **1973**, 317, IAEA/SM/171/21. IAEA, Vienna.
[36] Huff, H. B., et al., *Int J appl Radiat Isotopes*, **1970**, *21(2)*, 75-76.

Iodine-125 is usually produced in a reactor, and is generated by the $^{124}Xe(n,\gamma)^{125m}Xe$ and $^{124}Xe(n,\gamma)^{125g}Xe$ nuclear reactions. ^{125m}Xe and ^{125g}Xe are unstable and decay to ^{125}I with 57s and 16.9h half-lives, respectively. The amount of ^{124}Xe in natural xenon gas is very low (~0.1%); consequently, and in order to improve the efficiency of the nuclear reactions, the gas is pressurized to undergo neutron irradiation. After neutron beam, the gas is allowed to decay to eliminate short-lived radioisotopes and to allow ^{125g}Xe to decay into ^{125}I. The capsule containing the irradiated gas is cooled and free iodine is collected on the capsule sides; the gas is then released and finally the capsule is rinsed with aqueous NaOH solution to collect iodine as soluble iodide and hypoiodite. Purification using ion-exchange resins eliminates long-lived Caesium isotopes which are produced during the irradiation.

^{131}I has a half-life of 8.02 days, and decays 100% by electron emission, resulting also in the emission of gamma rays with a maximum at 364.5 keV (81.7%). Its β^- emission nature turns ^{131}I into a good alternative also for therapeutic use. ^{131}I can be produced using two different nuclear reactions. The first one comprises the neutron-irradiation of natural tellurium, yielding the nuclear reaction $^{130}Te(n,\gamma)^{131}Te$. ^{131}Te decays to ^{131}I with a half-life of 25 minutes. Usually, powder elemental tellurium is irradiated and then ^{131}I is separated by dry distillation. The element is finally dissolved in an alkaline solution, to produce ^{131}I as iodide and hypoiodite. The second method involves the irradiation of Uranium and chemical recovery from the fission products.

^{123}I has a relatively long half-life (13.22 hours), and decays by electron capture to ^{123}Te resulting in the emission of gamma rays with a major peak at 159 keV. It can be produced using different nuclear reactions, being $^{124}Te(p, 2n)^{123}I$ the most commonly used. High enrichment of tellurium is required: in addition to the (p,n) reaction on ^{124}Te to yield ^{124}I (see above), this impurity can also be formed via the $^{125}Te(p, 2n)^{124}I$ nuclear reaction [37].

Solid, liquid (or molten) and gaseous targets can be used for the production of ^{123}I, and indeed the three types of targets are currently used, depending on the energy of the cyclotron and the availability of enriched ^{124}Xe. The most commonly used are solid and gas targets. For solid targets, elemental tellurium or tellurium oxide is irradiated [30,38]. After irradiation, the ^{123}I is isolated by heating the irradiated material and distilling ^{123}I to a receiver vessel containing

[37] Kondo K, et al., *Int J Appl Radiat Isot*, **1977**, *28*, 395–401.
[38] Qaim SM, *Nucl Instrum Methods Phys Res A*, **1989**, *282*, 289–295.

a base solution. Alternatively, the irradiated target can be dissolved in an oxidizing alkaline solution, followed by reduction of the enriched tellurium to the elemental state and iodine to I^-. Precipitated tellurium metal is removed through filtration, and iodide is purified using a cation exchange resin.

The labelling strategies to incorporate ^{131}I, ^{123}I and ^{125}I into molecules are parallel to those mentioned above for ^{124}I. Of note, differences in specific activity might become significant depending on the production process, and hence optimization of experimental conditions or process-adaptation may be required when transitioning from one radioisotope to the next.

2.2.3. Image acquisition, reconstruction and analysis

Labelled molecules are subsequently used for *in vivo* imaging experiments. With that purpose, a small amount of the labelled species (usually activities below 37 MBq and mass amount below a few μg) is injected into the animal under investigation. Because a fast distribution of the tracer over the whole organism is preferred to prevent the formation of "hot spots" or areas with a high accumulation of radioactivity (which may complicate image reconstruction and analysis), administration takes place usually intravenously.

Concomitantly with the administration of the radiotracer, image acquisition starts. Of note, some tracers require incorporation time, and hence images are acquired after a certain time gap (e.g. 30 minutes). Either static or dynamic images can be acquired. Static images average the biodistribution of the radiotracer over time, while in dynamic acquisition, different (short) static images are acquired sequentially, and the distribution of the radiotracer for each time frame can be obtained.

The ultimate goal of nuclear imaging techniques is to obtain volumetric images providing information about the distribution of the radiotracer; this process requires two steps: (i) detection of emitted gamma-rays, which are emitted during radioactive decay or after annihilation of a positron with an electron, and (ii) determination of the direction in which the ray arrives to the detector, in order to get information of the precise position where the decay process occurs. Detection of the gamma rays is achieved using detectors, which contain scintillation crystals. When excited by a gamma ray, the crystals absorb its energy and re-emit a flash of light, typically in the ultra-violet range. This flash is detected by a photo-electronic system which records its location in the crystal and its intensity, which is proportional to the energy of the incidental

gamma-ray. Detection of the direction of the incoming ray differs between PET and SPECT. In PET, two photons (emitted 180° from each other) are generated simultaneously for each decay process. Hence, two detectors detecting simultaneously 2 gamma rays define a line of response (LOR), and the system assumes that within this line a decay process occurred. In SPECT, because only one photon is emitted, physical collimation is required. The collimators are usually made of a lead plate with holes. The role of the collimator is to stop all gamma rays which do not arrive perpendicular to the detector. In such a way, the collimator forms a projected image of the radioisotope distribution on the surface of the scintillation crystal.

Both SPECT and PET systems acquire a set of projections at different angular positions around the subject under investigation. Reconstruction tomography makes use of computers and mathematical algorithms to estimate the unknown distribution of radiotracer in the body from the detected projection data.

In a typical study, hundreds of thousands of photons are detected, and images are then derived by applying image reconstruction. To provide an exhaustive description of the different methods available is far beyond the scope of this PhD thesis. However, it is worth mention that reconstruction algorithms can be roughly divided into analytical and statistical methods. Analytical methods, such as Filtered-Back-Projection (FBP), solve the three-dimensional distribution of radiotracer from the projection data assuming ideal geometry and a rather simplistic physical model. Iterative statistical reconstruction methods such as OSEM (Ordered Subset Expectation Maximization) provide images with improved spatial resolution and better signal-to-noise ratios; however, increased computational time is required and unpredicted effects can appear in the final outcome.

After image reconstruction, quantification of the images will allow the determination of the concentration of radioactivity in a pre-defined volume of interest (VOI). Usually, units are nCi/cc or MBq/ml. Because cameras can only detect a small fraction of the gamma rays produced during spontaneous decay, it is necessary to calibrate these devices by scanning an object with a known activity concentration, record the number of detections, and derive a multiplicative calibration factor.

Because PET and SPECT images do not provide anatomical information, delineation of the VOIs directly on the PET or SPECT images to obtain quantitative data is very challenging. Because of this, and sequentially to PET or

SPECT images acquisition, anatomical images using e.g. computerized tomography (CT) or less often Magnetic Resonance Imaging (MRI) are acquired. Nuclear images and anatomical images can be then co-registrated, VOIs can be delineated on the anatomical images and translated to the nuclear images for quantification. This procedure has been applied for absolute quantification in the current PhD thesis.

2.3. Ex vivo studies: dissection and gamma counting

The determination of the biodistribution pattern of a molecule can be carried out, as described above, by using nuclear imaging techniques in combination with other anatomical techniques for localization of the radioactivity in the different organs/tissues. However, nuclear imaging techniques have a certain number of limitations that have to be taken into account.

The first limitation of nuclear imaging techniques is related to spatial resolution, which is usually in the range of the millimetre in the pre-clinical setting, and might be even lower in the case of SPECT. Hence, delineation of regions of interest in small volumes might lead to significant error due to partial volume effect and spill over. When the object or structure analyzed is smaller than 2-3 times the spatial resolution of the scanner (as measured by its Full Width at Half Maximum, FWHM), the values for the each pixel become diluted with signals from surrounding structures. If the region under analysis is surrounded by regions with less activity concentration, the result is an under estimation of the amount of activity in that region. This effect is known as Partial Volume Effect (PVE). If the region under analysis is surrounded by a region with a higher activity concentration, the values in the region under analysis will be over-estimated. This effect is called spill-over. Both effects can be corrected or mitigated to a certain extent by using appropriate reconstruction algorithms and factors, as previously reported in the literature [39,40].

The second limitation of nuclear imaging is closely related to the limited spatial resolution. Of course, with a 1 mm resolution the small blood vessels and the capillaries that irrigate the different organs or tissues cannot be discriminated. As a consequence, the amount of activity obtained in a volume of interest is always the sum of the activity in the organ/tissue plus the activity present in

[39] Srinivas SM, et al., *Ann Nucl Med*, **2009**, *23(4)*, 341-348.
[40] Fang YH, et al., *J Nucl Med* **2008**, *49*, 606-614.

blood. This contribution can be relevant if the accumulation of a tracer in an organ is low.

The third limitation relates to body motion. The duration of a PET scan to determine the spatiotemporal distribution of a tracer can be very long (up to a few hours in a single scan), depending on the half-life of the isotope and the pharmacokinetic properties of the molecule under investigation. During this period, and despite the animal is anesthetized, movement in the abdominal region may occur. Because only one CT scan for corregistration is usually acquired at the end of the PET scan, motion over the duration of the PET acquisition may introduce artefact.

Finally, delineation of VOIs in certain organs might be very challenging. One clear example is the intestine, due to its complex anatomical distribution. Also, organs which are not clearly visualized in the CT scan may be difficult to delineate correctly. In these cases, corregistration of PET images with MRI may solve the problem, but PET-MRI cameras are not fully standardized and they are not available in most of the research institutions.

Due to all the above mentioned limitations, the accurate determination of the biodistribution pattern of a radiotracer may require more invasive approaches. One of them is dissection and gamma counting. The general strategy behind this approach consist of: (i) administer to the animals a certain amount of radioactive compound; (ii) sacrifice the animals at pre-determined time points (potentially using perfusion with saline solution to remove the blood), (iii) harvest the organs and (iv) count the amount of activity for each organ in a gamma counter. By weighting the different organs, values of % of injected dose per gram of tissue can be obtained with high accuracy. Importantly, even very small organs can be quantified, and also organs with a complex anatomy within the organism or difficult to visualize on the CT images. This strategy has, however, one main drawback: the number of animals required is much higher, because different animals need to be sacrificed at each time point. For example, for the determination of the biodistribution pattern of a tracer at 3 different time points after administration, 9 animals would be required (assuming n=3 per time point) while only 3 animals would be required to get the information using PET (see Figure 2.14).

In the current PhD thesis, both approaches have been used. Occasionally, the results obtained using both methodologies have been compared and the differences (if existing) have been discussed.

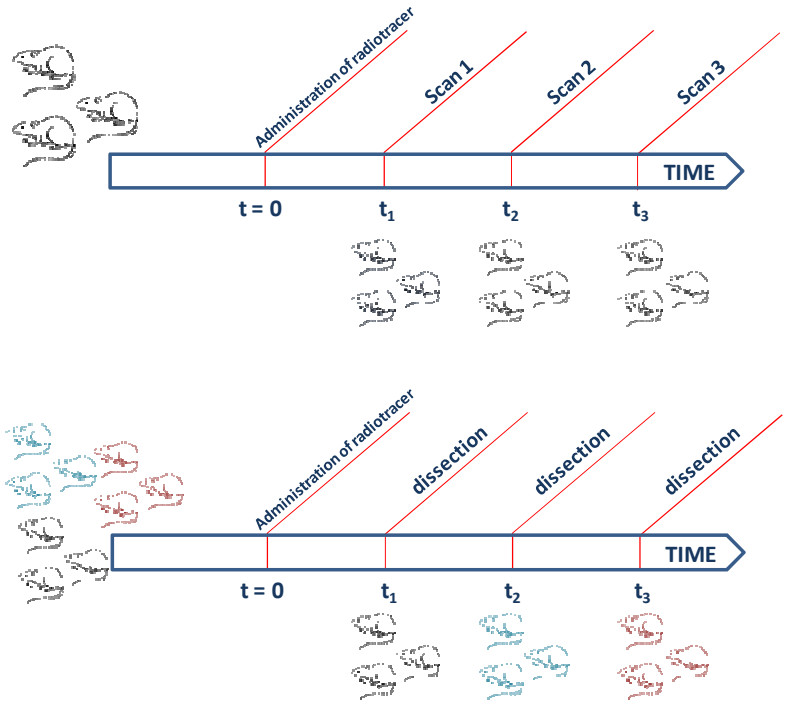

Figure 2.14. Experimental design to determine the biodistribution pattern of a radiotracer using nuclear imaging (top) and dissection/gamma counting (bottom). As it can be seen, the number of experimental animals is significantly higher in dissection/gamma counting.

3. BACKGROUND AND OBJECTIVES

3.1. Background

The current PhD thesis has been conducted in the Radiochemistry and Nuclear Imaging Group, led by Dr. Jordi Llop. The work has been developed in the context of the project entitled "Synthesis of PET radiotracers with application in BNCT", funded by the Ministry of Science and Innovation (*Ministerio de Ciencia e Innovación, project CTQ2009-08810*).

The main aim of this project was the development of strategies for the incorporation of radioactive isotopes (mainly positron and gamma emitters) in boron rich structures (carborane clusters), to enable the subsequent preparation of a library of potential BNCT drug candidates and their evaluation using nuclear imaging techniques such as PET and SPECT in combination with anatomical techniques such as CT. With that aim, the most widely used carborane clusters, namely dicarba-*closo*-dodecaboranes and cobalt-bis-dicarbiollide (COSAN), were selected.

3.2. Scope and achievements

For the preparation of labelled carboranes, two different strategies were investigated. The first strategy was based in the mono-[^{18}F]fluorination of carborane clusters *via* nucleophilic substitution, using cyclotron produced [^{18}F]F^{-} and carboranyl iodonium salts as non radioactive precursors. Further derivatization of the ^{18}F-labelled carboranes could be achieved by formation of the C_c-lithio salt and reaction with aldehydes. The second strategy was based in the preparation of labelled decaborane, to enable the subsequent formation of the labelled carborane analogues using the well known reaction of decaborane with acetylenes in the presence of a Lewis base. In this case, different radioisotopes of iodine (Iodine-125 and Iodine-131) were used for the radiolabelling. As a result of these works, two papers have been published in international *peer*-reviewed journals:

9- Gona KB, Gómez-Vallejo V, Padro D, Llop J; [^{18}F]Fluorination of *o*-carborane via nucleophilic substitution: towards a versatile platform for the preparation of ^{18}F-labelled BNCT drug candidates. *Chemical Communications*, **2013**. 49(98): 11491-11493.

10- Gona KB, Lakshmi VPN Thota J, Baz Z, Gómez-Vallejo V, Llop J, Straightforward synthesis of radioiodinated Cc-substituted o-carboranes: towards a versatile

platform to enable in vivo assessment of BNCT drug candidates. *Dalton Transactions*. **2015**. 44: 9915-9920.

One more paper is currently under preparation. The work concerning the radiolabelling of carboranes is included in Chapter 4 of this PhD thesis.

For the preparation of labelled COSAN analogues, palladium catalyzed isotopic exchange reactions were assayed, using ^{125}I (gamma emitter) and ^{124}I (positron emitter). Incorporation of ^{125}I and ^{124}I enabled the determination of the biodistribution pattern by using dissection/gamma counting and PET-CT, respectively. This work was conducted in collaboration with the group led by Prof. Francesc Teixidor and Prof. Clara Viñas, at Institut de Ciència de Materials de Barcelona (ICMAB-CSIC), and resulted in the publication of one scientific paper:

11- Gona KB, Zaulet A, Gómez-Vallejo V, Teixidor F, Llop J, Viñas C; COSAN as a molecular imaging platform: synthesis and "in vivo" imaging. *Chemical Communications*. **2014**. 50: 11415-11417.

One more paper is currently under preparation. The work concerning the radiolabelling of COSAN analogues is included in Chapter 5 of this PhD thesis.

Finally, part of the work conducted in the context of the current PhD thesis was oriented towards the development of strategies for the preparation of ^{11}C-labelled carborane analogues.

In chapter 6, the preparation of two analogues of 2-(4-aminophenyl) benzothiazole in which the phenyl ring has been substituted by a *m*-carborane cage is described, followed by the preparation of the *N*-[^{11}C]methylated derivatives. This work resulted in the publication of a scientific paper:

12- Gona KB, Lakshmi VPN Thota J, Baz Z, Gómez-Vallejo V, Llop J, Synthesis and ^{11}C-radiolabelling of 2-carboranyl benzothiazoles. *Molecules*. **2015**. 20: 7495-7508.

Finally, a method for the palladium catalyzed carbonylation of 1-iodo-1,7-dicarba-*closo*-dodecaborane, for the one-pot one-step formation of amides is presented in chapter 7. This work resulted in one scientific paper:

13- Gona KB, Gómez-Vallejo V, Llop J; Synthesis of m-carboranyl amides via palladium-catalyzed carbonylation. *Tetrahedron Letters*, **2013**. 54(8): 941-944.

Interestingly, the reaction reported in this work might be used for the preparation of ^{11}C-labelled carborane analogues, using the radioactive precursor [^{11}C]CO. Moving towards this application, a system for the generation of [^{11}C]CO from cyclotron-produced [^{11}C]CO_2 has been designed and implemented.

Besides the work described above, during the execution of the PhD thesis I was offered the opportunity to participate in scientific projects that, far from being directly related to the work included in the thesis, contributed to my education and provided a wider perspective of the possibilities of radiochemistry and nuclear imaging. As a result of these collaborations, I have been included as co-author in the following publications:

14- Soria FN, Pérez-Samartín A, Martin A, Gona KG, Llop J, Szczupak B, Chara JC, Matute C, Domercq M; Extrasynaptic glutamate release through cystine/glutamate antiporter contributes to ischemic damage. *The Journal of Clinical Investigation*. **2014**. 124: 3645-3655.

15- Gómez-Vallejo V, Vázquez N, Gona KB, Puigivila M, González M, San Sebastián E, Martin A, Llop J, Synthesis and *in vivo* evaluation of ^{11}C-labeled (1,7-dicarba-closo-dodecaboran-1-yl)-*N*-{[(2S)-1-ethylpirrolidin-2-yl]methyl}amide. *Journal of labeled compounds and radiopharmaceuticals*. **2014**. 57: 209-214. DOI: 10.1002/jlcr.3159

16- Gómez-Vallejo V, Gaja V, Gona KB, Llop J; Nitrogen-13: Historical review and future perspectives; *Journal of labeled compounds and radiopharmaceuticals*. **2014**. 57: 244-254.

3.3. Objectives

In the context of the above mentioned work, the specific objectives of the current PhD thesis were initially defined as follows:

1- To develop strategies for the preparation of ^{18}F-, ^{125}I- and ^{131}I-labelled *o*- and *m*-carborane analogues.
2- To develop strategies for the preparation of ^{124}I- and ^{125}I-labelled COSAN analogues, and evaluate the biodistribution properties of the most promising candidates in healthy animals and in animal models.
3- To implement a synthetic route for the preparation of 2-carboranyl benzothiazoles and subsequent radiolabelling using Carbon-11.

4- To develop a methodology for the preparation of carboranyl amides using palladium catalyzed carbonylation reactions.
5- Implement a system for the routine production of [^{11}C]CO from cyclotron-produced [^{11}C]CO_2.

4. SYNTHESIS OF ^{18}F-, ^{125}I- and ^{131}I-RADIOLABELLED CARBORANE ANALOGUES

4.1. Introduction

4.1.1. Dicarba-*closo*-dodecaboranes

4.1.1.1. General aspects

Dicarba-*closo*-dodecaboranes, commoly known as carboranes, are clusters composed of Boron, Carbon and Hydrogen atoms with the general formula $C_2B_nH_{n+2}$. Their rich derivative chemistry make carborane clusters, and particularly dicarba-*closo*-dodecaboranes, suitable building blocks with application for the preparation of macro-molecular and supramolecular entities [1], nonlinear optics [2] and medicinal chemistry, particularly in the context of BNCT (see references in chapter 1) and as hydrophobic pharmacophores of bioactive molecules [3].

Carboranes exist as *ortho*-, *meta*- and *para*- isomers (*o*-, *m*-, and *p*-carborane, respectively), which differ in the relative positions of the carbon atoms in the cluster (Figure 4.1). Whereas the *ortho*- and *meta*- isomers are widely available from a number of commercial sources at a modest expense, *para*-carborane can be nowadays hardly found.

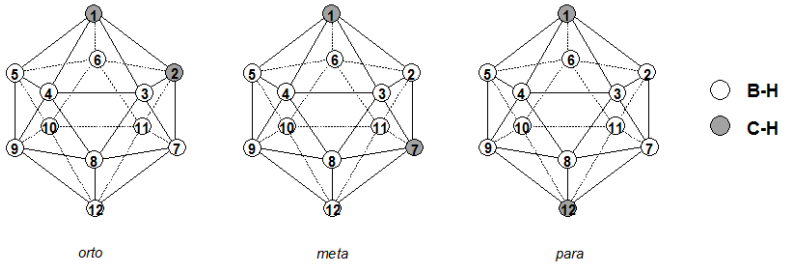

Figure 4.1. From left to right, chemical structure of *o*-, *m*- and *p*-carborane.

O-carborane can undergo a degradation process by removal of one of the boron atoms directly attached to the two cluster carbon atoms yielding the

[1] (a) Grimes, R. N. *Angew. Chem., Int. Ed. Engl.* **1993**, *32*, 1289; (b) Wedge, T. J. *et al.*, *Coord. Chem. Rev.* **2003**, *240*, 111. (c) Fox, M. A., *et al.*, *Coord. Chem. Rev.* **2004**, *248*, 457. (d) Puga, A. V., *et al. Chem. Eur. J.* **2009**, *15*, 9755; (e) Puga, A. V. *et al., Chem. Eur. J.* **2009**, *15*, 97641.
[2] (a) Murphy, D. M. *et al., J. Mater. Chem.* **1993**, *3*, 67; (b) Murphy, D. M., *et al., J. Mater. Chem.* **1993**, *3*, 139. (c) Pahomov, S., *et al., Inorg. Chem.* **2000**, 39, 2243. (d) Kaszynski, P. *et al., Collect. Czech. Chem. Commun.* **2002**, *67*, 1061.
[3] (a) Endo, Y., et al., *J. Med. Chem.* **1999**, *42*, 1501-1504; (b) Ogawa, T., et al., *Bioorg. Med. Chem. Lett.* **2006**, *16*, 3943-3946; (c) Vázquez, N., et al., *Tetrahedron. Lett.* **2011**, *52*, 615-618M; (d) Vázquez, N., et al., *Tetrahedron Lett.* **2012**, *53*, 4743-4746.

corresponding dicarbaundecaborate(1-) ion $(H_2C_2B_9H_{10})^-$ [4] or *nido*-carborane. The hydrogen atom, which was bond to the withdrawn boron atom, remains forming a bridge between two of the B-H units. This degradation occurs in the presence of strong bases such as sodium hydroxide. The formation of the *nido* derivatives is strongly dependent on the chemical properties of the substituents on the carborane cage and the relative position of the carbon atoms in the cluster. Basic or electron-withdrawing substituents (such as esters or aldehydes) on one of the CH vertices favour the degradation of the cluster [5], and the degradation is more favoured in *o*-carborane than in *m*-carborane.

4.1.1.2. Characterization of carboranes

Carboranes can be characterized by using different traditional techniques such as x-ray crystallography, nuclear magnetic resonance, infrared spectroscopy, etc [6]. In the particular case of IR, typical frequencies providing useful information during characterization of carboranes include B-H stretching (around 2600 cm^{-1} and 2520 cm^{-1} for *closo*- and *nido*-carboranes, respectively), and C-H stretching (appearing at 3079, 3070 and 3065 cm^{-1} for *ortho*-, *meta*- and *para*- carboranes, respectively). Regarding NMR, in the proton spectra carboranes show a broad signal between 3.00 and -0.75 ppm, corresponding to the protons directly attached to the boron atoms of the carborane cage. Protons attached to the carbon atoms appear as well defined singlets between 2.0 and 3.5 ppm. For carboranes in the *nido*- form, these appear as doublets between -2.5 and -3.0 ppm. For boron NMR, it is worth mentioning that only the most abundant isotope of boron (^{11}B, 80.3% abundancy) is used [6b]. The boron spectrum consists of a series of signals which appear as doublets due to coupling with hydrogen atoms (J = 125-205 Hz). These doublets become singlets when the spectrum is decoupled from proton. Boron atoms attached to e.g., iodine or carbon atoms, appear as singlets in both (coupled and decoupled) spectra, and hence NMR is extremely useful in substitution reactions on boron atoms of carborane cages.

4.1.1.3. Reactivity of carboranes

A unique aspect of carborane chemistry is that the carbon and boron vertices have orthogonal reactivities. The C_c-H groups are weakly acidic [7], and can be

[4] Williams, R.E; *Chem. Rev.* **1992**, *92*, 177-207.
[5] Powell, C.L, et al., *Tetrahedron Lett.* **2007**, *48*, 1251-1254.
[6] (a) Leites, L.A; *Chem. Rev.* **1992**, *92*, 279-323; (b) Heřmánek, S. *Chem. Rev.* **1992**, *92*, 325-362; (c) Reynhardt, E.C. *J. Mag. Res.* **1986**, *69*, 337-343.
[7] Leites, L. A. *Chem. Rev.* **1992**, *92*, 279.

readily deprotonated generating nucleophiles. In contrast, the boron vertices are derivatized by reactive electrophiles. Hence, C_c-selectively functionalized o-carboranes can be obtained by treatment of *o*-carborane with a strong base (e.g., alkyl lithium salts) and subsequent reaction with an electrophile. Unfortunately, monolithiation of o-carborane at carbon competes unfavourably with dilithiation, leading to complex mixtures (Figure 4.2.A). Despite smart and valid alternatives for the preparation of mono-substituted o-carboranes have been developed, e.g. blocking one of the C_c positions with a -$Si(Me)_2CMe_3$ (TBDMS) group to effect the desired reaction in the other C_c position followed by deprotection (Figure 4.2.B) [8], or using dimethoxyethane as a solvent (Figure 4.2.C) [9], fast and efficient alternative methods would be highly desirable.

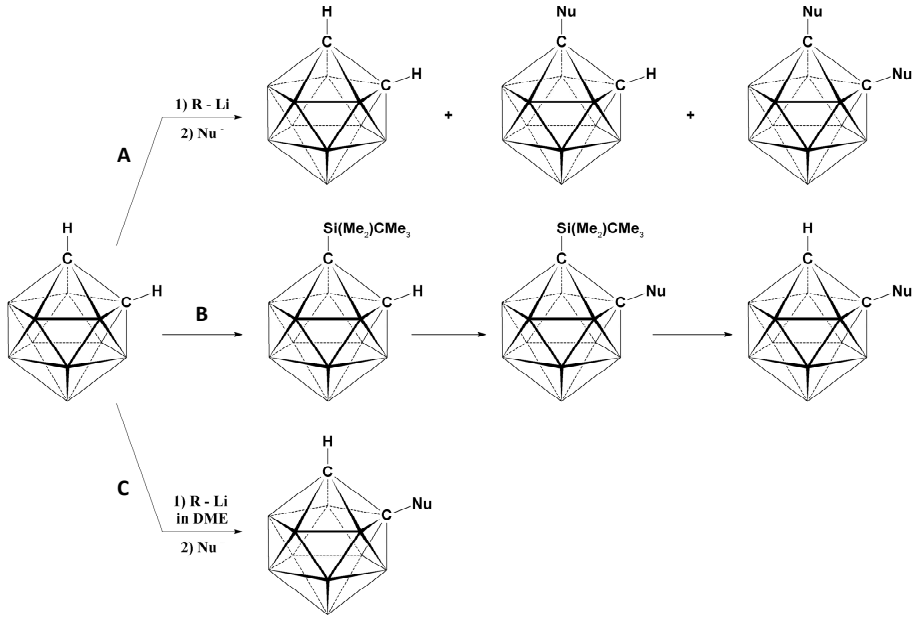

Figure 4.2. Different strategies for the preparation of C_c-substituted o-carboranes starting from $_o$-carborane.

The functionalization of carboranes on one of the boron atoms of the cluster has been less often exploited. However, incorporation of a halogen in the

[8] Kahl, S. B, *et. al*., *J. Am. Chem. Soc.* **1996**, *118*, 1223.
[9] Viñas, C. *et al.*, *Inorg. Chem.* **1995**, *34*, 3844.

presence of a Lewis acid (e.g. $AlCl_3$) has been reported [10]. Derivatization on boron vertices can also be achieved by treatment of *o*-carborane with liquid ammonia in the presence of alkali metals (Na, K) followed by oxidation using potassium permanganate or copper(i) chloride ($KMnO_4$ o CuCl), yielding 3-amino-*ortho*-carborane [11]. The amino group can be further converted into other functionalities by formation of the diazonium intermediate.

One convenient and straightforward strategy for the preparation of functionalized *o*-carboranes is based on the reaction of decaborane ($B_{10}H_{14}$) with a Lewis base in order to form a reactive complex ($B_{10}H_{12}L_2$) [12], which is further reacted under conventional heating with an alkyne to yield the corresponding *o*-carborane derivative (Figure 4.3.A).

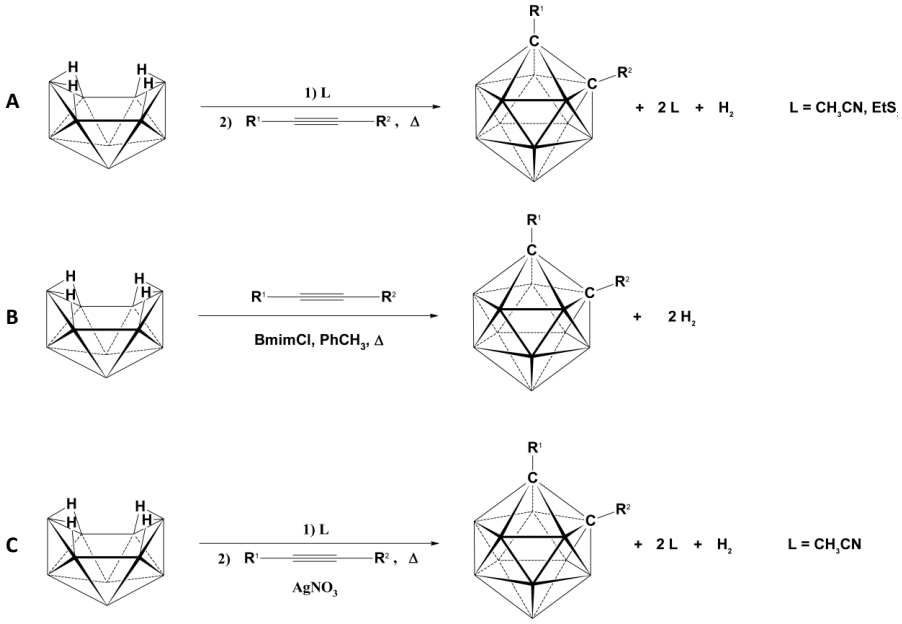

Figure 4.3. Different strategies for the preparation of Cc-substituted *o*-carboranes starting from decaborane.

Despite this methodology has been widely applied to the preparation of mono- and di- C_c-substituted *o*-carboranes, it usually offers variable chemical yields

[10] Jiang, W., et al., *Inorg. Chem.* **1995**, 34, 3491-3498.
[11] (a) Zakharkin, L.Iet al., *J. Organomet. Chem*, **1963**, *16*, 371-379; (b) Kasar, R.A., et al., *Inorg. Chem.* **1999**, *38*, 2936-2940.
[12] Schaeffer, R. *J. Am. Chem. Soc.* **1957**, *79*, 1006–1007.

and requires long reaction times at elevated temperatures, especially in the case of hindered alkynes. Sneddon and co-workers [13] recently reported the use of ionic liquids in which decaborane dehydrogenative alkyne-insertion reactions in biphasic ionic-liquid/organic solvent mixtures proceeded rapidly (<1 h) under conventional heating, with both terminal and internal alkynes and without the need of adding the Lewis base (Figure 4.3.B). The most effective method employed a catalytic amount of the ionic liquid 1-butyl-3-methyl-imidazolium chloride (bmimCl) and toluene. In a very recent work, the use of group 11(1B) metal salts to enhance the yields of *o*-caboranes produced when treating alkynes with $B_{10}H_{12}(CH_3CN)_2$ under microwave heating was investigated (Figure 4.3.C); $AgNO_3$ added in catalytic amounts resulted in improved yields when compared to the conventional method (without catalyst) or ionic liquids [14].

4.2. Aim and objectives

The above mentioned routes enable the preparation of a large collection of *o*-carborane derivatives, many of them with potential biomedical applications. However, their use *in vivo* requires a strategy suitable to determine their loci in a non invasive way. In this context, incorporation of a positron or gamma emitter into the chemical structure of the molecule under investigation and subsequent imaging studies using PET or SPECT may provide fruitful information about the spatiotemporal distribution of the boron-rich molecule.

To date, radiolabelling of carborane clusters with the radionuclide covalently attached to the carborane cage has been achieved using different iodine isotopes, i.e. Iodine-125 [15] and Iodine-131 [16]. Iodine-125 has a long half life (59.41 days) and decays by electron capture, with subsequent emission of low energy gamma rays (35.5 keV). These physical characteristics make the isotope attractive for *in vitro* studies, while *in vivo* investigation is constrained due to effective attenuation in the tissues. On the other hand, Iodine-131 emits higher energy gamma rays (364 keV), which are more convenient for *in vivo* imaging.

[13] Li, Y., *et al., Inorg. Chem.* **2008**, *47*, 9193-9202.
[14] Toppino, A., *et al.*, *Inorg. Chem.* **2013**, *52*, 8743-8749.
[15] (a) A. Varadarajan, et al., *Bioconjugate chem.* **1991**, *2*, 102; (b) D. S. Wilbur, et al., *Nuc. Med. Biol.*, **1994**, *21*, 601; (c) D. S. Wilbur, et al., *J. Label. Compd. Radiopharm.*, **1994**, *35*, 199; (d) F. J. Primus, et al., *Bioconjugate Chem.*, **1996**, *7*, 532; (e) R. J. Paxton, et al., *Bioconjugate Chem.*, **1992**, *3*, 241.
[16] V. A. Brattsev, et al., Eight International Symposium on Neutron Capture Therapy for Cancer; poster session, Chemistry and Physics; La Jolla; September, **1998**; 85.

However, β^- particles are simultaneously emitted and a greater radiation dose is released to tissue.

In this chapter, we present two different strategies for the incorporation of radioactive isotopes in functionalized carboranes. The first one relies in the mono-[^{18}F]fluorination of *o*-carborane *via* nucleophilic substitution, using cyclotron produced [^{18}F]F$^-$ and a carboranyl iodonium salt. Further derivatization of the ^{18}F-labelled carborane is achieved by formation of the C_c-lithio salt and reaction with aldehydes. The second strategy relies on the preparation of mono-radioiodinated decaborane *via* isotopic exchange, and subsequent reaction of the labelled species with acetylenes in acetonitrile under microwave heating to yield the corresponding labelled, C_c-substituted *o*-carboranes.

4.3. Results and discussion

4.3.1. [^{18}F]Fluorination of Carboranes

The [^{18}F]fluorination of *o*-carborane was achieved by reaction of cyclotron produced [^{18}F]F$^-$ and a carboranyl iodonium salt, as depicted in Figure 4.4.

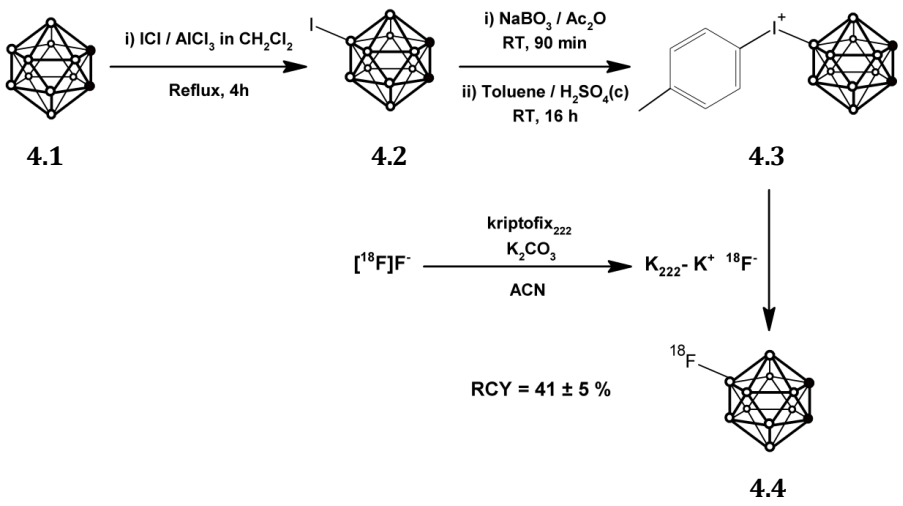

Figure 4.4. synthesis of 9-[^{18}F]fluoro-o-carborane ([^{18}F]**4.4**).

As shown in Figure 4.4, the first step consisted of the preparation of 9-Iodo-*o*-carborane (**4.2**), which was achieved by reaction of *o*-carborane with iodine monochloride in the presence of $AlCl_3$, following a previously reported method [17] (yield = 74%). The reaction of **4.2** with toluene in the presence of $NaBO_3$ and strong acidic conditions yielded *p*-tolyl-(9-*o*-carboranyl) iodonium bromide (3) in 30% yield. Finally, [^{18}F]**4.4** was prepared from [^{18}F]F^- (aqueous solution), which was generated by proton irradiation of ^{18}O-enriched water ([^{18}O]H_2O) via the ^{18}O(p,n) nuclear reaction. [^{18}F]F^- was first trapped in an anion exchange resin and subsequently eluted with K_2CO_3/H_2O and Kryptofix2.2.2/MeCN, which acts as phase transfer catalyst. After azeotropic evaporation of the solvent, the dried potassium [^{18}F]fluoride-Kryptofix2.2.2 complex was dissolved in dry MeCN and the resulting solution was reacted with **4.3**. Different experimental conditions (reaction temperature, reaction time and solvent) were investigated for the ^{18}F-fluorination step (Table 4.1) and radiochemical conversion (RCC) was calculated from chromatographic profiles [18]. Under identical reaction temperature and concentration of the precursor, higher RCC values were obtained when a mixture of 2-methyl-2-butanol/MeCN (9/1) was used as a solvent. At 100°C, RCC values of 75±8% were obtained when 20 mg of 3 were used. Undesired radiolabeled by-products were identified as free [^{18}F]F^- and minute amounts of *p*-[^{18}F]fluorotoluene (< 5%).

Table 4.1. Fluorination of **4.3** to yield [^{18}F]**4.4**.

Entry	C_P (mg/mL)[a]	RT (°C)	Solvent	RCC (%)[b]
1	10	80	MeCN	12 ± 3
2	20	80	MeCN	18 ± 7
3	10	100	MeCN	22 ± 6
4	20	100	MeCN	27 ± 5
5	10	80	2M2B/MeCN (9/1)	41 ± 9
6	20	80	2M2B /MeCN (9/1)	44 ± 9
7	10	100	2M2B /MeCN (9/1)	65 ± 3
8	20	100	2M2B /MeCN (9/1)	75 ± 8

[a] Concentration of the precursor. In all reactions, 1 mL of solution was used. [b] Radiochemical conversion, as determined by radio-HPLC; mean ± standard deviation, n=3. 2M2B: 2-methyl-2-butanol.

[17] Z. Zheng, et al., *Inorg. Chem.*, **1995**, *34*, 2095.

[18] It is important to note that the areas under the peaks in chromatographic profiles for radiometric detection are directly proportional to the amount of radioactivity present, when the signal is decay-corrected. Hence, integration of all the peaks in the chromatogram provides directly information about radiochemical conversion.

A purification step based on solid phase extraction (SPE) was implemented before approaching C_c-functionalization. The reaction mixture was diluted with water (20 mL) and flushed through a C-18 cartridge. After rinsing with water, [^{18}F]**4.4** could be eluted with 1 mL CH_2Cl_2 with overall decay-corrected radiochemical yield of 55%. Albeit radiochemical purity as determined by radio-HPLC was >98%, the precursor could not be removed quantitatively. Thus, a semi-preparative radio-HPLC method was implemented and [^{18}F]**4.4** was prepared in 44% decay corrected radiochemical yield in an overall synthesis time of 60 minutes. This radiochemical yield significantly exceeds the one previously reported using electrophylic substitution [19].

In order to show that the methodology proposed here was suitable for the preparation of functionalized *o*-carborane derivatives, the reaction of the labelled carboranes with aldehydes was approached.

C_c-derivatization of the ^{18}F-labelled carborane with 4-methoxybenzaldehyde was investigated first in cold (non radioactive) mode using 9-fluoro-*o*-carborane as starting material, following the synthetic route shown in Figure 4.5. Despite the well known difficulties associated to the monosubstitution of o-carborane [20], the reaction of the latter with aldehydes *via* formation of the lithium salt under controlled conditions is known to yield mainly monosubstituted derivatives [21]. In our case, 9-fluoro-*o*-carborane (**4.4**) was treated with *n*-ButLi (THF solution, 1:3 molar ratio) at low temperature and the resulting salt was reacted in situ with 4-methoxybenzaldehyde (MBA).

The reaction of C_c-lithio (unsubstituted) *o*-carborane with MBA has been reported previously [22]. In this previous work, the formation of two enantiomers was described. In our case, the formation of four different compounds could be anticipated due to the presence of the fluorine atom: Two positional isomers each one corresponding to the mixture of two enantiomers (**4.5a-4.5d**, Figure 4.5).

Compounds **4.5a-d** eluted as a single fraction under preparative chromatographic conditions (30% yield). Analysis of the purified fraction by ^{1}H{^{11}B}-NMR suggested the presence of two positional isomers in 1:1.5 molar

[19] G. W. Kabalka, S. K. Lee and C. P. D. Longford, J. Nuc. Med. 1996, S5, 43.
[20](a) F. Teixidor, et al., *Inorg. Chem.*, **1997**, *36*, 1719; (b) A.-R. Popescu, *et al.*, *Chem. Eur. J.*, **2012**, *18*, 3174.
[21]H. Nakamura, et al., *J. Organomet. Chem.*, **1999**, *574*, 107.
[22]H. Nakamura, et al., *J. Am. Chem. Soc.*, **1998**, *120*, 1167

ratio (Figure 4.6A). Analytical HPLC using a chiral column confirmed that compound 5 was indeed a mixture of four species (Figure 4.6B), with identical m/z (343.35) as measured by UPLC/ESI-MS, corresponding to **5a**-**5d**. ^{1}H-, ^{1}H{^{11}B}-, ^{11}B-, ^{11}B{^{1}H}-, {^{11}C}-NMR and ^{1}H,^{13}C-HSQC analyses corroborated the presence of two positional isomers.

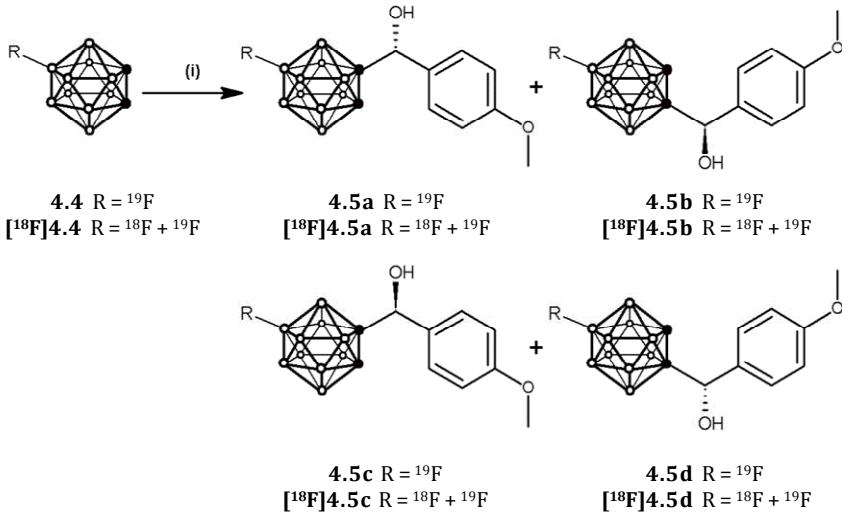

Figure 4.5. syntheses of ^{19}F- and ^{18}F-labelled C_c substituted *o*-carborane by reaction of 9-fluoro- and 9-[^{18}F]fluoro-*o*-carborane with MBA (4-methoxybenzaldehyde). (i) *n*-BuLi, THF, Δ; then MBA in THF. White dots stand for B-H; black dots stand for C/C-H

Translation of reaction conditions to ^{18}F-chemistry was not trivial. [^{18}F]F^- is produced in cyclotrons with high specific activity (in our hands, ~200 GBq/μmol at the end of the irradiation). Consequently, only nanomolar amounts of [^{18}F]**4.4** were obtained at the end of the synthetic procedure shown in Figure 4.4. Under these conditions, precise control of the desired molar ratio between compound [^{18}F]**4.4** and *n*-BuLi was anticipated to be unachievable; to overcome this problem, [^{18}F]**4.4** was diluted with **4.4** before approaching the synthesis of [^{18}F]**4.5**. Practically, the solution of [^{18}F]**4.4** resulting from elution of the C-18 cartridge with CH_2Cl_2 was first evaporated to dryness for complete removal of residual water. To the dry residue, compound **4.4** (10 mg, 62 μmol) was added and the solid was dried again under nitrogen flow (50°C, 5 min). Treatment with *n*-BuLi (2.6 M solution in THF, 71 μL, 186 μmol) and further reaction with MBA at 50°C for 10 minutes yielded a major radioactive species

(~80% RCC), which could be purified using radio-HPLC. Analysis of the collected fraction by chiral radio-HPLC confirmed the presence of 4 radioactive species, which co-eluted with non radioactive **4.5a**-**4.5d** (Figure 4.6C).

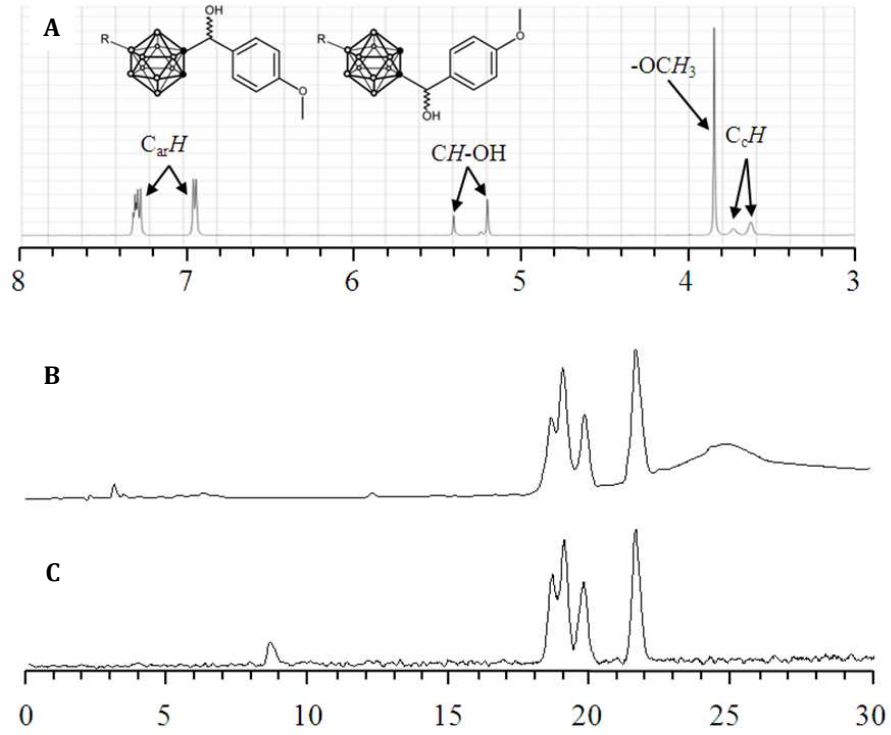

Figure 4.6. (a) ^{1}H{^{11}B}-NMR spectrum of **4.5**; (b) HPLC profile of **4.5** (UV detector) and [^{18}F]**4.5** (radiometric detector) obtained using a chiral column.

Inspired by the good results obtained, the incorporation of a moiety capable to target tumour tissue was pursuit. With this aim, [^{18}F]**4.4** was reacted with 1,2:3,4-di-O-isopropylidene-α-D-galacto-hexadialdo-1,5-pyranose (GLC) in the presence of TBAF to yield compound [^{18}F]**4.6** in 72% RCC (Figure 4.7).

Analysis of the reaction crude by HPLC-MS after complete radioactive decay confirmed the presence of **4.6** as a major peak with identical m/z+Na (443); Synthesis, isolation and characterization by HPLC-MS and ^{1}H-, ^{1}H{^{11}B}-, ^{11}B-, ^{11}B{^{1}H}- and {^{13}C}-NMR of the non radioactive analogue **4.6** corroborated the structure of the four labelled compounds as [^{18}F]**4.6a-d**.

The deprotection of the hydroxyl groups was not feasible with 2N HCl or with 2N NaOH, which led to quantitative hydrolysis for naked GLC. The hydrolysis of the carborane derivative was successfully achieved with a mixture of 90% TFA and 10% H_2O solution for 10 minutes.

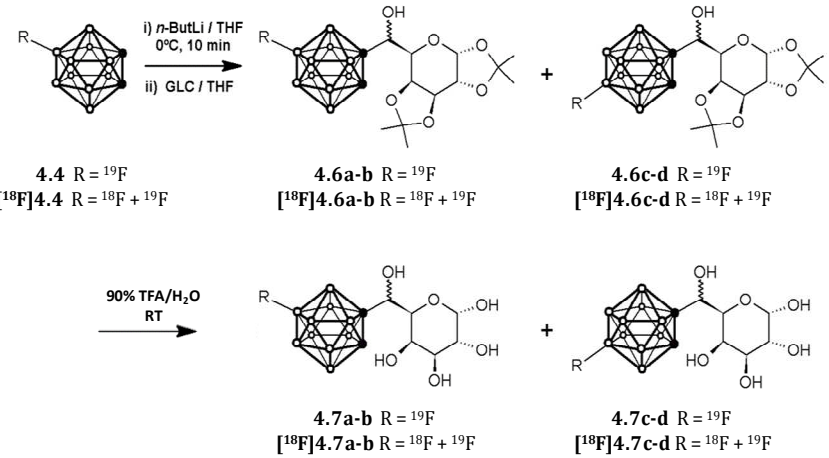

4.4 R = ^{19}F
[^{18}F]4.4 R = ^{18}F + ^{19}F

4.6a-b R = ^{19}F
[^{18}F]4.6a-b R = ^{18}F + ^{19}F

4.6c-d R = ^{19}F
[^{18}F]4.6c-d R = ^{18}F + ^{19}F

4.7a-b R = ^{19}F
[^{18}F]4.7a-b R = ^{18}F + ^{19}F

4.7c-d R = ^{19}F
[^{18}F]4.7c-d R = ^{18}F + ^{19}F

Figure 4.7. syntheses of ^{19}F- and ^{18}F-labelled C_c substituted *o*-carborane by reaction of 9-fluoro- and 9-[^{18}F]fluoro-*o*-carborane with 1,2:3,4-di-O-isopropylidene-α-D-galacto-hexadialdo-1,5-pyranose and hydrolysis.

It is worth mentioning that attempts for the isolation of the four radiolabelled isomers (**4.7a-d**) under semipreparative conditions were unsuccessful, mainly to the fact that, for safety reasons, the whole synthetic route is implemented in an automatic-remote controlled synthesis module, which is equipped with an isocratic pump and no gradients can be applied. Further investigation in the chromatographic conditions or, ultimately, installation of a new HPLC pump may result in separation of the four species.

4.3.2. Radioiodination of Carboranes

The above reported mono-[^{18}F]fluorination of *o*-carborane via nucleophilic substitution using the carboranyl iodonium salt as the precursor, and subsequent mono-functionalization at one of the C_c atoms by formation of the lithium salt and reaction with an aldehyde is a very novel strategy, and constitutes a step forward towards the possibility to visualize BNCT drug candidates using nuclear imaging. Indeed, the incorporation of the positron

emitter (^{18}F) should enable external tracking after administration into living organisms using PET. Despite the usefulness and novelty of this strategy, post-radiolabelling chemical reactions and tedious work-up are required, limiting the widespread application of the methodology.

In continuation of the above reported work, and in the pursuit of a general strategy for the preparation of radiolabelled *o*-carboranes, we tackled the preparation of radioiodinated carborane derivatives using a complete different approach, relying in the preparation of radiolabelled decaborane using ^{125}I (radioactive isotope which decays by electron capture with a half life of nearly 59 days) and catalytic isotopic exchange (Figure 4.8).

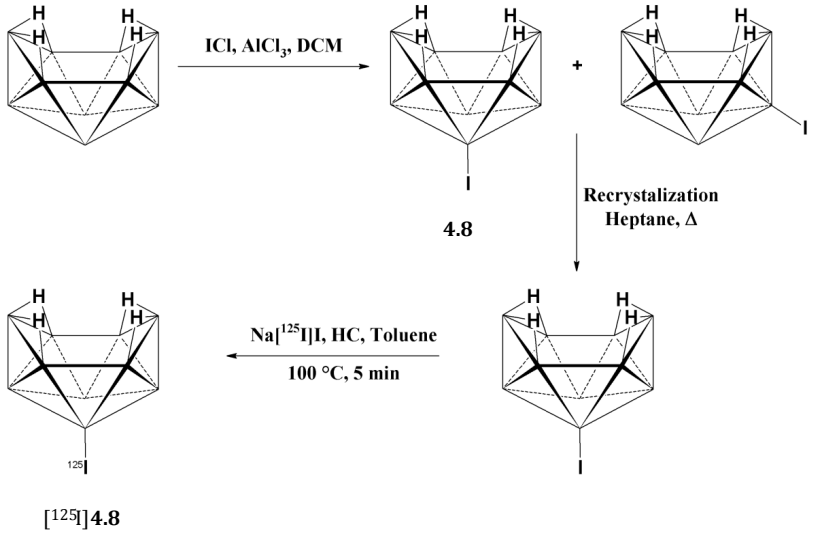

Figure 4.8. Schematic synthesis and purification of 1-Iododecaborane and radiolabelling by isotopic exchange using ^{125}I. The same synthetic strategy was used for the preparation of the ^{131}I-labelled derivative.

Further reaction with alkynes using acetonitrile, which acts both as a Lewis base and as the solvent, yielded the corresponding radiolabelled *o*-carborane derivatives in a one-pot, one-step reaction. The same synthetic strategy could be successfully translated to the preparation of analogues radiolabelled with ^{131}I (radioactive isotope which decays by beta and gamma emission, with a half-life of nearly 8 days). Hence, the general strategy reported here can be used for

the efficient preparation of a variety of radiolabelled o-carboranes by using the same radiolabelled precursor (^{125}I-labelled or ^{131}I-labelled iododecaborane) and just modifying the alkyne. Of note, translation of the methodology to other positron (^{124}I) or gamma (^{123}I) emitters, more convenient for their use *in vivo*, should be straightforward.

The mono-iodination of decaborane under non-radioactive conditions was first undertaken. Experimentally, decaborane was reacted with iodine monochloride and anhydrous $AlCl_3$ in dichloromethane to obtain two positional isomers (1- and 2-Iododecaborane, see Figure 4.8), which were separated by recrystallization in hot heptane following a previously reported method [23]. Previous results suggest a higher propensity of 2-iododecaborane to undergo deiodination [24], and hence 1-iododecaborane was used in subsequent radiolabelling experiments and preparation of o-carborane derivatives.

^{125}I-radiolabelling was carried out by adapting the previously reported palladium catalyzed iodine exchange reaction on iodinated dicarba-*closo*-dodecaboranes [25]. Briefly, 1-iododecaborane (4.04 μmol) in toluene (100 μl) was reacted with 370 KBq (10 μCi) of Na[^{125}I]I (solution in 0.1M aqueous NaOH) in the presence of Hermann's catalyst (HC, 0.1mg in 100 μl of toluene) at 100°C for 5min. Radiochemical conversion (RCC) values, as determined by high performance liquid chromatography (HPLC) using radiometric detection were 70±4% (see Figure 4.9A for example of chromatographic profile of the reaction crude).

Longer reaction times and higher temperature values led to a decrease in RCC values, suggesting a progressive deiodination of the precursor and the labelled species in competition with the isotopic exchange reaction.

The crude reaction was finally purified by solid phase extraction (SPE) to remove unreacted Na[^{125}I]I. With that aim, the reaction mixture was diluted with water and passed through a C-18 cartridge, which was further rinsed with water. Final elution with acetonitrile (1 mL) yielded pure 1-[^{125}I]iododecaborane in overall radiochemical yield of 58±7% (see Figure 4.9B for chromatographic profile of the purified product).

[23] A. V. Safronov, et al., *Inorg. Chem.*, **2012**, *51*, 2629
[24] K. J. Winberg, et al., *J. Organomet. Chem.* **2003**, *680*, 188
[25] F. F. Knapp, et al., *J. Med.Chem.*, **1984**, *27*, 57

The work reported herein was first conducted with ^{125}I, which was selected for convenience (it is widely available) and economical reasons. However, the results can be translated to other radioisotopes of iodine, more convenient for imaging studies and with shorter half lives such as ^{123}I (gamma emitter with $T_{1/2}$=13.2 h) or ^{124}I (positron emitter with $T_{1/2}$=4.2 days). In order to proof the suitability of the strategy when other iodine radioisotopes were used, the same procedure was repeated but Na[^{131}I]I (solution in 0.1M aqueous NaOH) was used as the labelling agent [26]. Equivalent radiochemical yields (56±4%) were achieved.

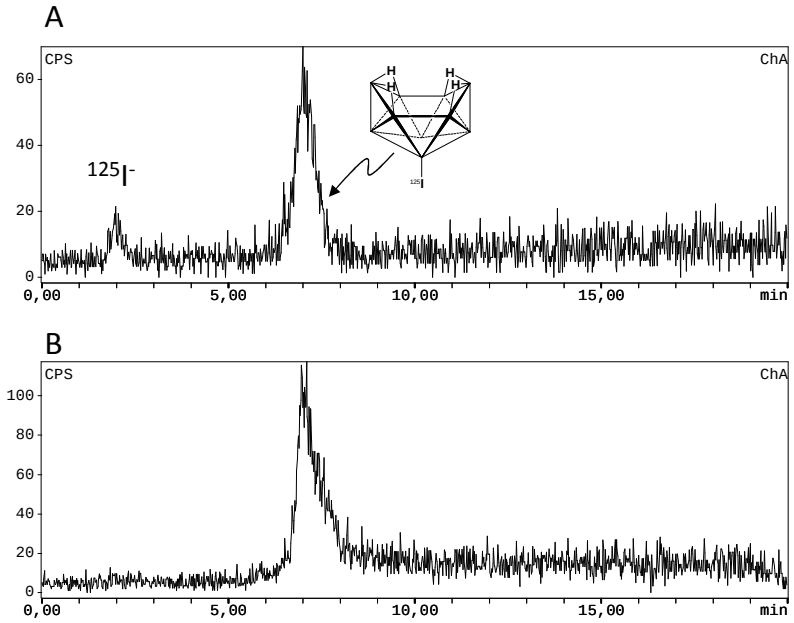

Figure 4.9. Chromatographic profiles (radiometric detection) for: (A) reaction crude and (B) pure 1-[^{125}I]decaborane.

In order to develop a methodology applicable to shorter lived radioisotopes of iodine (such as the above mentioned ^{123}I and ^{124}I) we emphasized in developing a one-pot, one-step, fast and efficient method for the reaction of 1-

[26] The reaction would have been ideally translated to ^{123}I or ^{124}I. However, the cost of these radionuclides is significantly higher than the cost for ^{131}I. Because no *in vivo* experiments with these labelled compounds were planned in the context of this PhD, ^{131}I was selected to demonstrate translation of the results to other radioisotopes of iodine, despite the emission spectra of this isotope is not compatible with our SPECT system (energy range 25-250 keV; energy emission for ^{131}I = 364 keV).

[^{125}I]iododecaborane (or 1-[^{131}I]iododecaborane) with different alkynes to obtain radiolabelled substituted o-carboranes. Generally, strategies involving Lewis bases require two steps, and hence our first attempts were performed with ionic liquids under microwave heating. Despite not previously reported in the context of the preparation of *o*-carboranes in ionic liquids, microwave heating was expected to significantly decrease reaction times. This was tested in model compounds using decaborane as the precursor (see table 4.2). Experimentally, decaborane and the corresponding alkyne (1:3 molar ratio) were dissolved in biphasic toluene/ionic liquid (1-butyl-3-methylimidazolium chloride, bmimCl) in a microwave vial and heated at 140°C under microwave irradiation for 1 minute (Figure 4.10, method A). Overall yields after purification for the six compounds assayed (**4.9**-**4.14**) ranged from 68±6% to 85±7%, resulting in a significant reduction of the reaction time when compared to conventional heating, according to published data (table 4.2). Unfortunately, the translation of these conditions to the preparation of ^{125}I-and ^{131}I-labelled analogues of compounds **4.9**-**4.14** resulted in low RCC values as determined by radio-HPLC (<5% in all cases). Longer reaction times (up to 20 min) only improved slightly RCC values up to 5-10%.

Table 4.2. Formation of *o*-carborane derivatives by reaction of decaborane with alkynes using ionic liquids (IL) and acetonitrile under microwave heating.

Compd.	Alkyne	Y. IL[a]	Y. MeCN[b]	Y. CH[c]
4.9	1-Octyne	85 ± 7 %	75 ± 7 %	91 %
4.10	Phenylacetylene	68 ± 6 %	65 ± 4 %	71 %
4.11	1-hexyne	71± 6 %	72 ± 9 %	NR
4.12	1,8-nonadiyne	72 ± 6 %	71 ± 7 %	63 %
4.13	4-Ethynyltoluene	75 ± 8 %	76 ± 3 %	NR
4.14	Ethyl propiolate	72 ± 4 %	69 ± 5 %	84 ± 4 %

[a] Yield obtained in this work: Microwave heating, reaction time of 1 min, using ionic liquids. [b] Yield obtained in this work: Microwave heating, reaction time of 20 min, using MeCN both as the Lewis base and solvent; [c] Yield reported in the literature, using ionic liquids under conventional heating (CH) with reaction time of 7 min; NR: not reported in the literature.

In the pursuit of simple alternatives applicable to the preparation of radioiodinated *o*-carboranes, we assayed an experimental scenario based on a one-pot, one-step, microwave-assisted synthetic route without using ionic liquids. Exploratory studies were initially conducted with non-labelled decaborane; in a typical experiment, decaborane and alkyne (1:3 molar ratio) were dissolved in acetonitrile in a microwave vial and heated at 120°C for 20

min under microwave irradiation (Figure 4.10, method B). Excellent yields were obtained for the six alkynes assayed (65±4 to 76±3%, table 4.2), while reaction times could be significantly decreased when compared to reported values using the conventional 2-step method (e.g., 23 h for Compound **4.9**, 10 h for compound **4.10**).

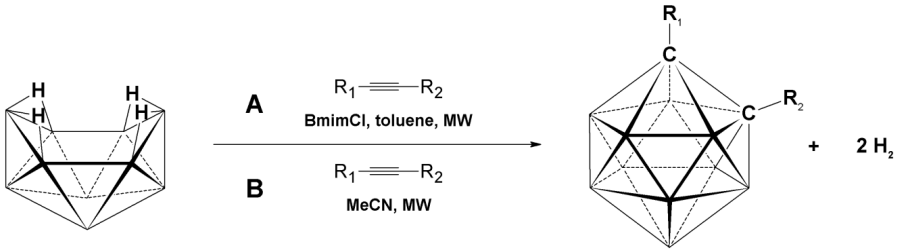

COMPOUND	R_1 , R_2
4.9	R_1 = H, R_2 = -$(CH_2)_5$-CH_3
4.10	R_1 = H, R_2 = -Ph
4.11	R_1 = H, R_2 = -$(CH_2)_3$-CH_3
4.12	R_1 = H, R_2 = -$(CH_2)_5$-C≡CH
4.13	R_1 = H, R_2 = 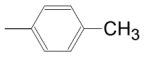
4.14	R_1 = H, R_2 = -COO-CH_2-CH_3

Figure 4.10. Scheme of the reaction for the preparation of *o*-carborane derivatives using microwave (MW) heating; Route **A**: Using ionic liquids; route **B**: Using acetonitrile both as the Lewis base and the solvent

Despite this method proved successful for the preparation of the substituted carboranes reported here, the determination of the real scope of MW-assisted formation of *closo*-carborane derivatives and the effect of different parameters (e.g. chemical properties of the alkynes, polarity, size, etc.) on the reaction yield and formation of by-products would require assays using a larger collection of alkynes and a more systematic analysis. Such investigation was out of the scope of the current work.

As a proof of concept that this strategy is suitable for the preparation of radiolabelled o-carboranes, these experimental conditions were applied to the preparation of four ^{125}I-labelled *o*-carboranes (Figure 4.11). Experimentally, the

purified labelled 1-[^{125}I]iododecaborane was dissolved in 100 µl of acetonitrile in a 2 mL microwave vial. The corresponding alkyne (14 µmol), was added and the mixture was heated under microwave irradiation at 120°C for 40 min. Good RCC values, as determined by radio-HPLC, were obtained (see table 4.3). Subsequent purification using radio-HPLC yielded pure compounds with overall radio chemical yields (RCYs) of 22±3%, 33±2%, 31±3% and 36±4%for [^{125}I]**4.15**, [^{125}I]**4.16**, [^{125}I]**4.17** and [^{125}I]**4.18**, respectively (Table 4.3). Compounds **4.15-4.18** were also prepared using ^{131}I, with equivalent radiochemical conversion and yields. Identification of the labelled compounds was carried out by radio-HPLC and co-elution with reference standard compounds (Figures 4.12-4.15).

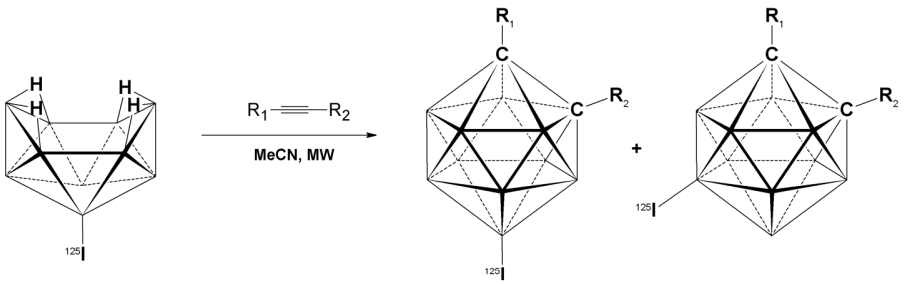

COMPOUND	R_1 , R_2
[^{125}I]**4.15**	R_1 = H, R_2 = -Ph
[^{125}I]**4.16**	R_1 = H, R_2 = 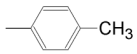
[^{125}I]**4.17**	R_1 = H, R_2 = -COO-CH_2-CH_3
[^{125}I]**4.18**	R_1 = H, R_2 = -$(CH_2)_5$-OTs

Figure 4.11. Scheme of the reaction for the preparation of ^{125}I-labelled o-carborane derivatives using microwave (MW) heating and acetonitrile as Lewis base and solvent in an one-step, one-pot reaction. The same strategy was used for the preparation of ^{131}I-labelled analogues

Table 4.3. Preparation of ^{125}I-labelled o-carboranes using acetonitrile acting both as the solvent and as the Lewis base, under microwave heating.

Compd.	Alkyne	RCC (%)	RCY (%)
[^{125}I]**4.15**	Phenylacetylene	69 ± 4	22 ± 3
[^{125}I]**4.16**	4-Ethynyltoluene	89 ± 3	33 ± 2
[^{125}I]**4.17**	Ethyl propiolate	84 ± 4	31 ± 3
[^{125}I]**4.18**	6-Heptyn-1-yl p-toluenesulfonate	70 ± 5	36 ± 4

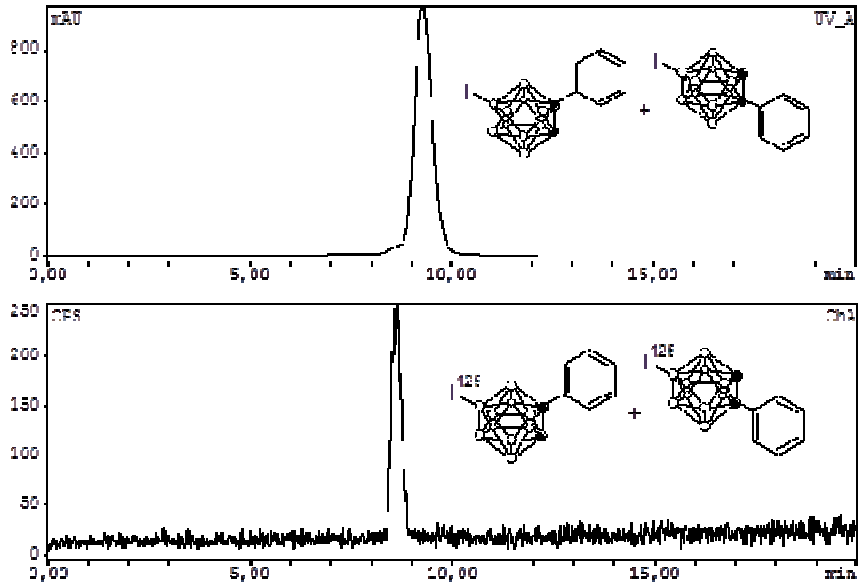

Figure 4.12: Chromatographic profiles (UV and radiometric detection) for reference compound **4.15** (top) and purified [^{125}I]**4.15** (bottom).

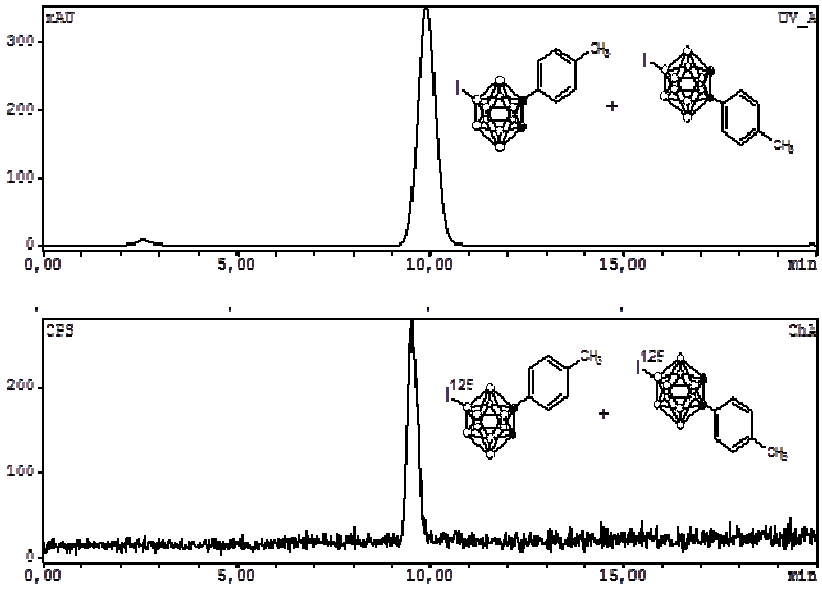

Figure 4.13: Chromatographic profiles (UV and radiometric detection) for reference compound **4.16** (top) and purified [^{125}I]**4.16** (bottom).

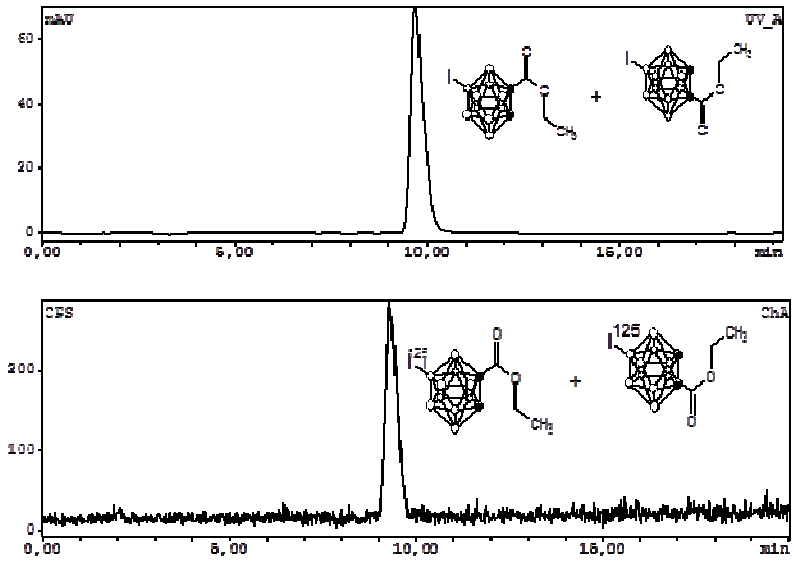

Figure 4.14: Chromatographic profiles (UV and radiometric detection) for reference compound **4.17** (top) and purified [^{125}I]**4.17** (bottom).

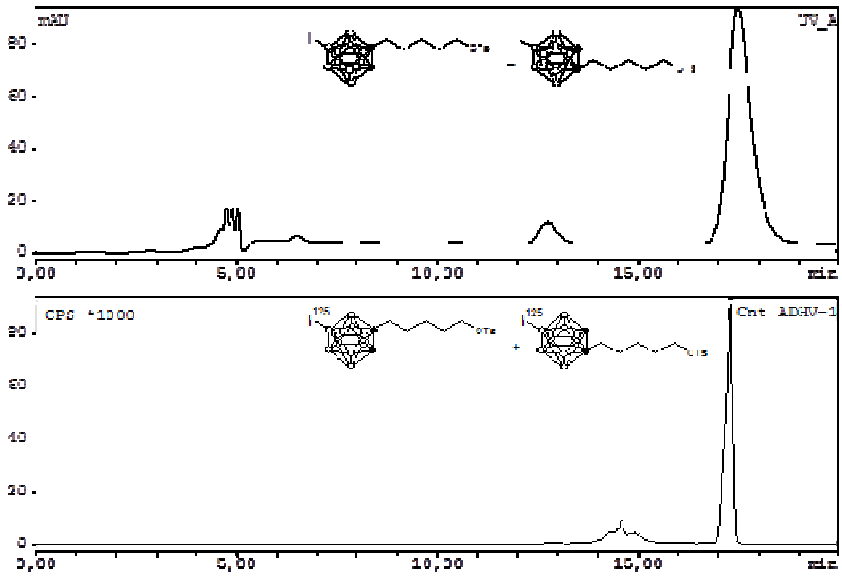

Figure 4.15: Chromatographic profiles (UV and radiometric detection) for reference compound **4.18** (top) and purified [^{125}I]**4.18** (bottom).

It is worth mentioning that when the iodinated decaborane is used (both in radioactive and in non radioactive conditions), the reaction with unsymmetrical acetylenes results is a mixture of two unavoidable positional isomers (see Figure 4.11), with the iodine atom attached to the 9- and 12-positions. Separation of these isomers was out of the scope of this work, although might be required for subsequent *in vivo* applications. This could be achieved, for example, using chiral HPLC. Additionally, the values of specific activity should be also taken into consideration, as they may gain relevance when moving to in vivo studies. Because the labelling strategy relies on isotopic exchange and low amounts of radioactivity were used, the final specific activity values were estimated to be around 0.1 MBq/μmol, taking into account that 10μCi (0.37 MBq) of radioiodine were used to label 1 mg of 1-iododecaborane. These values may be increased significantly by using higher amounts of radioactivity.

4.4. Materials and methods

4.4.1. [^{18}F]Fluorination of Carboranes

4.4.1.1. General procedures

1,2-dicarba-*closo*-dodecaborane was purchased from Katchem Ltd. (Prague, Czech Republic). All other reagents and anhydrous solvents, stored over 4 Å molecular sieves, were purchased from Aldrich Chemical Co. (Madrid, Spain) and used without further purification. HPLC grade ethanol, methanol, and acetonitrile were purchased from Scharlab (Sentmenat, Barcelona, Spain).

All reactions were performed under inert atmosphere. Flash chromatography was performed using silica gel 60 (Scharlab, Spain). Analytical thin layer chromatography (TLC) measurements were conducted with silica gel 60 F_{254} plates (Macherey-Nagel); for the visualization of carboranes, TLC plates were treated with an acidic solution of 1% $PdCl_2$ in methanol. NMR spectra were recorded on a 500-MHz Avance III Bruker spectrometer. To explain multiplicities the following abbreviations were used: s = singlet, d = doublet, t = triplet, q = quartet, m = multiplet.

UPLC/ESI-MS analyses were performed using an AQUITY UPLC separation module coupled to a LCT TOF Premier XE mass spectrometer (Waters, Manchester, UK). An Acquity BEH C18 column (1.7 µm, 5 mm, 2.1 mm) was used as stationary phase. The elution buffers were A (water and 0.1% formic acid) and B (Methanol and 0.1% formic acid). The column was eluted with a gradient: t=0 min, 95% A, 5% B; t=0.5 min, 95% A, 5% B; t=7.5 min, 1% A, 99% B; t=10min, 1% A, 99% B. Total run was 10 min, injection volume was 5 µL and the flow rate 300 µL/min. The detection was carried out in negative ion mode, monitoring the most abundant isotope peaks from the mass spectra.

4.4.1.2. Synthetic procedures and spectroscopic data

*Synthesis of 9-I-1,2-dicarba-closo-dodecaborane (**4.2**)*

The synthesis of the 9-I-1,2-dicarba-closo-dodecaborane (**4.2**) was based on a previously reported method [17]. Iodine monochloride (1.16 g, 7.1 mmol) and $AlCl_3$ (100 mg) were added to a cooled (0°C) solution of 1,2-dicarba-*closo*-dodecaborane (1.04 g, 7.1 mmol) in 25 mL of methylene chloride and the resulting mixture was refluxed for 4 h. The reaction mixture was then poured into 25 mL of ice-cold water, shaken and the organic phase was separated from the mixture. The aqueous phase was extracted twice with 25mL of CH_2Cl_2. The combined organic layer was sequentially washed with 10% aqueous $Na_2S_2O_3$

solution and water, and finally dried over Na_2SO_4. The mixture was concentrated and the crude product was purified using column chromatography (Silica gel 60, Hexane/Ethyl acetate = 90/10) to yield **4.2** as powdered white solid (1.4 g, 74%).

*Synthesis of p-tolyl-(9-o-carboranyl) iodonium bromide (**4.3**)*

The synthesis of **4.3** was based on a previously reported method [27]. $NaBO_3.H_2O$ (576 mg, 5.7 mmol) was suspended in Ac_2O (2.6 mL) and stirred at 25°C for 90 min; 9-I-1,2-dicarba-*closo*-dodecaborane (500 mg, 1.9 mmol) was added and the resulting mixture was further stirred at the same temperature for another 90 min. Toluene (1 mL, 9.6 mmol) was added, the reaction mixture was cooled to 0°C and concentrated H_2SO_4 (0.4 mL) was added dropwise while the internal temperature was maintained below 10°C. The resulting mixture was allowed to stir at room temperature for 16 h, poured into 25 mL of cold water and stirred for 30 min. The aqueous phase was washed twice with Et_2O (20 mL) to remove any unreacted organic substrates and the ethereal extracts were discarded. To the cooled aqueous phase, aqueous KBr solution (920 mg in 5 mL of water) was added with stirring. This mixture was allowed to stand in the fridge overnight. The precipitate formed was filtered, washed with water and Et_2O and dried under vacuum to yield **4.3** as a yellow solid (240 mg, 30 %).

*Synthesis of 9-[^{18}F]fluoro-1,2-dicarba-closo-dodecaborane ([^{18}F]**4.4**)*

[^{18}F]fluorine was produced by irradiation of [^{18}O]H_2O with 18MeV protons using an IBA Cyclone 18/9 cyclotron. [^{18}F]F^- was trapped in an Accell™ Plus QMA anion exchange resin (Waters) and pushed into a V-shaped vial with 15 mg of Kryptofix 2.2.2 in 1 mL of MeCN and 0.5 mL of aqueous solution containing 3 mg of K_2CO_3. The vial was heated at 80°C for 10 min under nitrogen flow to remove the MeCN-H_2O azeotrope; the temperature was increased to 100°C under vacuum for another 5min to remove any traces of water residues. To the dry potassium-[^{18}F]fluoride-Kryptofix$_{2.2.2}$ complex, *p*-tolyl-(9-*o*-carboranyl) iodonium bromide (10 mg dissolved in a mixture of 900 µL of 2-methyl 2-butanol and 100 µL of MeCN) was added. The mixture was heated at 100°C for 20 min. After cooling, the reaction crude was diluted with acetonitrile (1 mL) and water (1 mL) and the resulting mixture was passed through a Sep-Pak Alumina Plus cartridge (Waters) and loaded into an HPLC system for purification. A Mediterranean Sea18 column (10 x 250 mm, 5 µm) was used as stationary phase and MeCN/0.1M AMF (pH adjusted to 3.9 with

[27] A. Kryska, et al., *Molecules*, **2001**, *6*, 875

HCOOH) (60/40) as mobile phase at a flow rate of 8 mL/min. The desired fraction (retention time ~ 10 min) was collected, diluted with water (50 mL) and reformulated by trapping in a Sep-Pak C18 Plus Short Cartridge (waters) and further eluting with dichloromethane (1 mL). The radiochemical purity was determined by HPLC, using an Agilent 1200 Series HPLC system with a multiple wavelength UV detector (λ = 254 nm) and a radiometric detector (Raytest). A RP-C18 column (Eclipse XDB C18, 4.6x150 mm, 5 μm particle size) was used as stationary phase and water/MeCN 50/50 as a mobile phase with a flow rate of 2mL/min (retention time = 5.5 min). Total synthesis time was approximately 60 min from the end of irradiation (EOB).

*Synthesis of non radioactive (9-fluoro-o-carboranyl) (4-methoxyphenyl) methanol (**4.5**)*

To 10 mg of 9-fluoro-*o*-carborane (0.062 mmol) in 500 μL of ice cold THF, *n*-BuLi 2.6M solution in THF (71 μL, 0.186 mmol) was added and the mixture was heated at 50°C for 5 min. After cooling to 0-5°C, 4-methoxybenzaldehyde (MBA, 0.186 mmol) dissolved in TFH (500 μL) was added and the mixture was heated again at 50°C for 10 min. The reaction was quenched with 1N HCl and extracted with ethyl acetate. The organic layer was dried over Na_2SO_4, filtered, concentrated under vacuum and the crude was purified by column chromatography (silica gel, 10% Ethyl acetate/Hexane) to yield **4.5** as yellow solid (5.5 mg, 30 %).

*Synthesis of (9-[^{18}F]fluoro-o-carboranyl) (4-methoxyphenyl) methanol ([^{18}F]**4.5**)*

The precursor 9-[^{18}F]fluoro-*o*-carborane, obtained in 1 mL of dichloromethane, was dried over Na_2SO_4, decanted and mixed with 10 mg of non radioactive 9-fluoro-*o*-carborane (0.062 mmol). This mixture was dried under nitrogen flow at 50°C for 10 min. After complete evaporation, the residue was cooled to 0°C and 2.6M *n*-BuLi (71 μL, 0.186 mmol) in 500 μL of THF was added. The mixture was heated at 50°C for 5 min, cooled again back to 0-5°C and a solution of MBA (0.186 mmol) in TFH (500 μL) was added. After heating at 50°C for 10 min, the reaction was cooled to room temperature and quenched with 1M HCl. The radiochemical conversion was determined by radio-HPLC. A RP-C18 column (Eclipse XDB C18, 4.6x150 mm, 5 μm particle size) was used as stationary phase and water/MeCN 50/50 as a mobile phase with flow rate of 2 mL/min (retention time = 9.5 min). A fraction of the reaction crude was purified under identical chromatographic conditions and the purified fraction was analyzed by radio HPLC; a chiral column (ULTRON ES-OVM chiral analytical, 4.6x150mm)

was used as stationary phase. The column was eluted with A (water) and B (Ethanol) using a gradient: t=0 min, 95% A, 5% B; t=1min, 95% A, 5% B; t=20 min, 60% A, 40% B; t=32 min, 60% A, 40% B; t=40 min, 95% A, 5% B. The retention times of the four isomers were 17.5, 18, 20 and 21 min, respectively.

^{1}H{^{11}B} NMR (500 MHz, $CDCl_3$): δ 7.28 (C_{ar}*H*-C_{ar}-OCH_3, 2 H, dd, *J* 8.5, 4.5), 6.93 (C_{ar}*H*-C_{ar}-CH-, 2 H, d, *J* 8.6), 5.39 (C*H*-OH, 0.38 H, s), 5.19 (C*H*-OH, 0.59 H, s), 3.85 (O-CH_3, 3 H, s), 3.74 (C_c*H*, 0.37 H, s), 3.63 (C_c*H*, 0.62 H, s), 2.73 (O*H*, 1 H, s), 2.98 – 1.36 (B*H*, 10 H); ^{11}B{^{1}H} NMR (160 MHz, $CDCl_3$): δ 15.32 (*B*F), -5.08, -6.41, -10.44, -11.05, -13.08, -14.36, -15.68, -16.57, -17.53; ^{13}C NMR (126 MHz, $CDCl_3$): δ 160.57 (C_{ar}-OCH_3), 130.30 (C_{ar}-CH-), 127.89 (C_{ar}H-C_{ar}-OCH_3), 114.16 (C_{ar}H-C_{ar}-CH-), 74.72 (*C*H-OH), 73.46 (*C*H-OH), 55.35 (*C*H_3O-), 54.29 (C_cH), 42.94 (C_cH); ^{19}F NMR (471 MHz, $CDCl_3$): δ -184.37 (B*F,* 1F*, q*), -189.97(B*F,* 0.58F, *q*);43333 Elemental analysis: Measured: 40.1% C, 6.3% H; calculated: 40.26% C, 6.42% H.

Synthesis of non radioactive ***4.6***

To 35 mg of 9-fluoro-*o*-carborane (0.217 mmol) in 500 μL of ice cold THF, *n*-BuLi 1.6M solution in THF (160 μL, 0.260 mmol) was added and the mixture was heated at 50°C for 5 min. After cooling to 0-5°C, 158 mg of 1,2:3,4-di-O-isopropylidene-α-D-galacto-hexadialdo-1,5-pyranose (GLC) (0.652 mmol) dissolved in THF (500 μL) was added and the mixture was heated again at 50°C for 10 min. The reaction was quenched with 1N HCl and extracted with ethyl acetate. The organic layer was dried over Na_2SO_4, filtered, concentrated under vacuum and the crude was purified by column chromatography (silica gel, 15% Ethyl acetate/Hexane) to yield **4.6a-b** and **4.6c-d** as two different fractions**,** both as colorless solids, with an overall yield of 62 mg (32 %).

^{1}H{^{11}B} NMR (500 MHz, $CDCl_3$): δ 5.55 (C*H(*-O)$_2$, 1 H, dd, *J* 5.2, 2.5), 4.57 (C*H*-CH-CH*(*-O)$_2$, 1 H, dd, *J* 8.0, 2.4), 4.50 (C*H*-OH, 0.5 H, d, *J* 1.8), 4.31 (C*H*-OH, 0.5 H, d, *J* 1.8), 4.29 (C*H*-CH*(*-O)$_2$, 1 H, m), 4.28 (C*H*-CH-CHOH, 1 H, m), 4.20 (C_c*H*, 0.5 H, bs), 4.10(C_c*H*, 0.5 H, bs), 3.96 (O*H*, 0.5 H, bs), 3.90 (O*H*, 0.5 H, bs), 3.78 (C*H*-CHOH, 1 H, dt, *J* 4.2, 1.9), 1.50 (CH_3-C, 1.5 H, s), 1.48 (CH_3-C, 1.5 H, s), 1.41 (CH_3-C, 3 H, d, *J* 1.8), 1.28 ((CH_3)$_2$-C, 6 H, d, *J* 1.8), 2.68 – 1.80 (B*H*, 9 H); ^{11}B{^{1}H} NMR (160 MHz, $CDCl_3$): δ 15.53 (*B*F), -5.59, -10.63 , -11.56, -12.90, -15.56, -17.81; ^{13}C NMR (126 MHz, $CDCl_3$): δ 96.05, 73.5, 72.1, 71.5, 70.55, 70.2, 66.65, 53.51, 41.67, 25.7, 25.5, 24.50; LCMS (ESI) Experimental $[M+HCOO]^+$ m/z = 444.35.

^{1}H{^{11}B} NMR (500 MHz, $CDCl_3$): δ 5.53 (C*H*(-O)$_2$, 1 H, t, *J* 4.7), 4.65 (C*H*-CH-CH(-O)$_2$, 1 H, dd, *J* 7.8, 2.5), 4.47 (C*H*-CH(-O)$_2$, 1 H, ddd, *J* 12.7, 7.9, 2.0), 4.42 (C*H*-OH, 0.5 H, d, *J* 1.8), 4.38 (C$_c$*H*, 0.5 H, bs), 4.34 (C*H*-CH-CHOH, 1 H, m), 4.29 (C$_c$*H*, 0.5 H, bs), 4.22 (C*H*-OH, 0.5 H, d, *J* 1.8), 3.78 – 3.63 (C*H*-CHOH, 1 H, m), 3.24 (O*H*, 1 H, bs), 1.55 -1.53 (C*H*$_3$-C, 3 H, d, *J* 1.8), 1.45 (C*H*$_3$-C, 3 H, d, *J* 2.4), 1.37 – 1.34 (C*H*$_3$-C, 3 H, m), 1.33 (C*H*$_3$-C, 3 H, s). ^{11}B{^{1}H} NMR (160 MHz, $CDCl_3$): 15.51 (*B*F), -5.58, -10.91, -13.68, -16.31; ^{13}C NMR (126 MHz, $CDCl_3$): δ 110.03, 109.35, 96.62, 71.53, 71.18, 70.68, 70.03, 69.24, 68.65, 54.51, 42.85, 25.89, 25.67, 24.74, 24.50; LCMS (ESI) Experimental $[M+HCOO]^+$ m/z = 444.35.

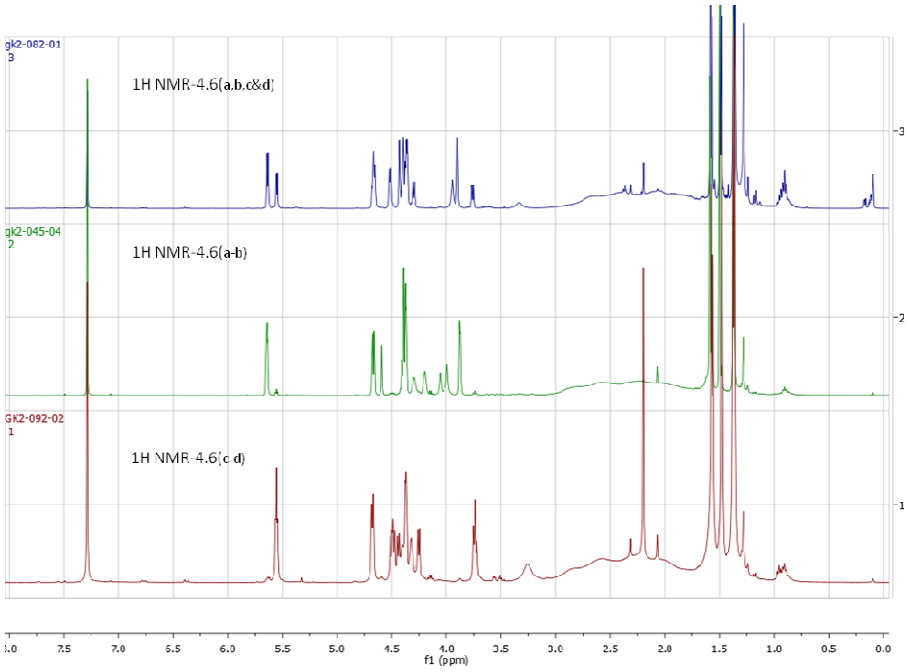

Figure 4.16: From top to bottom, ^{1}H-NMR spectra of 4.6(a-d), 4.6(a,b) and 4.6(c,d).

*Synthesis of [^{18}F]**4.6***

The precursor 9-[^{18}F]fluoro-*o*-carborane, obtained in 1 mL of dichloromethane, was dried over Na_2SO_4, decanted and concentrated under nitrogen flow at 50°C for 10 min. After complete evaporation, the residue was dissolved in 200µL of dry THF and 20µL of 1M THF solution of TBAF was added and heated at 40°C

for 5 min, followed by 20µL THF containing 4mg of GLC and heated at 40°C for 10 min. The reaction was cooled to room temperature and quenched with 1M HCl. The radiochemical conversion was determined by radio-HPLC. A RP-C18 column (Eclipse XDB C18, 4.6x150 mm, 5 µm particle size) was used as stationary phase and water/MeCN 60/40 as a mobile phase with flow rate of 2 mL/min (retention time = 10.9 min). The reaction crude was purified under radio HPLC conditions. A Mediterranean Sea18 column (10 x 250 mm, 5 µm) was used as stationary phase and MeCN/0.1M AMF (pH adjusted to 3.9 with HCOOH) (60/40) as mobile phase at a flow rate of 5 mL/min. The desired fraction (retention time ~ 11 min) was collected, diluted with water (50 mL) and reformulated by trapping in a Sep-Pak C18 Plus Short Cartridge (waters) and further eluting with dichloromethane (1 mL). The radiochemical purity was determined by HPLC, using the method used for determining RCC. The radiochemical purity was >95%.

*Synthesis of **4.7a-b and 4.7c-d***

To 15 mg of **4.6a-b** or **4.6c-d,** 1.5ml solution of 90%TFA and 10%H_2O was added. The mixture was stirred at room temperature for 10 min. The reaction mixture was concentrated on high vacuum pump, keeping the heating temperature below 30°C, and co-distilled twice with dichloromethane to give 6 mg (51%) of **4.7a-b** and 7.5 mg (65%) of ***4.7c-d***, both as colourless solids.

^{1}H{^{11}B} NMR (500 MHz, Methanol-d4): 5.17 – 5.09 (1 H, m), 4.40 – 4.36 (1 H, m), 4.23 – 4.18 (1 H, m), 4.03 (1 H, dd, *J* 13.6, 2.3), 3.85 (1 H, ddd, *J* 9.3, 4.7, 1.3), 3.72 (1 H, d, *J* 2.3), 3.45 (1 H, d, *J* 5.9); ^{11}B{^{1}H} NMR (160 MHz, Methanol-d4): 15.28 (BF), -5.93, -11.61, -15.18; LCMS (ESI) Experimental $[M+HCOO]^+$ m/z = 340.36.

^{1}H{^{11}B} NMR (500 MHz, Methanol-d4): 5.20 (1 H, t, *J* 3.2), 4.56 (1 H, dd, *J* 6.8, 1.7), 4.47 – 4.40 (2 H, m), 4.40 – 4.32 (2 H, m), 3.97 – 3.92 (1 H, m), 3.78 – 3.71 (2 H, m), 3.60 (1 H, q, *J* 1.7), 3.50 – 3.44 (1 H, m); ^{11}B{^{1}H} NMR (160 MHz, Methanol-d4): 15.27 ((BF), -5.95, -11.54, -15.16; ^{13}C NMR (126 MHz, Methanol-d4): 92.97 , 72.98 , 72.42 , 71.79 , 69.30 , 68.39; LCMS (ESI) Experimental $[M+HCOO]^+$ m/z = 340.36.

*Synthesis of [^{18}F]**4.7***

The dichloromethane solution containing *[^{18}F]**4.6,*** obtained after purification and reformulation of previous step, was dried over sodium sulfate, decanted and evaporated under nitrogen flow to dryness. Added 1ml solution of 90%

TFA and 10% H_2O, stirred at room temperature for 10 min. The reaction mixture was diluted with water (10 mL) and reformulated by trapping in a Sep-Pak C18 Plus Short Cartridge (waters) and further washed with 3ml of water and eluted with ethanol (0.5 mL). The radiochemical purity was determined by HPLC, using the method used for determining RCC (radiochemical purity > 95%). A RP-C18 column (Eclipse XDB C18, 4.6x150 mm, 5 µm particle size) was used as stationary phase and water/MeCN 60/40 as a mobile phase with flow rate of 2 mL/min (retention time = 2.3 min).

4.4.2. Radioiodination of Carboranes

4.4.2.1. General procedures

Decaborane was purchased from Katchem Ltd. (Prague, Czech Republic). All other reagents and anhydrous solvents, stored over 4 Å molecular sieves, were purchased from Aldrich Chemical Co. (Madrid, Spain) and used without further purification. HPLC grade ethanol, methanol, and acetonitrile were purchased from Scharlab (Sentmenat, Barcelona, Spain). 6-heptyn-1-yl p-toluenesulfonate was prepared following a previously described method [25].

General reactions and characterization of intermediate and final compounds were performed following the specifications in section 4.3.1. Microwave reactions were conducted in a Biotage Initiator Exp Eu system, and a power of 400W was used. All the reactions were performed in the vials specified by the manufacturer.

Synthetic procedure for microwave assisted alkyne-insertion to decaborane in ionic liquid.

In a clean and dry microwave vial, decaborane (1.636 mmol) and alkyne (5.235 mmol) were solved in biphasic toluene (8ml)/bmimCl (0.818 mmol). The vial was purged with nitrogen, properly capped, and reacted under microwave heating (140°C, 1 min). After cooling, the organic layer was withdrawn and the ionic liquid layer was extracted with ether (10 ml). The combined organic layer was evaporated and the crude was purified by silica gel column. The column was eluted with hexane (except compound **4.14**, which was eluted with 30% ethyl acetate in hexane), the product fractions were combined and the solvent was evaporated with a rotary evaporator.

Synthetic procedure for microwave assisted alkyne-insertion to decaborane in the absence of ionic liquid

In a clean and dry microwave vial, decaborane (1.636 mmol) and alkyne (5.235 mmol) were dissolved in acetonitrile (8ml). The vial was purged with nitrogen gas, properly capped and reacted under microwave heating (120°C, 20 min). After cooling, the solvent was evaporated and the residue was purified by silica gel column. The column was eluted with hexane (except compound **4.14**, which was eluted with 30% ethyl acetate in hexane), the product fractions were combined and the solvent was evaporated with a rotary evaporator.

Synthesis of 1-Iododecaborane

A previously described procedure was used [23]. Briefly: In a 100 ml SNRB flask, decaborane (5.00 g, 40.1 mmol) was dissolved in anhydrous dichloromethane (35 mL). Anhydrous $AlCl_3$ (0.546 g, 4.03 mmol) was added, the mixture was cooled to 0°C and a solution of ICl (2.08 mL, 41.5 mmol) in 20 mL of anhydrous dichloromethane was added drop wise. The dark brown reaction mixture was heated to reflux for 5 h. The reaction mixture was filtered and the solvent was evaporated to dryness. Recrystallization of the crude reaction mixture from hot heptane gave pure 2-Iododecaborane. 1-Iododecaborane was isolated by recrystallization of mother liquor.

Synthetic procedure for microwave assisted alkyne-insertion to 1-iododecaborane

In a cleaned and dry microwave vial, 1-iododecaborane (1.636 mmol) and alkyne (5.235 mmol) were dissolved in acetonitrile (8ml). The vial was purged with nitrogen gas, properly capped and reacted under microwave heating (120°C, 60 min). After cooling, the solvent was evaporated and the residue was purified by silica gel column. The column was eluted with 4% ethyl acetate/hexane, the product fractions were combined and the solvent was evaporated with a rotary evaporator.

Synthesis of ^{125}I- and ^{131}I-labelled 1-Iododecaborane

All the solvents were degassed for 10 minutes before use. 1 µL [^{125}I]NaI (solution in 0.1M NaOH, Perkin Elmer) or [^{131}I]NaI (solution in 0.1M NaOH, Perkin Elmer) and 200µL of acetonitrile (Sigma-Aldrich) were introduced in a 2.5 mL vial. The vial was heated at 100°C for 5 min under a constant helium flow to evaporate all the solvents. After complete evaporation, 1 mg of precursor solved in 100 µL of toluene and 0.1 mg (0.101 µmol) of Herrmann's catalyst (*trans*-Bis(acetato)bis[o-(di-o-tolylphosphino)benzyl] dipalladium(II), HC) solved in 100 µL of toluene were added. Reaction conditions were T=100˚C, t=5 min. After completion of the reaction, the solvent was removed with a constant helium flow and the radiochemical conversion was determined by

radio-HPLC. Analytical conditions were: Stationary phase: Mediterranea SEA18 column (15x0.46mm); mobile phase A: 0.1M ammonium formate (AMF) buffer pH= 3.9, B: acetonitrile; flow rate = 1mL/min. The following gradient was used; initial: A-80% & B-20%; 2min: A-80% & B-20%; 12min: A-20% & B-80%; 16min: A-20% & B-80%; 17min: A-80% & B-20%; 20min: A-80% & B-20%). Injected volume was 20 µL.

4.4.2.2. Spectroscopic data

*Compound 1-C_6H_{13}-1,2-$C_2B_{10}H_{11}$ (**4.9**)*

^{1}H NMR (500 MHz, $CDCl_3$): δ_H 3.58 (1H, s, C_C-*H*), 2.98-1.62 (m, 10H, B_{10}*H*$_{10}$), 2.25 – 2.18 (2H, m, C*H*$_2$- C_C), 1.53 – 1.39 (2H, m, C*H*$_2$-CH_2- C_C), 1.29 (6H, m, (C*H*$_2$)-(C*H*$_2$)-(C*H*$_2$)-CH_3), 0.91 (3H, t, C*H*$_3$); ^{11}B NMR (160 MHz, $CDCl_3$): δ_B -2.37 (d, 1*B*), -5.87 (d, 1*B*), -9.24 (d, 2*B*), -12.24 (q, 6*B*). Reported in Ref [13].

*Compound 1-C_6H_5-1,2-$C_2B_{10}H_{11}$ (**4.10**)*

^{1}H NMR (500 MHz, $CDCl_3$): δ 7.55-7.49 (m, 2H, C_{ar}*H*-C_{ar}-C_C), 7.45-7.40 (m, 1H, C_{ar}*H*-C_{ar}H-C_{ar}H-C_{ar}-C_C), 7.40-7.34 (m, 2H, C_{ar}*H*-C_{ar}H-C_{ar}-C_C), 4.00 (s, 1H, C_C-*H*), 3.30-1.70 (m, 10H, B_{10}*H*$_{10}$); ^{11}B NMR (160 MHz, $CDCl_3$): δ -2.01 (d, 1*B*), -4.32 (d, 1*B*), -8.91 (d, 2*B*), -9.92-14.44 (m, 6*B*); Reported in Ref [13].

Compound 1-C_4H_9-1,2-$C_2B_{10}H_{11}$ ***(4.11)***

^{1}H NMR (500 MHz, $CDCl_3$): δ_H 3.58 (s, 1H, C_C-*H*), 2.98-1.62 (m, 10H, B_{10}*H*$_{10}$), 2.28 – 2.17 (m, 2H, C*H*$_2$-C_C), 1.54 – 1.40 (m, 2H, C*H*$_2$-CH_2-C_C), 1.32 (m, 2H, C*H*$_2$-CH_3), 0.93 (t, 3H, C*H*$_3$); ^{11}B NMR (160 MHz, $CDCl_3$): -2.39 (d, 1*B*), -5.86 (d, 1*B*), -9.34 (d, 2*B*), -12.24 (q, 6*B*); ^{13}C NMR (126 MHz, $CDCl_3$): δ_C 75.44 (*C*$_C$-CH_2), 60.91 (*C*$_C$-H), 37.87 (*C*H$_2$-C_C), 31.23 (CH_2-*C*H$_2$-CH_2), 22.13 (*C*H$_2$-CH_3), 13.62 (*C*H$_3$); Elemental analysis: Theoretical: 35.97% C; 10.06% H. Experimental: 36.01% C; 10.15% H.

Compound 1-C_7H_{11}-1,2-$C_2B_{10}H_{11}$ ***(4.12)***

^{1}H NMR (500 MHz, $CDCl_3$): δ_H 3.58 (s, 1H, cage C-*H*), 2.29 – 2.16 (m, 4H, C*H*$_2$- C_C & C*H*$_2$-C), 1.97 (t, 1H, C*H*), 1.62 – 1.45 (m, 4H, C*H*$_2$- CH_2- C_C & C*H*$_2$-CH_2-C), 1.45 – 1.32 (m, 2H, C*H*$_2$- CH_2-CH_2- C_C); ^{11}B NMR (160 MHz, $CDCl_3$): -2.33 (d, 1*B*), -5.82 (d, 1*B*), -9.31 (d, 2*B*), -12.26 (q, 6*B*); Reported in Ref [13].

Compound 1-$C_6H_4CH_3$-1,2-$C_2B_{10}H_{11}$ ***(4.13)***

^{1}H NMR (500 MHz, $CDCl_3$): δ_H 7.46 – 7.33 (d, 2H, $C_{ar}H$-C_{ar}-C_C), 7.16 (d, 2H, $C_{ar}H$-C_{ar}-CH_3), 3.96 (s, 1H, cage C-*H*), 2.37 (s, 3H, CH_3); ^{11}B NMR (160 MHz, $CDCl_3$, decoupled):-2.02 (d, 1B), -4.52 (d, 1B), -10.94 (m, 8B); ^{13}C NMR (126 MHz, $CDCl_3$): δ_C 140.22 (C_{ar}-C_C), 130.67 (C_{ar}-CH_3), 129.48 (C_{ar}-C_{ar}-C_C), 127.49 (C_{ar}-C_{ar}-CH_3), 76.70 (C_C-C_{ar}), 60.37 (C_C-H), 20.9 (CH_3); Elemental analysis: Theoretical: 46.13% C; 7.74% H. Experimental: 45.90% C; 7.55% H.

Compound 1-C_2H_5OCO-1,2-$C_2B_{10}H_{11}$ ***(4.14)***

^{1}H NMR (500 MHz, $CDCl_3$): δ_H 4.29 – 4.25 (q, 2H, CH_2-O), 4.06 (s, 1H, cage C-*H*), 3.13 – 1.58 (m, 10B, $B_{10}H_{10}$), 1.31-1.28 (t, 3H, CH_3); ^{11}B NMR (160 MHz, $CDCl_3$, decoupled): -2.62 (d, 2*B*), -8.90 (d, 2*B*), -12.82 (dd, 6*B*); Reported in Ref [14].

Compound 1-C_6H_5-9-I-*closo*-1,2-$C_2B_{10}H_{10}$ ***(4.15)***

^{1}H NMR (500 MHz, $CDCl_3$): 7.51 (dd, 1H, $C_{ar}H$-C_{ar}H-C_{ar}H-C_{ar}-C_C), 7.49- 7.43 (m, 2H, $C_{ar}H$-C_{ar}-C_C), 7.43- 7.34 (m, 2H, $C_{ar}H$- C_{ar}H-C_{ar}-C_C), 4.29 (s, 0.3 H, cage C-*H*, isomer 1), 4.10 (s, 0.7 H, cage C-*H*, isomer 2), 3.39 – 2.02 (m, 9 H, B-*H*). Two different positional isomers (named as 1 and 2) are formed, in 0.3:0.7 ratio; ^{11}B NMR (160 MHz, $CDCl_3$): -0.02 – -0.95 (d, 1*B*), -6.73 – -7.72 (d, 2*B*), -9.90 – -14.47 (m, 6*B*), -16.15– -17.05 (s, 1*B*); ^{13}C NMR (126 MHz, $CDCl_3$): δ_C 130.36, 129.12, 127.49, 73.43, 61.06, 56.67; LCMS (ESI) Experimental $[M]^-$ m/z = 344.44; theoretical $[M]^-$ m/z = 345; FTIR (KBr, cm^{-1}): ν 3083, 2642, 2606, 2572, 1495, 1446. The typical strong bands corresponding to B-H stretching are seen in the range 2573-2642; Elemental analysis: Theoretical: 27.75% C; 4.37% H. Experimental: 27.95% C; 4.31% H.

Compound 1-$C_6H_5CH_3$-9-I-*closo*-1,2-$C_2B_{10}H_{10}$ ***(4.16)***

^{1}H NMR (500 MHz, $CDCl_3$): 7.36 – 7.32 (m, 2H, $C_{ar}H$-C_{ar}-C_C), 7.17 – 7.14 (m, 2H, $C_{ar}H$-C_{ar}-CH_3), 4.04 (s, 1H, cage C-*H*), 2.37 (s, 3H, CH_3-C_{ar}), 3.52 – 1.91 (m, 9H, B-*H*). Only one positional isomer is detected in this case; ^{11}B NMR (160 MHz, $CDCl_3$): -0.07 – -0.91 (d, 1*B*), -6.73 – -7.71 (d, 2*B*), -9.37 – -12.22 (m, 6*B*), -16.12– -17.11(s, 1*B*); ^{13}C NMR (126 MHz, $CDCl_3$): δ_C 140.67 (C_{ar}-C_C), 129.9 (C_{ar}-CH_3), 129.64 (C_{ar}H-C_{ar}-C_C), 127.39 (C_{ar}H-C_{ar}-CH_3), 73.48 (C_C-C_{ar}), 61.26 (C_{ar}-H), 21.00 (CH_3); LCMS (ESI) Experimental $[M]^-$ m/z = 358.18; theoretical $[M]^-$ m/z = 359; FTIR (KBr, cm^{-1}): ν 3078, 2647, 2602, 1506. The typical strong bands corresponding to B-H stretching are seen in the range 2602-2647; Elemental analysis: Theoretical: 30.01% C; 4.76% H. Experimental: 29.89% C; 4.79% H.

Compound 1-C_2H_5COO -9-I-*closo*-1,2-$C_2B_{10}H_{10}$ ***(4.17)***

^{1}H NMR (500 MHz, $CDCl_3$): δ_H 4.40 (s, 0.4H, cage C-*H*), 4.36-4.29 (dq, 2H, C*H*$_2$-O), 4.19 (s, 0.6H, cage C-*H*), 3.40-1.60 (bm, 9H, B-*H*), 1.37 – 1.33 (m, 3H, C*H*$_3$). The presence of two positional isomers in 0.6:0.4 ratio can be found; ^{11}B NMR (160 MHz, $CDCl_3$, decoupled): -0.70 – -1.69 (d, 1*B*), -6.70 – -7.69 (d, 2*B*), -11.19 – -14.05 (m, 6*B*), -15.85(s, 0.4*B*), -16.79 (s, 0.6*B*); ^{13}C NMR (126 MHz, $CDCl_3$): δ_C 160.4 (*C*O), 64.35 (*C*$_C$-CO), 56.81 (*C*$_C$-H), 52.14 (*C*H$_2$-O), 12.75 (*C*H$_3$); FTIR (KBr, cm^{-1}): ν 3079, 3002, 2987, 2581, 1740. The typical strong band corresponding to B-H stretching is seen at 2581; Elemental analysis: Theoretical: 17.55% C; 4.42% H. Experimental: 17.62% C; 4.51% H.

Compound 1-$(CH_2)_5OSO_2C_6H_4CH_3$-9-I-*closo*-1,2-$C_2B_{10}H_{10}$ ***(4.18)***

^{1}H NMR (500 MHz, $CDCl_3$): δ_H 7.79 (dd, 2H, C_{ar}*H*-C_{ar}-CH_3), 7.38 (dd, 2H, C_{ar}*H*-C_{ar}-S), 4.03 (q, 2H, C*H*$_2$-O), 3.88 (s, 0.3H, cage C-*H*), 3.69 (s, 0.7H, cage C-*H*), 2.48 (s, 3H, C*H*$_3$-C_{ar}), 2.28 – 2.14 (m, 2H, C*H*$_2$-CH_2O), 2.11 – 2.01 (t, 2H, CH_2- C_C), 1.66 (m, 2H, C*H*$_2$- CH_2- C_C), 1.53 – 1.30 (2H, m, C*H*$_2$-CH_2CH_2O); ^{11}B NMR (160 MHz, $CDCl_3$, decoupled): δ_B -0.72 (d, 1*B*), -7.56 (d, 2*B*), -12.39– -13.67 (hep, 6*B*), -16.48 (s, 0.3*B*), -18.45 (s, 0.7*B*). The presence of two peaks that remain as singlets in the ^{11}B NMR spectrum (-16.48 and -18.45 ppm, respectively) confirms the presence of two positional isomers in 0.3:0.7 ratio (as observed in the ^{1}H NMR spectrum; LCMS (ESI) Experimental $[M]^-$ m/z + $HCOO^-$ = 554.15; theoretical $[M]^-$ m/z = 554; Reported in Ref [28].

4.5. Summary and conclusions

In this chapter, an unprecedented strategy for the preparation of ^{18}F-labelled *o*-carborane via nucleophilic substitution using cyclotron produced $[^{18}F]F^-$ and *p*-tolyl-(9-o-carboranyl) iodonium bromide is presented. Excellent radiochemical yields were achieved. Because the ^{18}F atom is covalently attached to one of the boron atoms of the carborane cluster (B9), further functionalization on the C_c atoms can be achieved. The formation of the C_c-lithio derivatives and further reaction with aldehydes to yield the corresponding alcohols as a mixture of positional isomers and enantiomers is a proof of concept that the methodology reported here can be applied to the preparation of ^{18}F-labelled C_c-substituted carboranes. This methodology might be extended to the reaction of ^{18}F-labelled carboranes with other aldehydes, which may act as targeting moieties towards tumour tissue.

[28] R. Tiwari, et al. *Inorg. Chem.*, **2012**, 51, 629.

On the other hand, a straightforward methodology for the preparation of ^{125}I- and ^{131}I-labelled 1-iododecaborane is also reported. Subsequent reaction with alkynes using acetonitrile as the solvent under microwave heating results in the formation of the corresponding radiolabelled *o*-carborane derivatives through a one-pot, one-step reaction, with excellent yields in short reaction times. The experimental conditions might be directly translated to the preparation of radiolabelled carborane analogues using other radioisotopes of iodine such as ^{124}I or ^{123}I, which are more appropriate to conduct subsequent *in vivo* imaging studies. Hence, the combination of the methodologies developed herein may enable the preparation of a wide range of radioiodinated *o*-carborane derivatives, whose potential suitability as BNCT drug candidates might be easily investigated using non invasive, *in vivo* imaging techniques such as PET and SPECT. The preparation of radiolabelled carborane-bearing biomolecules is currently being explored using the methodology reported here.

5. SYNTHESIS OF RADIOLABELLED COSAN ANALOGUES

5.1. Introduction

5.1.1. Metallocarboranes

5.1.1.1. General aspects

Metallocarboranes are sandwich-type compounds in which a metal atom is sandwiched between two carboranyl clusters. For cobalt, iron and nickel, which are the most common metal atoms in metallocarboranes, the redox state of the metallic atom is (III), and it is coordinated via π bonds to 2 dicarbollide ([1,2-$C_2B_9H_{11}]^{2-}$) units. As a result, the final net charge of the complex is (-1), and the charge is delocalized in the whole cluster, resulting in a very low charge density.

First metallocarboranes were obtained as early as 1965 [1]. In this pioneering work, the structure of an iron (III) atom sandwiched between two dicarbollide units was reported. The similarity between the dicarbollide and the cyclopentadienide anions was indeed the key parameter to envisage the formation of such complexes. Only a few months later, a similar complex with Co(III) was reported [2] (Figure 5.1), and two years later the analogues containing Ni [3], Cr [4], Cu, Au and Pd [5] were reported. These sandwich complexes show significantly higher thermal and chemical stability than metallocenes, and higher oxidation states of the central metallic atom can be stabilized.

The structure of metallocarboranes exhibits both electrostatic interactions due to the above mentioned dispersed negative ionic charge covering the whole molecule, and non-bonding intermolecular interactions between its weakly polarized B–H and C–H bonds. Due to this duality, metallocarboranes possess simultaneously hydrophobic and hydrophilic character, being soluble in both water and oils.

5.1.1.2. Preparation and reactivity

Matallocarboranes can be prepared by different synthetic routes. The most common one consists of insertion of a transition metal into the *nido*- species formed from the respective carborane. In this methodology, the first step

[1] Hawthorne, M. F., et al., *J. Am. Chem. Soc.* **1965**, *87*, 1818.
[2] Hawthorne, M. F., et al., *Chem. Commun.* **1965**, 443.
[3] Warren, L. F. et al., *J. Am. Chem. Soc.* **1967**, *89*, 470.
[4] Ruhle, H., et al., *Inorg. Chem.* **1968**, *7*, 2279.
[5]Warren, L. F. et al., *J. Am. Chem. Soc.* **1968**, *90*, 4823.

consists of degrading the *o*-carborane cluster to the *nido*-derivative [7,8-*nido*-$C_2B_9H_{12}]^-$. This is followed by removal of the bridged hydrogen atom by treatment with a strong base (e.g. *n*-BuLi) to yield the dicarbollide anion [7,8-*nido*-$C_2B_9H_{11}]^{2-}$. Finally, the metal is added. For example, for the formation of Cobalt bis(dicarbollide) (COSAN), anhydrous $CoCl_2$ is added. The cobalt atom suffers a dismutation, yielding Co(III) and Co(0). The complex between two dicarbollide anion and the metallic atom is formed in situ yielding the resulting Cobalt bis(dicarbollide) anion.

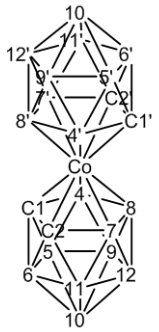

Figure 5.1. Structure and vertex numbering of COSAN.

Metallocarboranes show two differentiated reactive sites, which are C_C-H and B-H vertices [6]. The most reactive boron vertices are B(8) and B(8'), which are placed in the antipodes of the cluster carbon atoms and hence possess a negative charge density. This situation favours electrophilic induced nucleophilic substitution (EINS) reactions [7].

5.1.1.3. COSAN: a promising building block for in vivo applications

The Cobalt bis(dicarbollide) anion (COSAN) is probably the most widely studied metallocarborane. It shows an amphiphilic character in water [8], it has the ability to assemble into monolayer vesicles [9], it can cross through synthetic lipid membranes without disrupting membrane integrity [10] and accumulates *in vitro* within living cells [11].These properties, together with its

[6] (a) Churchill, M. R., et al., *J. Am. Chem. Soc.* **1969**, *91*, 1222; (b) Plesek, J. et al., *Collect. Czech. Chem. Commun.* **1995**, *60*, 1297; (c) Franken, A., et al., *Collect. Czech. Chem. Commun.* **1997**, *62*, 746.
[7] Khan, S. A., et al., *J. Chem. Soc. Pak.* **1997**, *19*, 103.
[8] N. Grimes. Carboranes. Academic Press: Burlington, MA, **2011**.
[9] P. Matějíček, et al., *Langmuir*, **2006**, *22*, 575.
[10] P. Bauduin, et al., *Angew. Chem. Int. Ed. Engl.*, **2011**, *50*, 5298.
[11] C. Verdiá-Báguena, et al., *Chem. Commun.*, **2014**, *50(51)*, 6677.

rich derivative chemistry, turn COSAN into a valuable building block for the preparation of boron-rich drugs with potential application in Boron Neutron Capture Therapy (BNCT).

For example, metallacarboranes containing nucleosides such as {8-[5-(N^3-thymidine)-3-oxa-pentoxy]-3-cobalt bis(1,2-dicarbollide)} and {8-[5-(O^4-thymidine)-3-oxa-pentoxy]-3-cobalt bis(1,2-dicarbollide)} (Figure 5.2) [12], conjugates of natural chlorins with COSAN (Figure 5.2) [13] and derivatives of naturally occurring amino acids (e.g. tyrosine) [14] have been developed, among others.

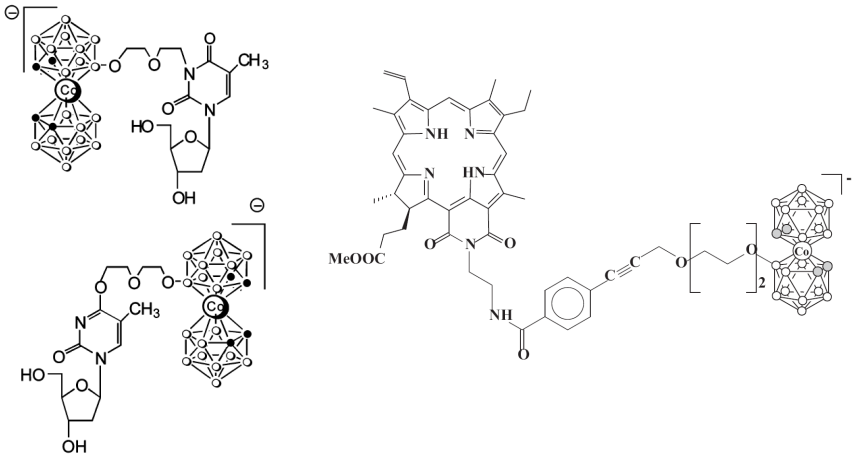

Figure 5.2. Left: Structure of {8-[5-(N^3-thymidine)-3-oxa-pentoxy]-3-cobalt *bis*(1,2-dicarbollide)} (top) and {8-[5-(O^4-thymidine)-3-oxa-pentoxy]-3-cobalt *bis*(1,2-dicarbollide)} (bottom). Adapted from [12]; right: Natural chlorins functionalized with COSAN. Adapted from [13].

5.2. Aim and objectives

Despite the fact that a large variety of COSAN analogues have been reported in the literature, some of them with potential application in the biomedical field and particularly in the context of BNCT, their use *in vivo* has been rarely reported. This is due, as in the case of carborane analogues (chapter 4) to the lack of a strategy suitable to determine their loci in a non invasive way. In this

[12] Lesnikowski, Z. J. et al., *Bioorg. Med. Chem.* **2005**, *13*, 4168-4175.
[13]Grin, M.A.,et al., *Russ. Chem.Bull.* **2010**, *59*, 219–224.
[14] Lobanova I.A., et al., *Russ. Chem. Bull.*, 2010, *59*, 2302–2308.

context, incorporation of a positron or gamma emitter into the chemical structure of the molecule under investigation and subsequent imaging studies using PET or SPECT may provide fruitful information about the spatiotemporal distribution of the boron-rich molecule.

To date, radiolabelling of COSAN with the radionuclide covalently attached to the carborane cage has not been reported. In this chapter, we present a strategy for the preparation of new bifunctional COSAN derivatives radiolabelled with either ^{125}I (gamma emitter) or ^{124}I (positron emitter) *via* palladium catalyzed isotopic exchange reaction. Incorporation of ^{125}I and ^{124}I enabled the determination of the biodistribution pattern by using dissection/gamma counting and PET-CT, respectively. With three of the compounds, Whole body biodistribution PET studies were carried out in subcutaneous PANC-1 (human pancreatic carcinoma) and A549 (carcinomic human alveolar basal epithelial cell line) xerograft mouse models. The concentration of boron-rich structures in the tumor at different time points after administration could be indirectly quantified from the PET images. Biodistribution studies with 2-deoxy-2-[^{18}F]fluoro-D-glucose ([^{18}F]FDG), the most commonly used PET contrast agent for the early detection of tumours in the clinical practice, were also performed on the same animals to assess tumour metabolism.

The work reported in this chapter has been conducted in collaboration with the group led by Prof. Francesc Teixidor and Prof. Clara Viñas, at Institut de Ciència de Materials de Barcelona (ICMAB-CSIC). The cold chemistry to prepare the functionalized COSAN analogues to perform the radiolabelling and subsequent *in vivo*/*ex vivo* studies was performed by the PhD student Adnana Zaulet under the supervision of Professors Teixidor and Viñas.

5.3. Results and discussion

5.3.1. Radiochemistry

Radiolabelling reactions on compounds [**5.1**]-, [**5.2**]-, [**5.3**]- and [**5.4**]$^-$ (Figure 5.3) were performed by adapting the previously reported palladium catalyzed iodine exchange reaction.

For all compounds, experimental conditions were first optimized using ^{125}I, which is a convenient radioisotope due to its low cost. Briefly, the appropriate precursor was reacted with 740-148 KBq (20-40 μCi) of Na[^{125}I]I (solution in 0.1M aqueous NaOH) in the presence of Hermann's catalyst (0.1mg). Radiochemical conversion values close to 85% were achieved for compound

[**5.1**]$^-$ when the reaction was conducted at 100°C for 3 min; longer reaction times did not improve radiochemical conversion. For compound [**5.2**]$^-$, the formation of unidentified labelled species was detected when the reaction was conducted at 100°C. Lower reaction temperatures (80°C) led to almost 80% radiochemical conversion after 8 min. Again, longer reaction times yielded lower incorporation yields, suggesting the degradation of the precursor and the radiolabelled compound. Radiochemical conversion values of 67±4% and 32±7% were obtained for compounds [**5.3**]$^-$ and [**5.4**]$^-$ when the reactions were carried out at 70°C for 15 min and 90°C for 10 min for [**5.3**]$^-$ and [**5.4**]$^-$, respectively.

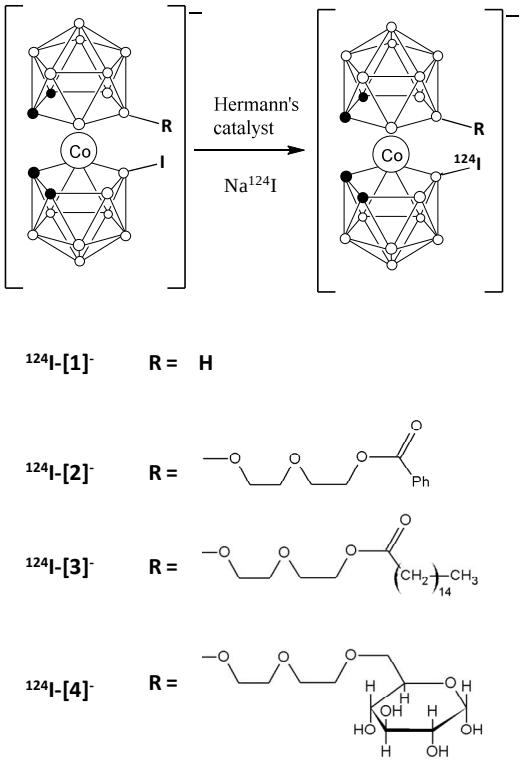

Figure 5.3. Radioiodination reaction of mono anionic species [**5.1**]-, [**5.2**]-, [**5.3**]- and [**5.4**]$^-$.

Purification of the labeled species could be achieved by using high performance liquid chromatography (HPLC), followed by solvent evaporation and reconstitution with C_2H_5OH/H_2O (1/9). This process resulted in injectable

solutions of chemically and radiochemically pure compounds (see Figure 5.4 for example of chromatographic profile for compound ^{124}I-[**5.1**]$^-$ after purification).

Experimental conditions were then translated to ^{124}I. The procedure was exactly the same, but Na^{124}I (solution in 0.2M NaOH) was used instead of Na^{125}I. After the labelling reaction, purification was achieved by semi-preparative HPLC followed by reconstitution with solid phase extraction, elution with ethanol, solvent evaporation and reconstitution with physiologic saline solution (see experimental section for details). Injectable solutions of chemically and radiochemically pure compounds could be obtained. Overall radiochemical yields (non-decay corrected) were 34±5%, 53±6% and 21±5% for [**1**]$^-$, [**2**]$^-$ and [**3**]$^-$, respectively; radiochemical purity was above 95% in all cases at injection time.

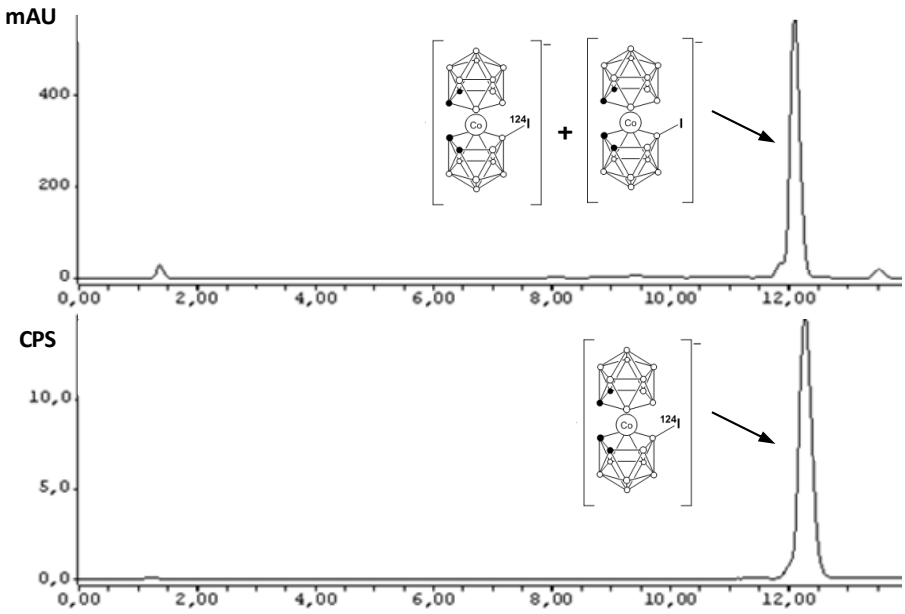

Figure 5.4. Chromatographic profiles corresponding to the quality control of ^{124}I-[**5.1**]$^-$; UV detector (top) and radiometric detector (bottom) profiles are shown. Connection of both detectors in series cause slight difference in retention times in both profiles.

5.3.2. In vivo/ex vivo studies

5.3.2.1. Biodistribution studies in healthy animals

Biodistribution studies in healthy animals were performed first with ^{125}I-labelled compounds [**5.1**]$^-$ and [**5.2**]$^-$ using dissection and gamma counting. The amount of radioactivity in the different organs was determined at three time points after administration of the radiolabelled species (10, 30 and 120 minutes, Figures 5.5a, 5.5b).

Very similar patterns were obtained for both compounds: high accumulation in liver throughout the duration of the study, increasing uptake in the lungs and moderate blood clearance. Uptake in the kidneys and the spleen was also significant and lower accumulation was detected in other organs. Progressive accumulation in the intestine and the low concentration of radioactivity in the bladder (urine) suggest biliary excretion.

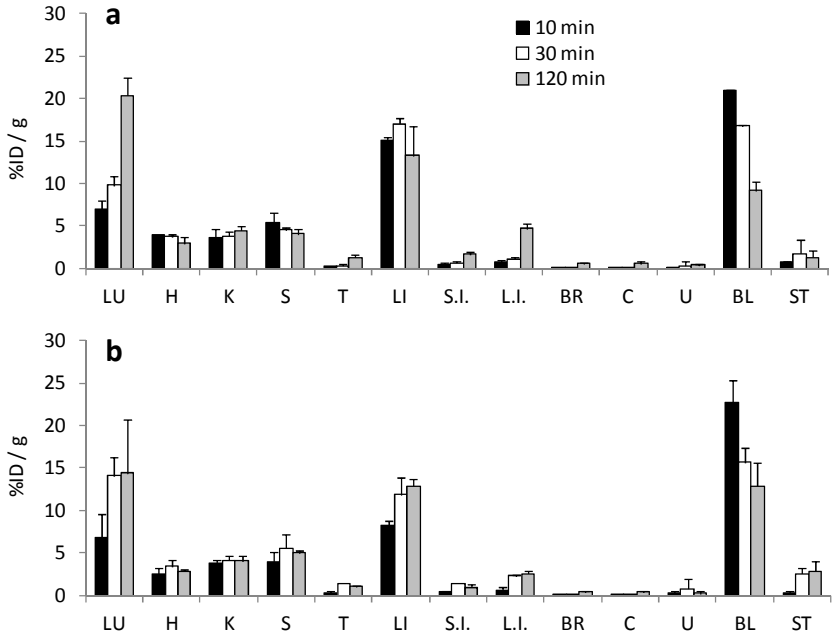

Figure 5.5.- Biodistribution of ^{125}I-[**5.1**]$^-$ (a) and ^{125}I-[**5.2**]$^-$ (b) in mice tissues (mean ± standard deviation, n=3) using the dissection method. Radioactivity is expressed as the percentage of the injected dose (ID) per gram of tissue. LU: Lungs; H: Heart; K: Kidneys; S: Spleen; T: Testicles; L: Liver; S.I.: Small intestine; L.I.: Large intestine; BR: Brain; C: Cerebellum; U: Urine; BL: Blood; ST: Stomach.

Moving towards *in vivo* application, the incorporation of the positron emitter ^{124}I was approached; with that aim, the radiolabelling process was performed following the optimized experimental conditions developed for ^{125}I, with equivalent incorporation ratios.

In vivo PET studies were conducted in combination with CT (Figures 5.6a, 5.6b), the latter for anatomical localization of the volumes of interest (VOIs). PET acquisitions were started concomitantly with the administration of the radiolabelled ^{124}I-[**5.1**]$^-$ and ^{124}I-[**5.2**]$^-$ species, and dynamic images were acquired (20 frames, total acquisition time of 130 min). In this case, only those organs clearly visualized on the CT images (lung, heart, kidney, liver, intestine, brain, bladder and stomach) were analyzed (Figures 5.7a and 5.7b). Good correlation between results obtained using both methodologies (*in vivo* imaging and dissection/gamma counting) were obtained (Figure 5.8), although significant differences were observed at different time points in the brain, the bladder and the lungs.

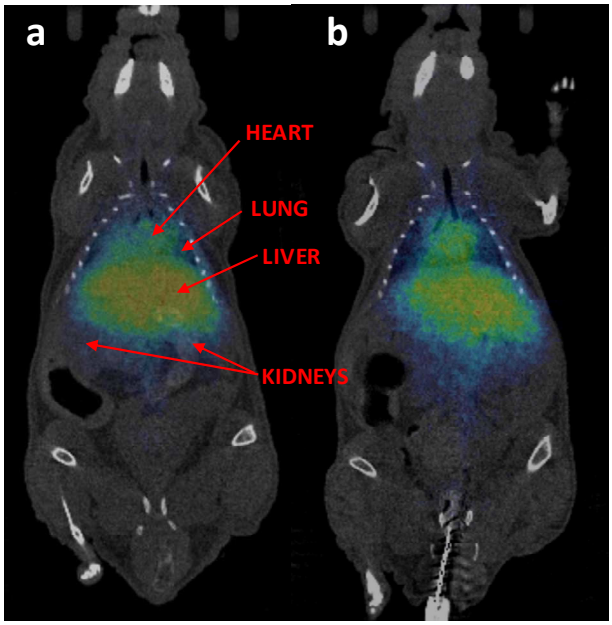

Figure 5.6. PET coronal projections resulting from averaged images (frames 12-20) obtained after administration of ^{124}I-[**5.1**]$^-$ (a) and ^{124}I-[**5.2**]$^-$ (b). Corregistration with CT images of the same animal is shown for localization of the radioactivity.

As a general trend, higher accumulation values in the brain were obtained *in vivo*, probably due to the contribution of the blood to the overall quantification of the uptake in this region. In the particular case of the lungs, the differences can be attributed to the fact that the percentage of injected dose (%ID) per gram of tissue is measured *ex vivo*, whereas *in vivo*, the %ID per cm^3 is obtained. Because the density of the lungs significantly differs from $1 g/cm^3$, the results obtained in both experiments cannot be directly compared. Differences observed in the bladder might be due to urination during image acquisition (*in vivo*) or uptake time (*ex vivo*). Interestingly, *in vivo* studies did not show accumulation of radioactivity in the thyroid gland, suggesting the stability of both ^{124}I-[**5.1**]$^-$ and ^{124}I-[**5.2**].

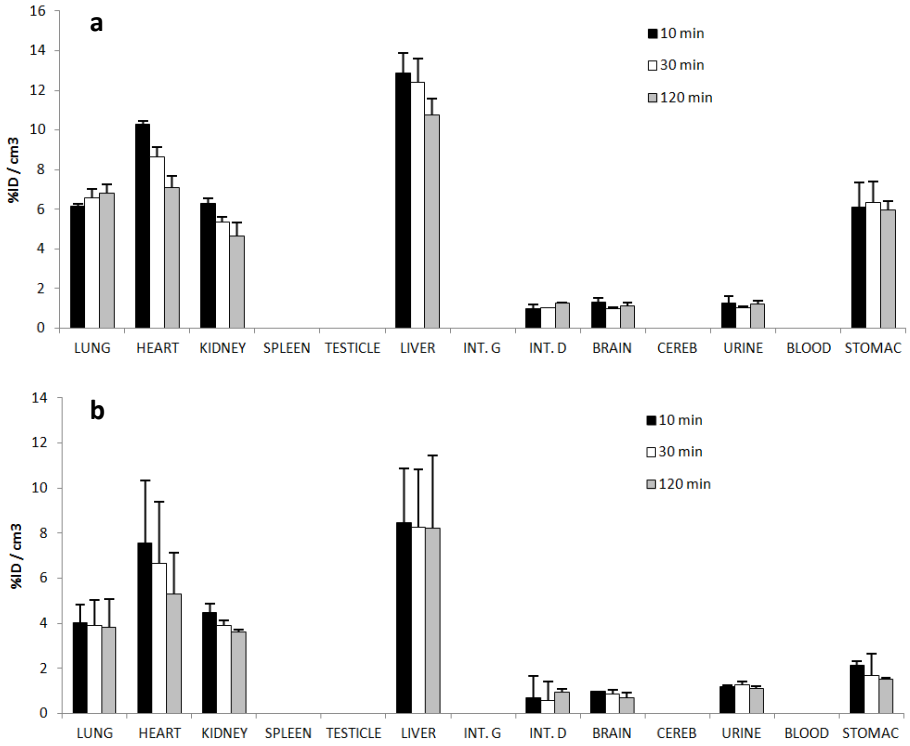

Figure 5.7 Accumulation of radioactivity in different organs for compound ^{124}I-[**5.1**]$^-$ (a) and ^{124}I-[**5.2**]$^-$ (b) determined by PET-CT at selected time points after administration; results are expressed as % of injected dose (%ID) per cm3 of tissue. Mean ± standard deviation values are presented (n=3).

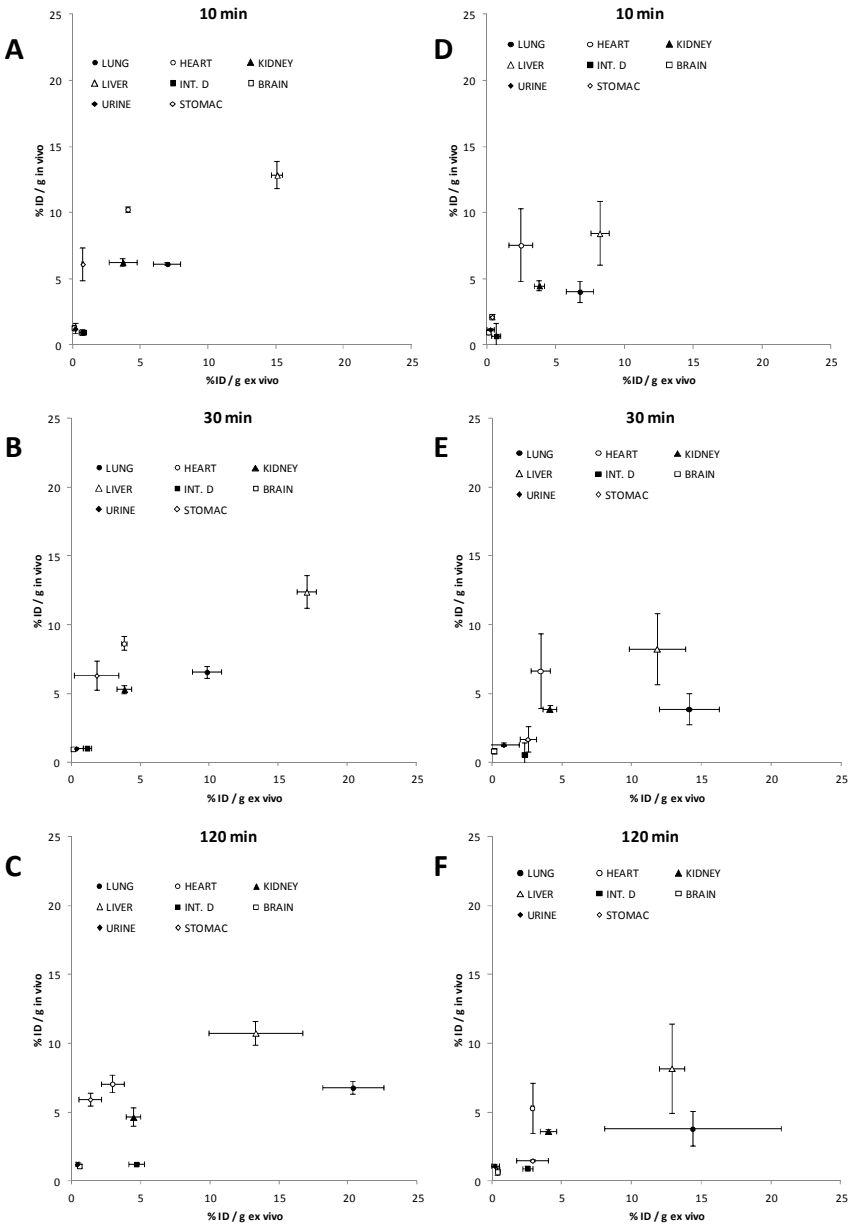

Figure 5.8. Correlation between results obtained using PET-CT (expressed as % of injected dose per cm^3 of tissue) and dissection and gamma counting (expressed as % of injected dose per gram of tissue) for compounds [**5.1**]$^-$ (A-C) and [**5.2**]$^-$ (D-F), at 10 (A, D), 30 (B, E) and 120 (C, F) minutes after administration.

5.3.2.2. Biodistribution studies in tumour bearing animals

Imaging studies were performed using two subcutaneous mouse tumour models: PANC-1 (human pancreatic carcinoma) and A549 (carcinomic human alveolar basal epithelial cell line), which were selected because of the high prevalence, morbidity and mortality associated to pancreatic ductal adenocarcinoma (PDAC) and non-small cell lung carcinoma (NSCLC). PDAC is currently the fourth leading cause of cancer death in the United States of America [15], and it is anticipated to become the second leading cause of cancer-related deaths in the year 2030 [16]. PDAC possesses a mortality rate of up to 80% within the first 6 months after diagnosis and the 5 years survival rate is only 6.7% [17]. On the other hand, lung cancer is a leading cause of malignancy-related death worldwide [18], being NSCLC the most common type, accounting for about 80% of lung cancers.

PET studies were conducted first with 2-deoxy-2-[^{18}F]fluoro-D-glucose ([^{18}F]FDG), a glucose analogue in which the hydroxyl group at the 2-position is substituted by an ^{18}F atom. This tracer is widely used in the clinical diagnostic arena for the early diagnose of a wide variety of tumours, as well as for the evaluation of the response to treatment. The basis behind accumulation of [^{18}F]FDG in tumour tissues is well known. This radiotracer is an analog of glucose with an ^{18}F atom in the 2 position in substitution of a hydroxyl group. [^{18}F]FDG is taken up by cells through the same pathways as glucose, phosphorylated and trapped in the cells (Figure 5.9); as a result, [^{18}F]FDG concentration increases in proportion to rate of utilization of glucose, and therefore it can be used as an indirect proliferation marker.

The typical biodistribution pattern for this tracer was observed in our studies (Figure 5.10A and 5.10B): High accumulation was detected in the kidneys and the bladder due to elimination mainly via urine, while significant uptake was also observed in the heart and the brain, organs which are known to consume a significant amount of glucose. For both models (PANC-1 and A549), the

[15] American-Cancer-Society, Cancer Facts & Figures 2014, in: A.C. Society (Ed.), American Cancer Society, Atlanta, **2014**
[16] L. Rahib, et al., *Cancer Res.*, **2014**, *74*, 2913-2921
[17] (a) T. Muniraj, et al., Pancreatic cancer: a comprehensive review and update, Dis. Mon., 59 (**2013**) 368-402; (b) NCI, SEER Stat Fact Sheets: Pancreas Cancer, in: N.C. Institute (Ed.), **2014**.
[18] (a) Goto H, et al., *Cancer Res* **2002**, *62*, 3711–3715

tumours could be clearly visualized on the images. Delineation of volumes of interest (VOIs) in the tumour on the CT images and subsequent quantification of the dynamic images resulted in time-activity-curves (TACs) as depicted in Figures 5.10C and 5.10D. As can be seen, the accumulation of [^{18}F]FDG in PANC-1 tumour follows a progressive increasing trend, reaching values close to 2%ID/mL at long times (t>1h) after administration. For A549 tumour, the TAC peaks at around 10 minutes after injection of the radiotracer. A progressive decrease to reach values slightly above 1%ID/mL is observed afterwards. These results confirm the presence of metabolic activity in the tumours and suggest the correct perfusion of the tumour tissue.

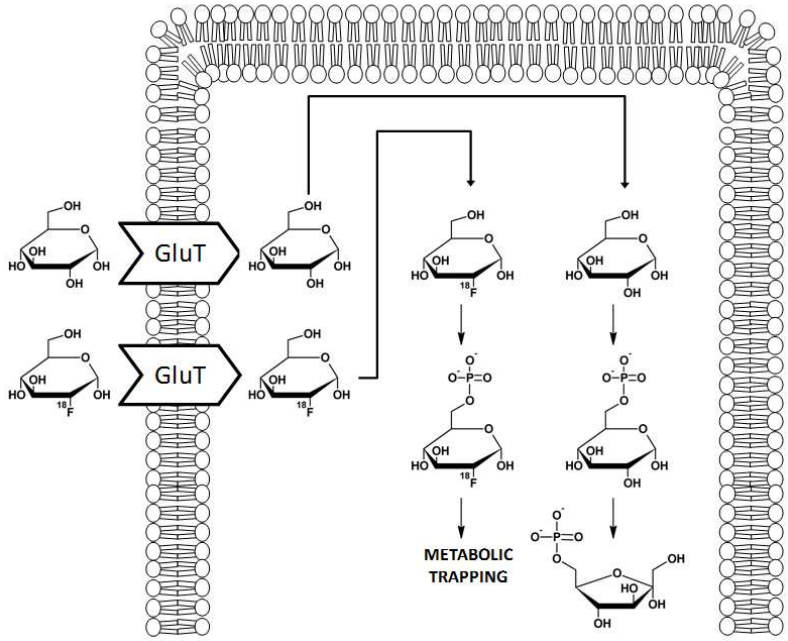

Figure 5.9. Intracellular metabolism of glucose and [^{18}F]FDG. Both are taken up by cells by means of glucose transporters (GluT). Once into the cell, they are phosphorylated to glucose-6-phosphate and [^{18}F]glucose-6-phosphate, respectively. Unlike glucose, [^{18}F]glucose-6-phosphate does not undergo further metabolism and is trapped in the cell. Obtained from [19].

[19] Gómez-Vallejo et al., New Molecular and Functional Imaging Techniques, Functional Imaging in oncology, Springer, **2014**, 491-522.

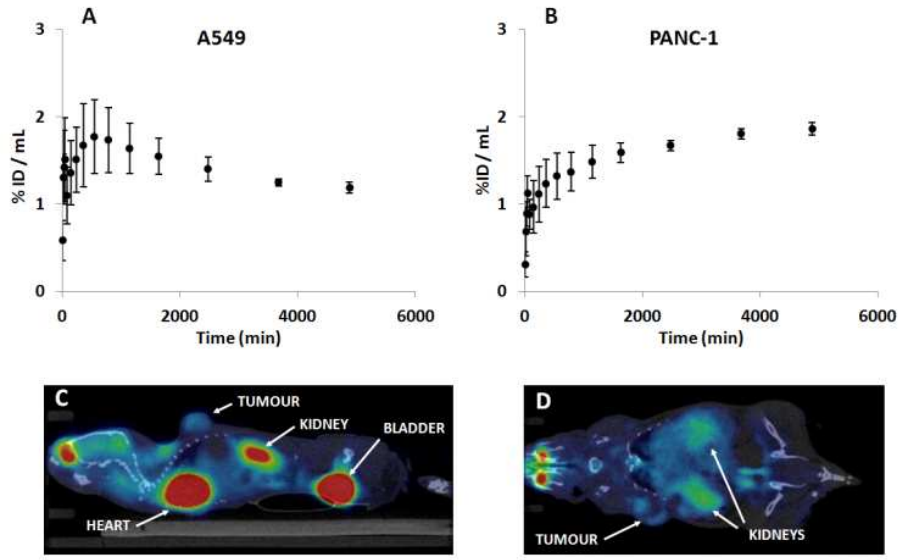

Figure 5.10. Biodistribution of [^{18}F]FDG in subcutaneous PANC-1 (human pancreatic carcinoma) and A549 (carcinomic human alveolar basal epithelial cell line) xerograft mouse models. Time-activity-curves in the tumour, expressed as the percentage of the injected dose (%ID) per cm^3 of tissue are shown in (A) and (B). PET sagital (C) and coronal (D) slices resulting from averaged images (frames 5-15) obtained after administration of [^{18}F]FDG in mice bearing A549 (C) and PANC-1 (D) tumours are shown; optimal view-point and slides were selected for correct visualization of the tumour.

The same animals were subsequently imaged using the newly developed labelled compounds (^{124}I-[**5.3**]$^-$ and ^{124}I-[**5.4**]$^-$) in order to determine the accumulation in the tumour tissue over time and to get an indication of the potential of the compounds as potential BNCT drugs. With that aim, dynamic scans were performed concomitantly with the administration of the labelled compounds. VOIs were drawn in major organs and the %ID/mL was determined as a function of time. Compound ^{124}I-[**5.1**]$^-$ was also investigated as the control.

The three labelled compounds showed a similar biodistribution pattern, irrespective of the tumour model (Figure 5.11). The high accumulation in heart suggest the long residence time of the labelled species in the blood pool. A significant uptake was observed in the liver (values of 12.9±2.4, 13.7±0.8 and 12.1±3.5 for [**5.1**]$^-$, [**5.3**]$^-$ and [**5.4**]$^-$, respectively, in A549 model; values of

9.5±2.4, 7.5±0.6 and 11.4±3.4 for [**5.1**]$^-$, [**5.3**]$^-$ and [**5.4**]$^-$, respectively, in PANC-1 model; t = 60 min post injection) and the kidneys, suggesting a combined elimination *via* the urinary and the hepatobiliary routes. Accumulation of the radiotracers could also be detected in the lungs, with values always below 5% ID/mL.

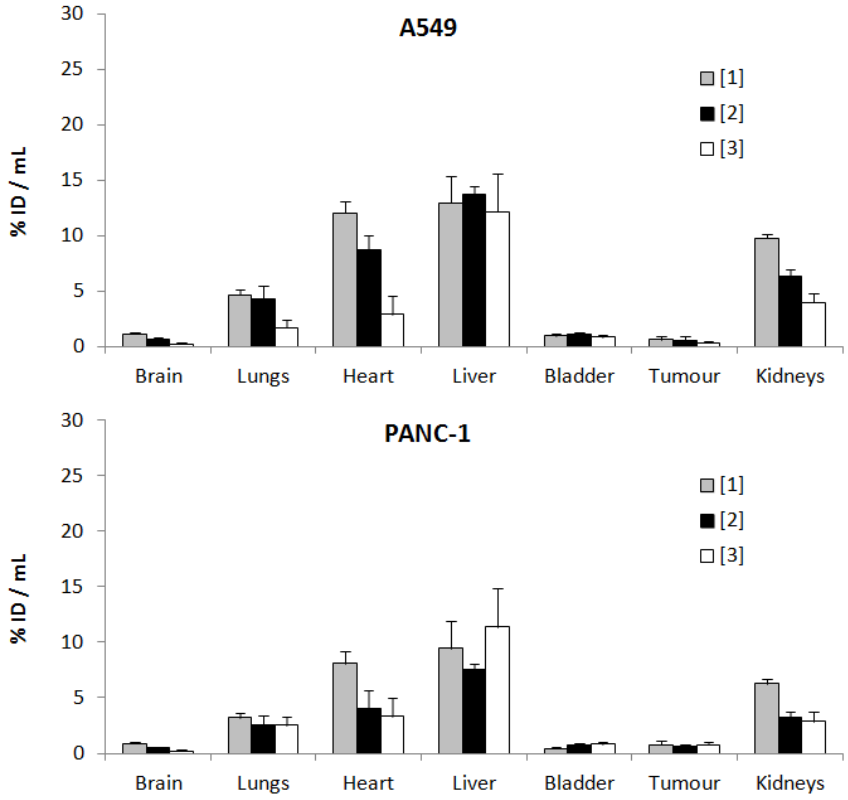

Figure 5.11. Biodistribution of ^{124}I-[**5.1**]$^-$, ^{124}I-[**5.3**]$^-$, and ^{124}I-[**5.4**]- in subcutaneous PANC-1 (human pancreatic carcinoma) and A549 (carcinomic human alveolar basal epithelial cell line) xerograft mouse models. Values are expressed as percentage of injected dose (%ID) per cm3 of tissue and correspond to t=60 minutes after administration of the radiotracer.

Accumulation in the tumour was relatively low, with values below 1%ID/g, irrespective of the compound and the tumour model. In all cases, the %ID/mL was below 1% at t=60 min after administration (A549: 0.60±0.31, 0.51±0.39 and 0.34±0.09% ID/g for [**5.1**]$^-$, [**5.3**]$^-$ and [**5.4**]$^-$, respectively; PANC-1:

0.78±0.31, 0.78±0.23 and 0.34±0.09% ID/g for [**5.1**]$^-$, [**5.3**]$^-$ and [**5.4**]$^-$, respectively).

5.4. Materials and methods

5.4.1. Cold chemistry

As mentioned above, this part of the PhD was conducted in collaboration with the group led by Prof. Francesc Teixidor and Prof. Clara Viñas, at Institut de Ciència de Materials de Barcelona (ICMAB-CSIC). The starting materials to perform the radiolabelling and subsequent *in vivo*/*ex vivo* studies (compounds **5.1**-**5.4**) were provided by this group. All the cold chemistry work was performed by the PhD student Adnana Zaulet, and the methods and characterization of the compounds can be found in her PhD thesis. They have not been included in this chapter.

5.4.2. Radiochemistry

5.4.2.1. General procedures

Radiolabelling reactions were performed by adapting the palladium catalyzed iodine exchange reaction previously reported for iodinated 1,2-dicarba-*closo*-dodecaborane (*o*-carborane) [20]. Incorporation of both ^{125}I (*ex vivo* experiments) and ^{124}I (*in vivo* experiments) was carried out.

Na[^{124}I]I (solution in 0.02M aqueous NaOH) and Na[^{125}I]I (solution in 0.1M aqueous NaOH) were obtained from Perkin Elmer and used without further purification. All solvents were HPLC grade and were degassed for 10 minutes before use.

The manipulation of radioactive materials was performed in lead-shielded cabinets (75 mm of lead) and all procedures were performed according to the current regulation on radioprotection and internal protocols.

5.4.2.2. Labelling procedure

Acetonitrile (200μL) was added to Na[^{124}I]I or Na[^{124}I]I (50 μL, 37 MBq) and the resulting solution was introduced in a 2.5 mL conic vial. The solvent was evaporated to dryness (100 °C, 5 min, constant helium flow at 20 mL/min) and 1 mg of precursor dissolved in acetonitrile (100 μL) was added together with *trans*-*bis*(acetate)*bis*[o-(di-o-tolylphosphino)benzyl] dipalladium (II)

[20] I. Rojo, et al., *Organometallics* **2003**, *22*, 3414

(Herrmann's catalyst, HC, 0.1 mg, 0.101 µmol) dissolved in toluene (100 µL). The reaction mixture was heated (100°C, 3 min for [**5.1**]$^-$; 80°C, 8 min for [**5.2**]$^-$; 70°C, 15 min for [**5.3**]$^-$; 90°C, 10 min for [**5.4**]$^-$), the solvent was removed under a constant helium flow and the resulting solid was dissolved in 1 mL of 0.1M ammonium formate (AMF)/acetonitrile (1/1) and purified by semi-preparative high performance liquid chromatography (HPLC). The purification conditions were: Stationary phase: Mediterranea Sea18 column (10x250 mm, 5 µm particle size); mobile phase: 0.1M ammonium formate (AMF) buffer pH=5.9 / acetonitrile; For compounds [**5.1**]$^-$, [**5.2**]$^-$ and [**5.3**]$^-$ isocratic elution was carried out with 80%B at a flow rate of 3 mL/min. For compound [**5.4**]$^-$, a gradient was applied: t=0 min: 70% B; t=15min: 70% B; t=18min: 100% B; t=26min: 100% B; t=28min: 70% B; t=30min: 70% B flow rate: 2ml/min. The purified fraction (RT: 13.5, 15.0, 13.75 and 11.5 min for [**5.1**]$^-$, [**5.2**]$^-$, [**5.3**]$^-$ and [**5.4**]$^-$, respectively) was reformulated by dilution with water, retention on a C-18 cartridge (Sep-Pak® Light, Waters) and further elution with ethanol (500 µL, Sigma-Aldrich). The final solution was evaporated to a final volume of 100 µL and reconstituted with saline (total volume = 1000 µL). Quality control was performed by radio-HPLC. Analytical conditions were: Stationary phase: Mediterranea Sea18 column (4.6x150 mm, 5 µm particle size); mobile phase A: 0.1M ammonium formate (AMF) buffer pH= 5.9; B: acetonitrile; flow rate = 2mL/min; In all cases, a gradient was applied. For compounds [**5.1**]$^-$, [**5.2**]$^-$ and [**5.3**]$^-$, the gradient was: t=0 min: 40% B; t=2min: 40% B; t=8min: 99% B; t=16min: 99% B; t=18min: 40% B; t=20min: 40% B. For compound [**5.4**]$^-$, the gradient was: t=0 min: 40% B; t=2min: 40% B; t=18min: 100% B; t=23min: 100% B; t=25min: 40% B; t=30min: 40% B. Retention times were 8.3, 10.0, 9.8 and 8.5min for [**5.1**]$^-$, [**5.2**]$^-$, [**5.3**]$^-$ and [**5.4**]$^-$, respectively.

5.4.3. In vivo/ex vivo studies:

5.4.3.1. Biodistribution studies in healthy mice: PET-CT

PET studies with ^{124}I-[**5.1**]$^-$ and ^{124}I-[**5.2**]$^-$ were carried out in mice (n=3 per compound) using an eXploreVista-CT small animal PET-CT system (GE Healthcare). Anesthesia was induced with 3% isoflurane and maintained by 1.5 to 2% of isoflurane in 100% O_2. For intravenous administration of the radiotracer, the tail vein was catheterized with a 24-gauge catheter and the radiotracer (250 ± 5 µCi, 100 µL) was injected concomitantly with the start of a PET dynamic acquisition.

Dynamic images (20 frames: 4x5s, 4x10s, 4x60s, 4X300s, 4x600s) were acquired in 2 bed positions in the 400-700 keV energetic window, with a total

acquisition time of 130 minutes; after each PET scan, CT acquisitions were also performed, providing anatomical information as well as the attenuation map for the later image reconstruction. Mice were kept normothermic throughout the scans using a heating blanket (Homeothermic Blanket Control Unit; Bruker).

Dynamic acquisitions were reconstructed (decay and CT-based attenuation corrected) with filtered back projection (FBP) using a Ramp filter with a cut off frequency of 1 Hz.

PET images were analyzed using PMOD image analysis software (PMOD Technologies Ltd, Zürich, Switzerland). Volumes of interest (VOIs) were manually drawn in the lungs, heart, kidneys, liver, small intestine, brain, bladder and stomach using the CT images as anatomical reference. VOIs were then transferred to the PET images and time activity curves (decay corrected) were obtained for each organ as cps/cm^3. Curves were transformed into real activity (Bq/cm^3) curves. Injected dose normalization was finally applied to data to get time activity curves as percentage of injected dose per cm^3 of tissue.

5.4.3.2. Biodistribution studies in healthy mice: dissection / gamma counting

Biodistribution studies using dissection and gamma counting were performed with ^{125}I-[**5.1**]$^-$ and ^{125}I-[**5.2**]$^-$. Three animals per compound and time point were used.

Anesthesia was induced with 3% isoflurane and maintained by 1.5 to 2% of isoflurane in 100% O_2. For intravenous administration of the radiotracer, the tail vein was catheterized with a 24-gauge catheter and the radiotracer (25 ± 5 µCi, 100 µL) was injected. The animals were kept under anesthesia throughout the duration of the study. At pre-selected time points (10, 30 and 120 minutes after administration) animals were sacrificed by exsanguination. The animals were perfused with saline solution, the organs were harvested, weighted and the amount of radioactivity was determined using a gamma counter. Comparison with a standard calibration curve enabled the determination of accumulated radiotracer as percentage of injected dose per gram of tissue.

5.4.3.3. Tumour model

Preparation of PANC-1 cells for production of xenografts consisted of collecting them in a pellet by centrifugation and a further suspension in Dulbecco's Phosphate Buffered Saline (PBS) (Lonza, Verviers, Belgium) at a concentration

of 20 x 10^6 cells/mL. The cell suspension was mixed with Matrigel (Becton Dickinson, Oak Park, Bedford, MA) and kept at 4 °C at a 1:1 (v/v) ratio. 200 µL of the mixture were used for each injection. Fifteen seven-week old male athymic-nude CD-1 Foxn1 nu/nu mice (Charles River Laboratories, Calco, Italy) were injected subcutaneously with 2 million PANC-1 cells in the upper left flank. Preparation of A549 cells was carried out following the same procedure, but the suspension in PBS was performed at a concentration of 10 x 10^6 cells/mL and mice were injected with 1 million cells.

During tumour growth, mice were housed in a controlled environment (12 hours:12 hours light/dark cycle with dawn and dusk transitional periods, room temperature 22 °C and 55% relative humidity) and maintained on an ad libitum access to commercially available pelleted diet (Teklad 2919, Harlan Laboratories, Inc.) and sterilized water. Animal weight and tumour size were monitored three times per week. The tumour volume was calculated using the formula $(L \times W^2)/2$ where L is the longest diameter (in mm) of the tumour and W (in mm) is the longest perpendicular diameter with respect to L. Both dimensions were determined with a caliper. Animals were subjected to the imaging sessions when tumour volumes reached above 150 mm^3.

5.4.3.4. Biodistribution studies in tumour-bearing mice: PET-CT

PET studies were performed using an eXploreVista-CT small animal PET-CT system (GE Healthcare). During PET studies, mice were kept normothermic using a heating blanket (Homeothermic Blanket Control Unit; Bruker). For each labelled compound, three animals were submitted to whole body (WB) scans to assess the biodistribution pattern. In all cases, anesthesia was induced with 2-4% isoflurane and maintained by 1.5 to 2% of isoflurane in 100% O_2. For administration of the labelled species, the tail vein was catheterised with a 24-gauge catheter and 10-15 MBq were injected in tandem with the start of a PET dynamic acquisition.

Dynamic images were acquired in 2 bed positions in the 400-700 keV energy window, with a total acquisition time of 68 minutes; after each PET scan, CT acquisitions were also performed, providing anatomical information as well as the attenuation map, for the later image reconstruction. Dynamic acquisitions were reconstructed (decay and CT-based attenuation corrected) with filtered back projection (FBP) using a Ramp filter with a cut off frequency of 1 Hz.

PET images were analysed using PMOD image analysis software (PMOD Technologies Ltd, Zürich, Switzerland). Volumes of interest (VOIs) were

manually drawn in the lungs, brain, liver, kidneys, bladder and tumour, using the CT images as anatomical reference. VOIs were then transferred to the PET images and the concentration of radioactivity was obtained as explained above. The same procedure was followed for [^{18}F]FDG studies, but ROIs were only drawn in the tumour.

5.5. Summary and conclusions

Compounds [**5.1**]$^-$, [**5.2**]$^-$, [**5.3**]$^-$ and [**5.4**]$^-$ could be efficiently labelled with ^{125}I and ^{124}I by isotopic exchange in the presence of a palladium catalyst. After optimization of experimental conditions, good-to-excellent radiochemical conversion values could be achieved, resulting in appropriate radiochemical yields to approach *in vivo* and *ex vivo* studies.

Biodistribution studies performed both with PET-CT and dissection/gamma counting with labelled [**5.1**]$^-$ and [**5.2**]$^-$ showed a similar pattern, with significant accumulation in the heart (suggesting the presence of the labelled species in the blood pool), the liver and the kidneys.

Accumulation of compounds ^{124}I-[**5.1**]$^-$, ^{124}I-[**5.3**]$^-$ and ^{124}I-[**5.4**]$^-$ was investigated also in animals bearing subcutaneous PAC-1 and A549 tumours. For all compounds, the accumulation in the tumour was low. Appropriate perfusion and metabolism in the tumours was confirmed by PET-[^{18}F]FDG.

6. SYNTHESIS AND RADIOLABELLING OF 2-CARBORANYL BENZOTHIAZOLES

6.1. Introduction

Outstanding advances in the early diagnosis and treatment of cancer have raised the 5-year relative survival rate for all cancers combined from 50% (1974) to 68% (2007) [1]; however, cancer still accounted for 8.2 million deaths worldwide in 2012 [2]. Hence, the identification of novel structures useful for the design of new, potent, selective and less-toxic anticancer agents is still a major challenge to medicinal chemistry researchers.

Benzothiazoles are fused bicyclic systems and show interesting biomedical properties such as neuron protective [3], anti-malarial [4], and anti-inflammatory [5] effects, among others [6]. However, one of the most promising fields for benzothiazole derivatives is the development of anti-cancer drugs. Indeed, the benzothiazole moiety with various substitutions shows anti-tumour activity and a series of potent and selective anti-tumour agents have been developed to date [7]. Different mechanisms of action are involved in the anti-cancer properties of substituted benzothiazoles, as they can act as replication and mitosis inhibitors (compounds **6.1**-**6.3**, Figure 6.1) [8], Topoisomerase II inhibitors (compounds **6.4**-**6.6**, Figure 6.1) [9], tyrosine kinase inhibitors (compound **6.7**, Figure 6.1) [10], and cytochrome P450 inhibitors (compound **6.8**, Figure 6.1) [11].

2-(4-Aminophenyl)benzothiazole (CJM 126, Figure 6.2), which was originally prepared as a synthetic intermediate for the preparation of polyhydroxylated 2-phenylbenzothiazoles, was found to elicit pronounced inhibitory effects against certain breast cancer cell lines in vitro [12]. Interestingly, structure-activity relationship studies performed with analogues of CJM 126 showed that

[1]National Cancer Institute at the National Institute of Health. Available online: http://www.cancer.gov /cancertopics/factsheet /cancer-advances-in-focus/cancer (accessed on 14 May 2014).
[2] International Agency for Research on Cancer. GLOBOCAN 2012: http://globocan.iarc.fr/Pages/fact_sheets_cancer.aspx (accessed on 14 May 2014).
[3] (a) Nogradi, A., ET AL., *Eur. J. Neurosci.* **2001**, *13*, 113-118; (b) Bae, H J., et al., *Neurosci. Lett.* **2000**, *294(1)*, 29-32
[4]Burger, A., et al., *J. Med. Chem.* **1968**, *11*, 270-273.
[5] Lee, Y. R., et al., *Biochem. Biophys. Res. Commun.* **2011**, *408(4)*, 625-629; (b) Paramashivappa, R., et al., *Bioorg. Med. Chem. Lett.* **2003**, *13(4)*, 657-60.
[6] Ahmed, K., et al., *Expert Opin. Investig. Drugs.* **2012**, *21(5)*, 619-635.
[7] Sharma, P. C., et al., *J. Enzyme Inhib. Med. Chem.* **2013**, *28(2)*, 240-66.
[8] Tuylu, B. A, et al., *Biologia* **2007**, *62*, 626-632.
[9] Choi, S. J.et al., *Bioorg. Med. Chem.* **2006**, *14*, 1229-1235.
[10] Bhuva, H. A., et al., *J. Mol. Graph. Model.* **2010**, *29*, 32-37.
[11] Hutchinson, I., et al., *Bioorg. Med. Chem. Lett.* **2003**, *13*, 471-474.
[12] Shi, D.-F., et al., *J. Med. Chem.* **1996**, *39*, 3375-3384.

substitution at 3-position in the phenyl ring with an halogen atom or alkyl group enhanced potency in breast carcinoma and extended the in vitro spectrum to ovarian, lung, renal and colon carcinoma human cell lines [12]. However, replacement of halogen atoms with cyano- or hydroxy- substituents at the 3-position and introduction of chloro- substituent at the 21-position of the aminophenyl group showed reduced activity compared to the parent amine CJM 126 [13]. These results suggest that small modifications in the structure severely influence the biological action of compounds in this series [14].

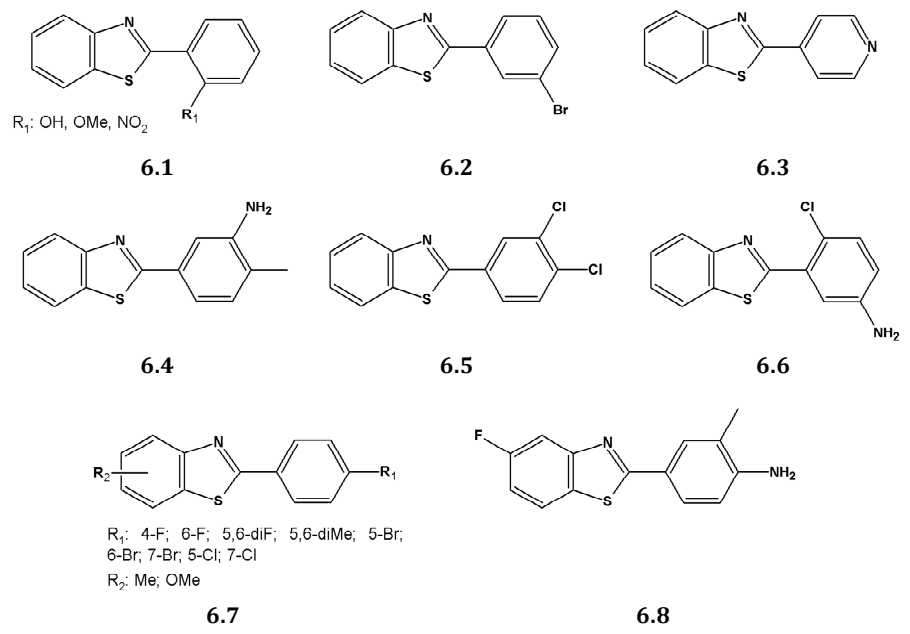

Figure 6.1. Chemical structure of benzothiazole derivatives with anticancer properties.

As mentioned above (see chapter 4), dicarba-*closo*-dodecaboranes (commonly known as carboranes) are polyhedral clusters containing boron, hydrogen and carbon atoms, and have unique structural and chemical properties, e.g. rigid geometry, rich derivative chemistry, thermal and chemical stability and exceptional hydrophobic character. Because of this, carboranes have been used in different fields. In the context of medicinal applications, Endo and co-

[13] Bradshaw, T. D.; et al., *Brit. J. Cancer* **1998**, *77(5)*, 745-752.
[14] Dubey, R.; et al., *Mini Rev. Med. Chem.* **2006**, *6*, 633-637.

workers [15] showed that 1,2- and 1,7-dicarba-*closo*-dodecaborane (*o*- and *m*-carborane) can act as a hydrophobic structure of different biologically active molecules, because the carborane cage has a rotating volume similar to the phenyl group. Based on a similar approach, our group recently reported the preparation of analogues of the D_2 receptor antagonist Raclopride, by replacing the poly-substituted phenyl moieties by different carborane clusters (*o*-carborane, *m*-carborane, and 1-methyl-*o*-carborane) [16], as well as the preparation of new analogues of Rimonabant (a CB1 receptor antagonist first developed by Sanofi-Aventis [17] which has recently been approved in the European Union for the treatment of obesity) incorporating different carborane cages in their structure [18].

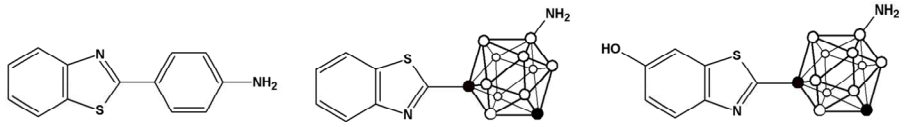

CJM 126 **6.15** **6.22**

Figure 6.2. Chemical structure of CJM 126 and the two analogues incorporating *m*-carborane, developed in the current work.

6.2. Aim and objectives

In this chapter, we include the preparation of two analogues of 2-(4-aminophenyl)benzothiazole in which the phenyl ring has been substituted by a m-carborane cage (compounds **6.15** and **6.22**, Figure 6.2). The inclusion of the carboranyl moieties may modulate the physic-chemical properties of the final compounds, which might result in an enhancement of the anti-tumour activity of the resulting benzothiazol derivatives.

Moving towards *in vivo* applications, strategies for the preparation of the *N*-[^{11}C]methylated derivatives of **6.15** and **6.22** have been implemented. Carbon-11 is a positron emitter with a half-life of 20.4 min; hence, the radiolabelled analogues might be used for the *in vivo* investigation in animal models using Positron Emission Tomography (PET).

[15] (a) Endo, Y., et al., *J. Med. Chem.* **1999**, *42*, 1501-1504; (b) Ogawa, T., et al., *Bioorg. Med. Chem. Lett.* **2006**, *16*, 3943-3946.
[16] Vázquez, N., et al., *Tetrahedron. Lett.* **2011**, *52*, 615-618.
[17] Rinaldi-Carmona, M., et al., *FEBS Lett.* **1994**, *350*, 240-244.
[18] Vázquez, N., et al., *Tetrahedron Lett.* **2012**, *53*, 4743-4746.

6.3. Results and discussion

One of the most convenient routes for the preparation of 2-substituted phenyl benzothiazoles consists of reacting benzoic acid with *o*-aminothiophenol in the presence of thionyl chloride [19], which leads to the in situ generation of the acid chloride and subsequent formation of the phenyl benzothiazole with excellent yields for a large collection of aromatic carboxylic acids. For the preparation of **6.15** we followed a similar strategy (see Figure 6.3) but starting from *m*-carboranyl carboxylic acid (6.10), obtained by reaction of *m*-carborane (6.9) with *n*-BuLi and CO_2. Further reaction with phosphorous pentachloride yielded the corresponding acid chloride (6.11), which was refluxed with 2-aminothiophenol and 2,4-bis(4-methoxyphenyl)-1,3,2,4-dithiadiphosphetane-2,4-dithione (Lawesson's reagent) in toluene to form 1-(1,7-dicarba-closo-dodecaboran-1-yl)-benzothiazole (6.12) in good overall yield (72.6%).

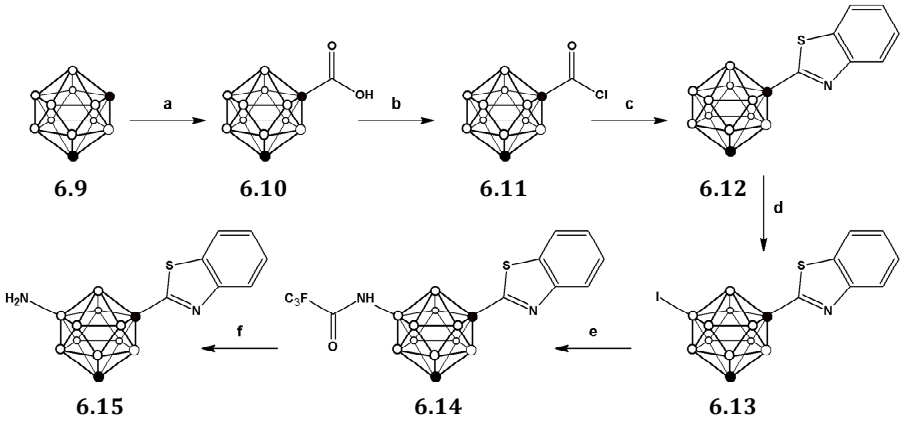

Figure 6.3. Schematic synthetic pathway followed for the preparation of compounds **6.10-6.15**; a) *n*-BuLi, CO_2; b) PCl_5; c) 2-aminophenol, Lawesson's reagent, toluene; d) ICl, $AlCl_3$; e) trifluoroacetamide, K_3PO_4, tris(dibenzylideneacetone)dipalladium, Davephos, toluene; f) NaOH.

In order to incorporate the amino group on the *m*-carborane cage, a previously reported methodology was applied [20]. Briefly, 1-(1,7-dicarba-closo-dodecaboran-1-yl)-benzothiazole dissolved in dichloromethane was iodinated using iodine monochloride (ICl) in the presence of catalytic amount of aluminum chloride. In principle, the incorporation of iodine can take place in

[19] Rudrawar, S., et al., *Synthesis* **2005**, *15*, 2521-2526.
[20] Sevryugina, Y., et al., *Inorg. Chem.* **2010**, *49*, 10627–10634.

different positions, either on the carborane cage or the aromatic ring. However, when one equivalent of iodine monochloride was used, the iodination took place preferentially on the *m*-carborane cage, leaving the phenyl ring unsubstituted as confirmed by ^{1}H-, and ^{11}B- and ^{11}B{^{1}H}-NMR (Figure 6.4). Boron atoms 9 and 10 have the highest electron density and hence these are the most susceptible positions to electrophilic halogenation [21]. In our case, the presence of only one boron atom which is a singlet both in ^{11}B- and ^{11}B{^{1}H}-NMR spectra (integration pattern 1:1:1:1:1:1:1:1:1:1, see Figure 6.4) confirmed the mono-substitution on the carborane cage.

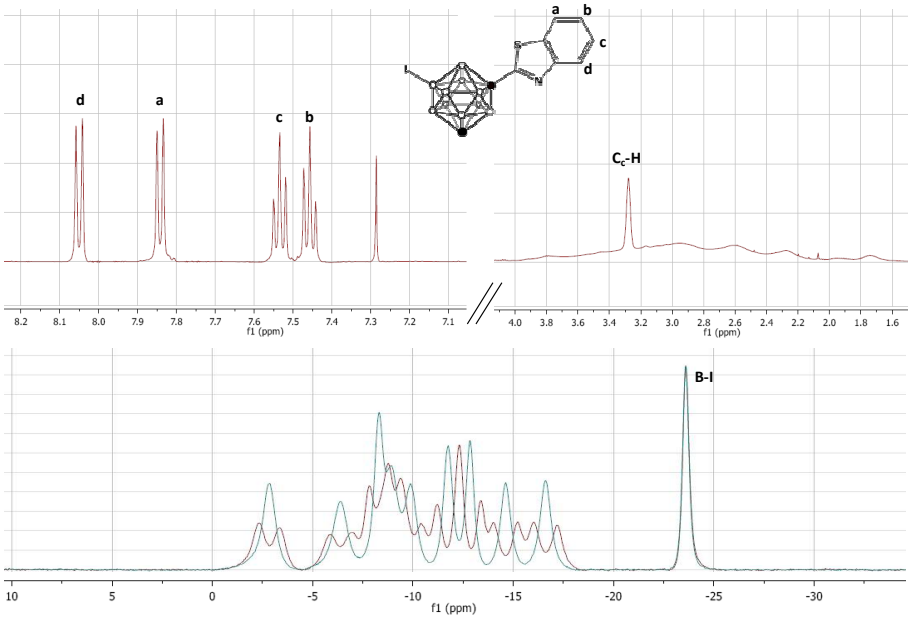

Figure 6.4. Top: ^{1}H-NMR spectra for compound **6.13**; bottom: ^{11}B- (red) and ^{11}B{^{1}H}-NMR (blue) spectra for compound **6.13**. The presence of 4 signals (integration 1:1:1:1) in the aromatic region and one signal (integration: 1) in the C_c-H region (top) together with the presence of a singlet in the ^{11}B-NMR spectra (-23.55 ppm) confirm the incorporation of the iodine atom on one of the boron atoms of the carborane cage.

The trifluoroacetamide group was subsequently introduced by palladium-catalyzed Buchwald-Hartwig amidation reaction to yield compound **6.14**; subsequent hydrolysis under basic conditions using sodium hydroxide resulted

[21] Grimes, R. N. Carboranes. New York: Academic Press Inc. **1970**.

in the formation of compound **6.15**, which was further used for the preparation of the *N*-[^{11}C]methylated derivative (*vide infra*).

The preparation of compound **6.22** (see Figure 6.5 for structure) was first envisioned using a similar synthetic strategy.

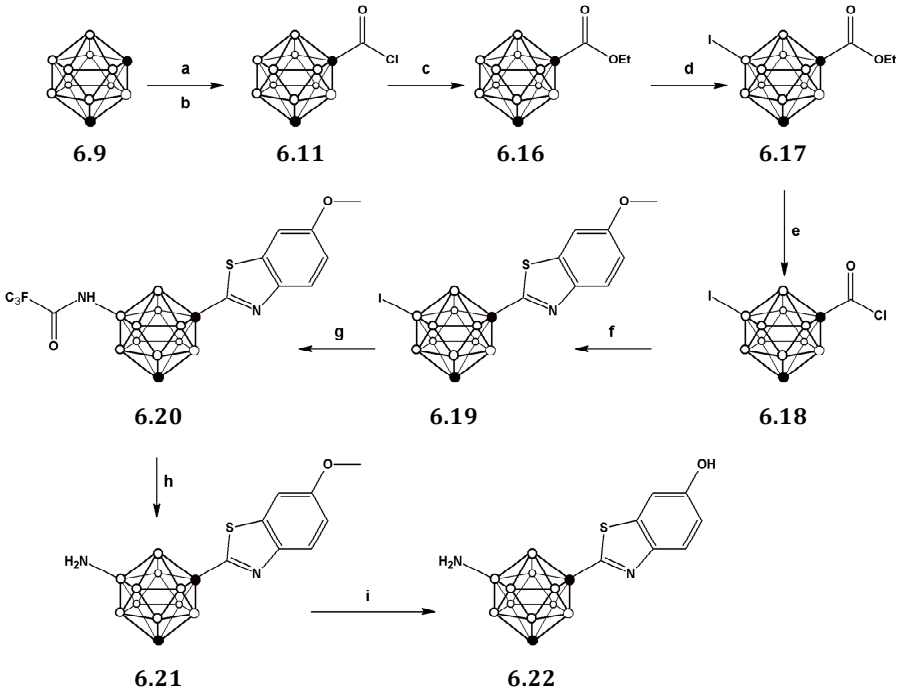

Figure 6.5. Schematic synthetic pathway followed for the preparation of compounds **6.16-6.22**; a) *n*-BuLi, CO_2; b) PCl_5; c) ethanol; d) ICl, $AlCl_3$; e) 2N aqueous NaOH, PCl_5; f) 2-amino-5-methoxythiophenol, Lawesson's reagent, toluene; g) trifluoroacetamide, tris(dibenzylideneacetone)dipalladium, Davephos, K_3PO_4, toluene; h) NaOH; i) 1M BBr_3 in DCM.

First, *m*-carboranyl carboxylic acid chloride (**6.11**) was prepared as above and further reacted with 2-amino-5-methoxythiophenol to yield 1-(1,7-dicarba-*closo*-dodecaboran-1-yl)-6-hydroxymethyl benzothiazole in good overall yield (71.2%). However, treatment of this compound with ICl in the presence of aluminum chloride resulted in preferential iodination on the phenyl ring, probably due to the electron-donnor character of the hydroxyl group which activates the *ortho* positions. Hence, an alternative synthetic route was

approached; in this case, iodination was performed before attaching the substituted benzothiazole ring (Figure 6.5). Briefly, the *m*-carboranyl carboxylic acid chloride (**6.11**) was esterified by treatment with ethanol, and subsequently iodinated using ICl in the presence of a catalytic amount of aluminum chloride to yield **6.17**. Compound **6.18**, obtained after hydrolysis and treatment with phosphorous pentachloride, was reacted with 2-amino-5-methoxythiophenol to yield **6.19**. Buchwald-Hartwig amidation using trifluoro acetamide followed by hydrolysis produced compound **6.21**, which after O-demethylation yielded compound **6.22** with overall yield of 6.4% (starting from compound **6.9**). This compound was also used for subsequent radiolabelling (*vide infra*).

The development of new drugs requires several steps before moving to clinical trials. Apart from evaluating *in vitro* efficacy and toxicity, one of the first steps is the determination of the pharmacokinetic properties (Absorption, Distribution, Metabolism and Elimination, ADME) in experimental animals. In this context, one attractive alternative consists of incorporating in the molecules under investigation a radioactive atom (namely, a positron or gamma emitter) which enables the subsequent non-invasive investigation of the biodistribution pattern using nuclear imaging techniques such as PET and SPECT. In this work, we selected Carbon-11 for the preparation of N-[^{11}C]methylated derivatives of compounds **6.15** and **6.22**. This positron emitter with a half-life of 20.4 minutes can be efficiently obtained in commercially available cyclotrons as [^{11}C]CH_4 or [^{11}C]CO_2, which can be robustly converted into a convenient methylating agents (e.g. [^{11}C]CH_3I or [^{11}C]CH_3OTf).

Radiolabelling of compounds **6.15** and **6.22** to yield [^{11}C]**6.23** and [^{11}C]**6.24** (Figure 6.7) was achieved by using two synthesis boxes, as schematized in Figure 6.6. The methylation reaction was conducted by treatment of the appropriate precursor with [^{11}C]CH_3OTf, which was synthesized with high specific activity following a well-established methodology in our laboratory [22]. Briefly, [^{11}C]CH_4 was generated by proton irradiation of a gas N_2/H_2 mixture and allowed to react with iodine at a temperature of 720°C to form [^{11}C]CH_3I, which was selectively trapped and subsequently distilled under continuous helium flow through a trap filled with silver triflate fixed on Carbowax® 1500 80/100 in an online flow-through process at 180°C to produce [^{11}C]CH_3OTf. The methylation reaction was conducted in a 2 mL

[22] Gómez-Vallejo, V., et al., *Nucl. Med. Commun.* **2011**, *32(11)*, 1011-1017.

stainless steel loop at room temperature, previously charged with a solution of the precursor (**6.15** or **6.22**).

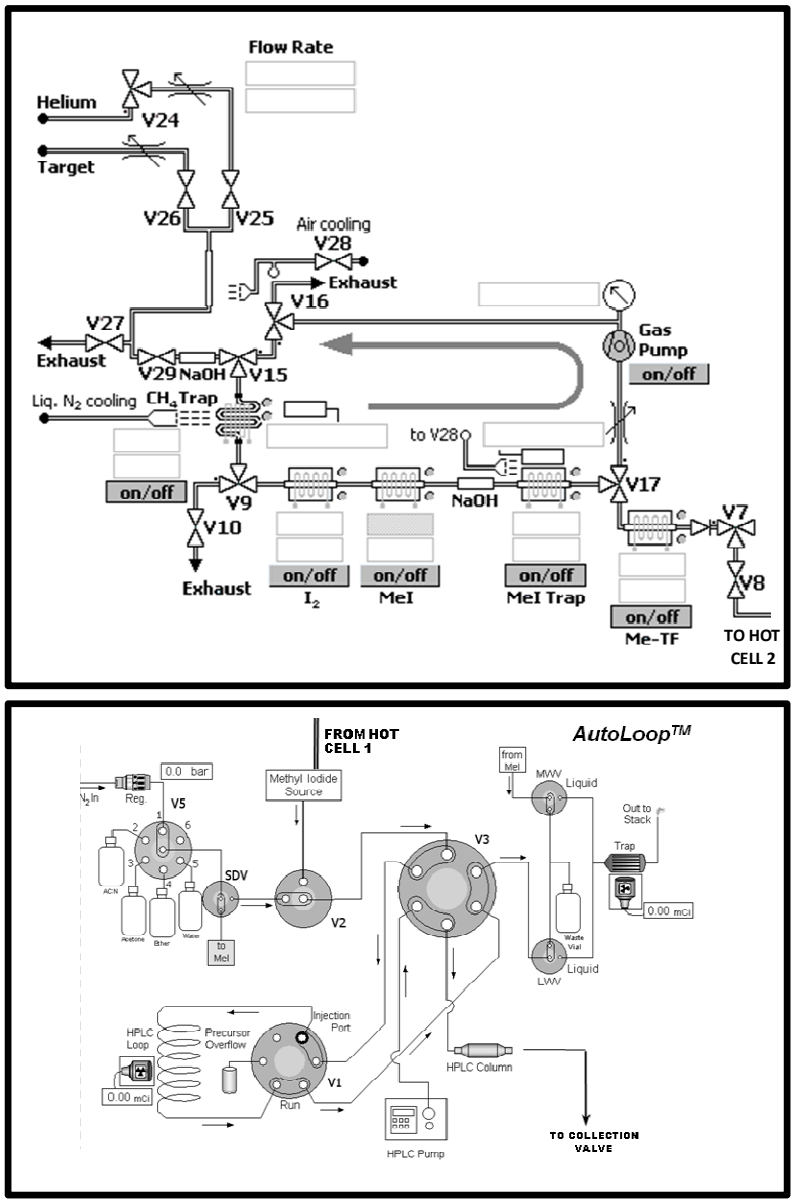

Figure 6.6. Schematic diagram of the two synthesis boxes used for the preparation of [^{11}C]**6.23** and [^{11}C]**6.24**.

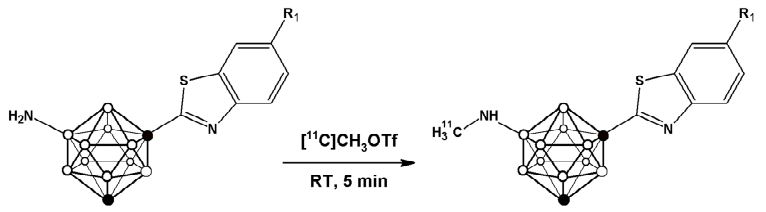

6.15 R_1 = H
6.22 R_1 = OH

[^{11}C]**6.23** R_1 = H
[^{11}C]**6.24** R_1 = OH

Figure 6.7. Schematic reaction for the preparation of [^{11}C]**6.23** and [^{11}C]**6.24** using [^{11}C]CH_3OTf as the labelling agent.

Initially, the methylation reaction was attempted using [^{11}C]CH_3I as the labeling agent and DMSO as the solvent. Radiochemical conversion values below 30% (as calculated from chromatographic profiles) were obtained when 10M aqueous NaOH was used as the base, irrespective of the amount of base (2-20 μL) and the reaction time (1-10 min). In our configuration, *in-loop* reactions have to be conducted at room temperature, and hence [^{11}C]CH_3OTf, which is a better methylating agent, was considered as a suitable alternative. When this labeling agent was used, radiochemical conversion values of 72±4% and 67±7% were obtained for **6.15** and **6.22**, respectively, when the reaction was carried out for 5 min at room temperature using 1 mg of precursor; interestingly, the addition of a base was not required.

Complete syntheses for both molecules were conducted including purification (carried out by High Performance Liquid Chromatography -HPLC-). The collected fractions (retention times of 9.2 and 6.4 minutes for [^{11}C]**6.23** and [^{11}C]**6.24**, respectively; see Figures 6.8A-B and 6.9A-B for examples of chromatographic profiles) were reformulated by trapping in a C-18 cartridge, further elution with ethanol and reconstitution with physiologic saline solution. Average production times from the end of the bombardment were 36 and 32 min for [^{11}C]**6.23** and [^{11}C]**6.24**, respectively; decay corrected radiochemical yields were 31.7 ± 5.6% and 20.5 ± 6.1%, respectively. The radiochemical purity at the end of the synthesis, as determined by HPLC (see experimental section, retention times of 11.5 and 9.0 minutes for [^{11}C]**6.23** and [^{11}C]**6.24**, respectively) was >98% (see Figures 6.10-6.11 for examples of chromatographic profiles after purification). Specific radioactivity values, according to historical values obtained in our laboratory with the same automatic configuration, were estimated to be in the range 80–120GBq/μmol

(EOS). Identification of the labelled species was carried out by HPLC-MS on the collected fractions after complete decay. The measured mass of the molecules were detected as $[M + H]^+$ (m/z = 307.2 and retention time = 9.51 min for [^{11}C]**6.23**; m/z = 323.2 and retention time = 8.39 min for [^{11}C]**6.24**; Theoretical m/z = 307.4 and 323.4, respectively; see Figures 6.8C-D and 6.9C-D for example of chromatographic profile and MS spectrum).

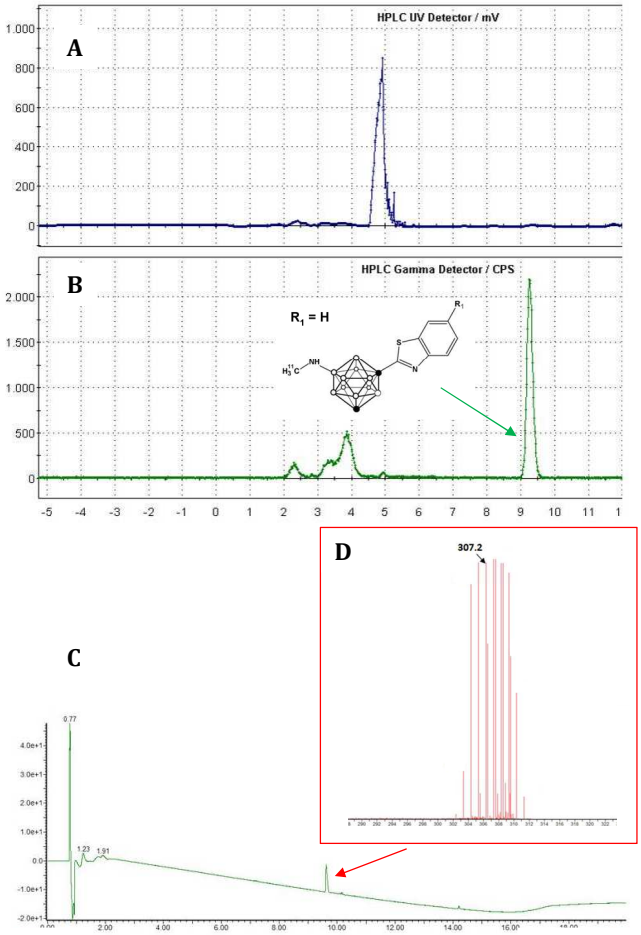

Figure 6.8. (A, B) Chromatographic profiles corresponding to the purification of [^{11}C]6.**23**: (A) UV detector and (B) radiometric detector. The collected fraction is indicated with an arrow in the radiometric profile; (C) chromatographic profile corresponding to LC-MS analysis of pure [^{11}C]**6.23** after complete decay; (D) MS spectrum for maximum intensity peak.

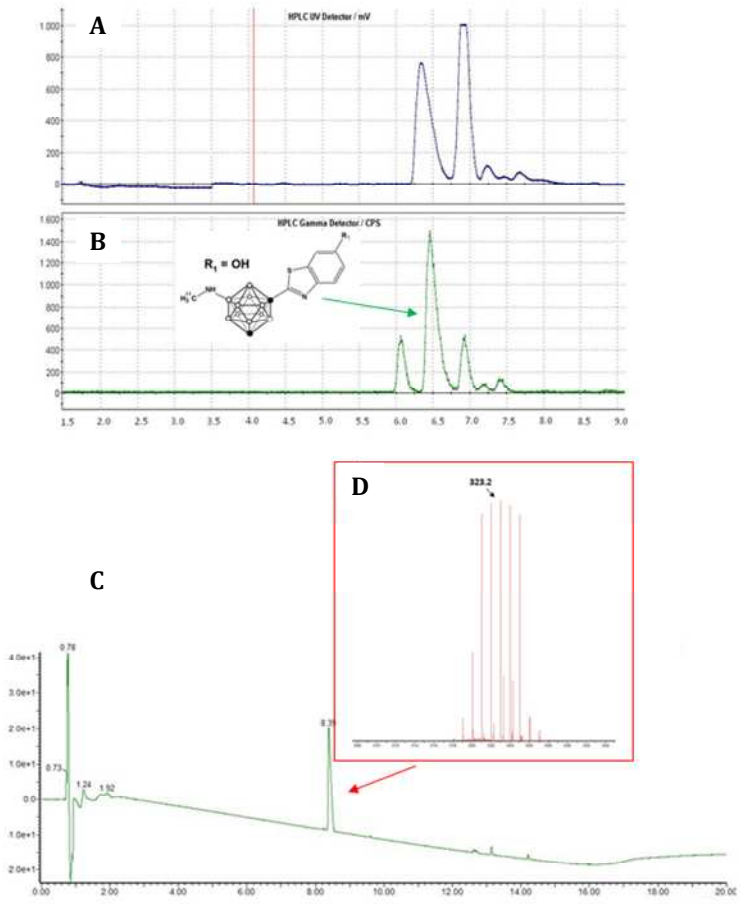

Figure 6.9. (A, B) Chromatographic profiles corresponding to the purification of [^{11}C]**6.24**: (A) UV detector and (B) radiometric detector. The collected fraction is indicated with an arrow in the radiometric profile; (C) chromatographic profile corresponding to LC-MS analysis of pure [^{11}C]**6.24** after complete decay; (D) MS spectrum for maximum intensity peak.

Despite not performed in the context of this PhD thesis, yield, specific activity, and radiochemical purity values obtained at the end of the synthetic process should enable subsequent *in vivo* investigations in animal models.

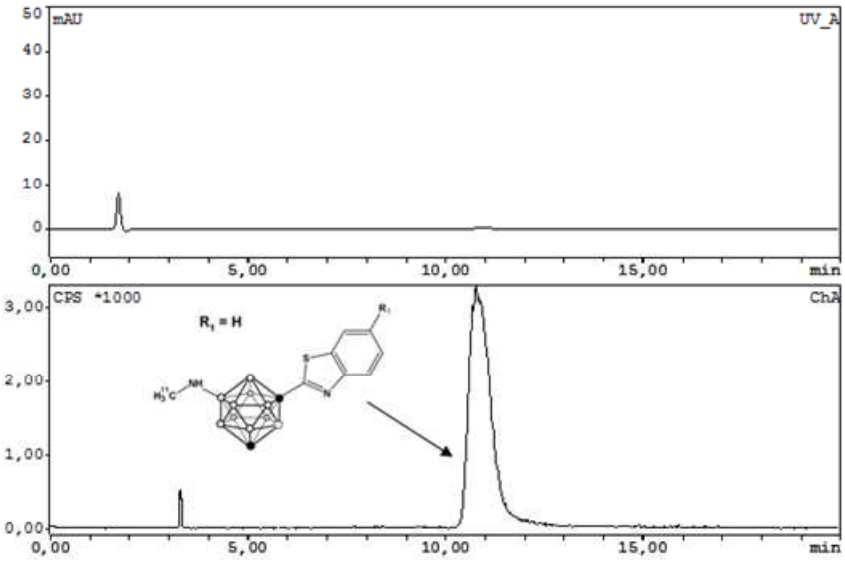

Figure 6.10. Chromatographic profiles corresponding to the quality control of [^{11}C]**6.23**: UV detector (top) and radiometric detector (bottom).

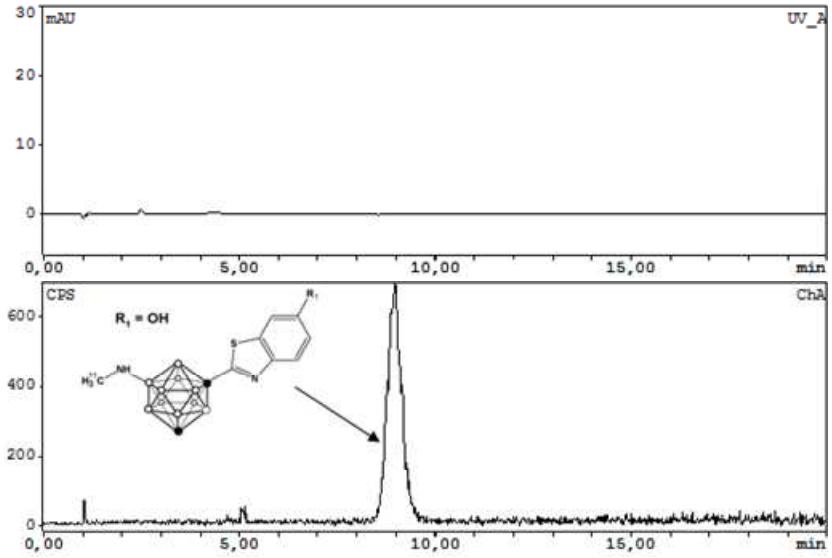

Figure 6.11. Chromatographic profiles corresponding to the quality control of [^{11}C]**6.24**: UV detector (top) and radiometric detector (bottom).

6.4. Materials and methods

6.4.1. Cold chemistry

6.4.1.1. General procedures

1,7-dicarba-*closo*-dodecaborane was purchased from Katchem Ltd. (Prague, Czech Republic); All other reagents and anhydrous solvents, stored over 4 Å molecular sieves, were purchased from Aldrich Chemical Co. (Madrid, Spain) and used without further purification. HPLC grade solvents (ethanol, methanol, and acetonitrile) were purchased from Scharlab (Sentmenat, Barcelona, Spain) and used as received. Reactions were performed under inert atmosphere. Analytical thin layer chromatography (TLC) measurements were conducted with silica gel 60 F254 plates (Macherey-Nagel). Visualization was accomplished with a UV source (254, 365 nm) and by treatment with an acidic solution of 1% PdCl2 in methanol. Carboranes charred as black spots on TLC. Manual chromatography was performed with silica gel 60 (70-230 mesh) from Scharlau.

^{1}H-, ^{11}B- and ^{11}B{^{1}H}-NMR spectra were recorded on a 500-MHz Avance III Bruker spectrometer. Chemical shifts were reported in ppm with the solvent resonance as the internal standard (CHCl3: δ 7.26 ppm). ^{13}C-NMR spectra were recorded on an Avance III Bruker spectrometer (126 MHz) with complete proton decoupling. Chemical shifts are reported in ppm with the solvent resonance as the internal standard ($CDCl_3$: δ 77.0 ppm).

UPLC/ESI-MS analyses were performed using an AQUITY UPLC separation module coupled to a LCT TOF Premier XE mass spectrometer (Waters, Manchester, UK). An Acquity BEH C18 column (1.7 μm, 5 mm, 2.1 mm) was used as stationary phase. The elution buffers were A (water and 0.1% formic acid) and B (Methanol and 0.1% formic acid). The detection was carried out in both positive & negative ion modes, monitoring the most abundant isotope peaks from the mass spectra.

6.4.1.2. Synthetic procedures and spectroscopic data

*Synthesis of 1,7-dicarba-closo-dodecarborane-1-carboxylic acid (**6.10**) and 1,7-dicarba-closo-dodecarborane-1-carboxylic acid chloride (**6.11**)*

Compounds **6.10** and **6.11** were prepared following previously reported methods [23]. Briefly, *m*-carborane (3.0 g, 20.97 mmol) was dissolved in diethylether (150 mL) and treated with *n*-BuLi (14.4 mL, 23.07 mmol, 1.6 M in hexane) at -78°C. The resulting mixture was stirred for 20 min and then dry ice (7.5 g) was added. The mixture was brought to room temperature and further stirred for 1 h. The solvent was removed under reduced pressure, water (100 mL) was added to the residue and unreacted *m*-carborane was extracted with hexane (2 x 50 mL). The aqueous phase was acidified with 3 N HCl and extracted with hexane (4 x 40 mL).

The organic layers were combined, dried over Na_2SO_4, and concentrated to yield 1,7-dicarba-*closo*-dodecarborane-1-carboxylic acid (3.52g, 90% yield) as a white solid.

^{1}H-NMR (500 MHz, $CDCl_3$): δ 8.89, (1H, bs, COOH), 3.05 (1H, s, cage C-H), 3.70-1.20 (10H, m, $B_{10}H_{10}$); ^{13}C-NMR (126 MHz, $CDCl_3$): 167.15, 71.16, 54.85; ^{11}B-NMR (160 MHz, $CDCl_3$): -4.87 (d, 1B), -6.49 (d, 1B), -10.52 (d, 2B), -11.25 (d, 2B), -13.15 (d, 2B) , -15.63 (d, 2B).

*Synthesis of 1-(1,7-dicarba-closo-dodecaboran-1-yl)-benzothiazole (**6.12**)*

To a solution of 1,7-dicarba-*closo*-dodecarborane-1-carboxylic acid chloride (0.55 g, 2.67 mmol) in dry toluene (15ml), 2-aminothiophenol (860 µl, 8.02 mmol) and Lawesson's reagent (378 mg, 0.96 mmol) were added and the resulting mixture was refluxed for 14h. The mixture was concentrated, water (100 mL) was added and the mixture was extracted with dichloromethane (3 x 50 mL). The combined organic layers were dried over Na_2SO_4, concentrated and purified using silica gel column chromatography (starting mobile phase: hexane; final mobile phase: 3% ethyl acetate) to afford 1-(1,7-dicarba-*closo*-dodecaboran-1-yl)-benzothiazole (610mg, 83% yield) as a yellow solid.

^{1}H-NMR (500 MHz, $CDCl_3$): 8.05 (1 H, dt, CH, phenyl), 7.83 (1 H, dt, CH, phenyl), 7.52 (1 H, ddd, CH, phenyl), 7.44 (1 H, ddd, CH, phenyl), 3.17 (1 H, d, cage C-H), 3.70-1.70 (10H, m, $B_{10}H_{10}$); ^{13}C-NMR (126 MHz, $CDCl_3$): 162.39, 152.57, 135.86, 126.73, 126.17, 123.83, 121.32, 73.37, 55.34; ^{11}B-NMR (160 MHz, $CDCl_3$): -3.82 (d, 1B), -7.51 (d, 1B), -10.26 (dd, 4B), -13.09 (d, 2B), -14.72 (d, 2B).

[23] Kahl, S. B., et al., *J. Am. Chem. Soc.* **1996**, *118*, 1223-1224.

*Synthesis of 1-(9-iodo-1,7-dicarba-closo-dodecaboran-1-yl)-benzothiazole (**6.13**)*

To a solution of 1-(1,7-dicarba-*closo*-dodecaboran-1-yl)-benzothiazole (0.50 g, 1.811 mmol) in dry dichloromethane (15ml), aluminum chloride (50 mg, 0.37 mmol) and iodine monochloride (95 µl, 1.811 mmol) were added. The mixture was refluxed for 14h, cooled to room temperature, and excess iodide was quenched with 5% sodium thiosulfate solution (50 ml). The products were extracted with dichloromethane (3 x 50 mL), the organic layers were combined, dried over Na_2SO_4, concentrated with a rotary evaporator and the crude was purified using silica gel column chromatography (starting mobile phase: hexane; final mobile phase: 3% ethyl acetate) to yield 1-(9-iodo-1,7-dicarba-*closo*-dodecaboran-1-yl)-benzothiazole (550 mg, 75% yield) as a yellow solid.

^{1}H-NMR (500 MHz, $CDCl_3$): 8.05 (1 H, dt, CH, phenyl), 7.84 (1 H, dt, CH, phenyl), 7.54 (1 H, ddd, CH, phenyl), 7.46 (1 H, ddd, CH, phenyl), 3.28 (1 H, s, cage C-H), 3.70-1.70 (10H, m, $B_{10}H_{10}$); ^{13}C-NMR (126 MHz, $CDCl_3$): 161.02, 152.49, 135.85, 126.98, 126.47, 123.93, 121.45, 74.57, 56.27; ^{11}B-NMR (160 MHz, $CDCl_3$): -2.85 (d, 1B), -6.43 (d, 1B), -8.31 (d, 1B), -8.90 (d, 1B), -9.88 (d, 1B), -11.75 (d, 1B) , -12.84 (d, 1B), -14.61 (d, 1B), -16.61 (d, 1B), -23.64 (s, 1B).

*Synthesis of 1-(9-trifluoroacetylamino-1,7-dicarba-closo-dodecaboran-1-yl)-benzothiazole (**6.14**)*

To a solution of 1-(9-iodo-1,7-dicarba-*closo*-dodecaboran-1-yl)-benzothiazole (800 mg, 1.985 mmol), trifluoroacetamide (673 mg, 5.955 mmol) and tripotassium phosphate (2.1 g, 9.925 mmol) in dry toluene, tris(dibenzylideneacetone)dipalladium (45.5 mg, 0.049 mmol) and 2-dicyclohexylphosphino-2′-(*N*,*N*-dimethylamino)biphenyl (Davephos, 39mg, 0.099 mmol) were added. The mixture was refluxed for 14 hours, filtered, concentrated using rotary evaporator and the crude was purified using silica gel column chromatography (starting mobile phase: hexane; final mobile phase: 10% ethyl acetate) to afford 1-(9-trifluoroacetylamino-1,7-dicarba-*closo*-dodecaboran-1-yl)-benzothiazole (630mg, 81% yield) as a yellow solid.

^{1}H-NMR (500 MHz, $CDCl_3$): 8.05 (1 H, dt, CH, phenyl), 7.84 (1 H, dt, CH, phenyl), 7.53 (1 H, ddd, CH, phenyl), 7.46 (1 H, ddd, CH, phenyl), 5.93 (1 H, s, NH), 3.18 (1 H, s, cage C-H), 3.70-1.70 (10H, m, $B_{10}H_{10}$); ^{13}C-NMR (126 MHz, $CDCl_3$): 161.16, 152.49, 135.85, 126.95, 126.45, 123.92, 121.44, 70.80, 52.56; ^{11}B-NMR (160 MHz, $CDCl_3$): -1.71 (s, 1B), -4.30 (d, 1B), -7.91 (d, 1B), -10.88 (dd, 2B), -11.65 (d, 1B), -13.69 (d, 1B), -14.82 (d, 1B), -16.21 (d, 1B), -18.71 (d, 1B).

*Synthesis of 1-(9-amino-1,7-dicarba-closo-dodecaboran-1-yl)-benzothiazole (**6.15**)*

To a solution of 1-(9-trifluoroacetylamino-1,7-dicarba-*closo*-dodecaboran-1-yl)-benzothiazole (150 mg, 0.38 mmol) in methanol (1.5ml), tetrahydrofuran (1.5ml), isopropanol (1.5ml), water (6ml) and sodium hydroxide (900mg, 22.5 mmol) were added. The resulting mixture was stirred at room temperature for 72h and concentrated below 30°C. Extraction was carried out with ethyl acetate (3 x 50 mL), the organic layers were combined, dried over sodium sulfate, concentrated using rotary evaporator and the crude was purified using silica gel column chromatography (starting mobile phase: hexane; final mobile phase: 50% ethyl acetate) to achieve 1-(9-amino-1,7-dicarba-*closo*-dodecaboran-1-yl)-benzothiazole (35 mg, 31% yield) as a white solid.

^{1}H-NMR (500 MHz, $CDCl_3$): 8.03 (1 H, dt, CH, phenyl), 7.80 (1 H, dt, CH, phenyl), 7.50 (1 H, ddd, CH, phenyl), 7.42 (1 H, ddd, CH, phenyl), 5.19 (2H, bs, NH_2), 3.03 (1 H, s, cage C-H), 3.70-1.70 (10H, m, $B_{10}H_{10}$); ^{13}C-NMR (126 MHz, $CDCl_3$): 162.20, 152.52, 135.83, 126.75, 126.19, 123.81, 121.35, 69.40, 51.37; ^{11}B-NMR (160 MHz, $CDCl_3$): -1.72 (s, 1B), -4.04 (d, 1B), -8.05(d, 1B), -10.72 (dd, 2B), -13.89 (d, 1B), -15.24 (d, 1B), -16.90 (d, 1B), -20.50 (d, 1B), -22.92 (d, 1B); LCMS (ESI) Experimental $[M + H]^+$ m/z = 293.12 (theoretical value: 293.41).

*Synthesis of 1,7-dicarba-closo-dodecarborane-1-ethylcarboxylate (**6.16**)*

A solution of 1,7-dicarba-*closo*-dodecarborane-1-carboxylic acid chloride (5.5 g, 26.7 mmol) was refluxed in ethanol (150 ml) for 4h. After cooling, the mixture was concentrated to yield 1,7-dicarba-*closo*-dodecarborane-1-ethylcarboxylate (5.7g, 98% yield) as brown viscous liquid, which was used without further purification. ^{1}H-NMR (500 MHz, $CDCl_3$): 4.20 (2 H, q, CH_2CH_3), 3.02 (1 H, s, cage C-H), 1.29 (3 H, t, CH_3CH_2), 3.70-1.70 (10H, m, $B_{10}H_{10}$); ^{13}C-NMR (126 MHz, $CDCl_3$): 161.75, 63.75, 54.67, 13.76; ^{11}B-NMR (160 MHz, $CDCl_3$): -4.89 (d, 1B), -6.98 (d, 1B), -10.69 (d, 2B), -11.28 (d, 2B), -13.32 (d, 2B), -15.65 (d, 2B).

*Synthesis of (9-iodo-1,7-dicarba-closo-dodecarborane-1-yl)-ethylcarboxylate (**6.17**)*

Prepared according to the procedure described for compound **6.13**; yield after purification: 78%.

^{1}H-NMR (500 MHz, $CDCl_3$): 4.22 (2H, q, CH_2CH_3), 3.15 (1H, s, cage C-H), 3.70-1.70 (10H, m, $B_{10}H_{10}$), 1.30 (3H, t, CH_3CH_2); ^{13}C-NMR (126 MHz, $CDCl_3$): 160.72,

73.65, 64.19, 55.64, 13.77. ^{11}B-NMR (160 MHz, $CDCl_3$): -3.84 (d, 1B), -5.91 (d, 1B), -8.55 (d, 1B), -10.12 (d, 1B), -11.15 (d, 1B), -11.99 (d, 1B) , -13.12 (d, 1B), -15.59 (d, 1B), -17.58 (d, 1B), -23.76 (s, 1B).

*Synthesis of (9-iodo-1,7-dicarba-closo-dodecarborane-1-yl)-carboxylic acid chloride (**6.18**)*

To a solution of (9-iodo-1,7-dicarba-*closo*-dodecarborane-1-yl)-ethylcarboxylate (4.3g, 12.6 mmol) in ethanol (30ml), 2N NaOH solution (30ml) was added and the mixture was stirred at room temperature for 30min. The solvent was evaporated below 30°C, and the residue was neutralized with 2N HCl, extracted with ethylacetate (3 x 50 mL), and the combined organic layers were dried over sodium sulfate. After solvent evaporation, (9-iodo-1,7-dicarba-*closo*-dodecarborane-1-yl)-carboxylic acid (3.99g, 98% yield) was obtained.

^{1}H-NMR (500 MHz, $CDCl_3$): 9.35 (1H, bs, COOH), 3.18 (1H, s, cage C-H), 3.70-1.70 (10H, m, $B_{10}H_{10}$); ^{13}C-NMR (126 MHz, $CDCl_3$): 166.03, 72.25, 55.83; ^{11}B-NMR (160 MHz, $CDCl_3$): -3.81 (d, 1B), -5.82 (d, 1B), -8.50 (d, 1B), -10.09 (d, 1B), -11.12 (d, 1B), -11.93 (d, 1B), -13.05 (d, 1B) , -15.56 (d, 1B), -17.54 (d, 1B), -23.74 (s, 1B).

The acid chloride was prepared by reacting compound **6.18** (3.99g, 12.7 mmol) dissolved in toluene (40 ml) with phosphorous pentachloride (2.88g, 13.86 mmol) at room temperature for 6h. The reaction mixture was concentrated under high vaccum and used for the next step without purification.

*Synthesis of 1-(9-iodo-1,7-dicarba-closo-dodecaboran-1-yl)-6-hydroxymethyl benzothiazole (**6.19**)*

Compound **6.19** was prepared according to the procedure described for compound **6.12**, but 2-amino-5-methoxi phenol was used instead of 2-aminophenol, with a yield of 73.8 % starting from acid.

^{1}H-NMR (500 MHz, $CDCl_3$): 7.91 (1 H, d, CH, phenyl), 7.25 (1 H, d, CH, phenyl), 7.12 (1 H, dd, CH, phenyl), 3.89 (3 H, s, CH_3O-), 3.26 (1 H, s, cage C-H), 3.70-1.70 (10H, m, $B_{10}H_{10}$); ^{13}C-NMR (126 MHz, $CDCl_3$): 158.60, 158.12, 147.00, 137.34, 124.46, 116.59, 103.52, 74.71, 56.18, 55.87; ^{11}B-NMR (160 MHz, $CDCl_3$): -2.90 (d, 1B), -6.62 (d, 1B), -8.42 (d, 1B), -8.81 (d, 1B), -9.90 (d, 1B), -11.85 (d, 1B), -12.94 (d, 1B), -14.66 (d, 1B), -16.64 (d, 1B), -23.63 (s, 1B).

*Synthesis of 1-(9-trifluoroacetylamino-1,7-dicarba-closo-dodecaboran-1-yl)-6-hydroxymethyl benzothiazole (**6.20**)*

Compound **6.20** was prepared according to the procedure described for compound **6.14**; yield 72%.

^{1}H-NMR (500 MHz, $CDCl_3$): 7.91 (1 H, d, CH, phenyl), 7.25 (1 H, d, CH, phenyl), 7.12 (1 H, dd, CH, phenyl), 5.93 (1 H, s, NH), 3.89 (3 H, s, CH_3O-), 3.17 (1 H, s, cage C-H), 3.70-1.70 (10H, m, $B_{10}H_{10}$); ^{13}C-NMR (126 MHz, $CDCl_3$): 159.49 (q), 158.60, 158.24, 146.99, 137.34, 124.44, 116.59, 103.50, 70.95, 55.85, 52.47; ^{11}B-NMR (160 MHz, $CDCl_3$): -1.77 (s, 1B), -4.33 (d, 1B), -8.09 (d, 1B), -10.93 (dd, 2B), -11.70 (d, 1B), -13.74 (d, 1B), -14.87 (d, 1B), -16.23 (d, 1B), -18.71 (d, 1B).

*Synthesis of 1-(9-amino-1,7-dicarba-closo-dodecaboran-1-yl)-6-hydroxymethyl benzothiazole (**6.21**)*

Compound **6.21** was prepared according to the procedure described for compound **6.15**; yield 32%. ^{1}H-NMR (500 MHz, $CDCl_3$): 7.89 (1 H, d, CH, phenyl), 7.23 (1 H, d, CH, phenyl), 7.09 (1 H, dd, CH, phenyl), 3.87 (3 H, s, CH_3O-), 3.46 (2H, bs, NH_2), 3.03 (1 H, s, cage C-H), 3.70-1.70 (10H, m, $B_{10}H_{10}$); ^{13}C-NMR (126 MHz, $CDCl_3$): 159.25, 158.44, 146.98, 137.26, 124.32, 116.37, 103.51, 69.79, 55.83, 51.56; ^{11}B-NMR (160 MHz, $CDCl_3$): 3.77 (s, 1B), -4.53 (d, 1B), -8.38 (d, 1B), -10.57 (dd, 2B), 12.42 (d, 1B), -13.79 (d, 1B), -15.38 (d, 1B), -16.96 (d, 1B), -21.91 (d, 1B).

*Synthesis of 1-(9-amino-1,7-Dicarba-closo-dodecaboran-1-yl)-6-hydroxy benzothiazole (**6.22**)*

A solution of 1-(9-amino-1,7-dicarba-*closo*-dodecaboran-1-yl)-6-hydroxy-methyl benzothiazole (**6.21**, 30mg, 0.088 mmol) in dry dichloromethane (1ml) was cooled to 0^{o}C and 1M solution of BBr_3 in dichloromethane (0.44ml, 0.44 mmol) was added dropwise. The mixture was allowed to stir at room temperature for 12h. Sodium bicarbonate (10% aqueous solution, 1ml) was added. The solution was extracted with dichloromethane (3 x 5 mL), the organic layers were combined, dried over sodium sulfate, and concentrated to yield 1-(9-amino-1,7-dicarba-*closo*-dodecaboran-1-yl)-6-hydroxy benzothiazole (**6.22**, 20 mg, 71% yield) as a white solid.

^{1}H-NMR (500 MHz, CD_3OD): 7.78(1 H, d, CH, phenyl), 7.25 (1 H, d, CH, phenyl), 7.03 (1 H, dd, CH, phenyl), 3.85 (1 H, bs, cage C-H), 3.83-1.70 (10H, m, $B_{10}H_{10}$); ^{13}C-NMR (126 MHz, CD_3OD): 154.48, 153.67, 143.41, 135.06, 122.41, 115.69,

105.39, 72.59, 55.92; ^{11}B-NMR (160 MHz, CD_3OD): 1.48 (s, 1B), -4.71 (d, 1B), -8.28 (d, 1B), -10.86 (dd, 2B), -12.01 (d, 1B), -13.67 (d, 1B), -14.88 (d, 1B), -16.35 (d, 1B), -20.71 (d, 1B); LCMS (ESI) Experimental $[M + H]^+$ m/z = 308.5 (theoretical value: 308.4).

6.4.2. Radiochemistry

$[^{11}C]CH_3OTf$ synthesis was carried out using a TRACERlab FX_C Pro synthesis module (GE Healthcare). A N_2/H_2 gas mixture was irradiated with 18 MeV protons (target current=22μA, integrated current = 2 μAh) in an IBA 18/9 Cyclone cyclotron (IBA) to generate $[^{11}C]CH_4$. The radioactive gas was trapped in Carbosphere 60/80 (Alltech Associates, Inc.) at -140°C. After complete trapping, $[^{11}C]CH_4$ was desorbed by heating at 80°C and converted into $[^{11}C]CH_3I$ in a gas circulating process by reacting with molecular iodine at 720°C. The $[^{11}C]CH_3I$ was selectively retained in a trap containing Porapak™ Q (50– 80 mesh, Waters Corporation) at room temperature, while the unreacted $[^{11}C]CH_4$ was recirculated (total number of cycles: 8-9). The trapped $[^{11}C]CH_3I$ was distilled by heating the Porapak™ Q trap at 190°C under continuous helium flow (20 mL/min) for 2.5 min, and passed through a trap filled with 150– 200 mg of silver triflate fixed on Carbowax® 1500 80/100 (Grace Davison Discovery Science) in an online flow-through process at 180°C to produce $[^{11}C]CH_3OTf$.

The $[^{11}C]CH_3OTf$ was finally introduced in the reaction loop (AutoLoop™ system, Bioscan Inc.), pre-charged with a solution of the precursor and the solvent (total volume: 100 μL). The reaction was allowed to occur at room temperature (see Figure 6.12 for example of the curve representing trapping of the activity in the loop and subsequent elution). During process optimization, the crude reaction mixtures were directly collected in vials by pushing with acetonitrile and the resulting solutions were analyzed by radio-HPLC to obtain radiochemical conversion. For final runs under optimal conditions, the reaction mixture was directly pushed to a semi-preparative HPLC column (Meditarian Sea18 C18 column, 250×10mm, 5μm, Teknokroma, Spain) using aqueous 0.1M AMF (pH adjusted to 3.9 using HCOOH)/MeCN in a ratio of 50/50 as the mobile phase (flow rate of 3mL/min). The desired fraction (retention time=9.2 min & 6.4 min for $[^{11}C]$**6.23** and $[^{11}C]$**6.24** respectively on radiometric and UV detection) was collected and reformulated by diluting with water (20mL), trapping in a C-18 cartridge and eluting to the final vial with ethanol (1 mL), using the TRACERlab FX_C Pro synthesis module. The amount of radioactivity obtained was measured in a dose calibrator (PETDOSE HC, Comecer).

Radiochemical purity of the final compound was determined by radio-HPLC, using an Agilent 1200 Series HPLC system equipped with a multiple wavelength UV detector (λ=254nm) and a radiometric detector (Gabi, Raytest). An Eclipse C18 column (4.6 × 150 mm, 5 µm particle size) was used as stationary phase and aqueous 0.1M AMF (pH adjusted to 3.9 using HCOOH)/MeOH 55/45 as the mobile phase. The retention times of [^{11}C]**6.23** and [^{11}C]**6.24** were 11.5 and 9.0 minutes respectively.

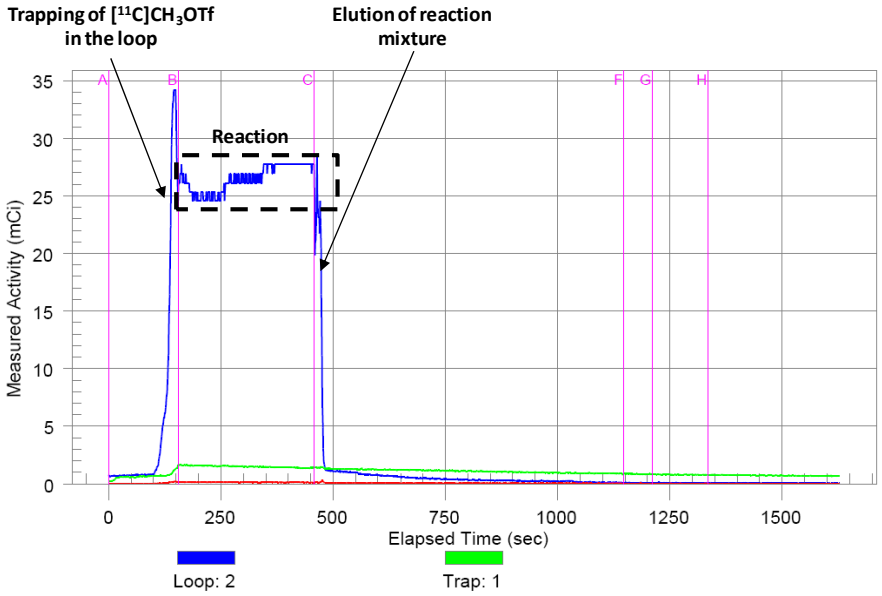

Figure 6.12. Typical curves obtained in the AutoLoopTM system. The activity ([^{11}C]CH_3OTf) is trapped in the loop (blue line) and the methylation reaction is allowed to occur. After a pre-determined time, the reaction crude (containing either [^{11}C]**6.23** or [^{11}C]**6.24** is transferred to a vial or purification system.

Identification of the desired species was carried out by HPLC-MS performed on the purified fraction after complete decay, using an AQUITY UPLC separation module coupled to a LCT TOF Premier XE mass spectrometer (Waters, Manchester, UK). An Acquity BEH C18 column (1.7 µm, 5 mm, 2.1 mm) was used as stationary phase. The elution buffers were MEOH (A) and 0.1% formic acid aqueous solution (B). The column was eluted with a gradient: t=0min, 95% B; t=0.5min, 95% B; t=16 min, 1% B; and t = 20 min, 1%B. Total run length was 20 min; injection volume was 5 µL, and the flow rate was 0.3 mL/min. The

detection was carried out in positive ion mode, monitoring the most abundant isotope peaks from the mass spectra. Compounds [^{11}C]**6.23** and [^{11}C]**6.24** were detected as a protonated species, m/z = 306.1 and m/z = 322.1 respectively.

6.5. Summary and conclusions

The synthesis of 1-(9-amino-1,7-dicarba-*closo*-dodecaboran-1-yl)-benzothiazole could be achieved by reaction of *m*-carboranyl carboxylic acid chloride with 2-aminothiophenol and Lawesson's reagent, followed by iodination using iodine monochloride in the presence of aluminum chloride, subsequent palladium-catalyzed Buchwald-Hartwig amidation reaction to incorporate the trifluoroacetamide group and final hydrolysis under basic conditions. The preparation of 1-(9-amino-1,7-dicarba-*closo*-dodecaboran-1-yl)-6-hydroxy benzothiazole required a different approach, based on the preparation of the iodinated *m*-carboranyl carboxylic acid chloride in a first step, followed by reaction with 2-amino-5-methoxythiophenol, Buchwald-Hartwig amidation, hydrolysis and finally O-demethylation. Both compounds could be efficiently labeled with Carbon-11 to yield the corresponding *N*-[^{11}C]methylated derivatives, which might be used for subsequent *in vivo* investigation using Positron Emission Tomography.

7. Synthesis of *m*-carboranyl amides via palladium-catalyzed carbonylation: Towards ^{11}C-radiolabelling using ^{11}C-carbonylation.

7.1. Introduction

As previously mentioned in this PhD thesis, dicarba-*closo*-dodecaboranes, possess a rich derivative chemistry, which turns carboranes into suitable building blocks with application in different fields (see chapter 4)

Independently of their isomeric form (*o*-, *m*-, and *p*-carborane), carboranes can be attached to other molecules either via their carbon or boron atoms. Up to date, functionalization of carboranes at the carbon position has been extensively studied [1]. One of the commonly used strategies for such functionalization consists on the formation of carboxyl-substituted carboranes via reactions of C-lithio or C-MgBr derivatives with CO_2 followed by acidification [2]. The carboxylic acids can be further converted into the corresponding acid chlorides [3] which in turn can combine with alcohols or amines to form esters [4] or amides [5], respectively.

Surprisingly, other strategies for the preparation of amides like the Heck carbonylation reaction [6], which is a powerful method for the synthesis of secondary and tertiary amides by reaction of aryl bromides and vinyl iodides with primary or secondary amines under CO atmosphere in the presence of a palladium complex acting as a catalyst, have not been assayed to date for the preparation of carborane derivatives substituted either at the carbon or boron positions. Such strategy might be anticipated to be suitable for the preparation of carborane derivatives due to the three-dimensional delocalization of skeletal electrons which derive in a three-dimensional aromaticity, as supported by different theoretical investigations [7].

In this chapter, a method for the palladium catalyzed carbonylation of 1-iodo-1,7-dicarba-*closo*-dodecaborane for the one-pot one-step formation of amides is presented. The reported reaction, employed herein for the preparation of amides, might be used as well for the preparation of other carboxyl-substituted

[1] V. Bregadze, *Chem. Rev*. **1992**, *92*, 209.
[2] (a) V. I. Stanko, et al., *Zh. Obshch. Khim.* **1966**, *36*, 165; (b) V. I. Stanko, et al., *Zh. Obshch. Khim*. **1976**, *46*, 869.
[3] (a) L. I. Zakharkin, et al., *Izv. Akad. Nauk. SSSR Ser. Khim.* **1970**, 912; (b) V. I. Stanko, et al., *Zh. Obshch. Khim.* **1970**, *40*, 1523.
[4] (a) E. A. Dikusar, et al., *Russ. J. Gen. Chem.* **2005**, *75*, 575; (b) E. A. Dikusar, et al., *Russ. J. Gen. Chem.* **2008**, *78*, 424; c) E. A. Dikusar, et al., *Russ. J. Gen. Chem.* **1996**, *66*, 1766.
[5] (a) J. R. Reiner, *et al., Inorg. Chem.* **1966**, *5*, 1460; (b) L. I. Zakharkin, et al., *Russ. Chem. Bull.* **1996**, *45*, 680.
[6]A. Schoenberg, et al., *J. Org. Chem.* **1974**, *39*, 3327.
[7] (a) A. J. Stone, et al., *Inorg. Chem.* **1982**, *21*, 2297; (b) P. V. R. Schleyer, et al., *Inorg. Chem.* **1998**, *37*, 3454; (c) B. M. Gimarc, et al., *Inorg. Chem.* **1996**, *35*, 825.

carboranes and could be potentially extended also to the preparation of *o*- and *p*-carboranyl derivatives. Interestingly, the reaction conditions might be also easily translated into the radiochemistry field, where radiosynthetic routes for the preparation of ^{11}C-labelled radiotracers starting from the radioactive precursor [^{11}C]CO have been developed so far [8].[12] Thus, the biological activity of the resulting radiotracers could be assessed *in vivo* by using positron emission tomography (PET) a non-invasive, ultra-sensitive molecular imaging technique. Moving towards the preparation of ^{11}C-labelled carborane derivatives using the methodology reported here, an automated system for the generation of [^{11}C]CO has been developed and tested.

7.2. Results and discussion

7.2.1. Cold chemistry

The scheme of the reaction used for the synthesis of carboranyl amides *via* the Heck carbonylation reaction is shown in Figure 7.1.

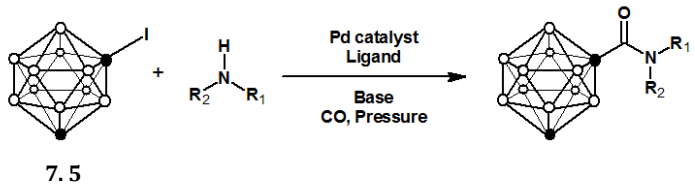

7. 5

R_1	R_2	Compound
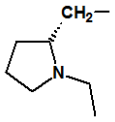	H	**7. 1**
$-CH_2-(CH_2)_3-CH_2-$		**7. 2**
$-CH_2-(CH_2)_2-CH_2-$		**7. 3**
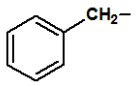	H	**7.4**

Figure 7.1. Aminocarbonylation reaction of **7.5** with primary and secondary amines to yield the corresponding amides (**7.1** – **7.4**).

[8] J. Eriksson, et al., *J. Label. Compds. Radiopharm.* **2012**, *55*, 223, and references therein.

In first instance, we investigated the carbonylation reaction of **7.5** (synthesized following a previously reported method [9] with minor modifications, see experimental section for details) with [(2R)-1-ethyl-2-pyrrolidinyl]methanamine to yield **7.1**. In order to assess the effects of the catalyst, the ligand and the base in the carbonylation reaction, a set of runs was carried out using different catalysts ($Pd_2(dba)_3$, $Pd(OAc)_2$, $PdCl_2$, $PdCl_2(PPh_3)_2$ and $Pd(PPh_3)_4$), ligands (BINAP, DPPE, DPPF, TPP, Xantphos and 2,2'-bipyridine, see Figure 7.2) and bases (K_2CO_3, triethylamine, K^{t}OBu and K_3PO_4) in a carbon monoxide atmosphere at 2 bar. In a typical experiment, compound **7.5** (25 mg, 0.09 mmol) was dissolved in THF (1 mL) and introduced in a glass Tiny-clave (nominal volume: 25 mL). The catalyst, the base, the ligand and the nucleophile were added, the system was closed, and carbon monoxide was introduced until the appropriate pressure was reached. The reaction mixture was heated under stirring at 85°C. After 2 hours, the reaction was cooled at room temperature, carbon monoxide was flushed and a sample was analysed by GC-MS (see supplementary information for details) to assess the chemical conversion, using reference compound **7.5** as internal standard.

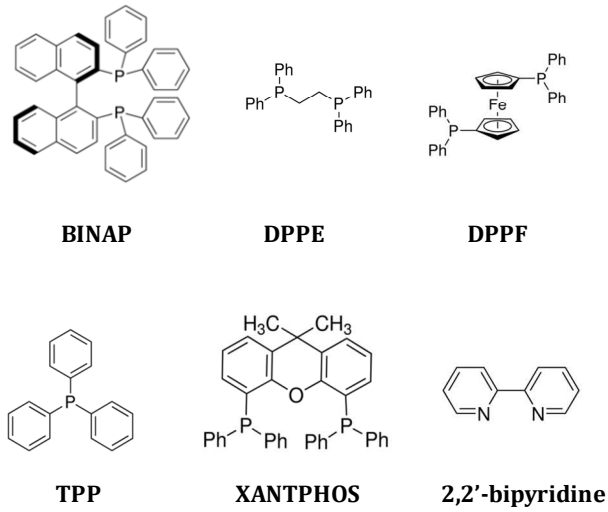

Figure 7.2. Chemical structure of the ligands used in the current work.

First screening experiments were performed to choose the most appropriate catalyst. BINAP, a bidentate ligand with a bite angle of 90-91°, was used as a

[9]D. Grafstein, et al., *Inorg. Chem.* **1963**, *2*, 1120.

ligand and K_3PO_4 was used as a base. The formation of **7.1** could not be detected after 2 hours of reaction when $Pd_2(dba)_3$, $Pd(OAc)_2$ and $PdCl_2$ were used. Interestingly, formation of the desired product could be observed when $PdCl_2(PPh_3)_2$ and $Pd(PPh_3)_4$ were used, with chemical conversions of 10.5% and 15.3%, respectively (Table 7.1, entries 1-2). Thus, all subsequent reactions were performed with $Pd(PPh_3)_4$. To assess the effect of the base, different experiments were performed using $Pd(PPh_3)_4$/BINAP as catalyst/ligand. The addition of K_2CO_3 and triethylamine led to moderately lower chemical conversions when compared to K_3PO_4 (Entries 3-4, Table 7.1), while the use of K^tOBu decreased the reaction rate with respect to K_3PO_4 by a factor of ~30 (Entry 5).

To assess the effect of the ligand, the reaction was repeated using DPPF, DPPE, Xantphos and bipyridine. All combinations led to lower conversion values than those obtained with BINAP (Table 7.1, entries 2 and 6-9). The effect of the catalyst and ligand concentrations was also investigated by using $Pd(PPh_3)_4$/BINAP at different molar ratios with respect to compound **7.5**. As can be seen in table 7.1 (entries 2, 10 and 11) higher amounts of catalyst and ligand offered significantly lower chemical conversion values.

The substitution of the iodine atom by bromine in the starting m-carborane (compound **7.6**) did not lead to improved results (0.7% conversion after 2 h reaction, entry 12) while no desired compound could be detected when 1-trifluoromethanesulfonyl-1,7-dicarba-*closo*-dodecaborane (**7.7**) was used as starting material (entry 13).

The kinetic profile of the reaction was monitored by GC-MS under optimized conditions, this is, using $Pd(PPh_3)_4$/BINAP/K_3PO_4. The reaction proceeded fast during the first 2 hours (chemical conversions of 8.5% and 15.3% after 1 and 2 hours, entries 16 and 2, respectively). However, at longer times the reaction rate significantly decreased until a plateau was reached at conversions ~ 25% (entries 18 and 19). Significant amounts of *m*-carborane could be detected in the chromatograms of the corresponding reaction crudes, suggesting the de-iodination of **7.5**. Parallely, increasing amounts of the undesired symmetrical urea were observed while increasing reaction time. The relative formation rate of the urea with respect to the desired amide decreased when the CO pressure was decreased to 1 bar, and increased when the pressure was increased to 10 bar, although chemical conversion for the amide was lower than the one obtained at P=2 bar (Table 7.1, entries 2, 14 and 15)

Table 1. Experimental conditions and reaction extent for the synthesis of *m*-carboranyl secondary and tertiary amides via the Heck carbonylation reaction.

Entry[a]	Prec.	Catalyst	Amount catalyst (eq)[b]	Ligand	Amount ligand (eq)[b]	Base[c]	Reaction time (h)	P_{CO} (bar)	% reaction[d]
1	7.5	$Pd(PPh_3)_2Cl_2$	0.02	BINAP	0.04	K_3PO_4	2	2	10.5
2	7.5	$Pd(PPh_3)_4$	0.02	BINAP	0.04	K_3PO_4	2	2	15.3
3	7.5	$Pd(PPh_3)_4$	0.02	BINAP	0.04	K_2CO_3	2	2	4.3
4	7.5	$Pd(PPh_3)_4$	0.02	BINAP	0.04	TEA	2	2	5.2
5	7.5	$Pd(PPh_3)_4$	0.02	BINAP	0.04	K^tOBu	2	2	0.4
6	7.5	$Pd(PPh_3)_4$	0.02	DPPF	0.04	K_3PO_4	2	2	1.7
7	7.5	$Pd(PPh_3)_4$	0.02	DPPE	0.04	K_3PO_4	2	2	3.2
8	7.5	$Pd(PPh_3)_4$	0.02	Xantphos	0.04	K_3PO_4	2	2	1.5
9	7.5	$Pd(PPh_3)_4$	0.02	Bipyridine	0.04	K_3PO_4	2	2	2.1
10	7.5	$Pd(PPh_3)_4$	0.10	BINAP	0.20	K_3PO_4	2	2	7.7
11	7.5	$Pd(PPh_3)_4$	0.20	BINAP	0.40	K_3PO_4	2	2	1.5
12	7.6	$Pd(PPh_3)_4$	0.02	BINAP	0.04	K_3PO_4	2	2	0.7
13	7.7	$Pd(PPh_3)_4$	0.02	BINAP	0.04	K_3PO_4	2	2	0.0
14	7.5	$Pd(PPh_3)_4$	0.02	BINAP	0.04	K_3PO_4	2	1	14.4
15	7.5	$Pd(PPh_3)_4$	0.02	BINAP	0.04	K_3PO_4	2	10	2.1
16	7.5	$Pd(PPh_3)_4$	0.02	BINAP	0.04	K_3PO_4	1	2	8.5
17	7.5	$Pd(PPh_3)_4$	0.02	BINAP	0.04	K_3PO_4	4	2	18.1
18	7.5	$Pd(PPh_3)_4$	0.02	BINAP	0.04	K_3PO_4	16	2	25.3
19	7.5	$Pd(PPh_3)_4$	0.02	BINAP	0.04	K_3PO_4	24	2	26.7

[a] All reactions were carried out in THF (1 mL) using 25 mg (0.09 mmol) of carborane precursor and 0.15 mmol of amine. [b] With respect to carborane precursor. [c] Amount of base: 0.27 mmol. [d] Chemical conversion as determined by GC-MS; TEA: triethylamine; P_{CO}: CO pressure.

Optimized experimental conditions (entry 19 in Table 7.1) were applied to the synthesis of compounds **7.1**-**7.4** (Figure 7.1). After purification by chromatography (see materials and methods section for details), yields of 21%, 15%, 16% and 10%, respectively, were obtained. All compounds were characterized by ^{1}H NMR, {^{1}H–^{11}B} NMR, ^{13}C NMR, ^{11}B NMR, {^{11}B-^{1}H} NMR, ^{1}H-^{13}C HSQC and high resolution mass spectrometry.

7.2.2. Radiochemistry

In the current work, a system for the automatic production of [^{11}C]CO from cyclotron-produced [^{11}C]CO_2 was implemented.

The preparation of [^{11}C]CO has been widely reported in the literature. It is usually produced through the reduction of cyclotron generated [^{11}C]CO_2 over zinc or molybdenum [10]. The reduction under zinc is carried out at 400 °C, which is very close to the melting point of zinc (419.5°C). Thus, extremely accurate control on the temperature regulator is required; too high temperatures lead to zinc melting and subsequent blocking of the system, while too low temperatures lead to ineffective or incomplete reduction. Reduction using molybdenum takes place at higher temperature. Typically, molybdenum wire or powder is introduced in a quartz glass tube and heated at 850°C. The installation of cold traps before and after reduction steps increases the concentration factor and improves the overall reaction yield.

Although [^{11}C]CO is a very attractive radioactive precursor for the preparation of labelled structures, its use has been historically limited because of its low reactivity and solubility. Because of this, recirculation techniques and the use of high pressure reactors to increase the trapping efficiency (e.g., the high pressure system reported by the Uppsala group [11] and the system developed by Hostetler and Burns [12], see Figures 7.3 and 7.4).

Recently, the problem of transferring [^{11}C]CO into the reaction mixture was resolved by careful selection of the carrier gas (Figure 7.5) [13]. [^{11}C]CO was taken up from the cold trap using xenon, and transferred to a septum-capped glass vial containing THF solution of other reactants. Since xenon is very soluble in THF, [^{11}C]CO is almost quantitatively trapped in the reaction vial and

[10] Zeisler, S. K.; et al., *Appl. Radiat. Isot.* **1997**, *48 (8)*, 1091-1095.
[11] (a) Kihlberg, T., et al., WO, 2002102711 A1, **2002.** (b) Itsenko, O., et al., *Nat. Protoc.* **2006**, *1 (2)*, 798-802.
[12] Hostetler, E. D., et al., *Nucl. Med. Biol.* **2002**, *29 (8)*, 845-848.
[13] Eriksson, J., et al, J. Labelled Compd. Radiopharm. **2012**, *55(6)*, 223-228.

carbonylation reactions can be conducted with excellent radiochemical conversion values.

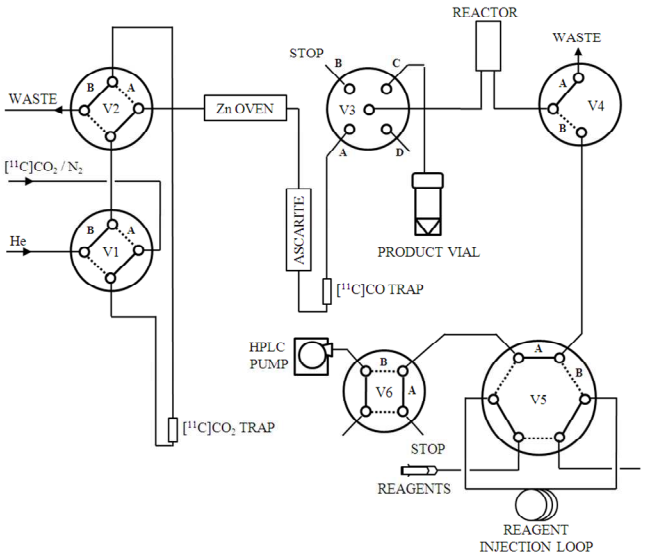

Figure 7.3: Schematic system for the production of [^{11}C]CO from cyclotron generated [^{11}C]CO_2 and further reaction at high pressure (Kihlberg et al., 2002). The system is divided into two main parts: one to reduce the accelerator-produced [^{11}C]CO to [^{11}C]CO_2, and another to deliver liquid reagents into the reactor and pressurize it.

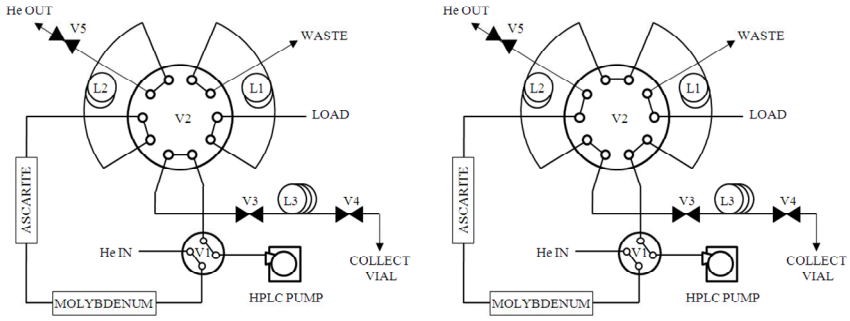

Figure 7.4: Schematic system for the production of [^{11}C]CO from cyclotron generated [^{11}C]CO_2 and further reaction at high pressure (Hostetler et al., 2002). V3, V4 and V5 are high pressure valves. In status 1 (left) the precursor is loaded into L1 and the [^{11}C]CO is trapped in L2. In status 2 (right) the precursor and [^{11}C]CO are pushed into L3 where reaction takes place.

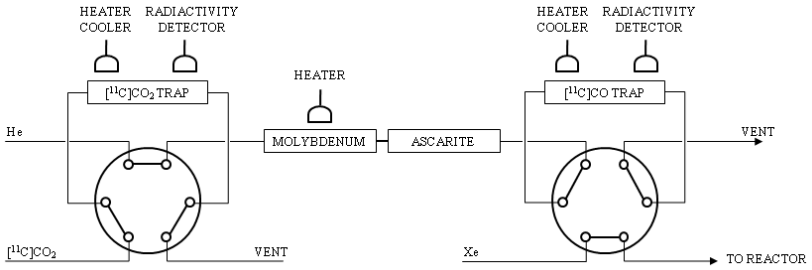

Figure 7.5: Schematic system for the production of [^{11}C]CO from cyclotron generated [^{11}C]CO_2 and further introduction into a reactor at atmospheric pressure. In step 1 (valves position as shown in the figure) [^{11}C]CO_2 is trapped in the [^{11}C]CO_2 trap (liquid nitrogen). Then V1 is switched and [^{11}C]CO_2 is pushed with helium, reduced in the molybdenum column, purified ([^{11}C]CO_2 is trapped in ascarite) and trapped in the [^{11}C]CO trap. Finally, V2 is switched and [^{11}C]CO is pushed with Xenon and trapped in the reactor at low pressure.

In this work, the procedure previously implemented by *Eriksson et al*. was followed. However, low pressure 2- and 3-way valves were used instead of 6-port valves. Good conversion values from [^{11}C]CO_2 to [^{11}C]CO were obtained (65±12%, decay corrected) in overall production times of 13 minutes. Despite the resulting [^{11}C]CO was not used for subsequent radiolabelling and the fact that the procedure may still be optimized, the system was working robustly and it is a good starting point to approach carbonylation reactions in the near future.

7.3. Materials and methods

7.3.1. Cold chemistry

7.3.1.1. General procedures

1,7-dicarba-*closo*-dodecaborane was purchased from Katchem Ltd. (Prague, Czech Republic); carbon monoxide was purchased from Air Liquide. All other reagents were purchased from Aldrich Chemical Co. and used without further purification. Dry solvents, stored over 4 Å molecular sieves, were also purchased from Aldrich Chemical Co. All reactions, except cross-coupling, were carried out under nitrogen atmosphere and were followed by thin-layer chromatography carried out on silica gel 60 F_{254} plates (Macherey-Nagel). Visualization was accomplished with a UV source (254, 365 nm) and by

treatment with an acidic solution of 1% $PdCl_2$ in methanol. Carboranes charred as black spots on TLC.

The kinetics of the cross coupling reaction was followed by GC-MS. GC-MS analyses were performed on an Agilent 7820A network GC with manual injector combined with Agilent 5975c inert XL MSD with Triple axis detector. An HP-5 column (length: 30 m, internal diameter: 0.25 mm) was used as stationary phase. The inlet conditions were 250°C, 25 psi and a flow rate of 20.65 ml/min using a 1:1 split injector with helium (99.9999%) as the carrier gas. The oven initial temperature was set of 120 °C with a hold time of 2 min. After that, a temperature ramp of 50°C/min was applied until reaching 300°C; then, a hold time of another 10 min was applied. Retention times for Compounds **7.1**-**7.4** were, respectively, 7.68, 7.66, 7.03 and 6.87 minutes.

Manual chromatography was performed with silica gel 60 (70-230 mesh) from Scharlau. ^{1}H, ^{13}C and ^{11}B spectra were recorded on a 500-MHz Avance III Bruker spectrometer. To explain multiplicities the following abbreviations were used: s = singlet, d = doublet, t = triplet, q = quartet, m = multiplet. Masses were determined by the LCT Premier XE from Waters (10000 FWHM).

7.3.1.2. Synthesis and characterization

*Synthesis of 1-iodo-1,7-dicarba-closo-dodecaborane (**7.5**) and 1-bromo-1,7-dicarba-closo-dodecaborane (**7.6**)*

To a solution of *m*-carborane (3.5mmol) in 5ml of anhydrous diethyl ether at -78°C, *n*-butyl lithium 1.6M solution in THF (3.8mmol) was added dropwise. The solution was allowed to reach 5°C within 1 hour and was then cooled back to -78°C. The halogen (I_2 or Br_2, 3.5 mmol) was added slowly and the mixture was allowed to reach 5°C in 2h while stirring. After reaching 5°C, the reaction was maintained at this temperature for 2 hours. The reaction was quenched with 10% aqueous $Na_2S_2O_3$ solution (10 mL), extracted with ether and the organic phase dried over Na_2SO_4. Evaporation of the dry organic phase gave pure 1-halo carborane. (Yields: 75% for 1-iodo-1,7-dicarba-*closo*-dodecaborane, 72% for 1-bromo-1,7-dicarba-*closo*-dodecaborane)

*Synthesis of 1-trifluoromethanesulfonyl-1,7-dicarba-closo-dodecaborane (**7.7**)*

To a solution of 1-hydroxy-*m*-carborane (3.12 mmol, prepared as described previously [14]) in pyridine (5 mL), triflic anhydride (4.6mmol) was added dropwise at 0°C. The reaction was allowed to occur for 2h at 0°C. Then, the reaction mixture was concentrated in a rotary evaporator to remove pyridine, and water and diethyl ether (10 mL each) were added for extraction. The organic layer was dried over Na_2SO_4, decanted and concentrated under reduced pressure to yield the pure triflate (yield: 55%).

Typical Procedure for cross-coupling reaction

In a clean and dry Tiny-clave reactor covered with aluminum foil, 1-iodo-*m*-carborane (0.09 mmol), amine (0.135 mmol), base (0.27 mmol) and ligand (4 mol% with respect to carborane) were solved in degassed dry THF (1 mL). The catalyst (2 mol% with respect to carborane) was added and the solution was degassed one more time. The reactor was closed and filled with the required pressure of CO, placed in a pre heated oil bath and heated at 85°C. Progress of the reaction was monitored by GC-MS analysis. After finishing the reaction, the oil bath was removed, cooled at room temperature and the CO was flushed with nitrogen. The reaction mixture was filtered through a celite bed. The celite was washed with ethyl acetate and the collected filtrates were concentrated and purified by column chromatography. Conditions were as follows: Compound **7.1**: chloroform/ethanol 75/25; Compound **7.2**: chloroform/ethanol 95/05; Compound **7.3**: chloroform/ethanol 92/08; Compound **7.4**: chloroform/ethanol 92/08.

Characterization

Compound **7.1**: ^{1}H NMR (500 MHz, $CDCl_3$): δ 6.89 (1 H, s), 3.40 (1 H, ddd, *J* 13.6, 7.1, 3.0), 3.24 (1 H, dd, *J* 24.8, 5.9), 3.13 (1 H, d, *J* 13.6), 3.04 (1 H, s), 2.84 – 2.72 (1 H, m), 2.70 (1 H, d, *J* 18.3), 2.27 (2 H, ddd, *J* 23.9, 11.1, 5.7), 1.90 (1 H, ddd, *J* 16.9, 12.9, 8.5), 1.75 (2 H, dd, *J* 7.4, 3.6), 1.57 – 1.40 (1 H, m), 1.14 (3 H, dd, *J* 13.8, 6.7); ^{11}B NMR (160 MHz, $CDCl_3$, decoupled) δ -5.7 (1B), -7.6 (1B), -10.9 (4B), -13.3 (2B), -15.7 (2B); ^{13}C NMR (126 MHz, $CDCl_3$) δ 160.6 (*C*=O), 75.9 (C_c-C=O), 61.9 (*C*H-NEt), 54.8 (C_c-H), 53.4 (CH_2-NEt), 48.2 (CH_3-CH_2-N), 41.4 (CH_2-NHCO), 28.2 (CH_2-CHNEt), 23.0 (CH_2-CH_2NEt), 13.8 (CH_3-CH_2N); HRMS (ESI) Experimental $[M+Na]^+$ m/z = 321.2943, Calculated m/z = 321.2951, Deviation = 2.5 ppm.

[14] K. Ohta, et al., *Inorg. Chem.* **2007**, *46*, 3966.

Compound **7.2**: ^{1}H NMR (500 MHz, $CDCl_3$): δ 7.36 – 7.25 (3 H, m), 7.16 (2 H, d, J 7.1), 6.39 – 6.02 (1 H, m), 4.48 – 4.29 (2 H, m), 3.52-1.76 (10 H, m), 3.02 (1 H, s); ^{11}B NMR (160 MHz, $CDCl_3$, decoupled): δ -5.8 (1B), -7.4 (1B), -10.8 (2B), -11.5 (2B), -13.1 (2B), -15.6 (2B); ^{13}C NMR (126 MHz, $CDCl_3$): δ 160.3 (*C*=O), 136.9 (*C*-CH_2NHCO), 128.9 (2C, *C*H-CCH_2NHCO), 127.9 (*C*H-CHCHCCH_2NHCO), 127.3 (2C, *C*H-CHCCH_2NHCO), 75.5 (C_c-CO), 55.0 (C_c-H), 44.7 (*C*H_2-NHCO); HRMS (ESI) Experimental $[M+Na]^+$ m/z = 300.2352, Calculated m/z = 300.2373, Deviation = 7 ppm.

Compound **7.3**: ^{1}H NMR (500 MHz, $CDCl_3$): δ 3.69 – 3.52 (4 H, m), 2.99 (1 H, s), 3.43 – 1.69 (10 H, m), 1.65 (2 H, dt, *J* 11.4, 3.5), 1.59 – 1.50 (4 H, m); ^{11}B NMR (160 MHz, $CDCl_3$, decoupled): δ -5.1 (1B), -6.2 (1B), -11.1 (4B), -13.4 (2B), -14.4 (2B); ^{13}C NMR (126 MHz, $CDCl_3$): δ 158.6 (*C*=O), 75.9 (C_c-CO), 54.3 (C_c-H), 47.9 (*C*H_2-CH_2CH_2NCO), 26.2 (2C, *C*H_2-NCO), 24.2 (2C, *C*H_2-CH_2NCO); HRMS (ESI) Experimental $[M+Na]^+$ m/z = 278.2514, Calculated m/z = 278.2528, Deviation = 5 ppm.

Compound **7.4**: ^{1}H NMR (500 MHz, $CDCl_3$): δ 3.67 (2 H, s), 3.50 (2 H, s), 3.01 (1 H, s), 3.40 – 1.57 (10 H, m), 1.92 (2 H, d, *J* 4.4), 1.82 (2 H, d, *J* 4.8); ^{11}B NMR (160 MHz, $CDCl_3$, decoupled): δ -5.5 (1B), -6.3 (1B), -11.0 (4B), -13.3 (2B), -14.6 (2B); ^{13}C NMR (126 MHz, $CDCl_3$): δ 158.2 (*C*=O), 54.6 (C_c-H), 49.8 (*C*H_2-NCO), 49.2 (*C*H_2-NCO), 27.3 (*C*H_2-CH_2NCO), 23.1 (*C*H_2-CH_2NCO); HRMS (ESI) Experimental $[M+Na]^+$ m/z = 264.2368, Calculated m/z = 264.2371, Deviation = 1.1 ppm

7.4. Summary and conclusions

We present here an unprecedented strategy for the synthesis of 1-*m*-carboranyl amides via the one-pot one-step reaction of 1-iodo-*m*-carborane with primary or secondary amines under CO atmosphere in the presence of a palladium complex acting as a catalyst. The effects of the catalyst, the ligand, the base, CO pressure and reaction time have been investigated. Under optimized conditions, slightly lower yields than those previously reported using alternative strategies have been obtained, but both the number of steps and the workup required have been substantially decreased. To the best of our knowledge, the preparation of carboranyl derivatives using the Heck carbonylation reaction has not been reported to date and could be a powerful tool for the synthesis of more complex molecules containing a carborane cage. Moreover, this strategy should be suitable for the preparation of ^{11}C-labelled carboranyl amides using [^{11}C]CO as labeling agent for further *in vivo* evaluation using PET. This work will be approached in our lab in the next future.

8. General conclusions.

1- The preparation of ^{18}F-labelled *o*-carborane can be achieved via nucleophilic substitution using cyclotron produced [^{18}F]F$^-$ and *p*-tolyl-(9-o-carboranyl) iodonium bromide. Further functionalization on the C_c atoms can be approached by formation of the C_c-lithio derivatives and reaction with aldehydes, to yield the corresponding alcohols as a mixture of positional isomers and enantiomers.
2- The preparation of ^{125}I- and ^{131}I-labelled 1-iododecaborane can be achieved by palladium catalyzed isotopic exchange reaction starting from 1-iododecaborane. Subsequent reaction with alkynes using acetonitrile as the solvent under microwave heating results in the formation of the corresponding radiolabelled *o*-carborane derivatives through a one-pot, one-step reaction, with excellent yields in short reaction times.
3- Functionalized 8-I-cobaltabisdicarbollide (I-COSAN) derivatives can be efficiently labelled with ^{125}I and ^{124}I by isotopic exchange in the presence of a palladium catalyst with excellent radiochemical conversion values. Biodistribution studies performed both with PET-CT and dissection/gamma counting showed a similar pattern for all investigated compounds, with significant accumulation in the heart, the liver and the kidneys. Low accumulation was observed in the tumour when mice bearing subcutaneous PANC-1 and A549 tumours were investigated, irrespectiove of the functionality attached to the COSAN complex.
4- The synthesis of 1-(9-amino-1,7-dicarba-*closo*-dodecaboran-1-yl)-benzothiazole could be achieved by reaction of *m*-carboranyl carboxylic acid chloride with 2-aminothiophenol and Lawesson's reagent, followed by iodination using iodine monochloride in the presence of aluminum chloride, subsequent palladium-catalyzed Buchwald-Hartwig amidation reaction to incorporate the trifluoroacetamide group and final hydrolysis under basic conditions. The preparation of 1-(9-amino-1,7-dicarba-*closo*-dodecaboran-1-yl)-6-hydroxy benzothiazole required a different approach, based on the preparation of the iodinated *m*-carboranyl carboxylic acid chloride in a first step, followed by reaction with 2-amino-5-methoxythiophenol, Buchwald-Hartwig amidation, hydrolysis and finally O-demethylation. Both compounds could be efficiently labeled with Carbon-11 to yield the corresponding *N*-[^{11}C]methylated derivatives.
5- The synthesis of 1-*m*-carboranyl amides can be achieved via the one-pot one-step reaction of 1-iodo-*m*-carborane with primary or secondary amines under CO atmosphere in the presence of a palladium complex acting as a catalyst.

9. NMR spectra

Compound Reference Number: 4.2

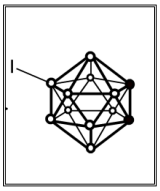

Name: 9-I-1,2-dicarba-closo-dodecaborane
Molecular Formula: $C_2B_{10}H_{11}I$
Molecular Weight: 270.12

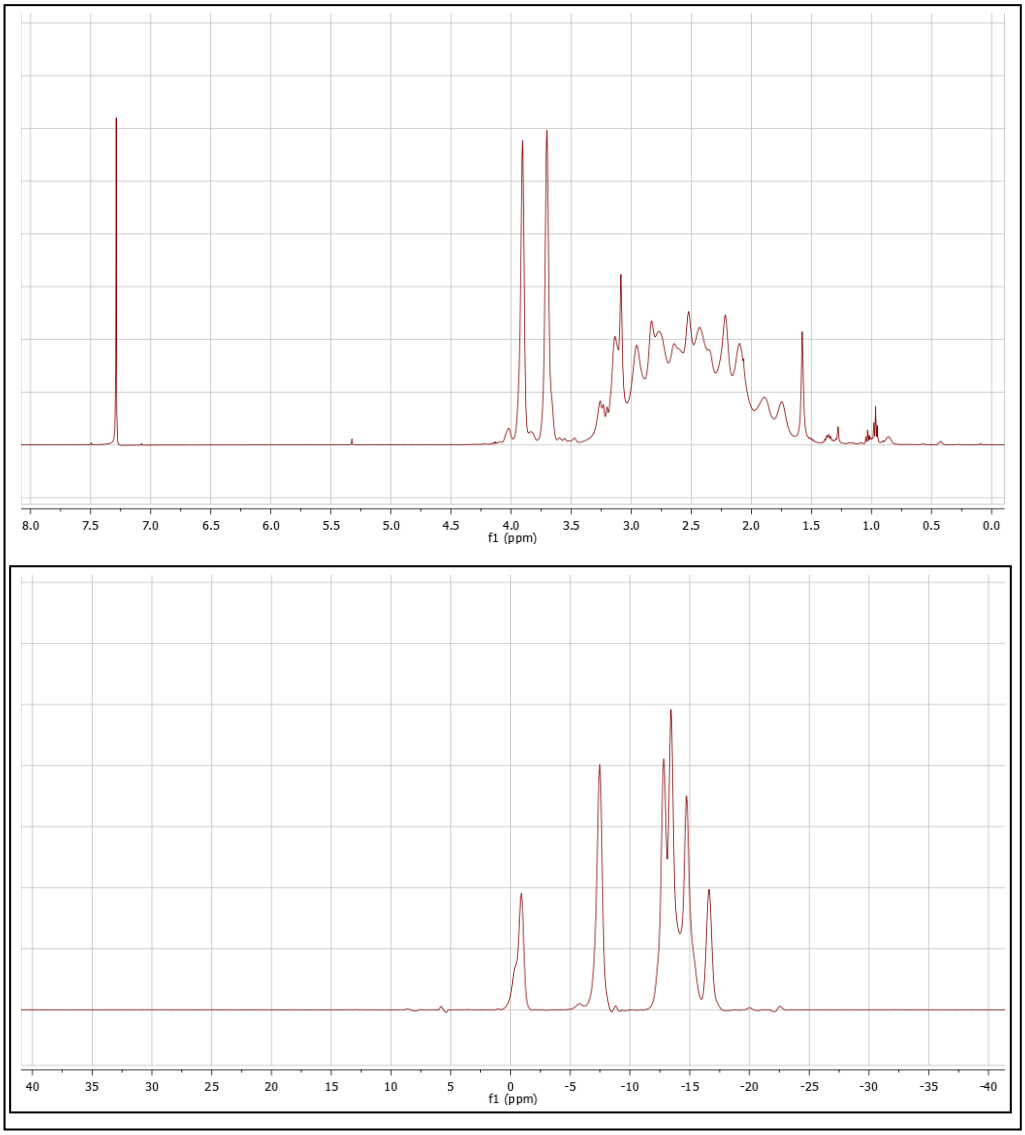

Compound Reference Number: 4.3

Name: p-tolyl-(9-o-carboranyl) iodonium bromide
Molecular Formula: $C_9B_{10}H_{18}IBr$
Molecular Weight: 441.16

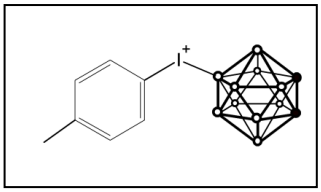

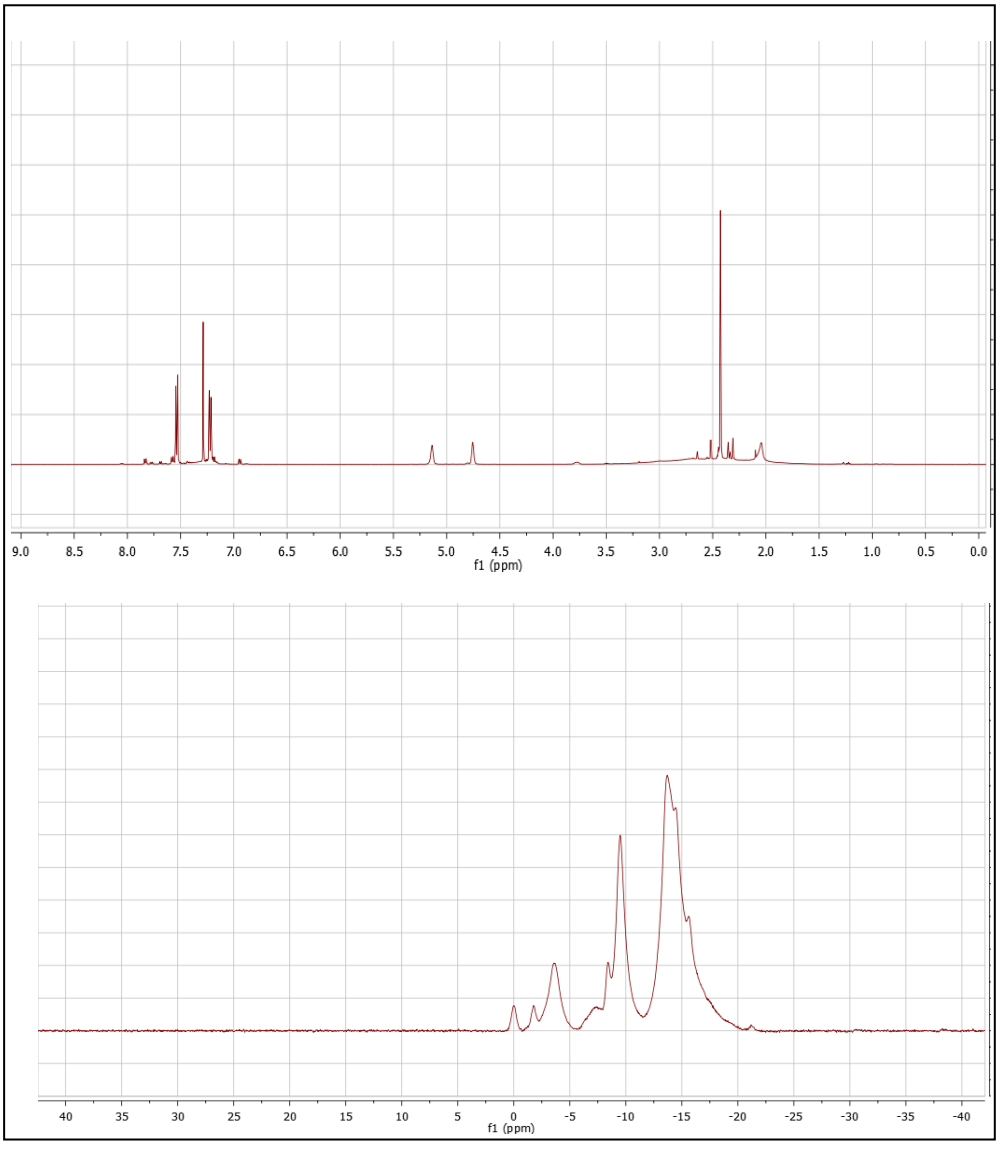

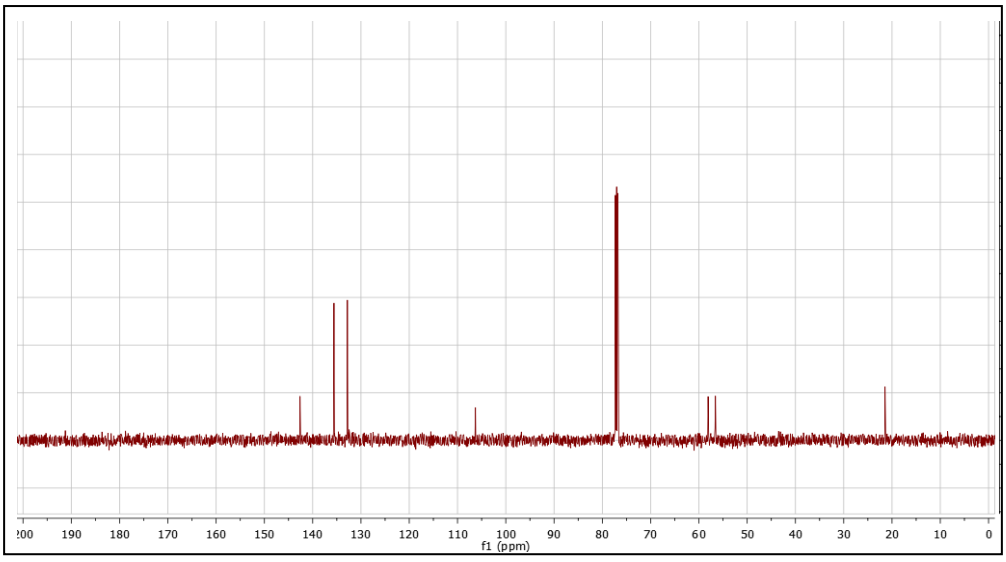
200
190
180
170
160
150
140
130
120
110
100
90
80
70
60
50
40
30
20
10
0
f1 (ppm)

Compound Reference Number: 4.4

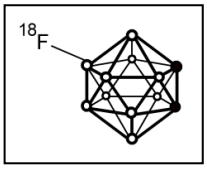

Name: 9-F-1,2-dicarba-closo-dodecaborane
Molecular Formula: $C_2B_{10}H_{11}F$
Molecular Weight: 162.2

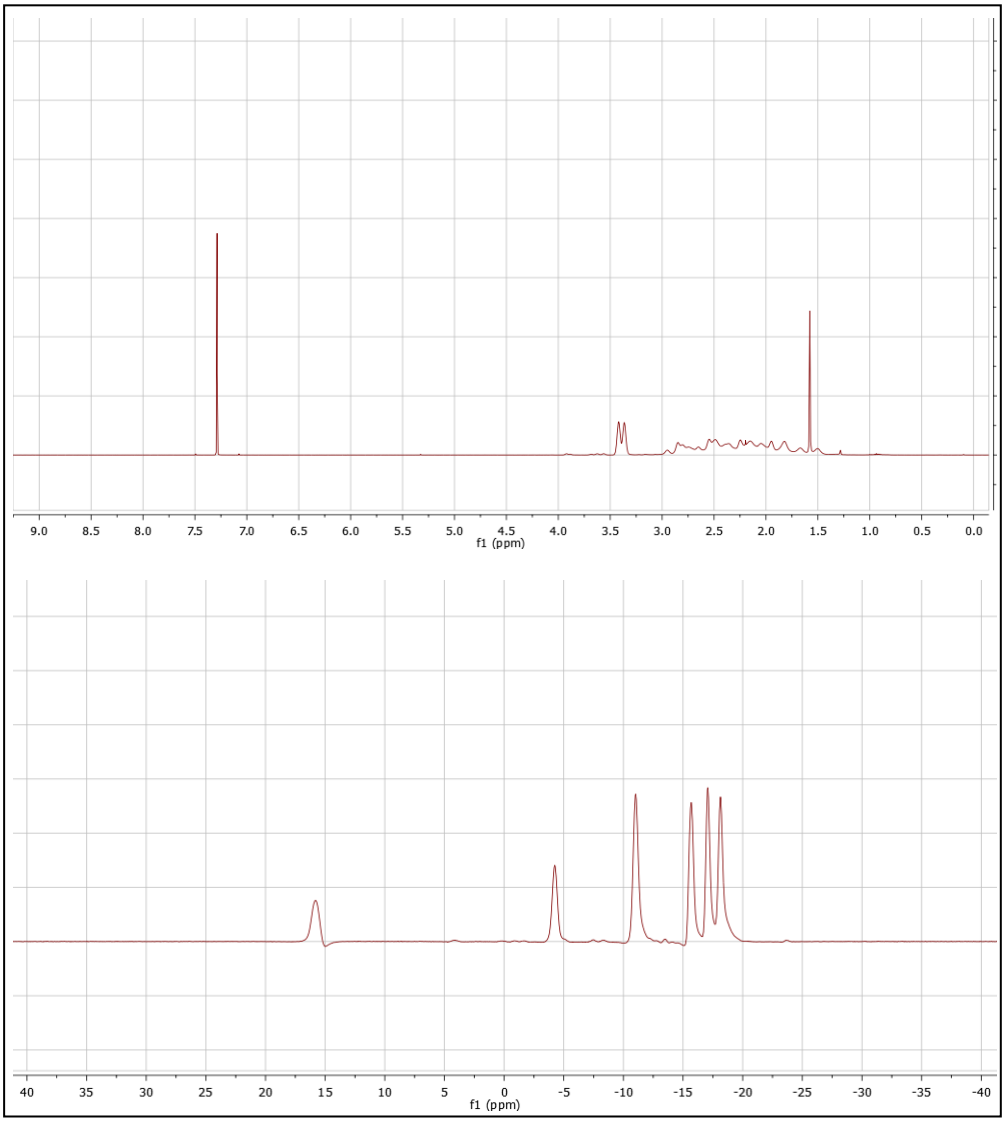

Compound Reference Number: 4.5

Name: 9 (9-fluoro-o-carboranyl) (4-methoxyphenyl) methanol
Molecular Formula: $C_{10}B_{10}H_{19}FO_2$
Molecular Weight: 298.36

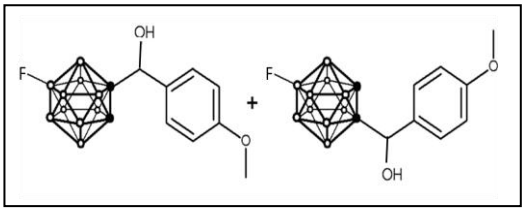

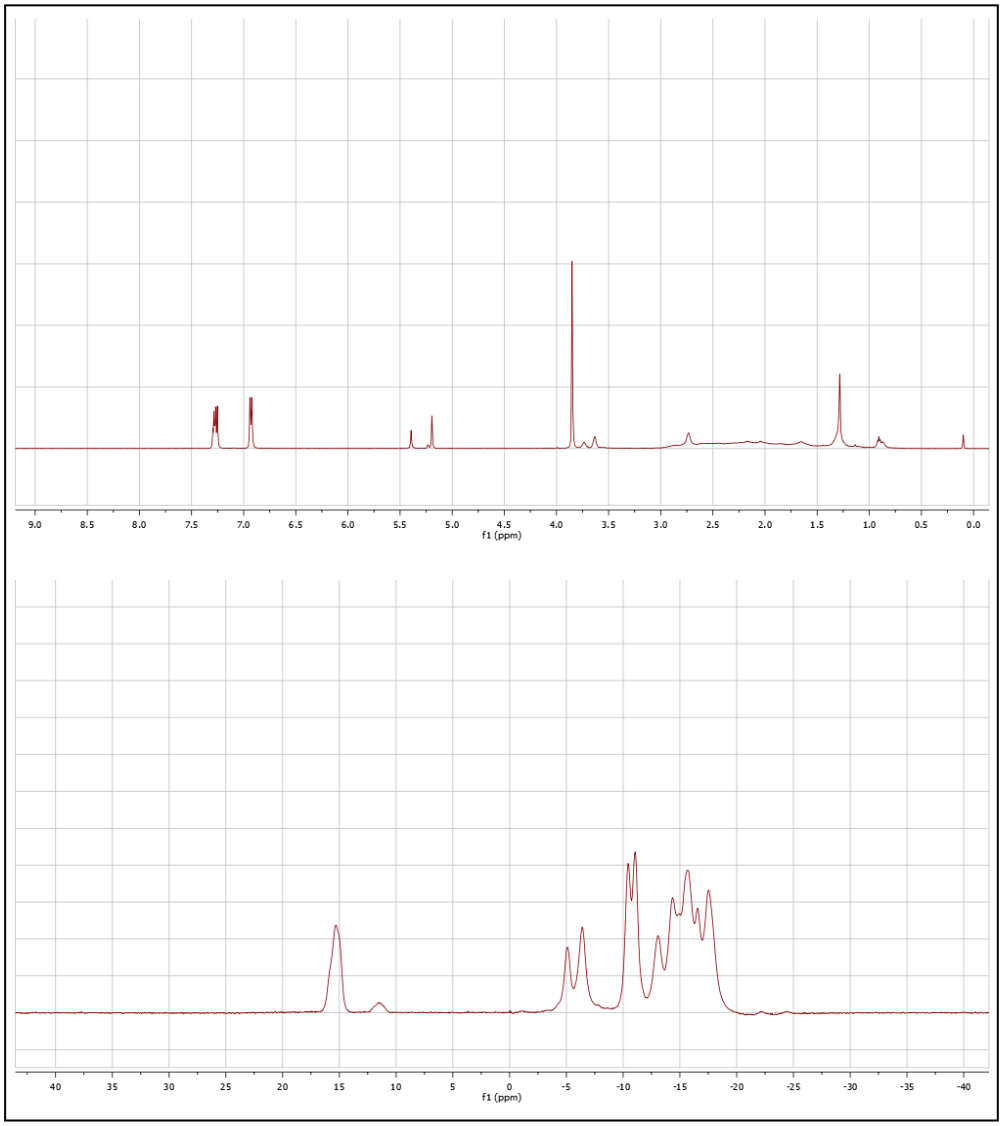

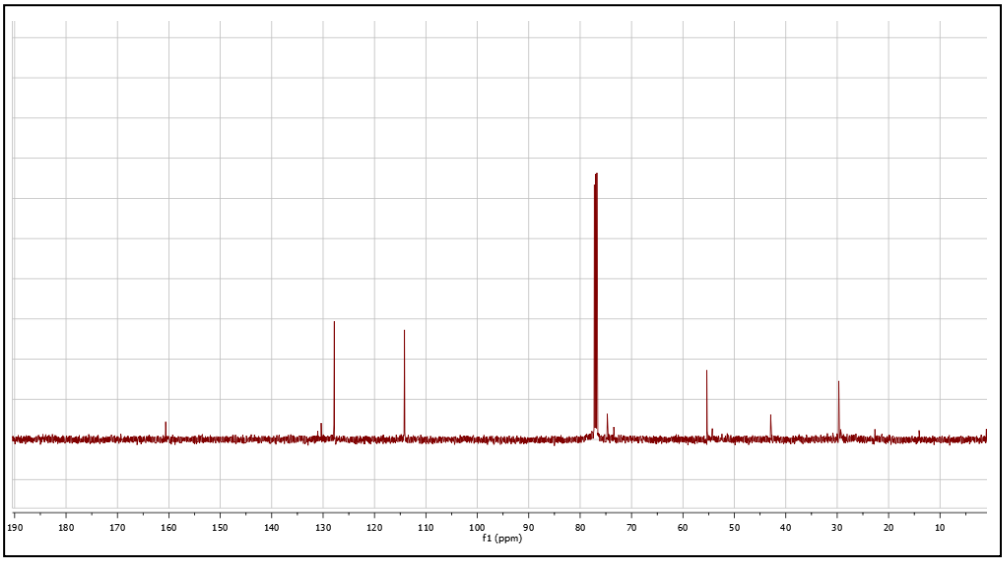
190
180
170
160
150
140
130
120
110
100
90
80
70
60
50
40
30
20
10
f1 (ppm)

Compound Reference Number: 4.6 (a&b)

Name: (9-fluoro-o-carboranyl) (1,2:3,4-Di-o-isopropylidene-l-arabinopyranose) methanol

Molecular Formula: $C_{14}B_{10}H_{31}FO_6$

Molecular Weight: 422.50

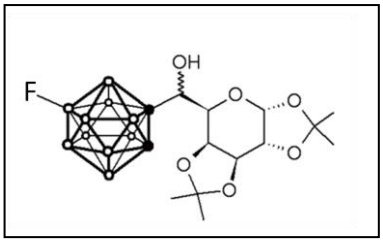

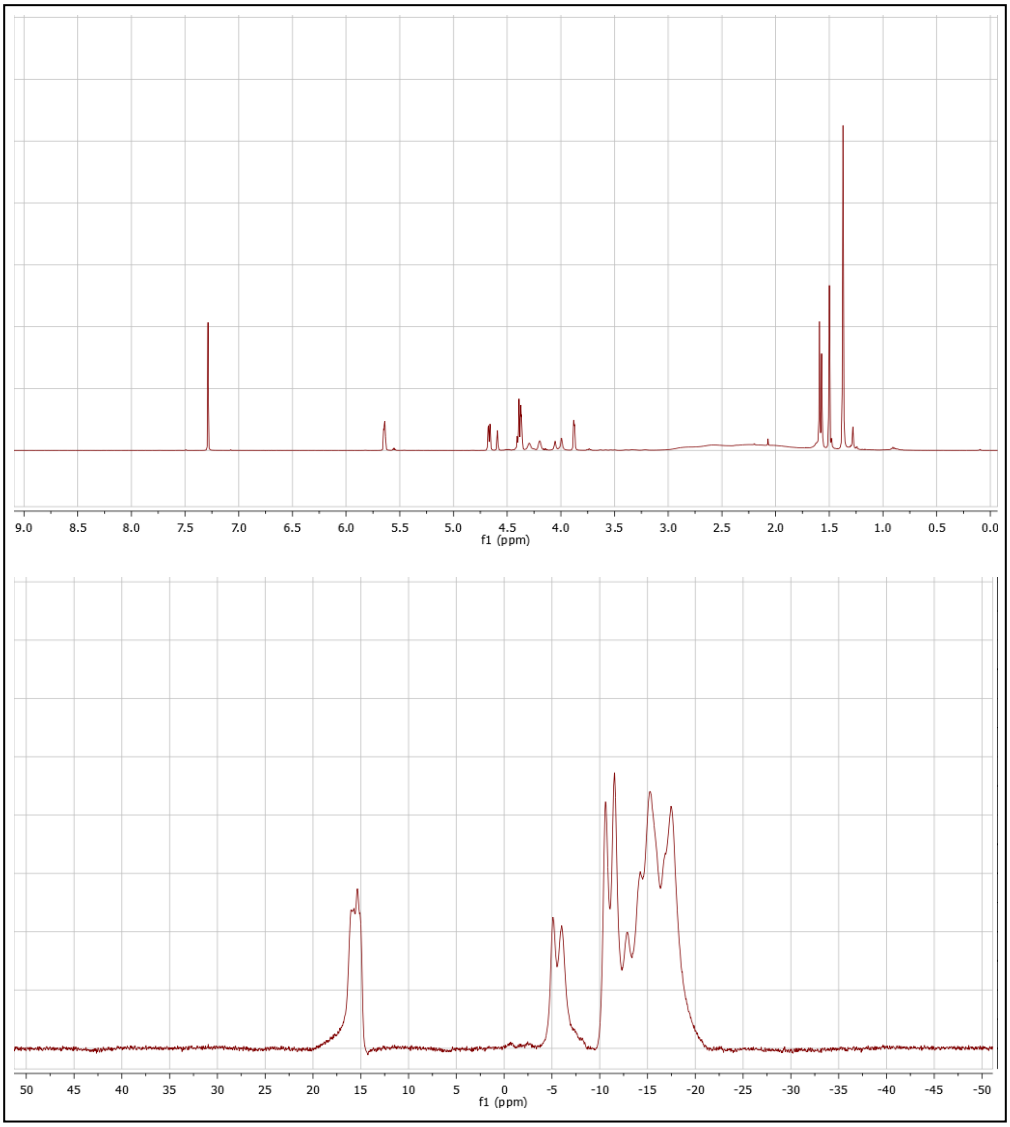

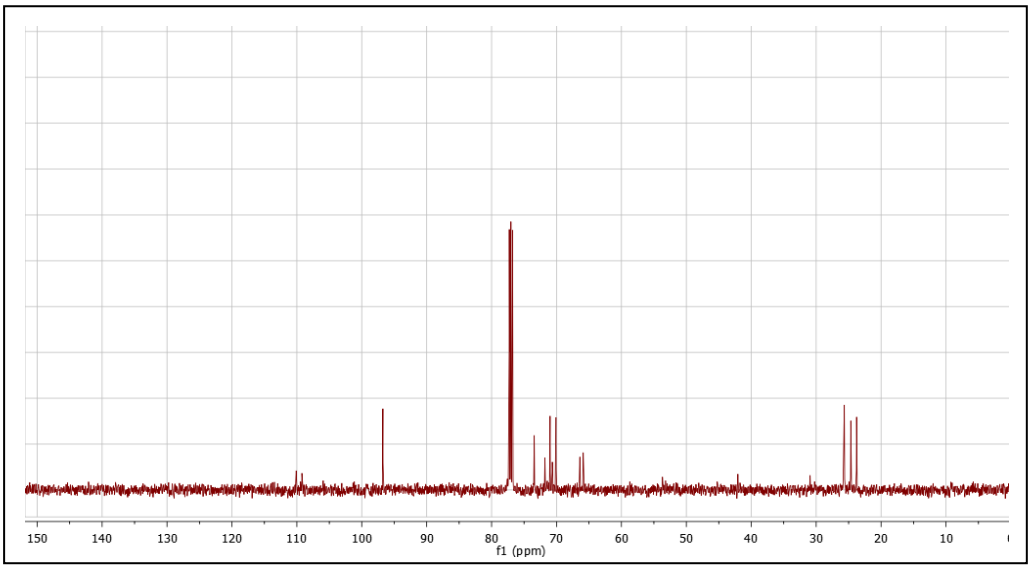
150
140
130
120
110
100
90
80
70
60
50
40
30
20
10
f1 (ppm)

Compound Reference Number: 4.6(c&d)

Name: (12-fluoro-o-carboranyl) (1,2:3,4-Di-o-isopropylidene-l-arabinopyranose) methanol
Molecular Formula: $C_{14}B_{10}H_{31}FO_6$
Molecular Weight: 422.50

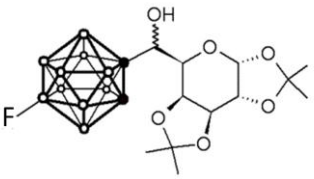

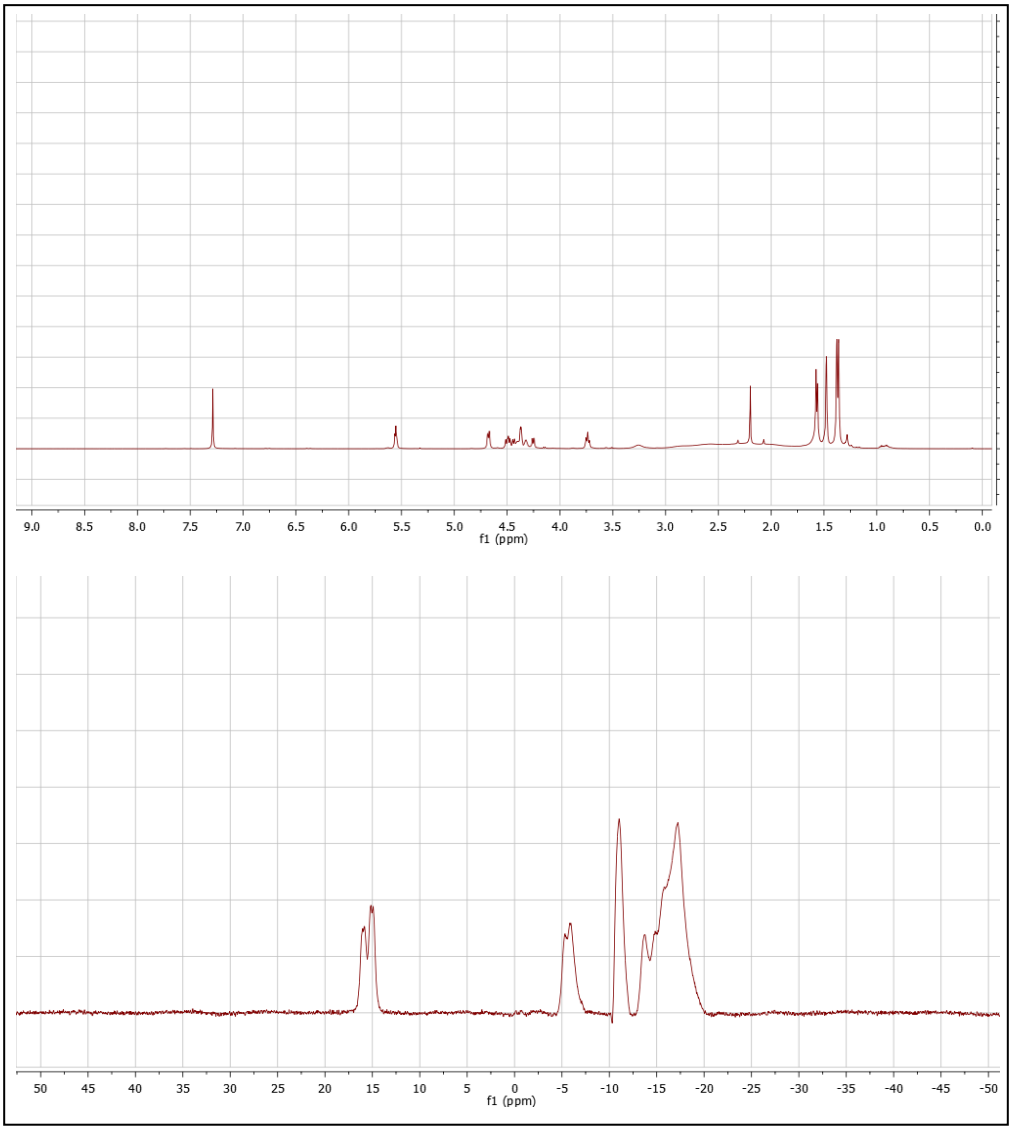

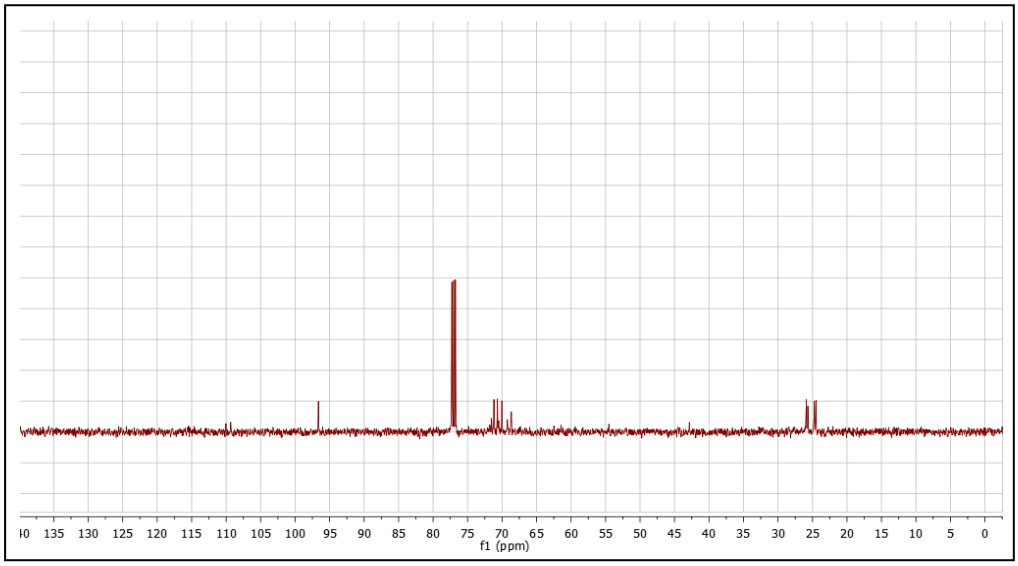
140 135 130 125 120 115 110 105 100 95 90 85 80 75 70 65 60 55 50 45 40 35 30 25 20 15 10 5 0
f1 (ppm)

Compound Reference Number: 4.7 (a&b)

Name: (9-fluoro-o-carboranyl) (l-arabinopyranose) methanol
Molecular Formula: $C_8B_{10}H_{23}FO_6$
Molecular Weight: 342.37

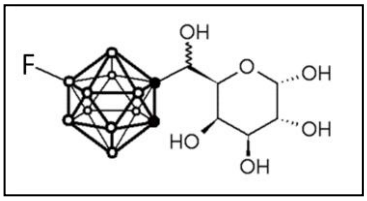

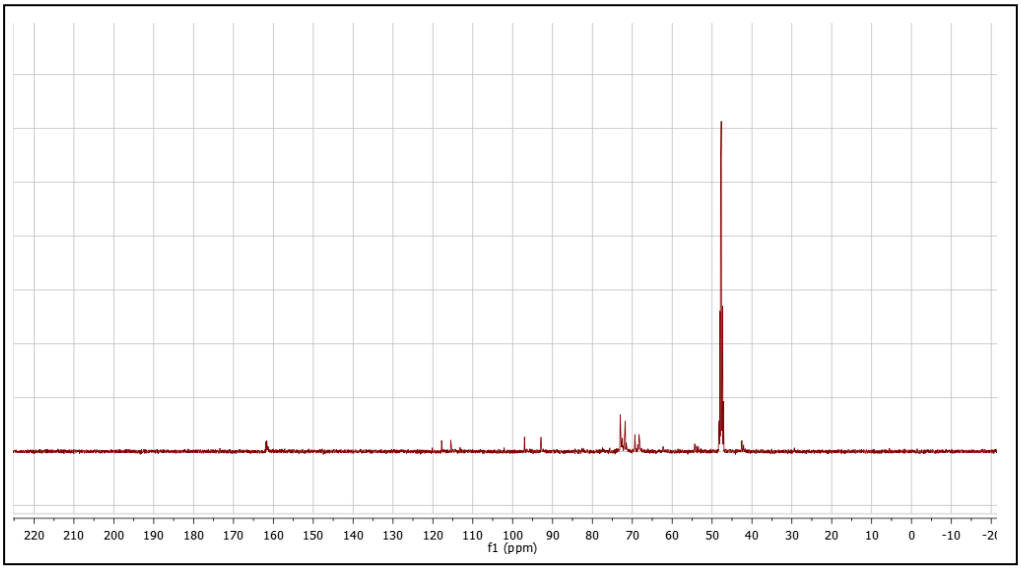
220 210 200 190 180 170 160 150 140 130 120 110 100 90 80 70 60 50 40 30 20 10 0 -10
f1 (ppm)

Compound Reference Number: 4.7 (c&d)

Name: (12-fluoro-o-carboranyl) (l-arabinopyranose) methanol
Molecular Formula: $C_8B_{10}H_{23}FO_6$
Molecular Weight: 342.37

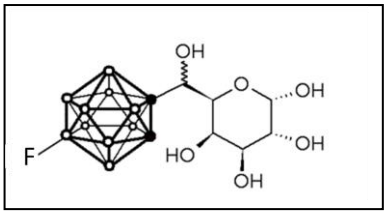

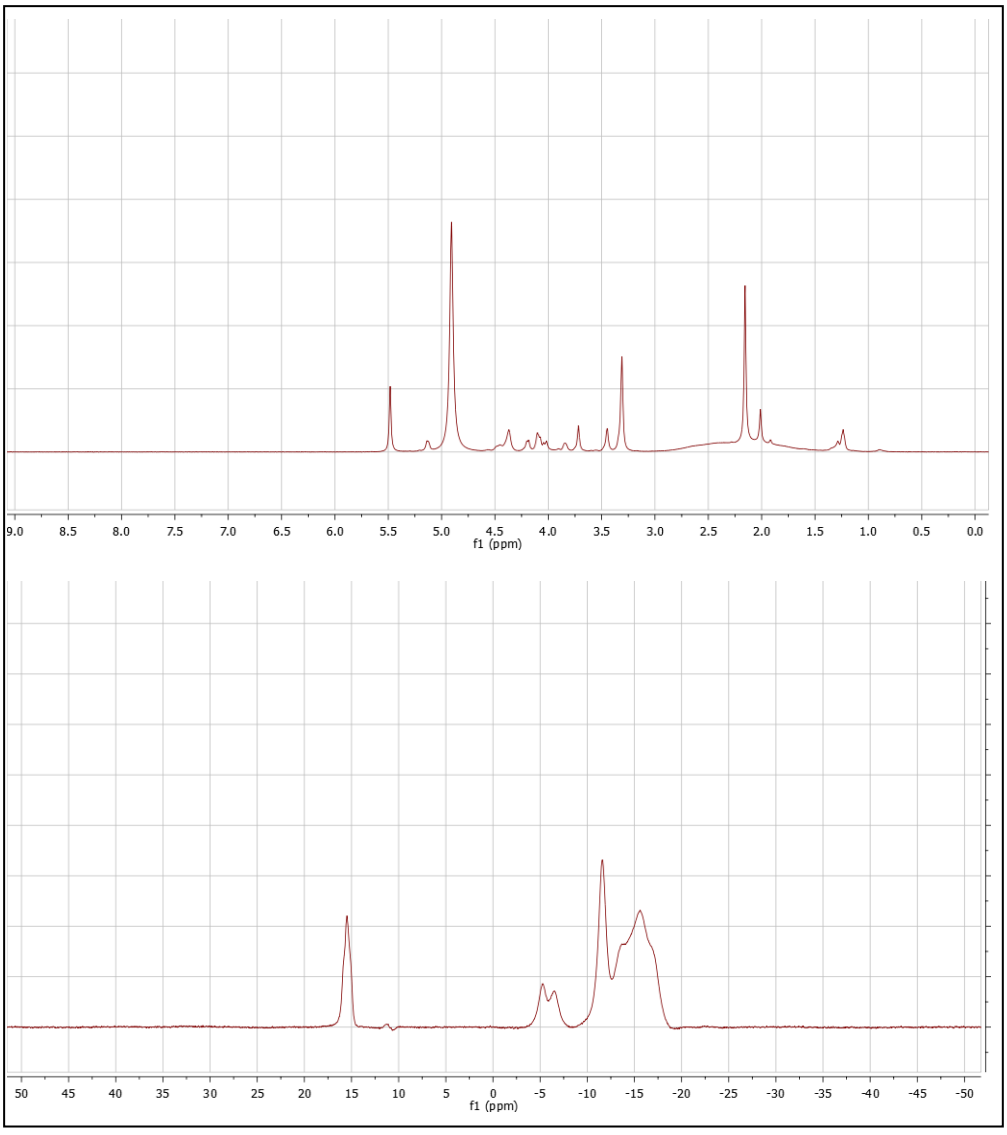

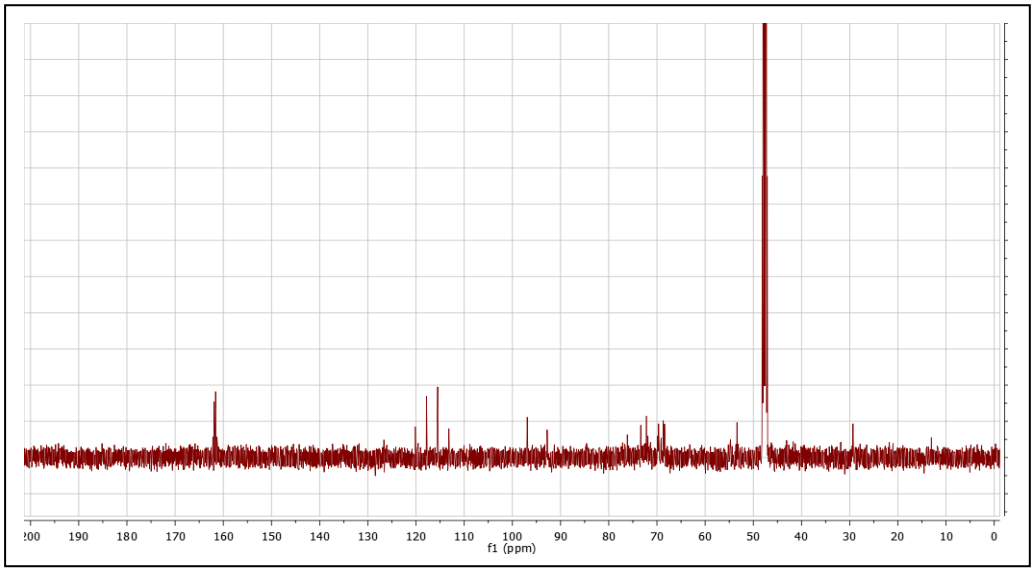
200
190
180
170
160
150
140
130
120
110
100
90
80
70
60
50
40
30
20
10
0
f1 (ppm)

Compound Reference Number: 4.8

Name: 1-Iododecaborane
Molecular Formula: $B_{10}H_{13}I$
Molecular Weight: 248.12

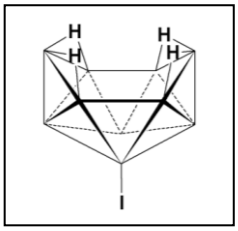

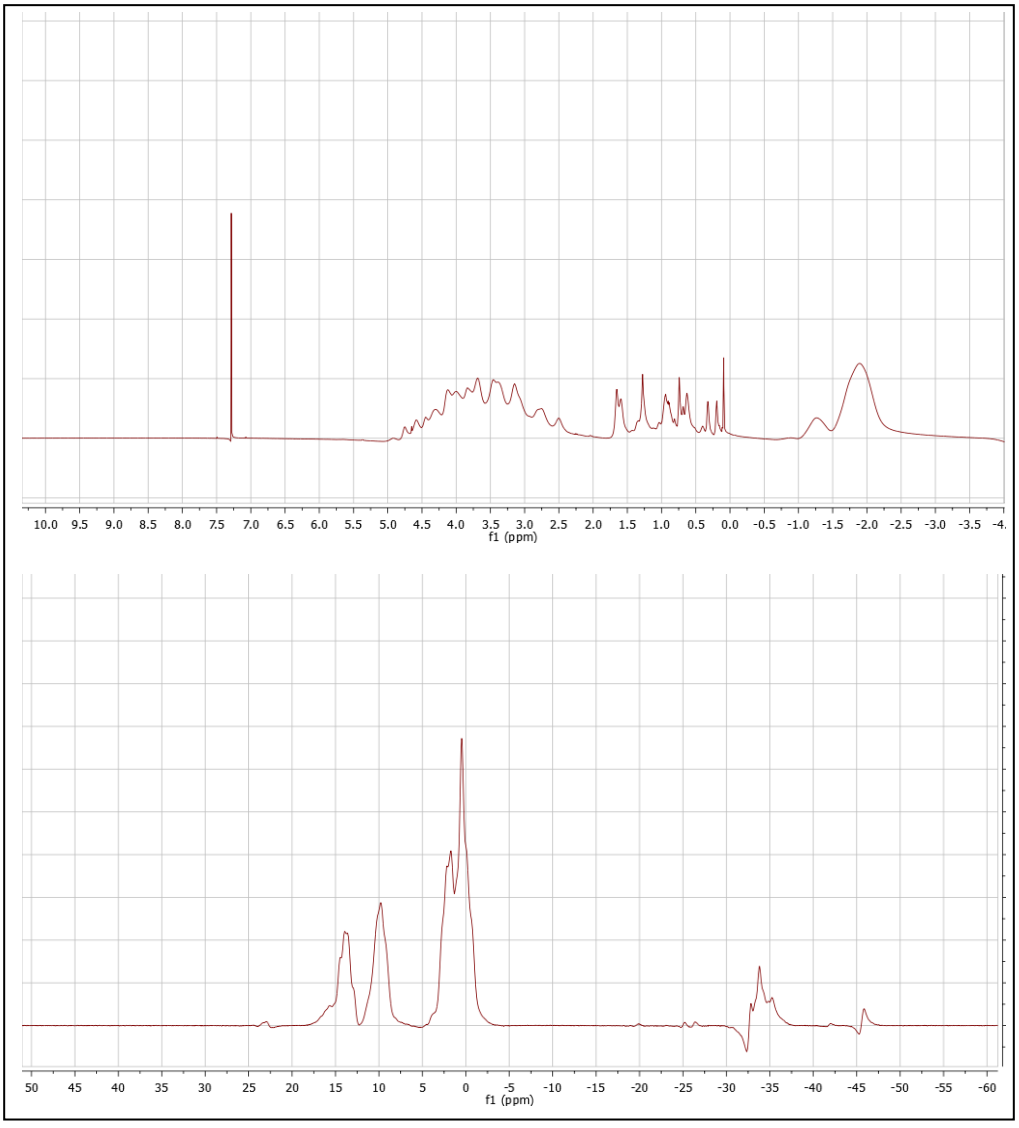

Compound Reference Number: 4.9

Name: 1-octyl-1, 2-closo-dodecaborane
Molecular Formula: $C_{10}B_{10}H_{24}$
Molecular Weight: 252.41

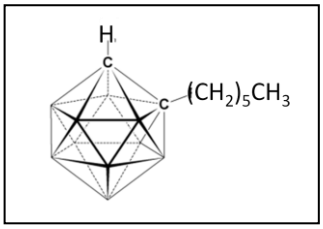

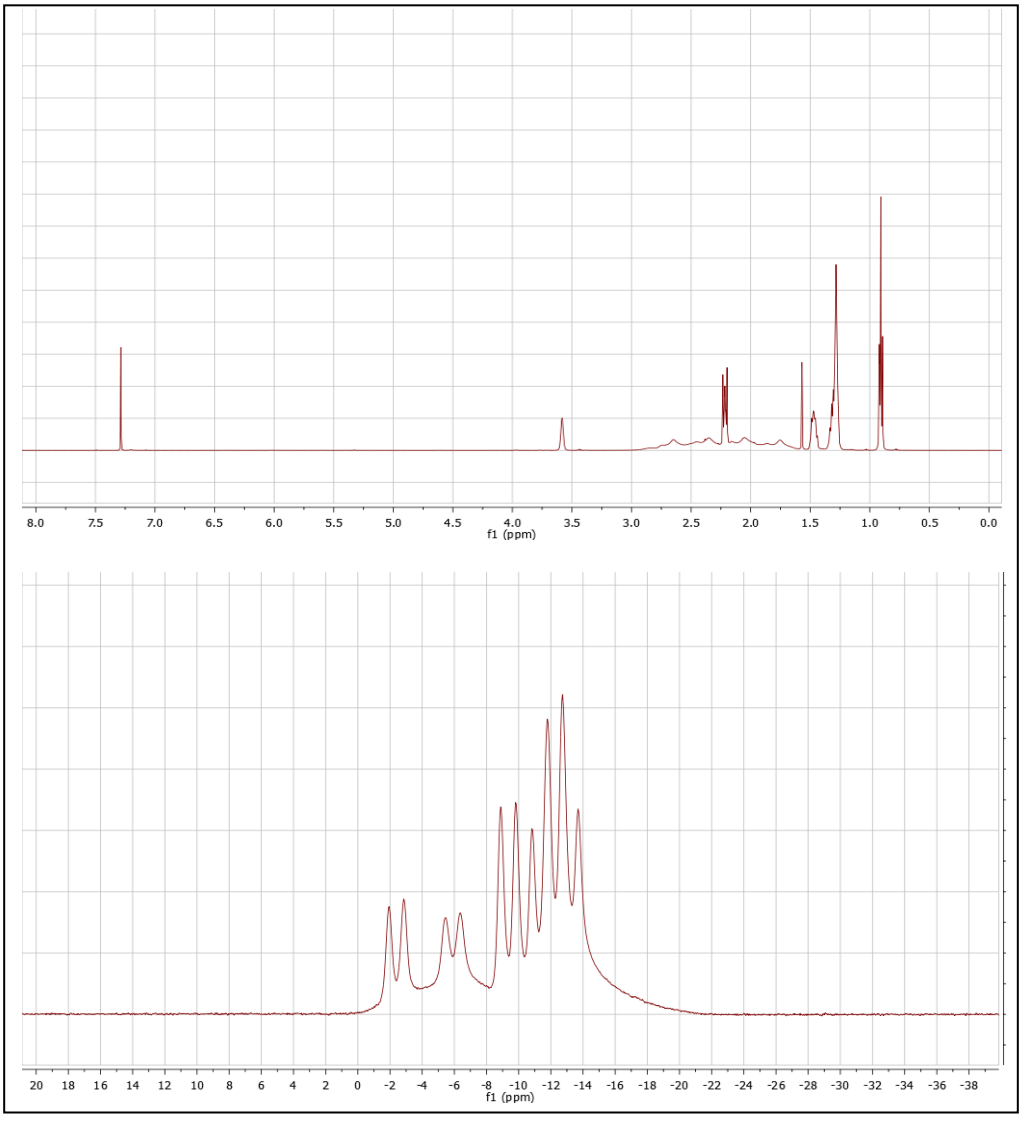

Compound Reference Number: 4.10

Name: 1-phenyl-1, 2-closo-dodecaborane
Molecular Formula: $C_8B_{10}H_{16}$
Molecular Weight: 220.32

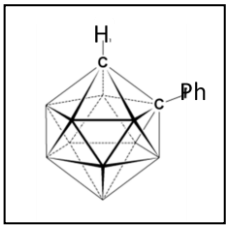

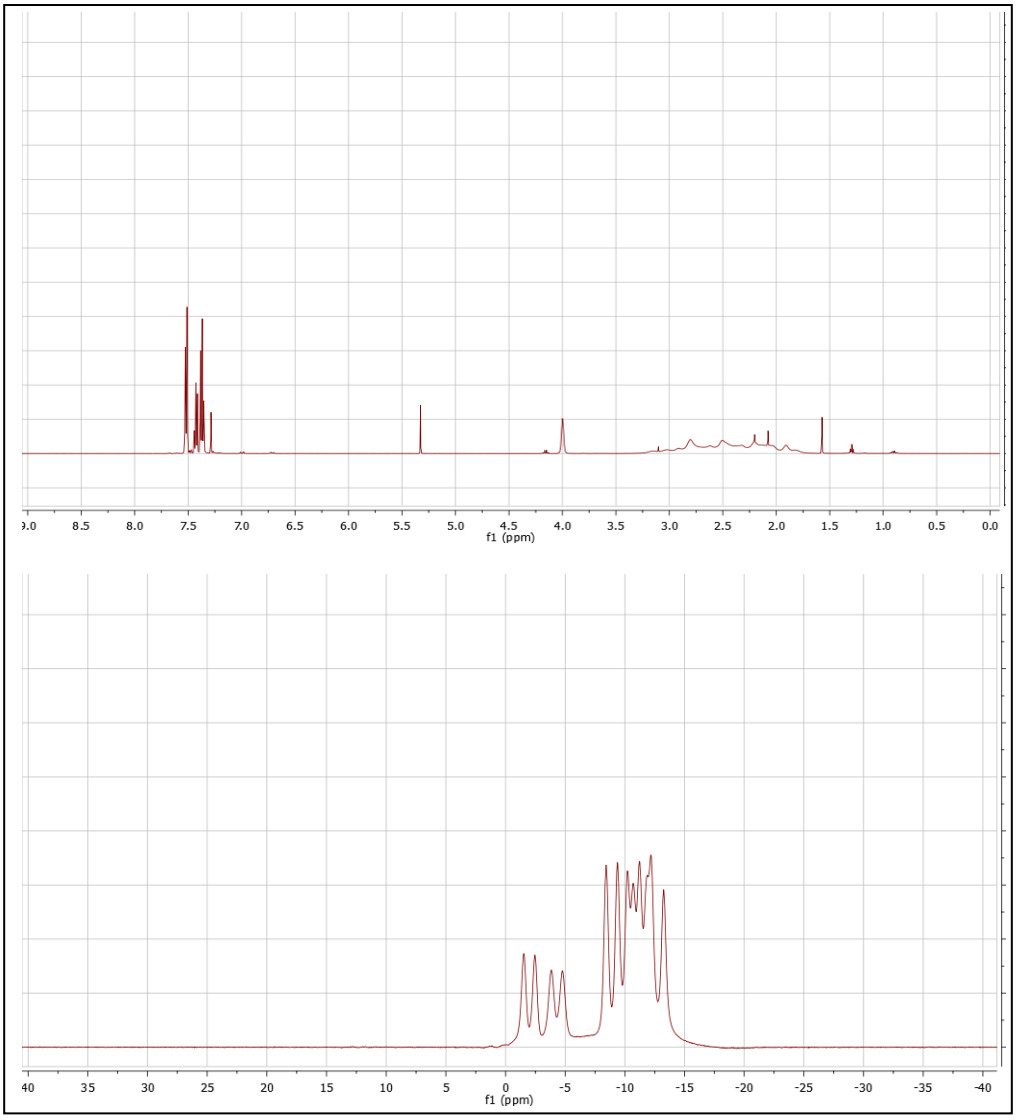

Compound Reference Number: 4.11

Name: 1-butyl-1, 2-closo-dodecaborane
Molecular Formula: $C_6B_{10}H_{20}$
Molecular Weight: 200.33

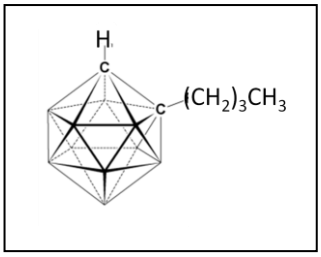

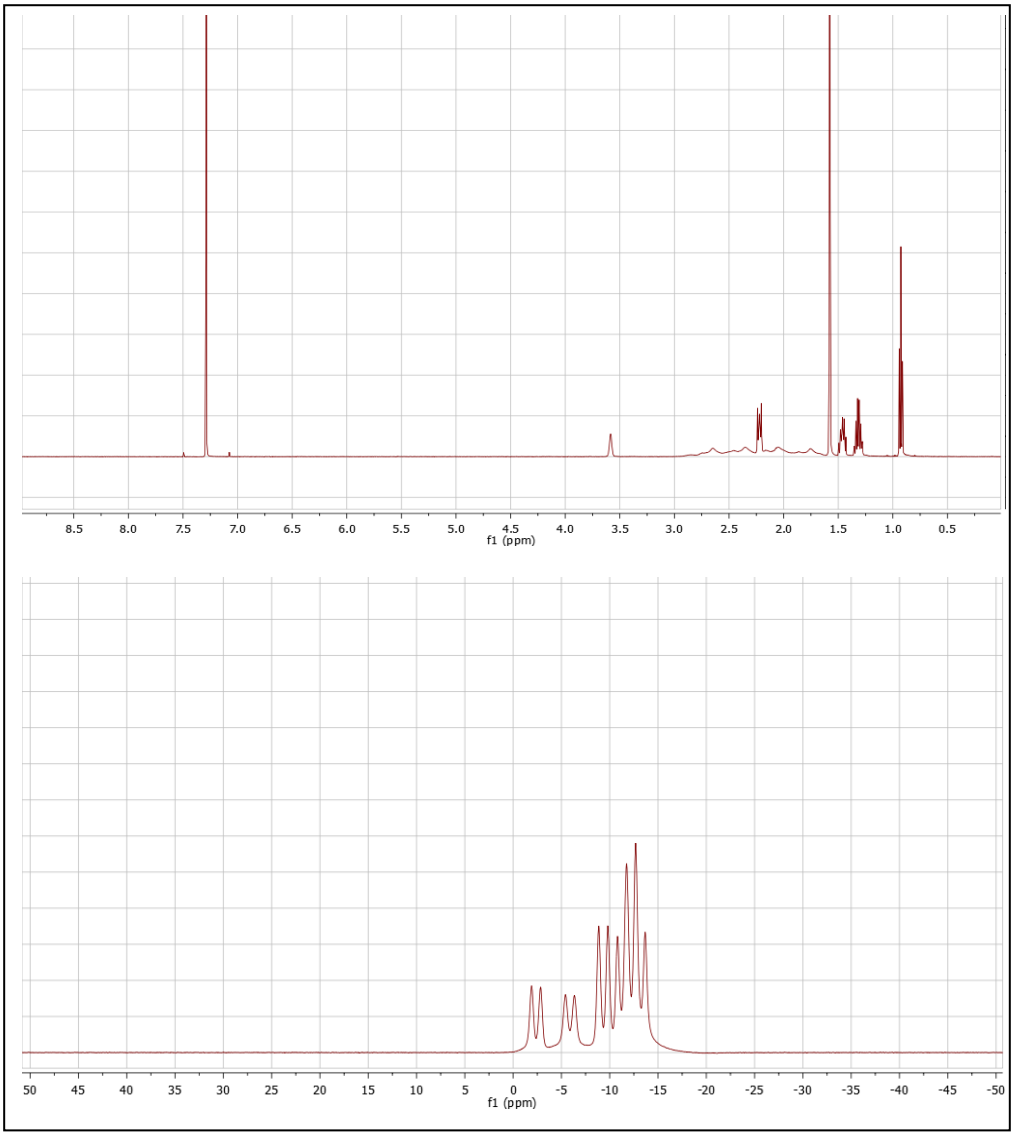

Compound Reference Number: 4.12

Name: 7-hep-1-yl-1, 2-closo-dodecaborane
Molecular Formula: $C_9B_{10}H_{22}$
Molecular Weight: 238.38

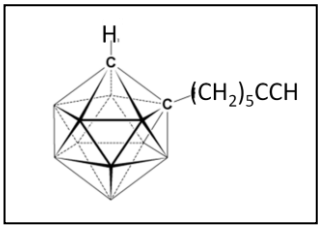

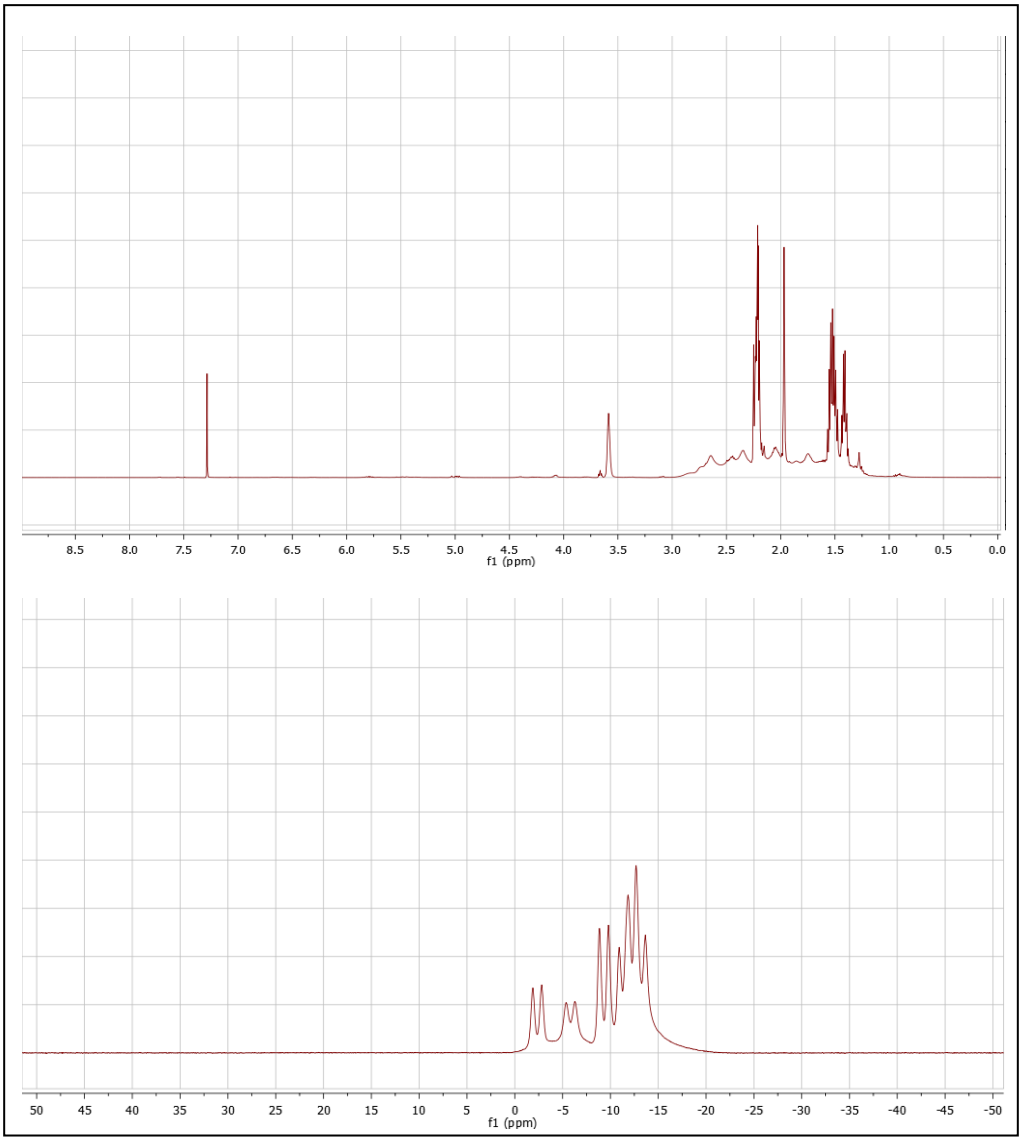

Compound Reference Number: 4.13

Name: 1-methylphenyl-1, 2-closo-dodecaborane
Molecular Formula: $C_9B_{10}H_{18}$
Molecular Weight: 234.35

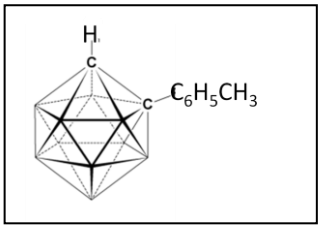

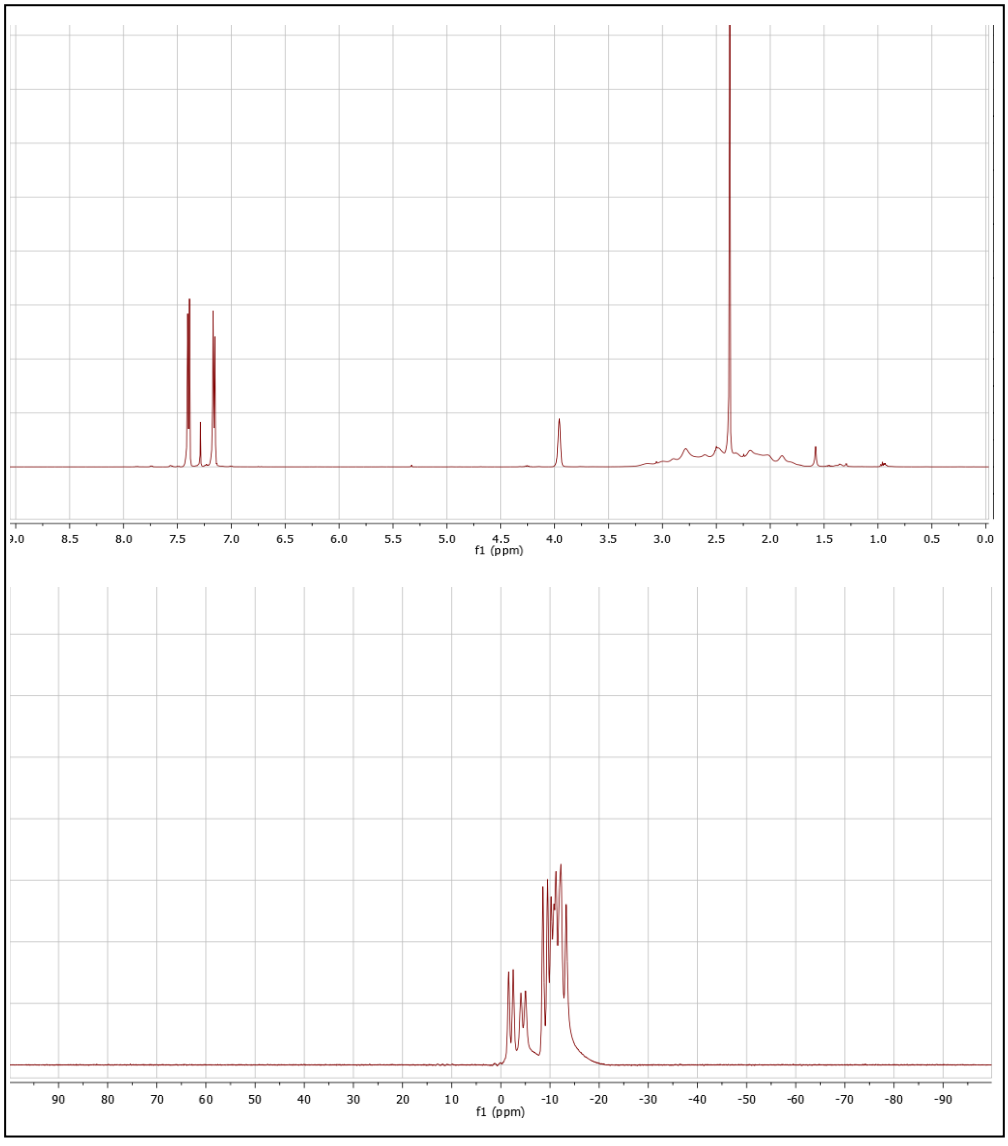

Compound Reference Number: 4.15

Name: 1-phenyl-9-I-1, 2-closo-dodecaborane &
1-phenyl-12-I-1, 2-closo-dodecaborane
Molecular Formula: $C_8B_{10}H_{15}I$
Molecular Weight: 346.22

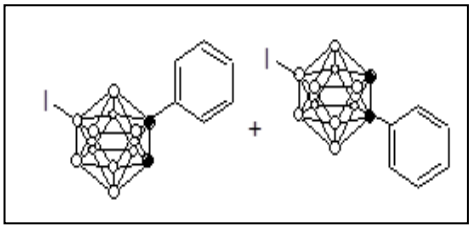

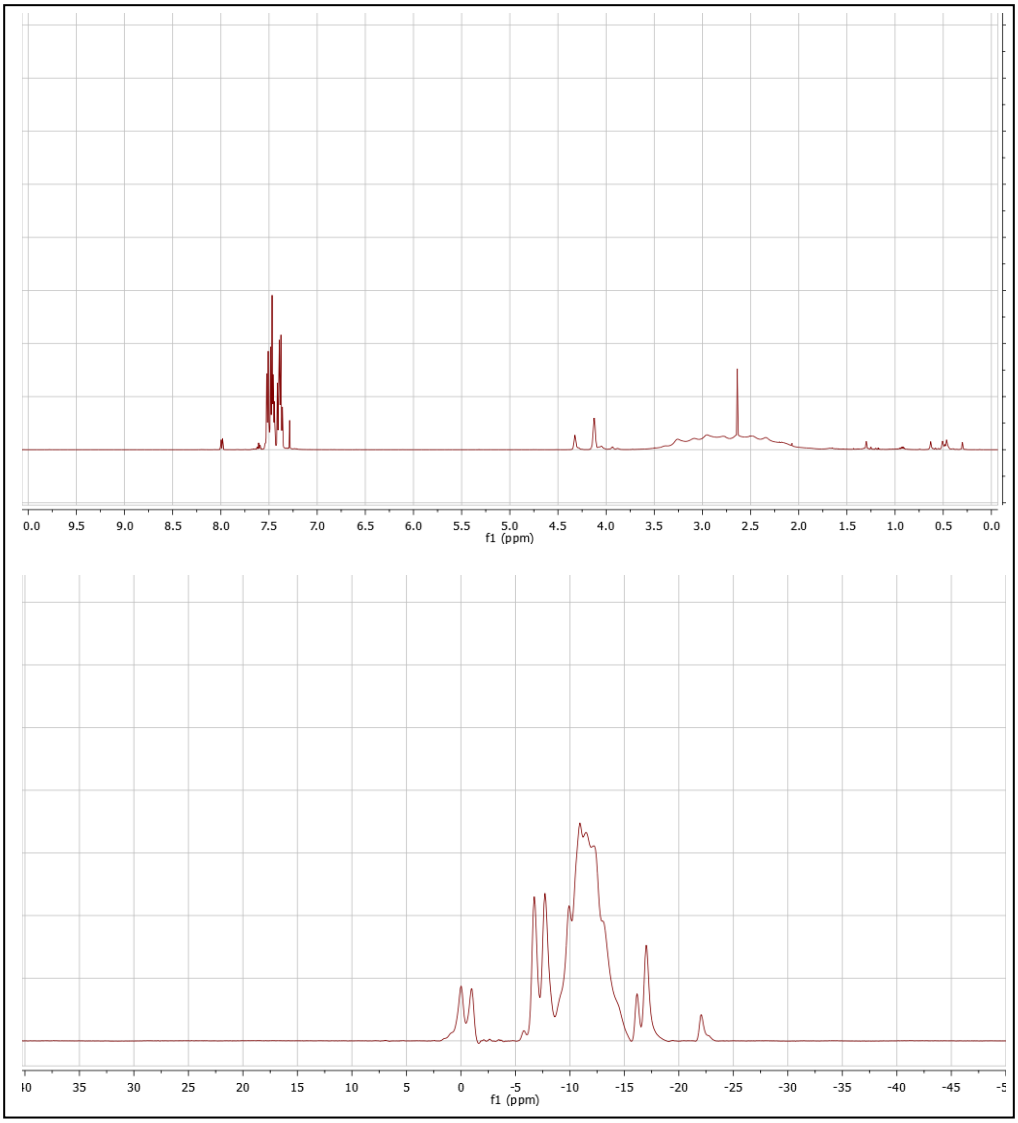

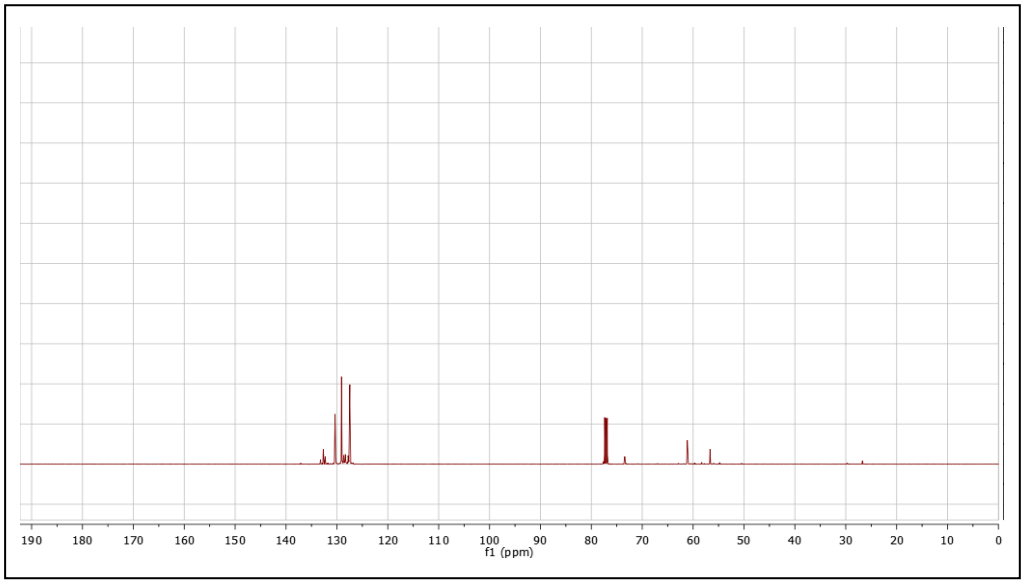
190
180
170
160
150
140
130
120
110
100
90
80
70
60
50
40
30
20
10
0
f1 (ppm)

Compound Reference Number: 4.16

Name: 1-methylphenyl-9-I-1, 2-closo-dodecaborane & 1-methylphenyl-12-I-1, 2-closo-dodecaborane
Molecular Formula: $C_9B_{10}H_{17}I$
Molecular Weight: 360.25

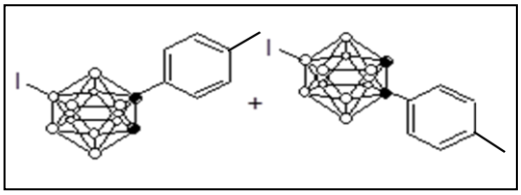

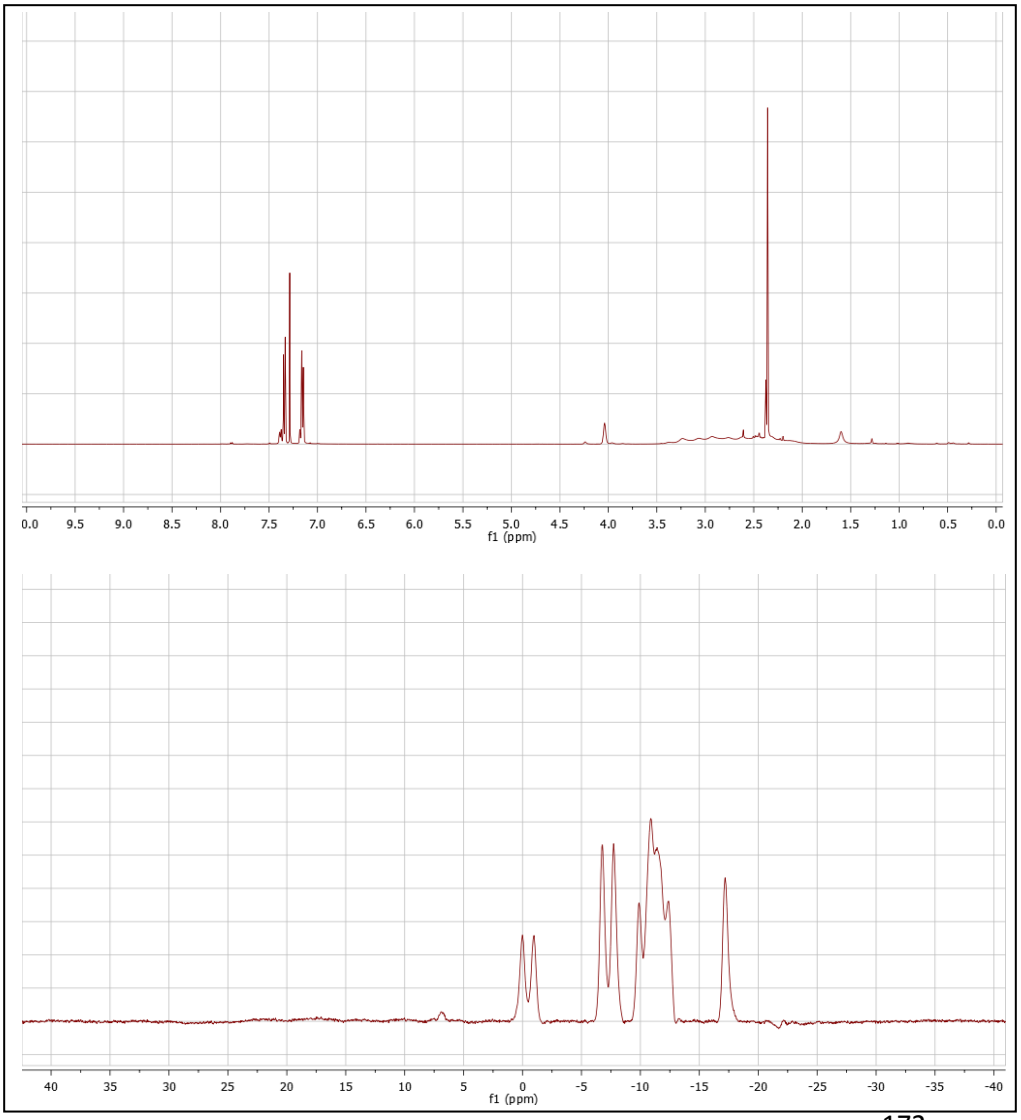

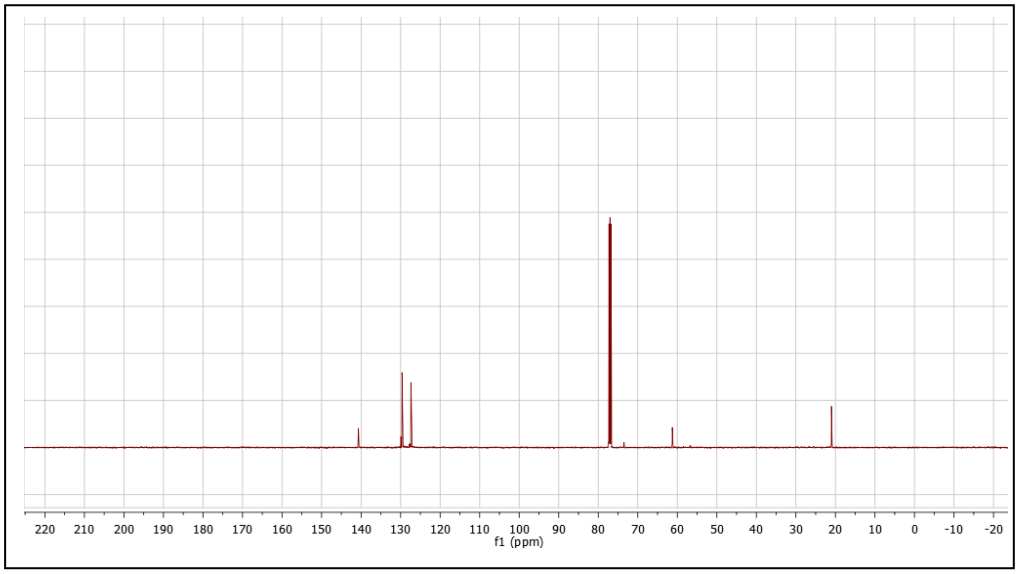
220 210 200 190 180 170 160 150 140 130 120 110 100 90 80 70 60 50 40 30 20 10 0 -10 -20
f1 (ppm)

Compound Reference Number: 4.17

Name: 1-ethylpropiolyl-9-I-1, 2-closo-dodecaborane & 1-ethylpropiolyl-12-I-1, 2-closo-dodecaborane
Molecular Formula: $C_5B_{10}H_{15}O_2I$
Molecular Weight: 342.19

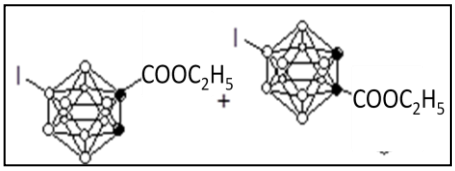

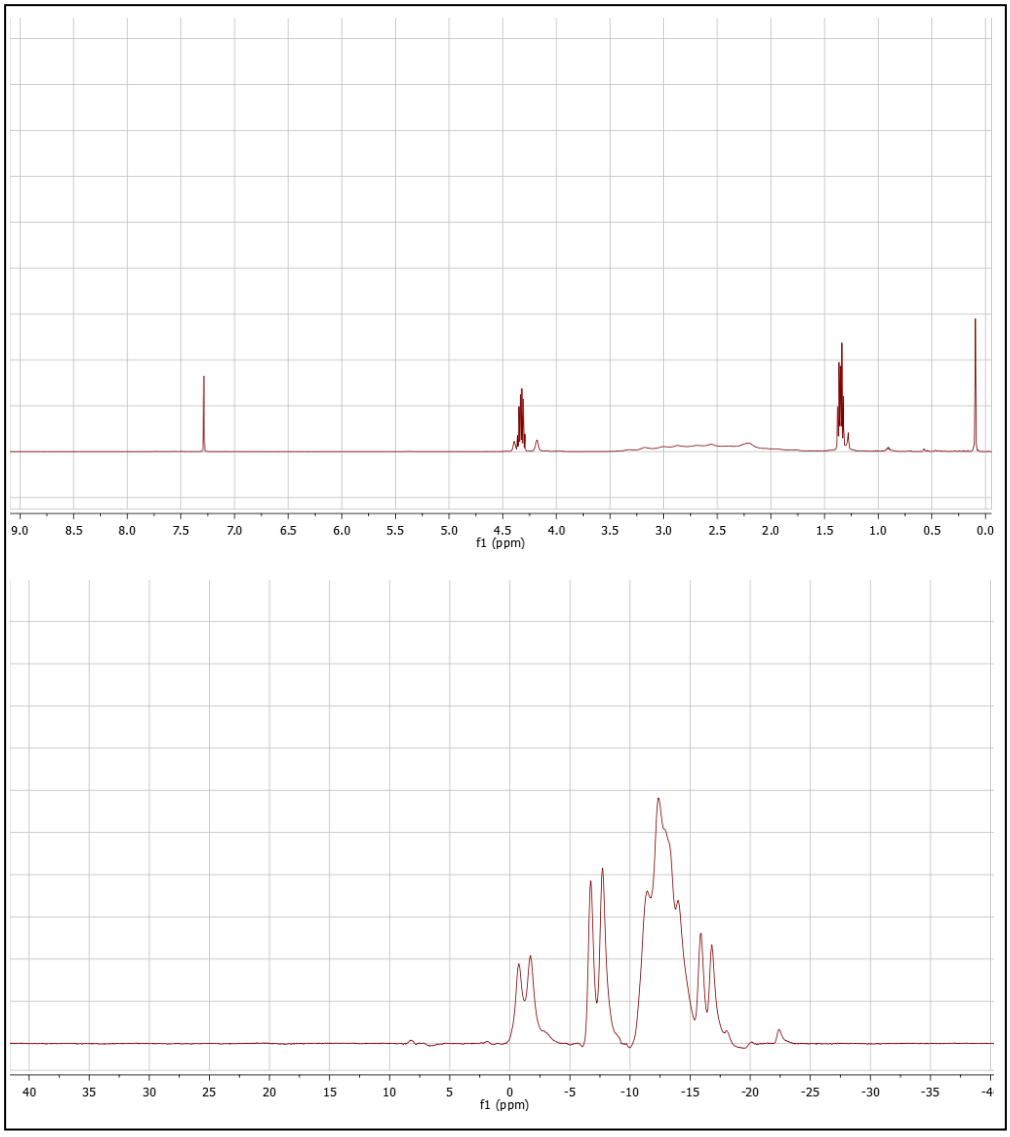

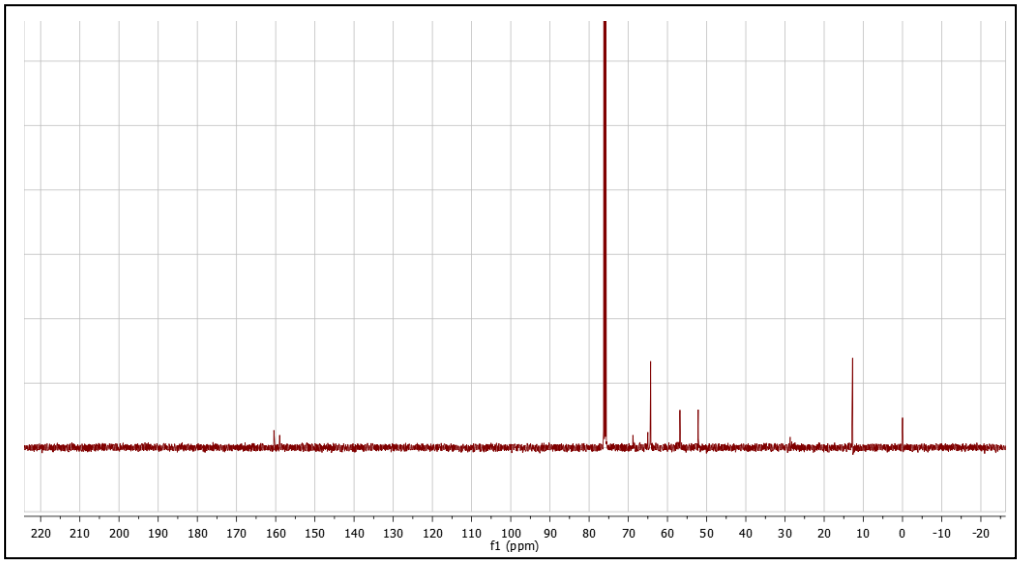
220 210 200 190 180 170 160 150 140 130 120 110 100 90 80 70 60 50 40 30 20 10 0 -10 -20
f1 (ppm)

Compound Reference Number: 4.18

Name: 1-pentyl-5-O-tosyl-9-I-1, 2-closo-dodecaborane & 1- pentyl-5-O-tosyl -12-I-1, 2-closo-dodecaborane
Molecular Formula: $C_{14}B_{10}H_{27}SO_3I$
Molecular Weight: 510.44

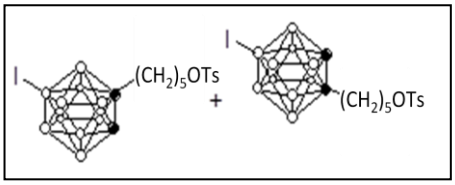

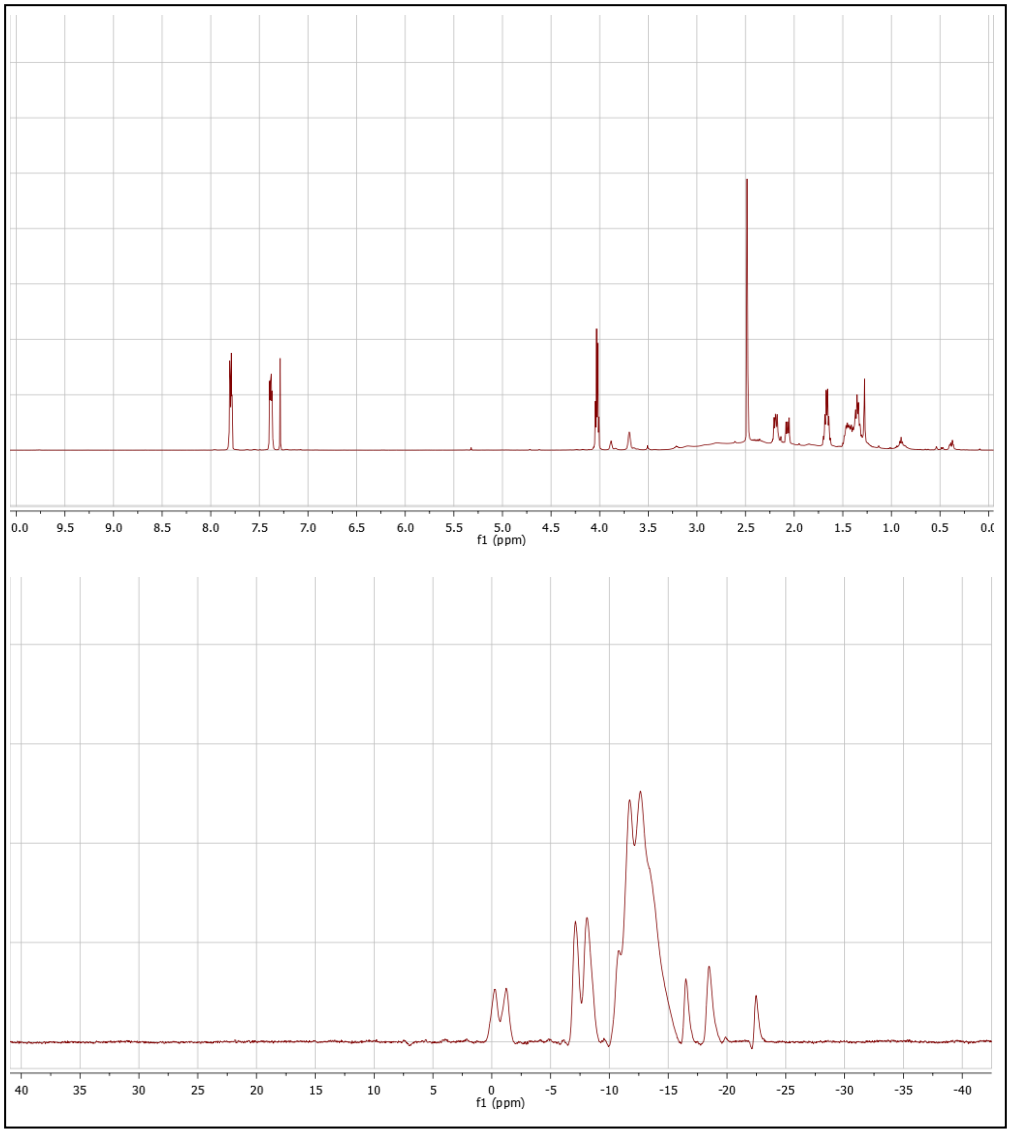

Compound Reference Number: 6.10

Name: 1,7-dicarba-closo-dodecarborane-1-carboxylic acid
Molecular Formula: $C_3B_{10}H_{12}O_2$
Molecular Weight: 188.24

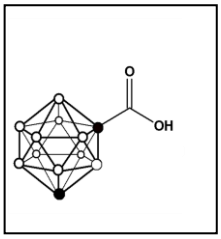

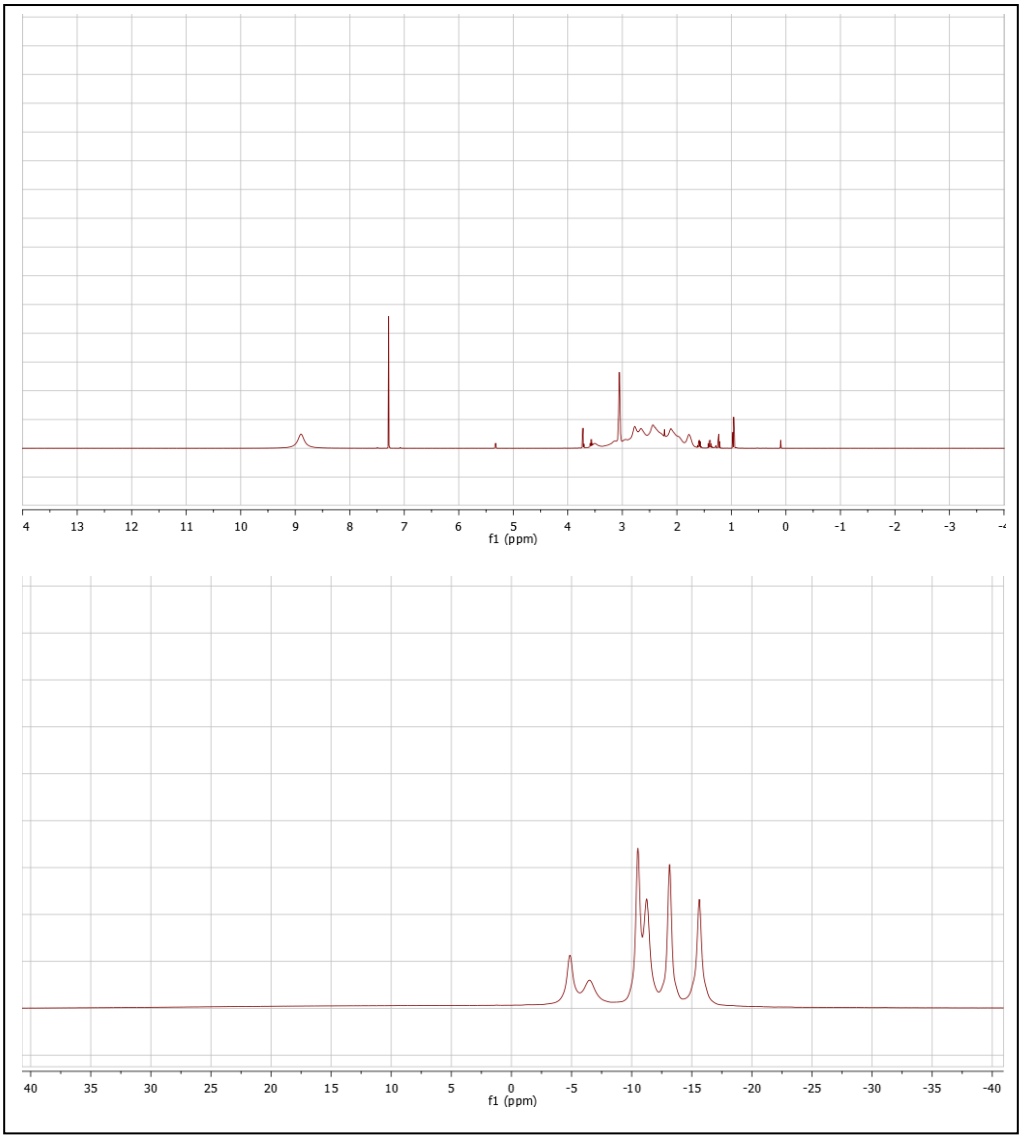

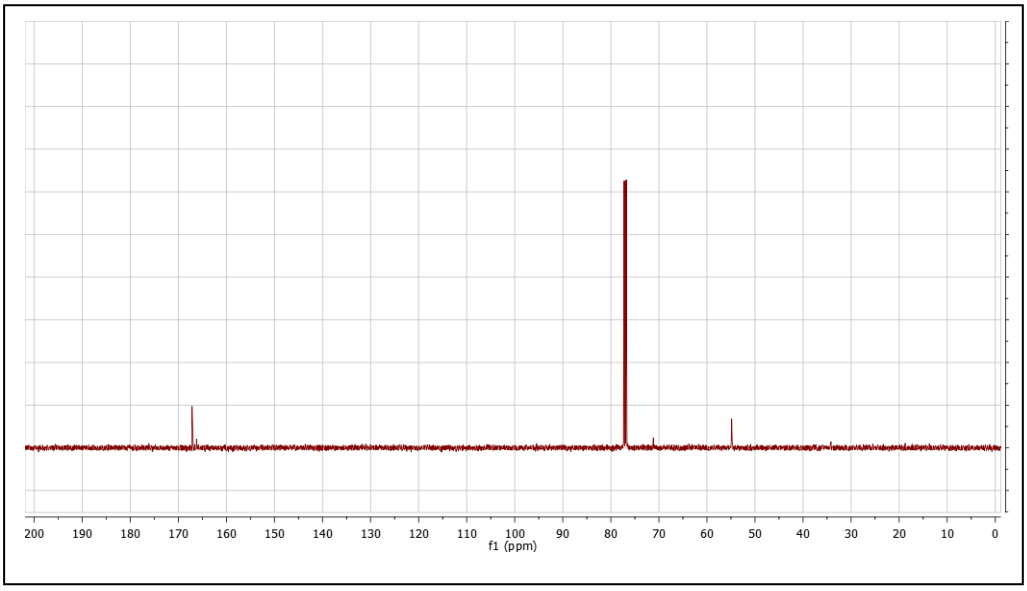
200
190
180
170
160
150
140
130
120
110
100
90
80
70
60
50
40
30
20
10
0
f1 (ppm)

Compound Reference Number: 6.12

Name: 1-(1,7-dicarba-closo-dodecaboran-1-yl)-benzothiazole
Molecular Formula: $C_9B_{10}H_{16}NS$
Molecular Weight: 278.40

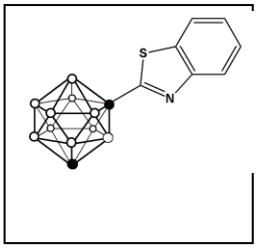

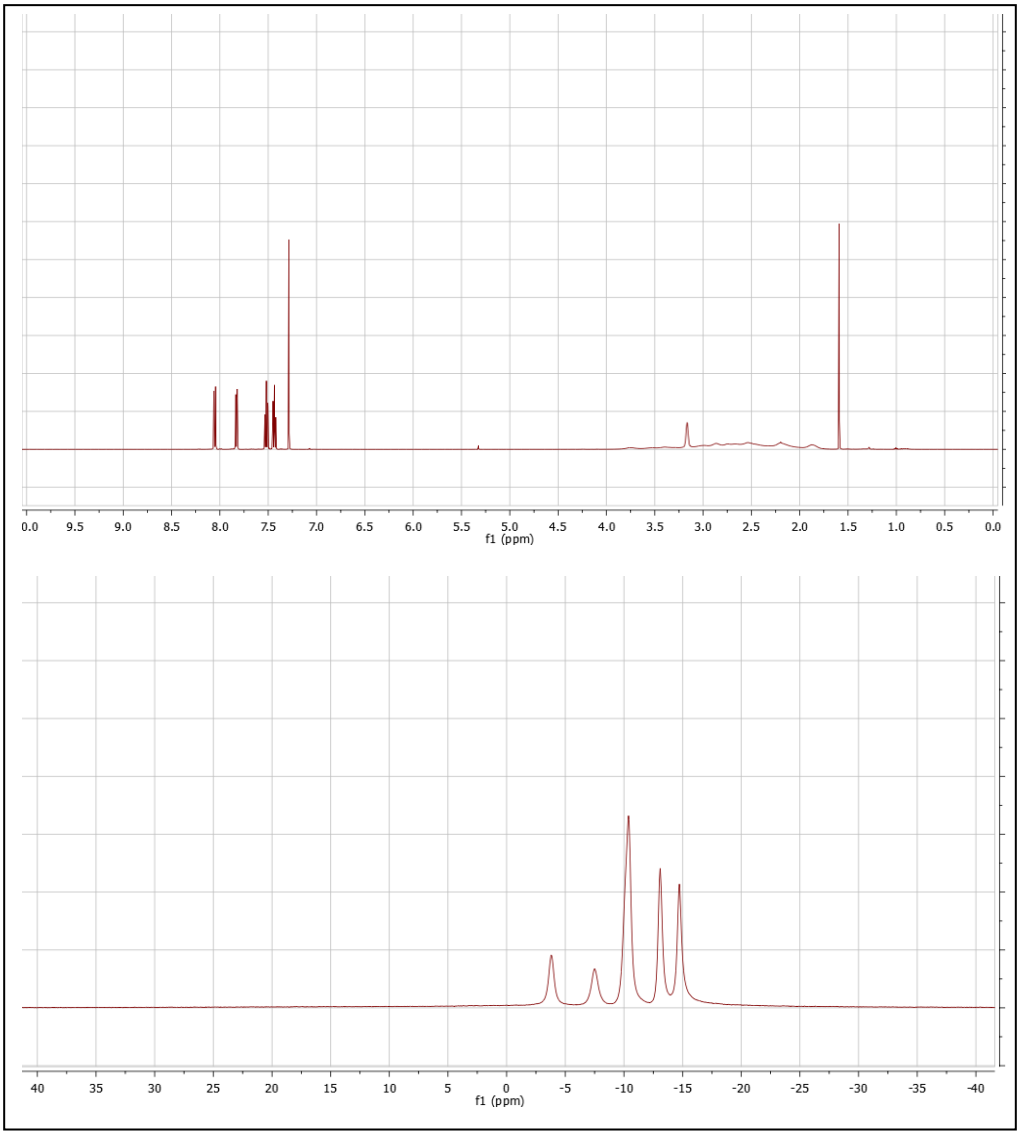

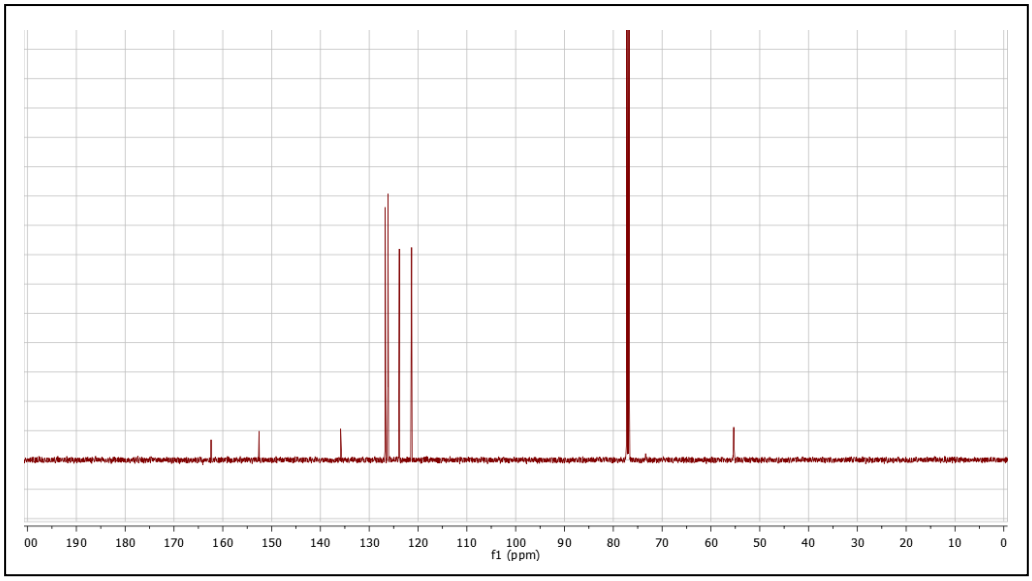
00 190 180 170 160 150 140 130 120 110 100 90 80 70 60 50 40 30 20 10 0
f1 (ppm)

Compound Reference Number: 6.13

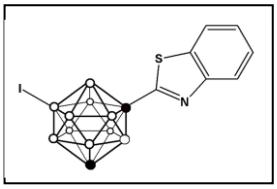

Name: 1-(9-iodo-1,7-dicarba-closo-dodecaboran-1-yl)-benzothiazole
Molecular Formula: $C_9B_{10}H_{14}INS$
Molecular Weight: 403.29

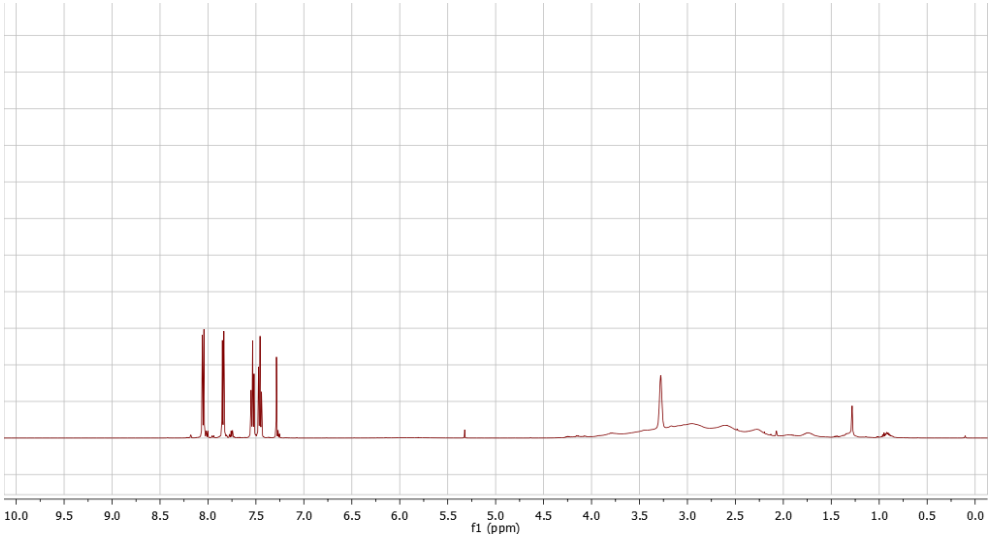

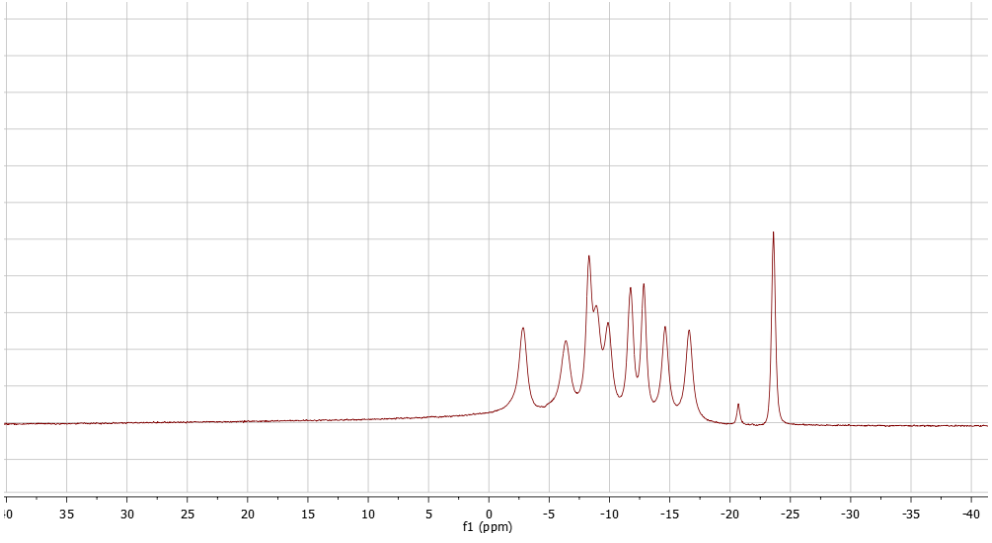

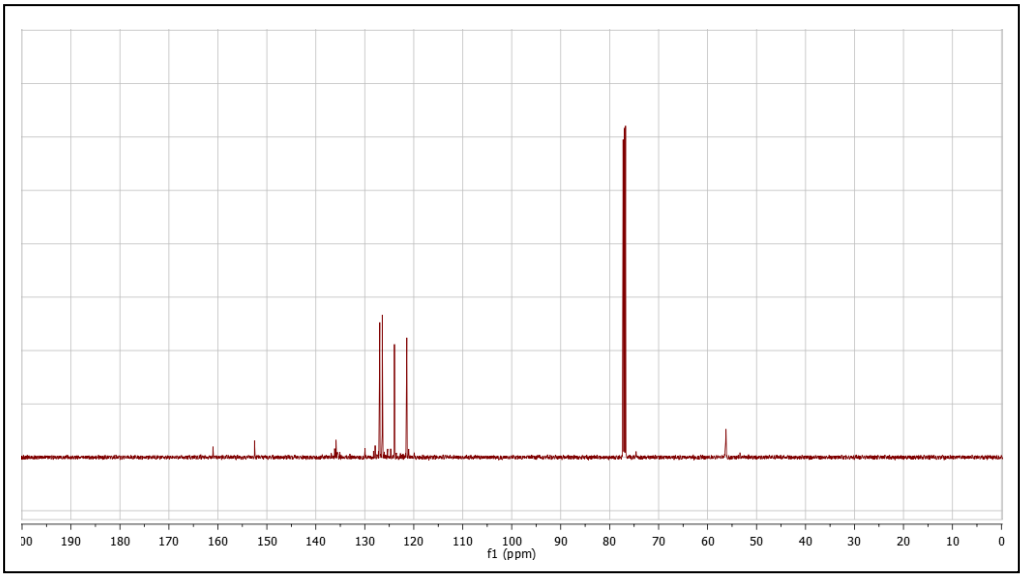
190
180
170
160
150
140
130
120
110
100
90
80
70
60
50
40
30
20
10
0
f1 (ppm)

Compound Reference Number: 6.14

Name: 1-(9-trifluoroacetylamino-1,7-dicarba-closo-dodecaboran-1-yl)-benzothiazole

Molecular Formula: $C_{11}B_{10}H_{15}F_3N_2OS$

Molecular Weight: 388.42

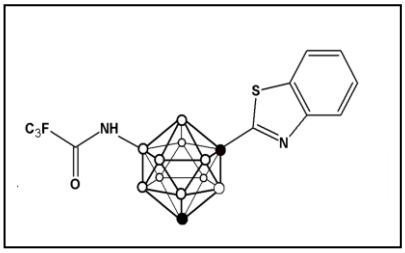

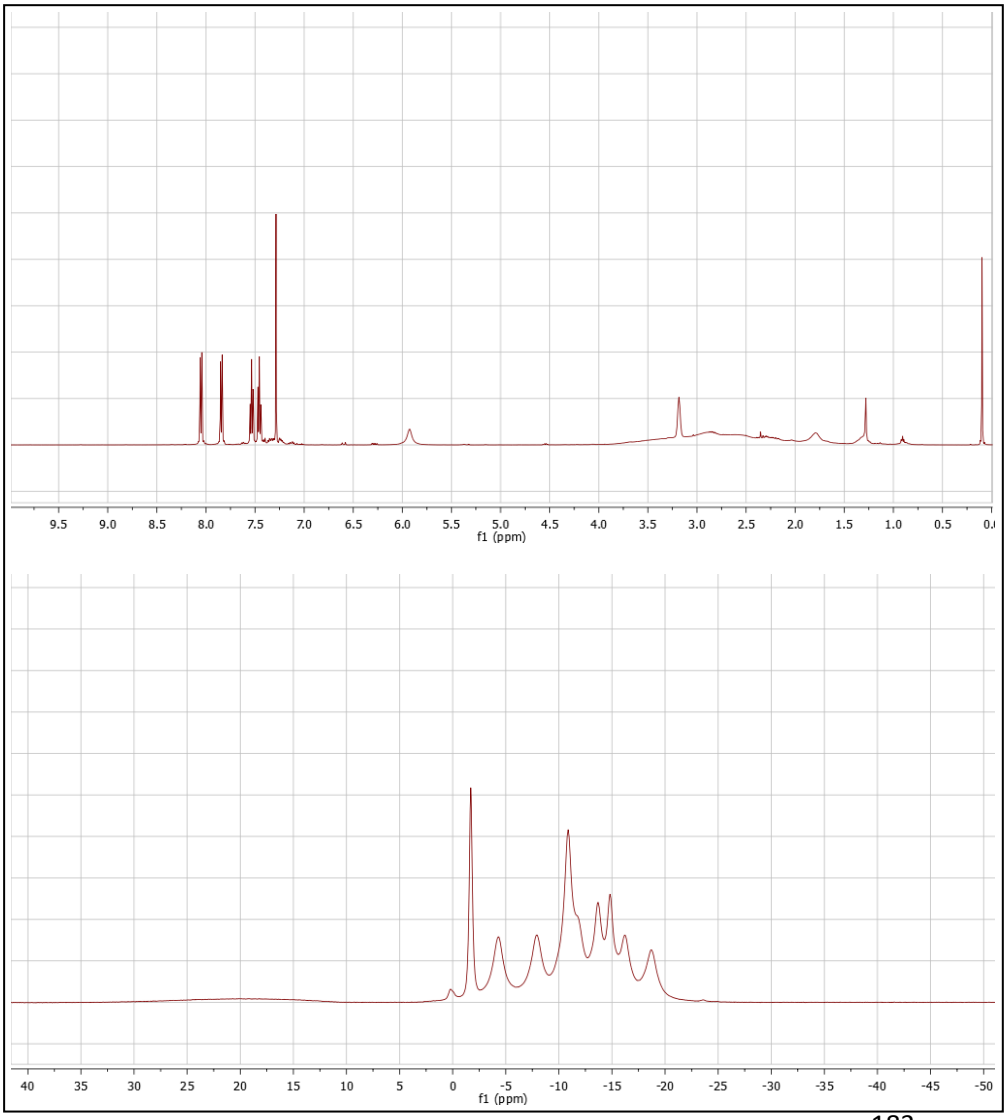

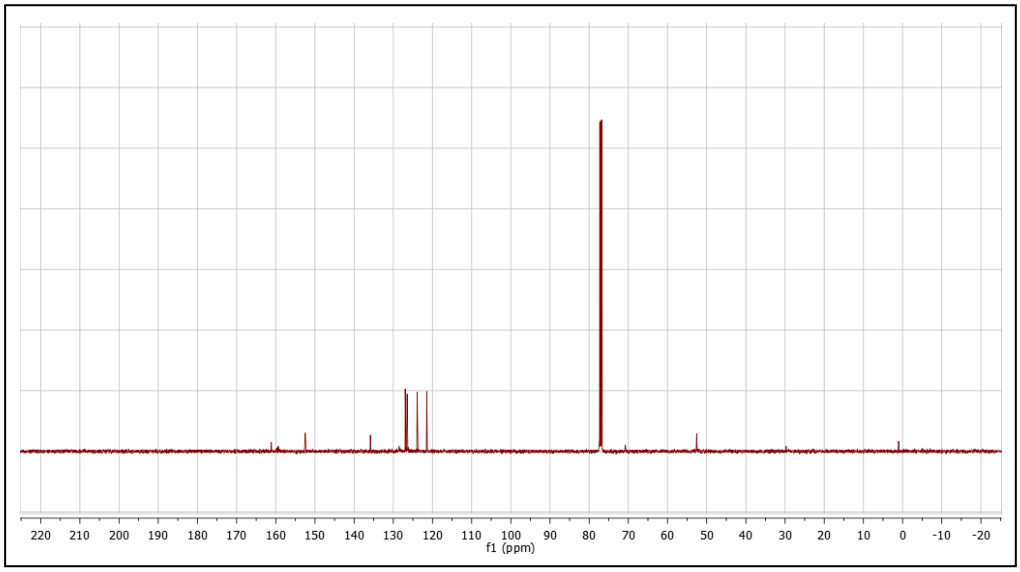
220 210 200 190 180 170 160 150 140 130 120 110 100 90 80 70 60 50 40 30 20 10 0 -10 -20
f1 (ppm)

Compound Reference Number: 6.15

Name: 1-(9-amino-1,7-dicarba-closo-dodecaboran-1-yl)-benzothiazole
Molecular Formula: $C_9B_{10}H_{16}N_2S$
Molecular Weight: 292.41

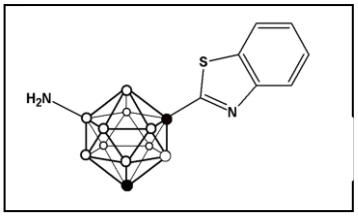

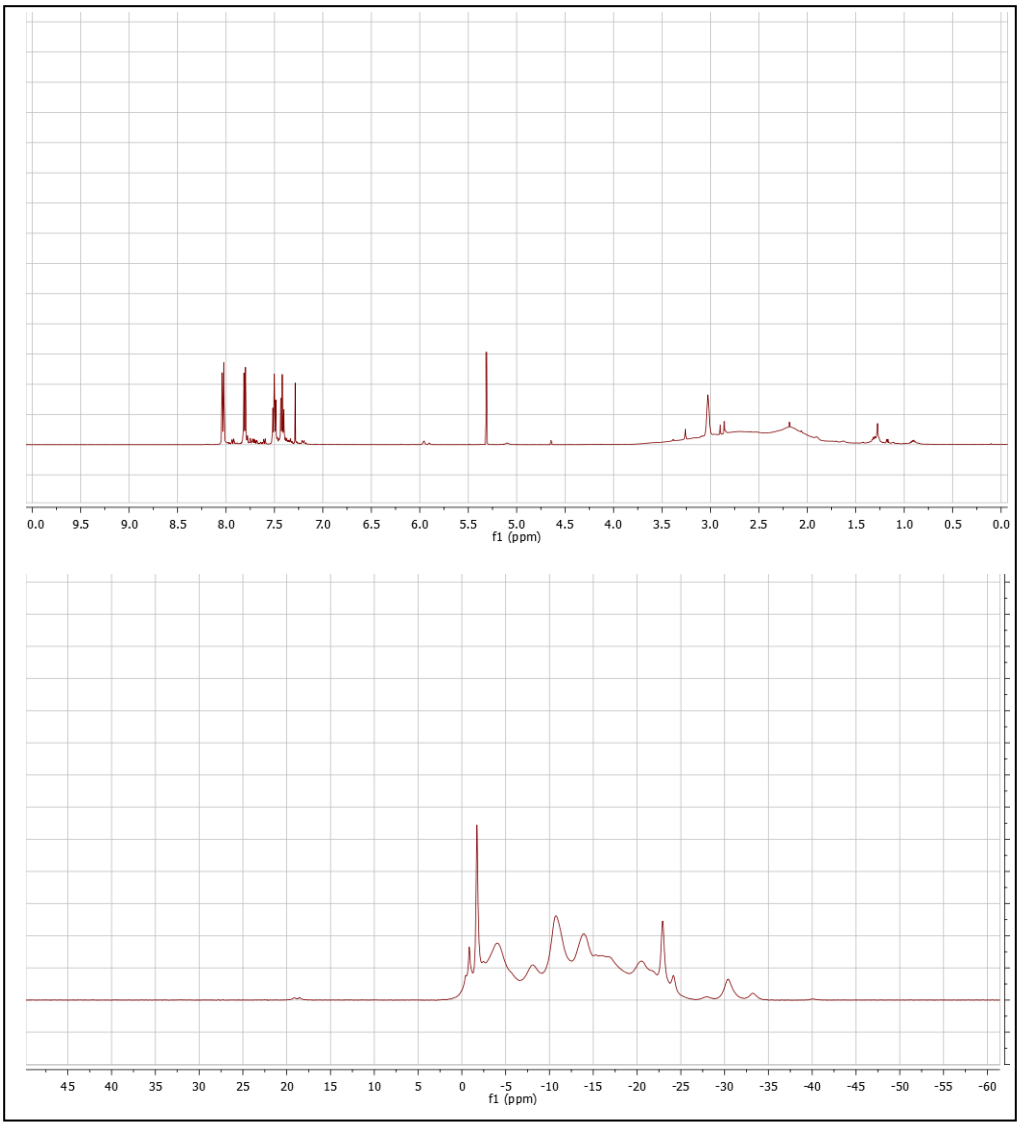

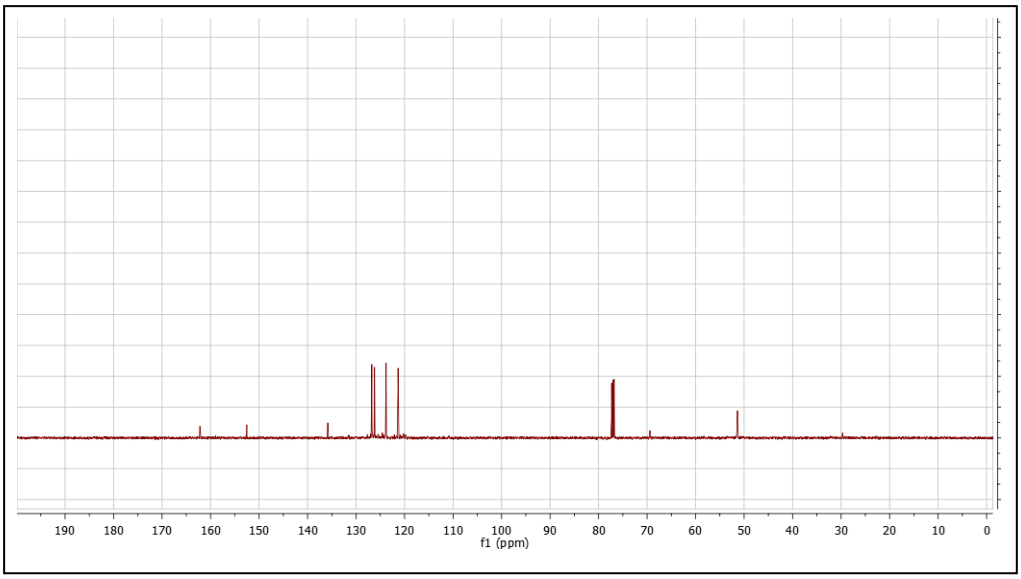
190
180
170
160
150
140
130
120
110
100
90
80
70
60
50
40
30
20
10
0
f1 (ppm)

Compound Reference Number: 6.16

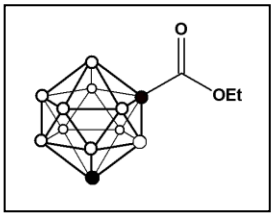

Name: 1,7-dicarba-closo-dodecarborane-1-ethylcarboxylate
Molecular Formula: $C_5B_{10}H_{16}O_2$
Molecular Weight: 216.29

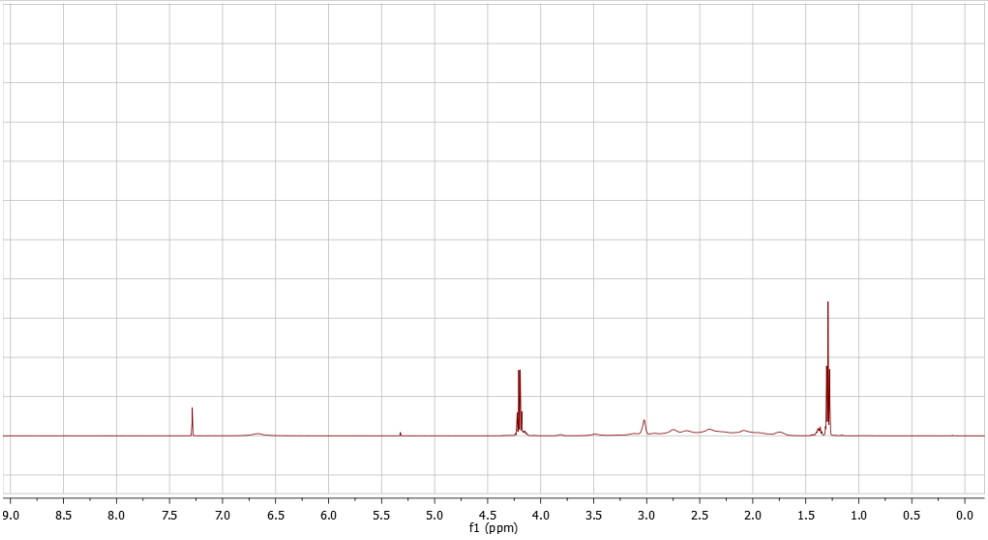

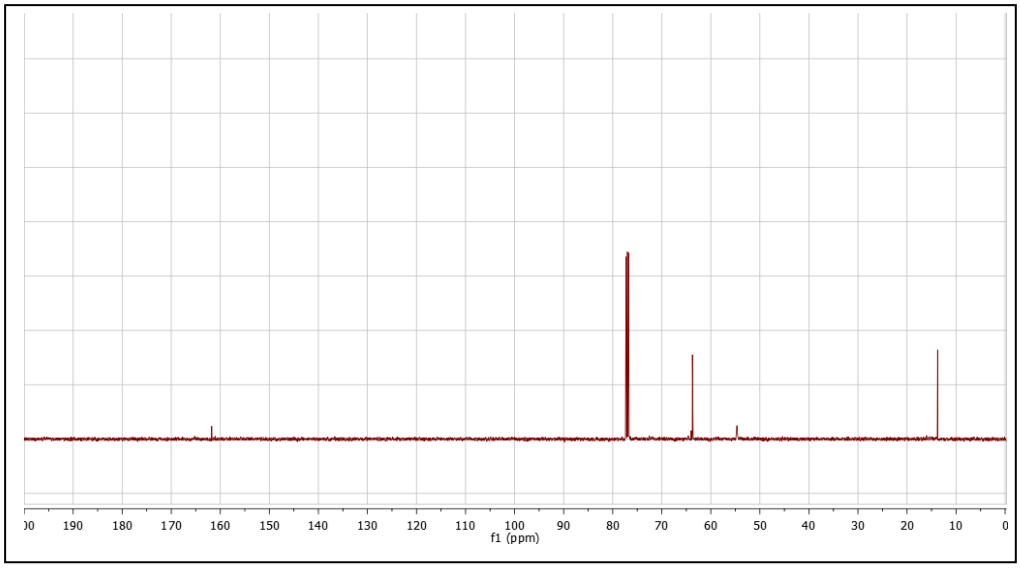
190
180
170
160
150
140
130
120
110
100
90
80
70
60
50
40
30
20
10
0
f1 (ppm)

Compound Reference Number: 6.17

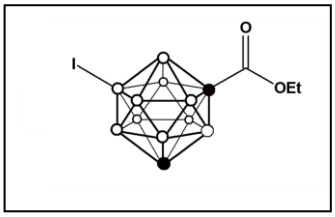

Name: (9-iodo-1,7-dicarba-closo-dodecarborane-1-yl)-ethylcarboxylate
Molecular Formula: $C_5B_{10}H_{15}IO_2$
Molecular Weight: 342.19

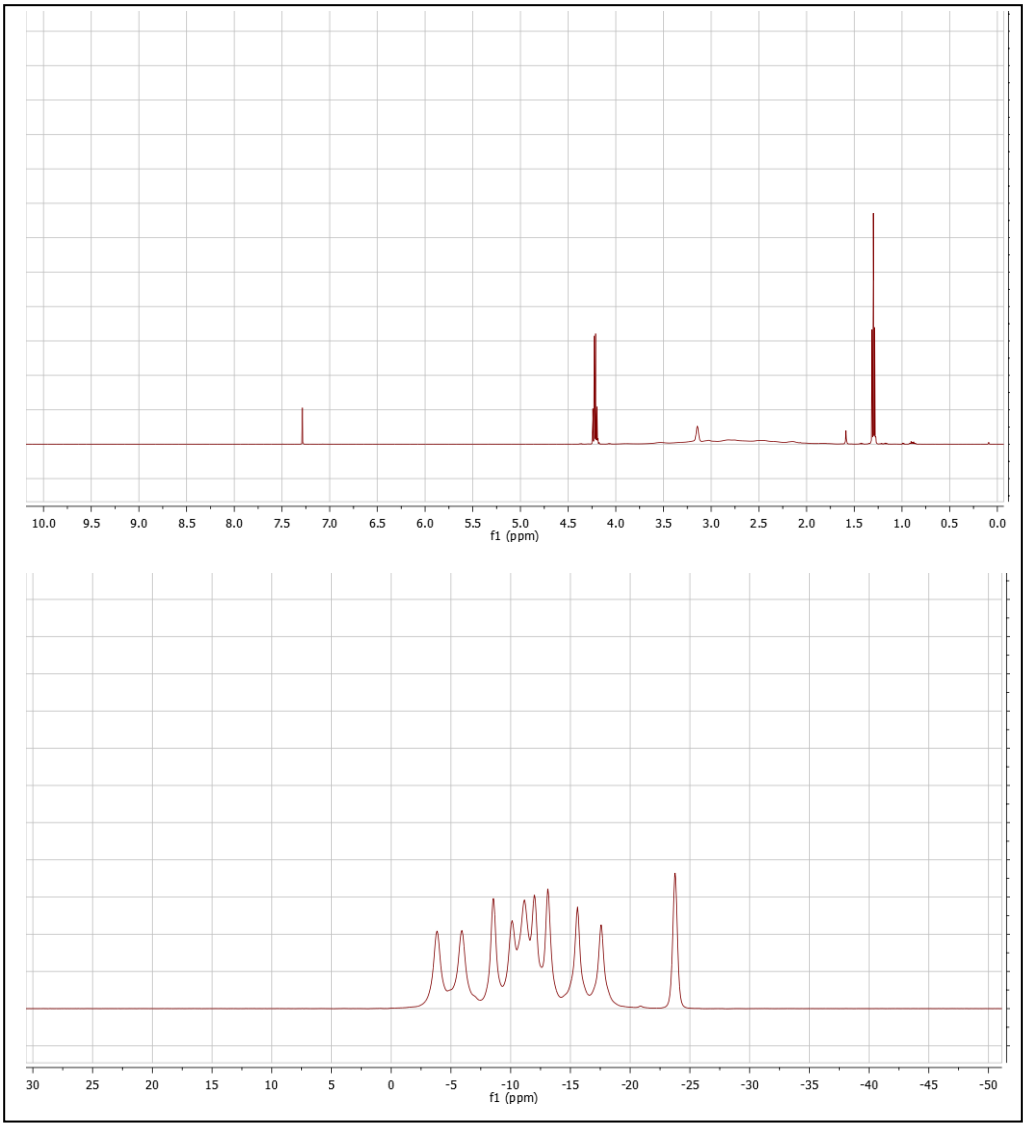

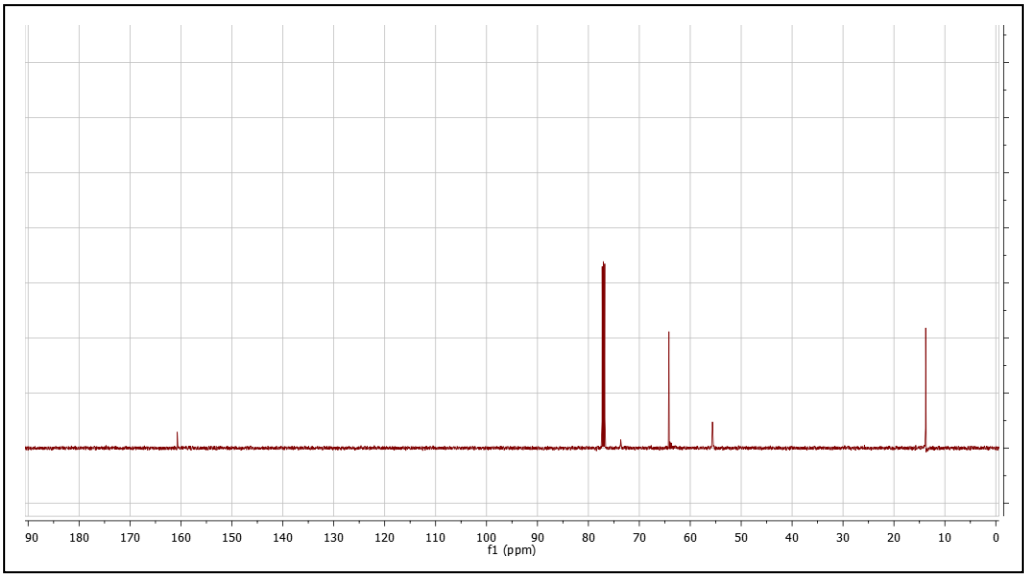
90
180
170
160
150
140
130
120
110
100
90
80
70
60
50
40
30
20
10
0
f1 (ppm)

Compound Reference Number: 6.19

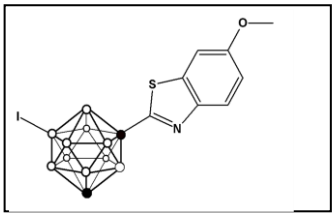

Name: 1-(9-iodo-1,7-dicarba-closo-dodecaboran-1-yl)-6-hydroxymethyl benzothiazole
Molecular Formula: $C_{10}B_{10}H_{16}INOS$
Molecular Weight: 433.32

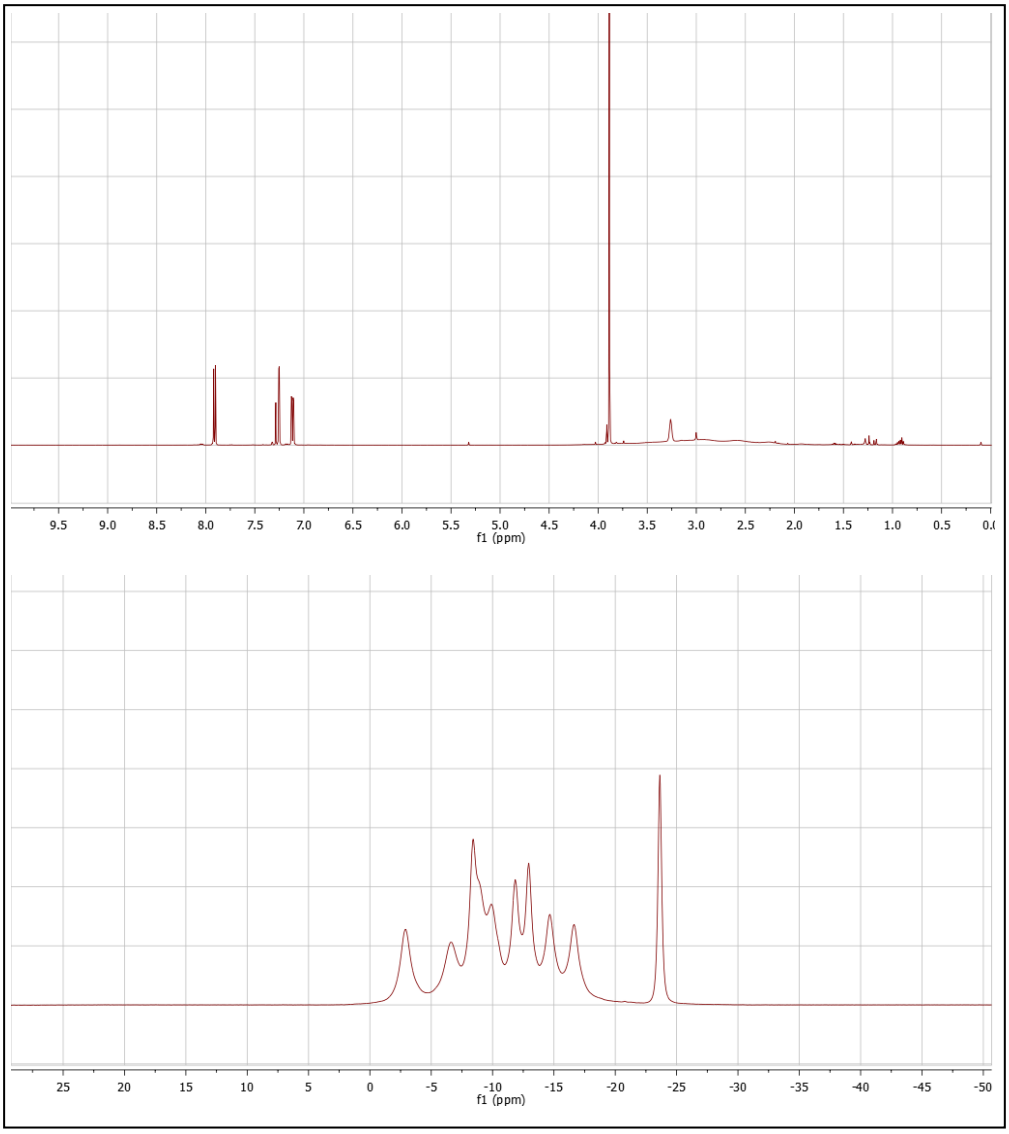

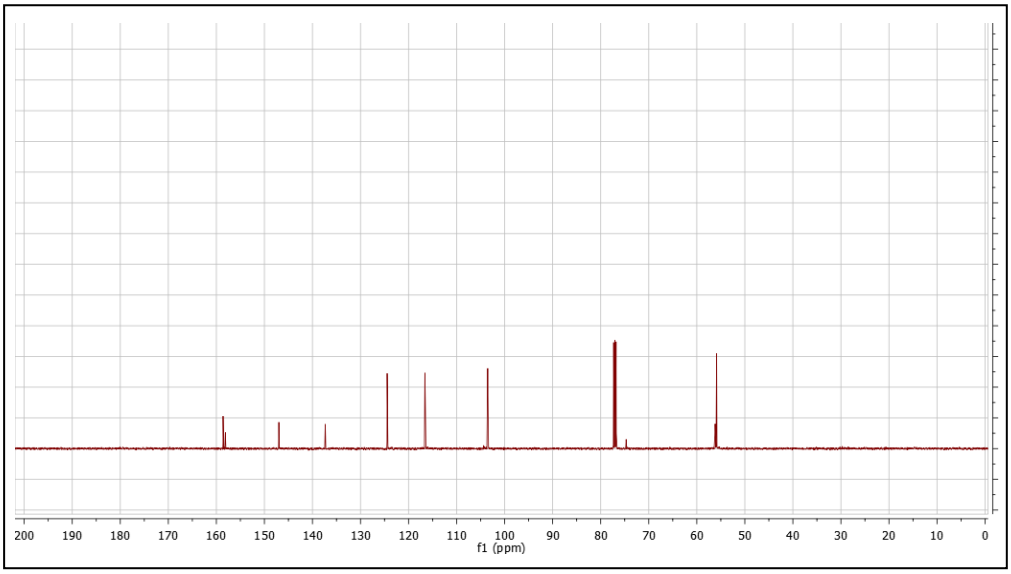
200
190
180
170
160
150
140
130
120
110
100
90
80
70
60
50
40
30
20
10
0
f1 (ppm)

Compound Reference Number: 6.20

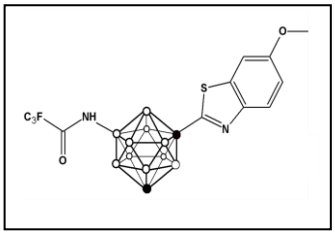

Name: 1-(9- trifluoroacetylamino -1, 7-dicarba-closo-dodecaboran-1-yl)-6-hydroxymethyl benzothiazole

Molecular Formula: $C_{12}B_{10}H_{17}F_3N_2O_2S$

Molecular Weight: 418.45

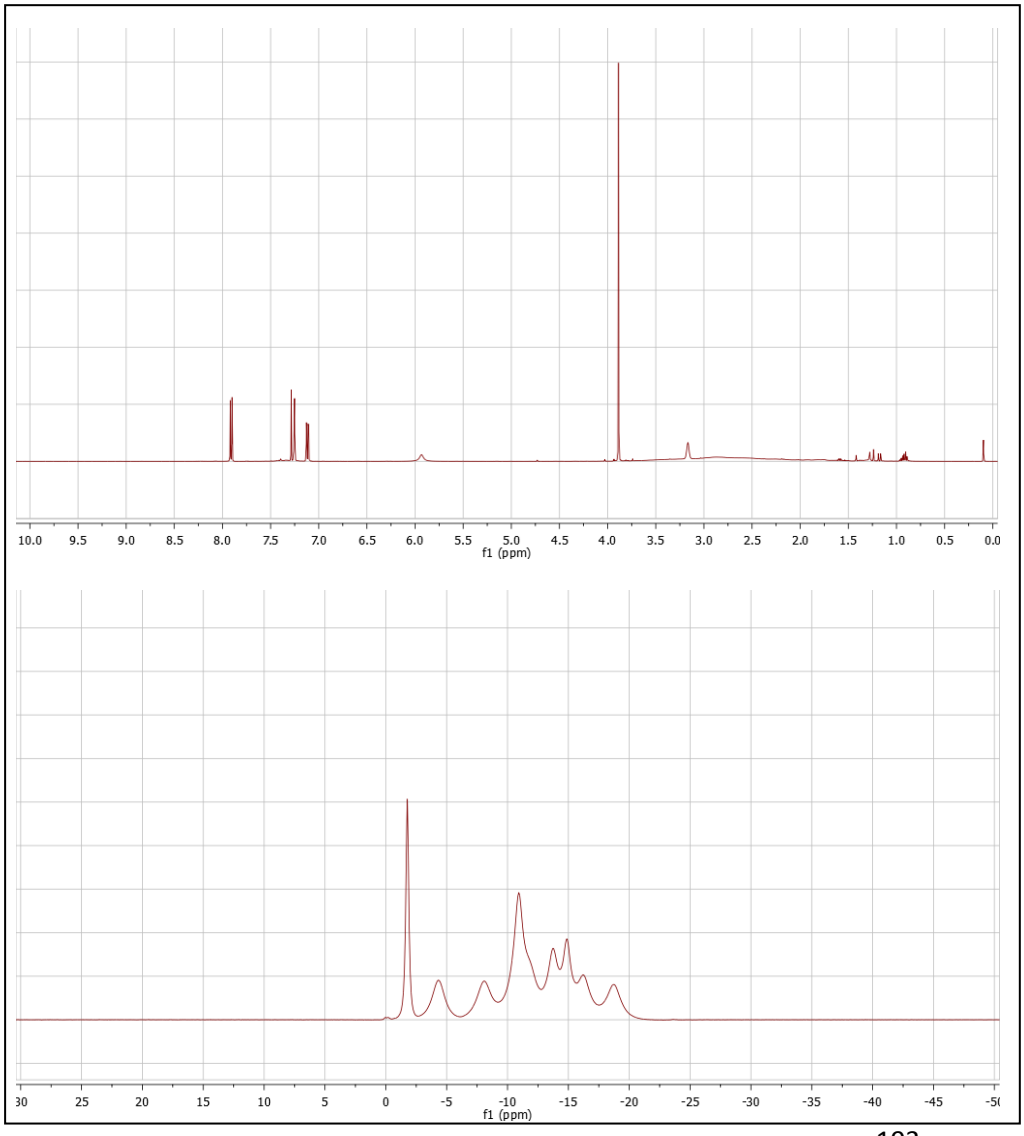

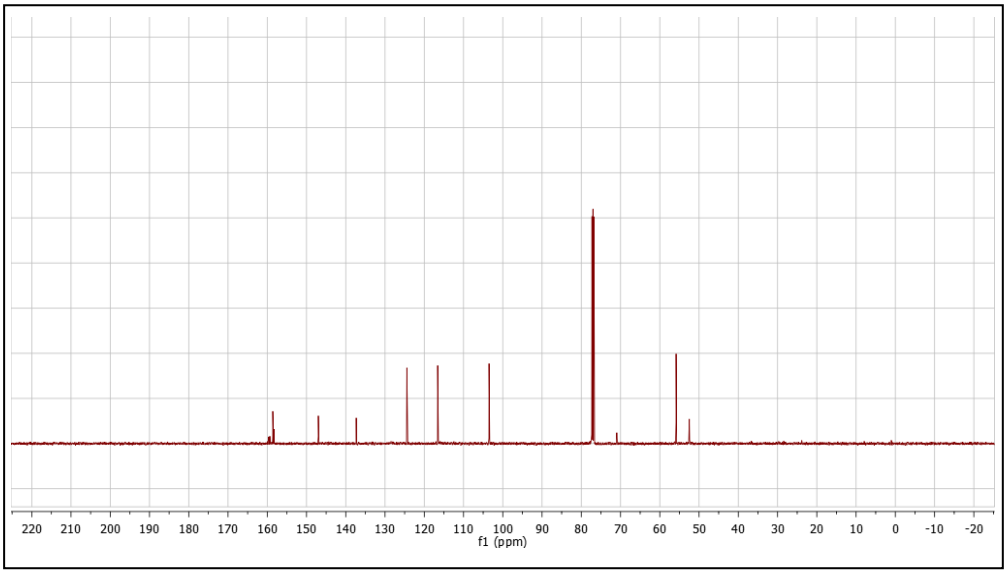
220 210 200 190 180 170 160 150 140 130 120 110 100 90 80 70 60 50 40 30 20 10 0 -10 -20
f1 (ppm)

Compound Reference Number: 6.21

Name: 1-(9-amino -1, 7-dicarba-closo-dodecaboran-1-yl)-6-hydroxymethyl benzothiazole

Molecular Formula: $C_{10}B_{10}H_{18}N_2OS$

Molecular Weight: 322.44

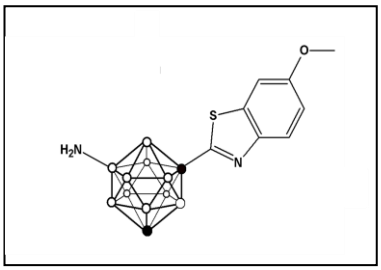

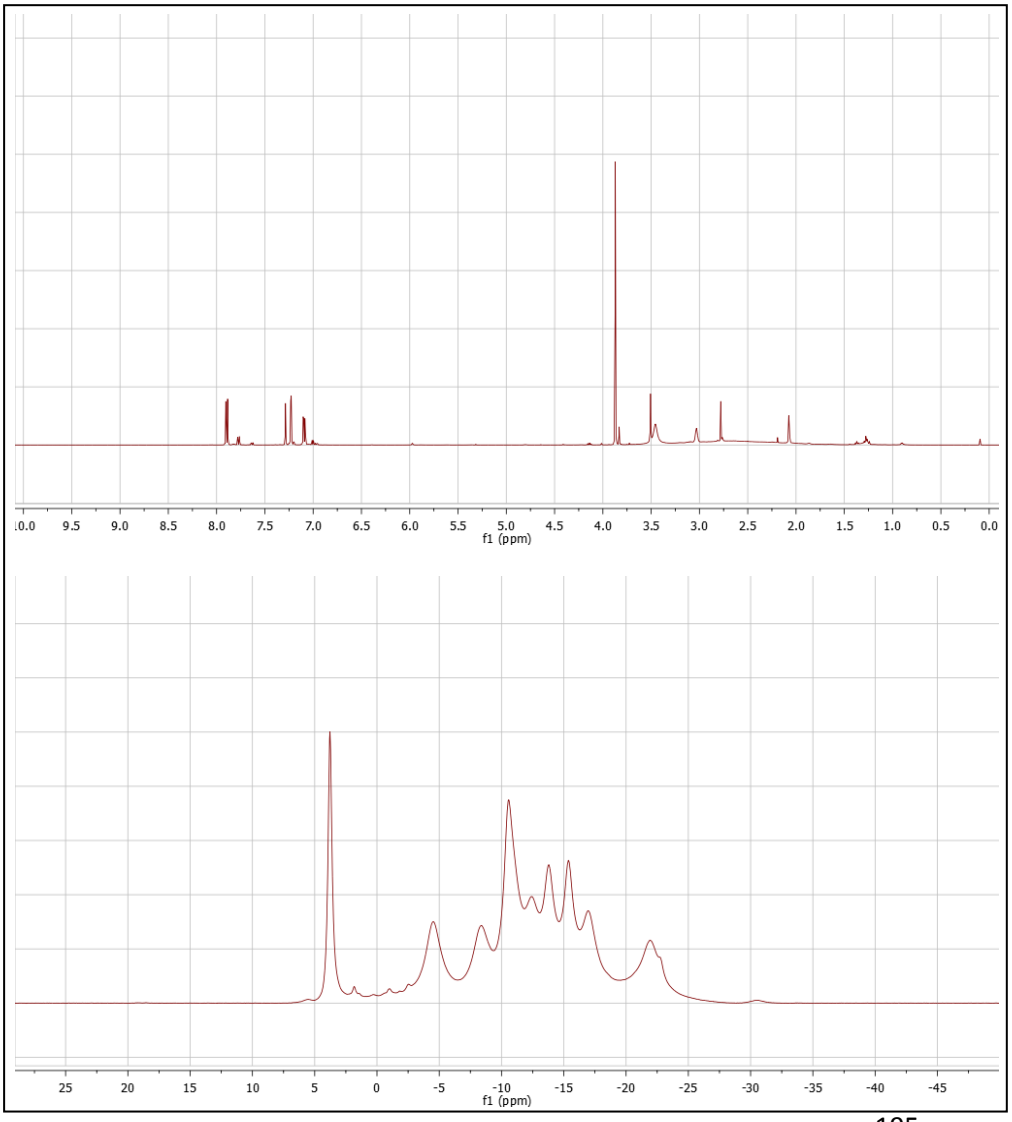

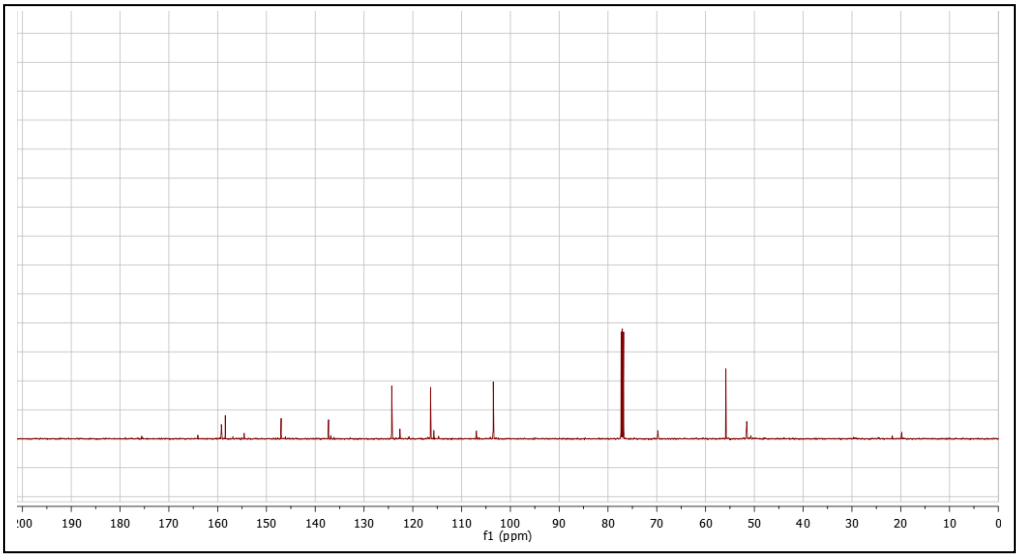
200
190
180
170
160
150
140
130
120
110
100
90
80
70
60
50
40
30
20
10
0
f1 (ppm)

Compound Reference Number: 6.22

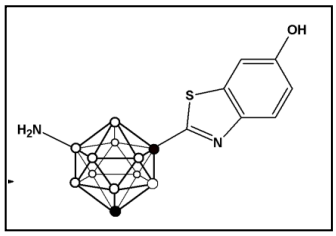

Name: 1-(9-amino -1, 7-dicarba-closo-dodecaboran-1-yl)-6-hydroxybenzothiazole

Molecular Formula: $C_9B_{10}H_{16}N_2OS$

Molecular Weight: 308.41

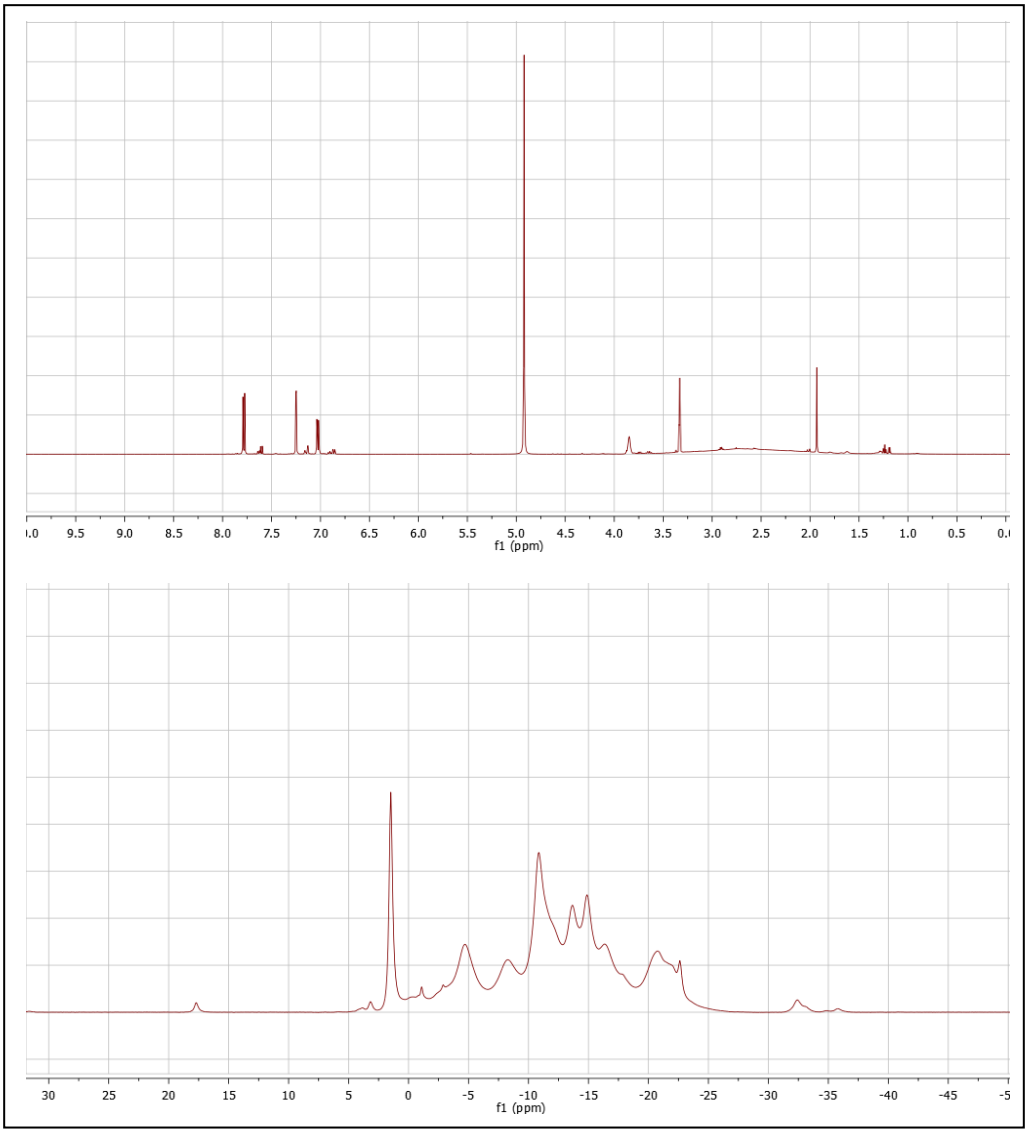

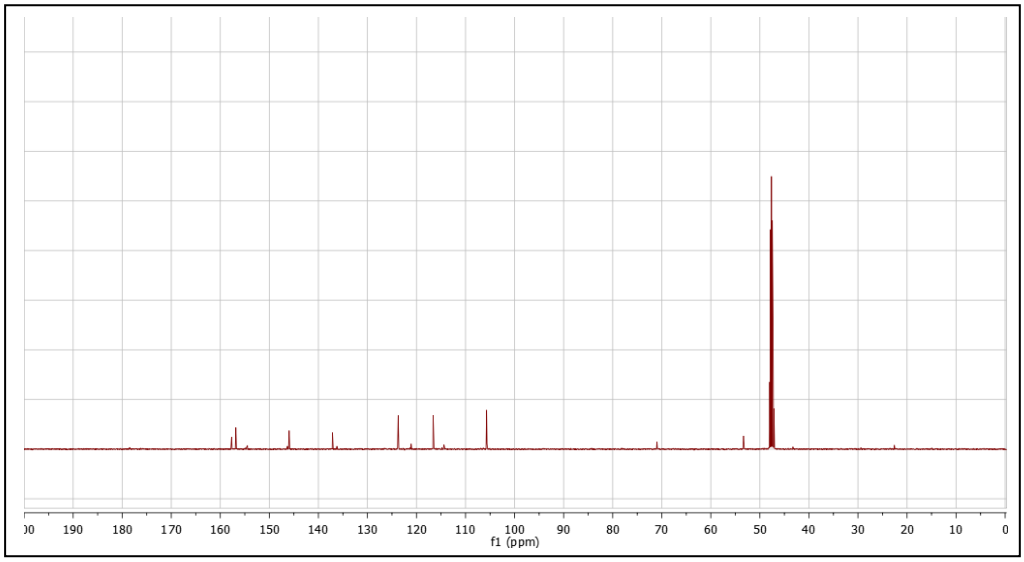
190
180
170
160
150
140
130
120
110
100
90
80
70
60
50
40
30
20
10
0
f1 (ppm)

Compound Reference Number: 7.1

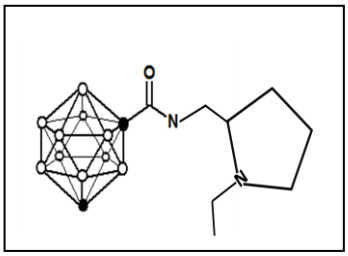

Name: 1,7-dicarba-*closo*-dodecaboran-1-yl-*N*-{[(2S)-1-ethylpyrrolidin-2-yl]methyl}amide
Molecular Formula: $C_{10}B_{10}H_{25}N_2O$
Molecular Weight: 297.43

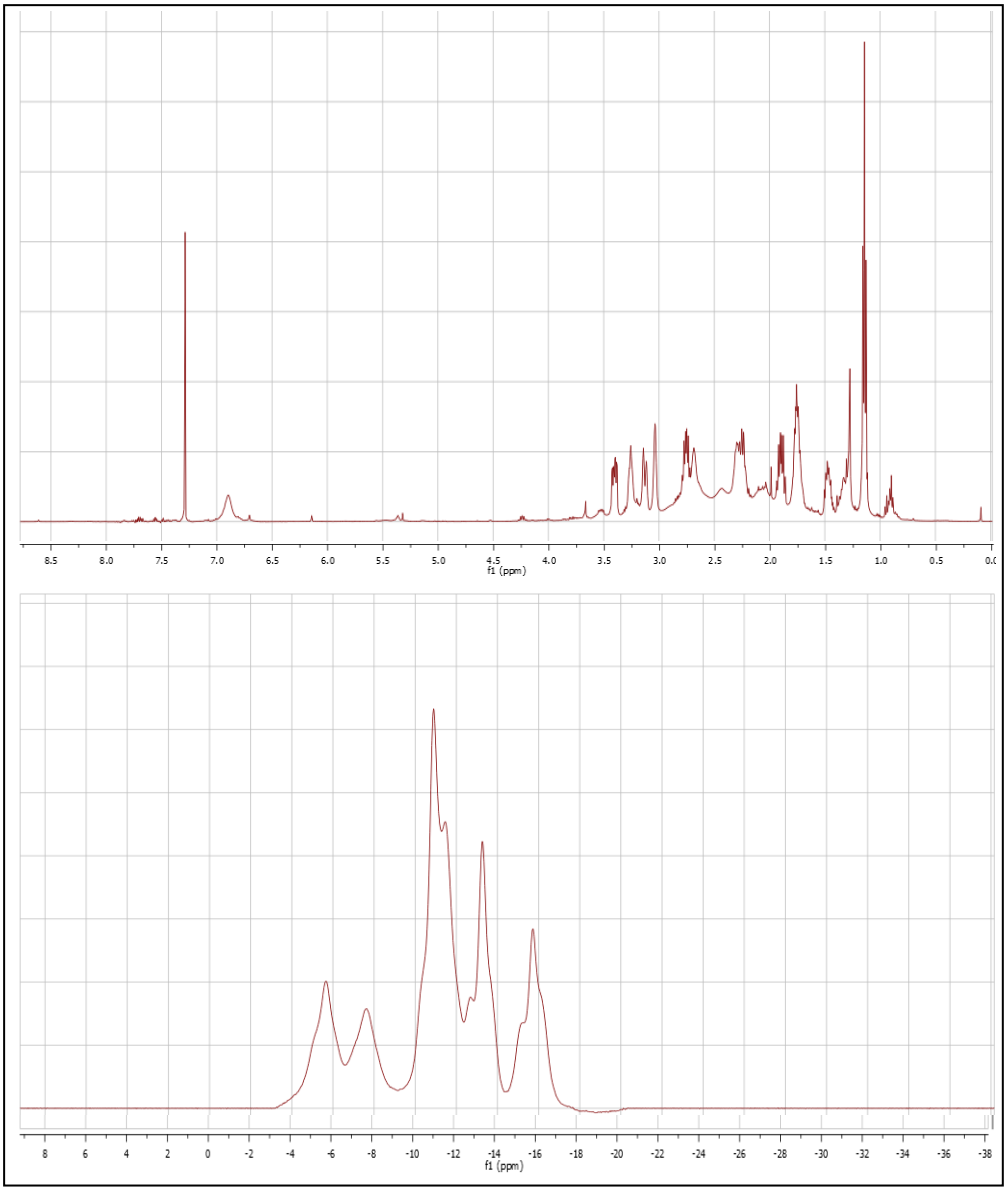

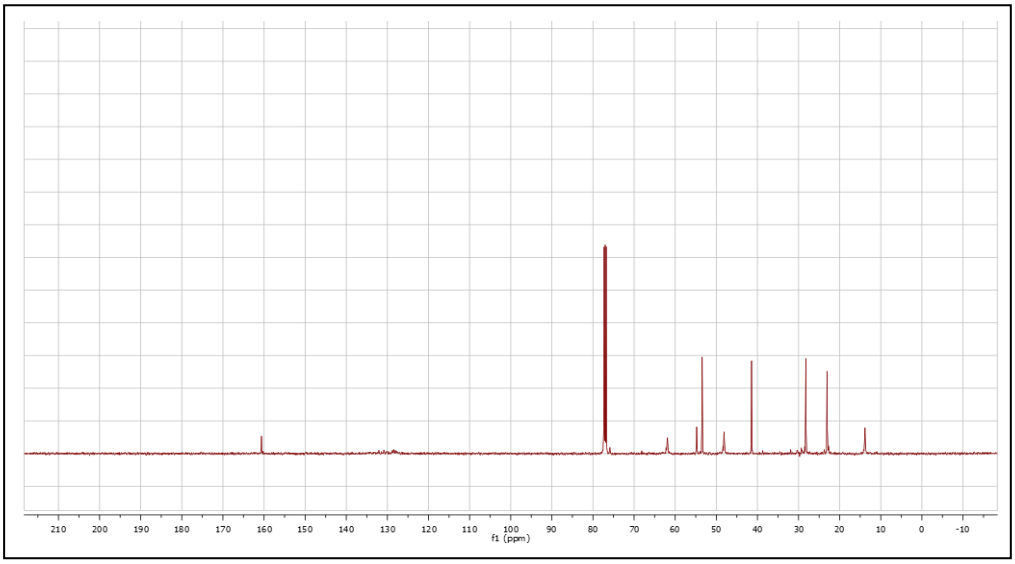
210
200
190
180
170
160
150
140
130
120
110
100
90
80
70
60
50
40
30
20
10
0
-10
f1 (ppm)

Compound Reference Number: 7.2

Name: 1,7-dicarba-*closo*-dodecaboran-1-yl-piperidine
Molecular Formula: $C_8B_{10}H_{21}NO$
Molecular Weight: 255.37

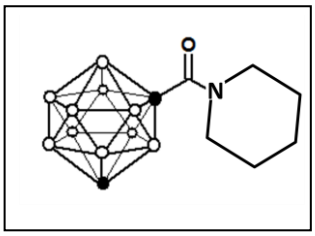

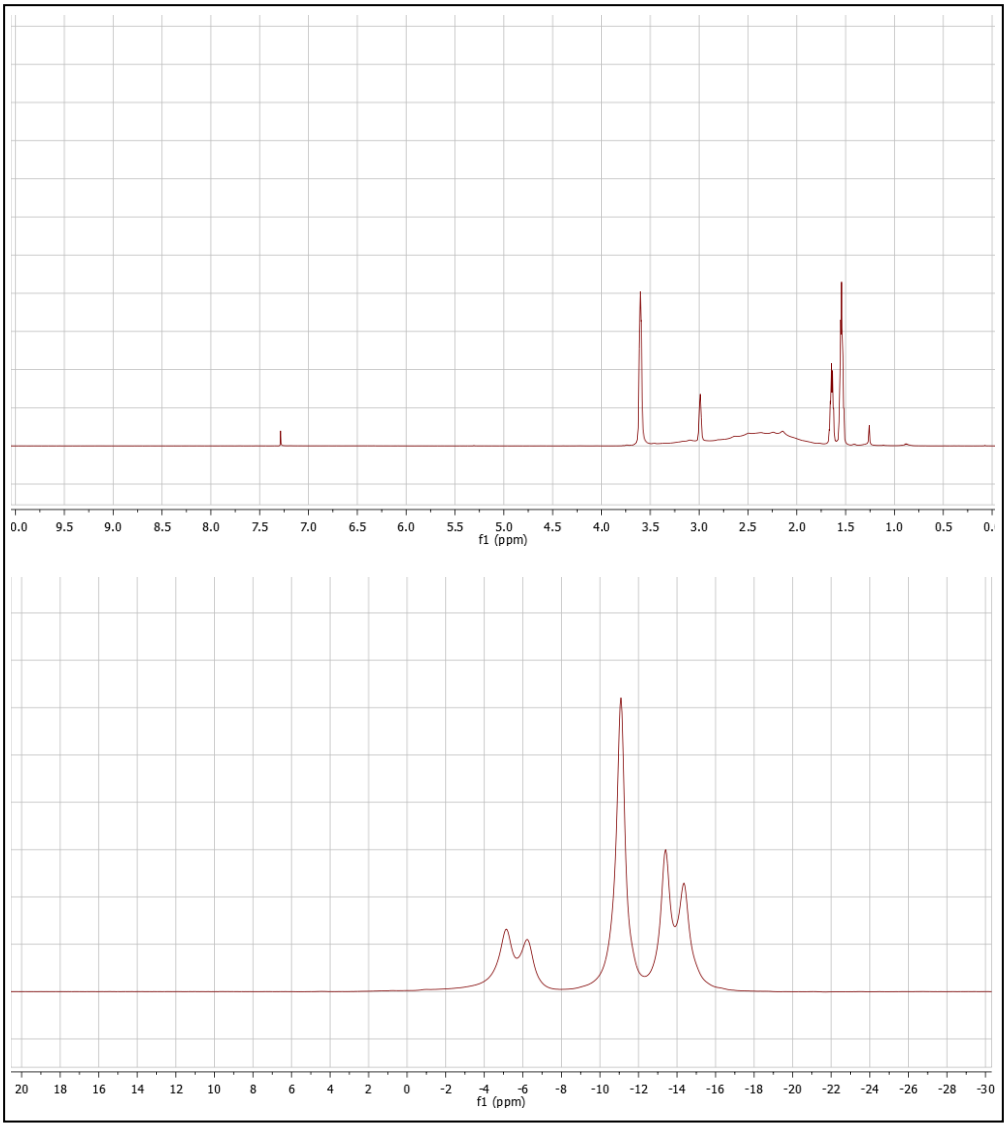

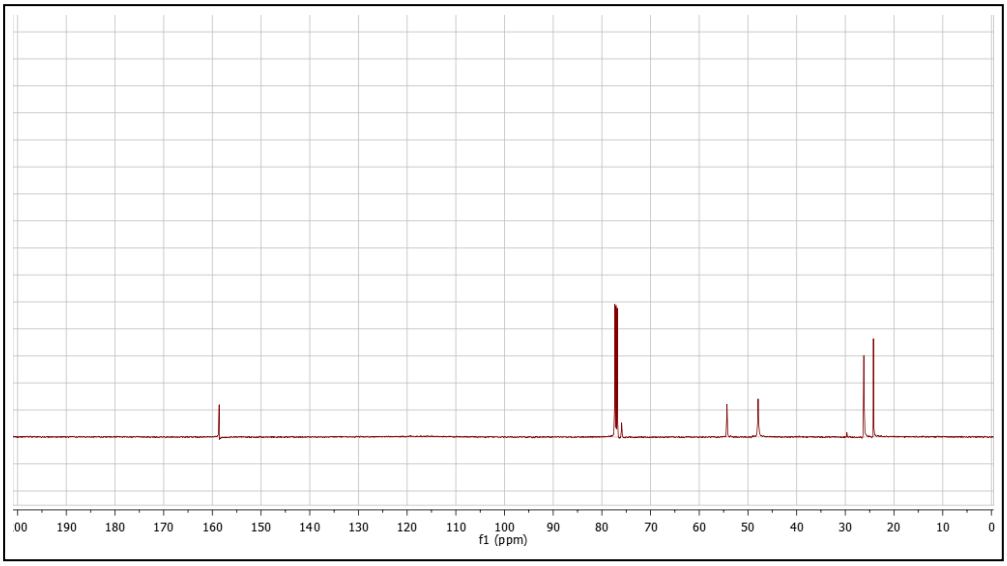
00
190
180
170
160
150
140
130
120
110
100
90
80
70
60
50
40
30
20
10
0
f1 (ppm)

Compound Reference Number: 7.3

Name: 1, 7-dicarba-*closo*-dodecaboran-1-yl-pyrrolidine
Molecular Formula: $C_7B_{10}H_{19}NO$
Molecular Weight: 241.34

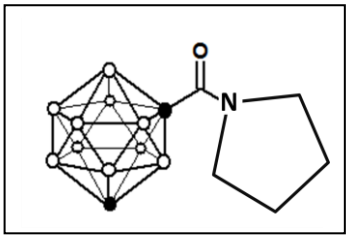

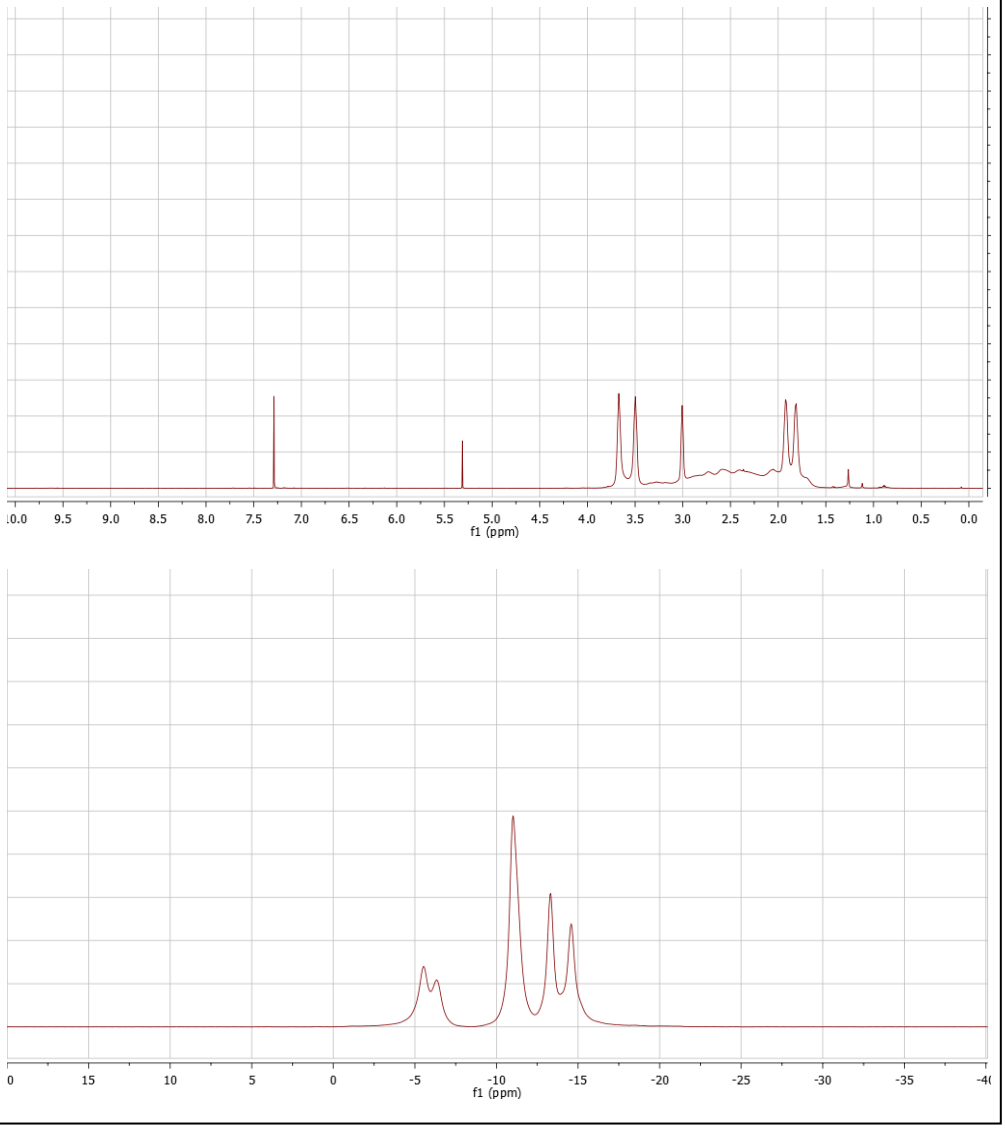

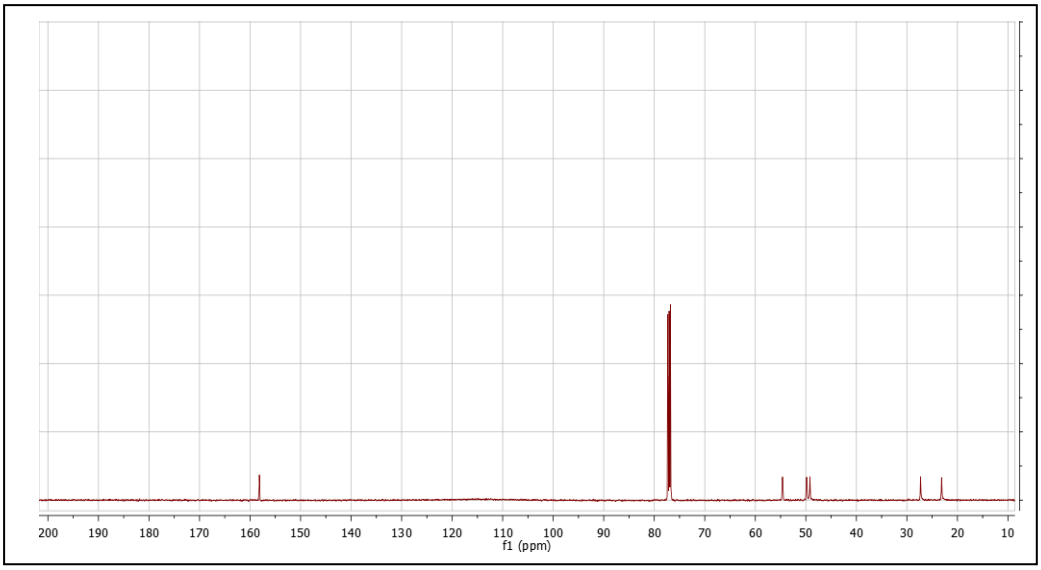
200
190
180
170
160
150
140
130
120
110
100
90
80
70
60
50
40
30
20
10
f1 (ppm)

Compound Reference Number: 7.4

Name: 1, 7-dicarba-*closo*-dodecaboran-1-yl-benzene
Molecular Formula: $C_{10}B_{10}H_{19}NO$
Molecular Weight: 277.37

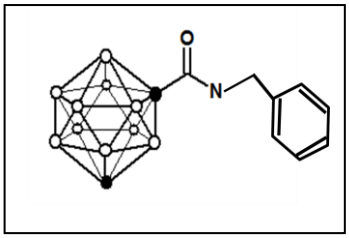

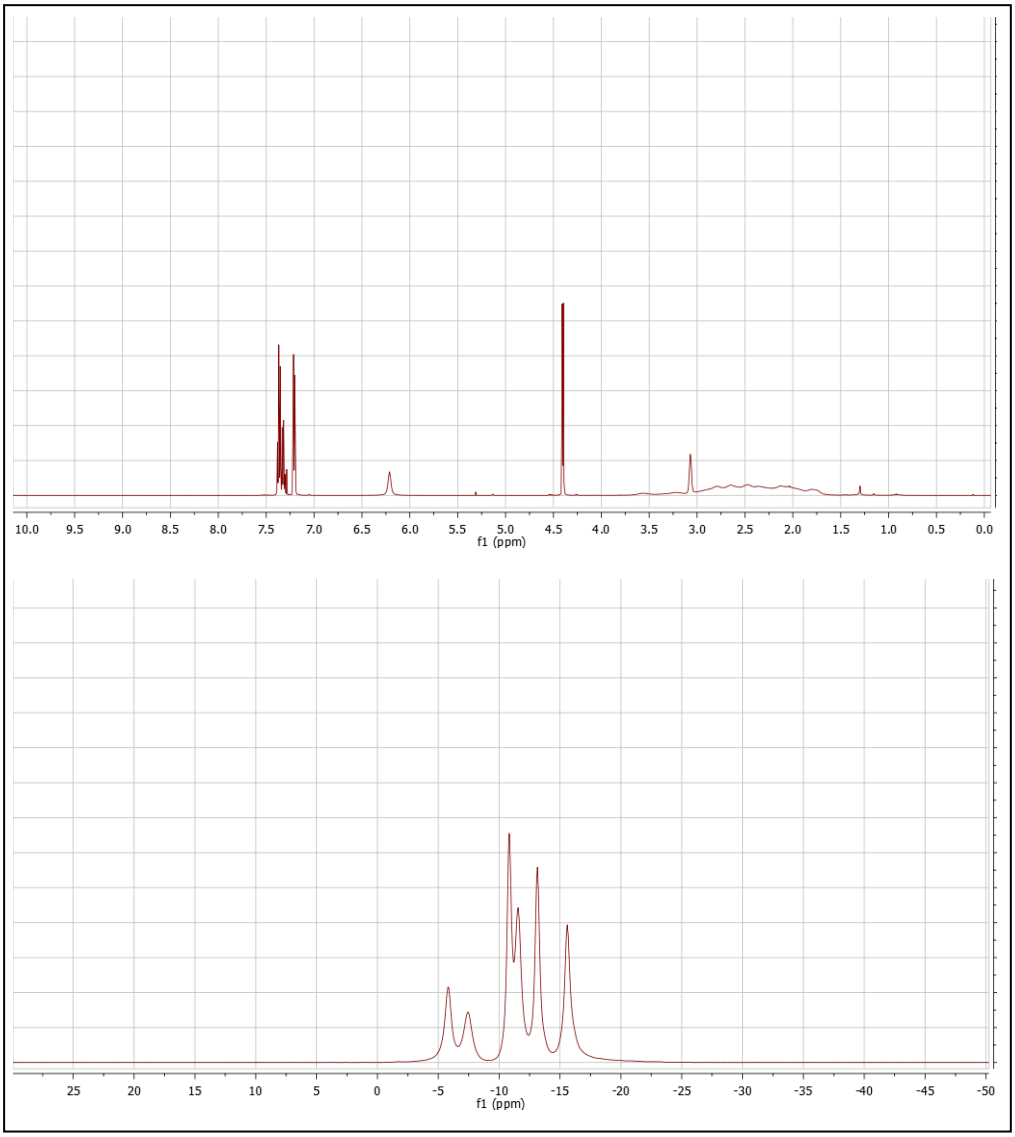

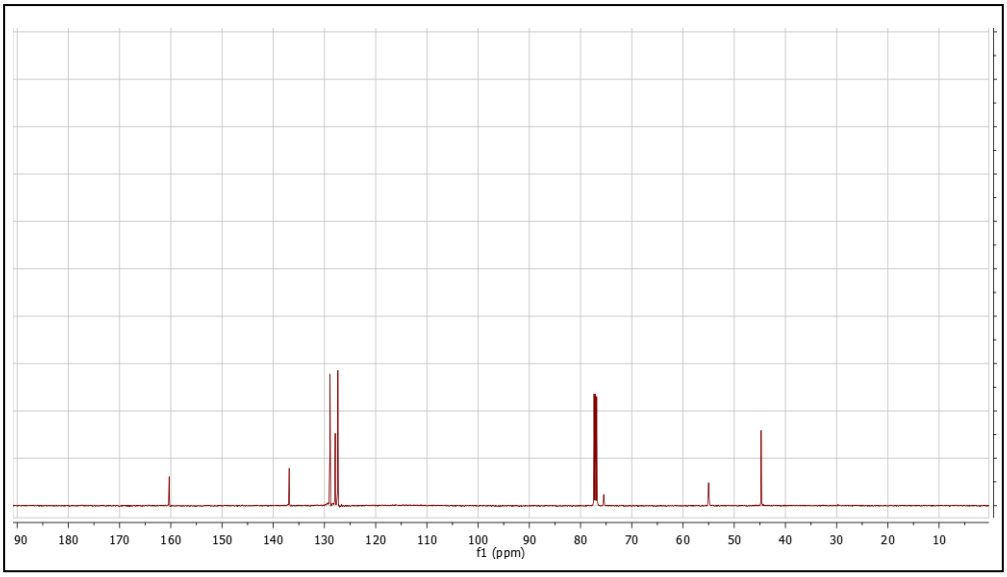
90
180
170
160
150
140
130
120
110
100
90
80
70
60
50
40
30
20
10
f1 (ppm)

Compound Reference Number: 7.5

Name: 1-iodo-1, 7-dicarba-closo-dodecaborane
Molecular Formula: $C_2B_{10}H_{11}I$
Molecular Weight: 270.12

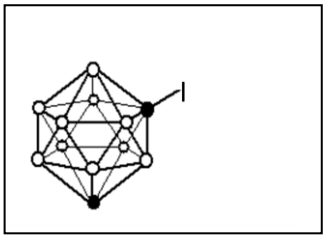

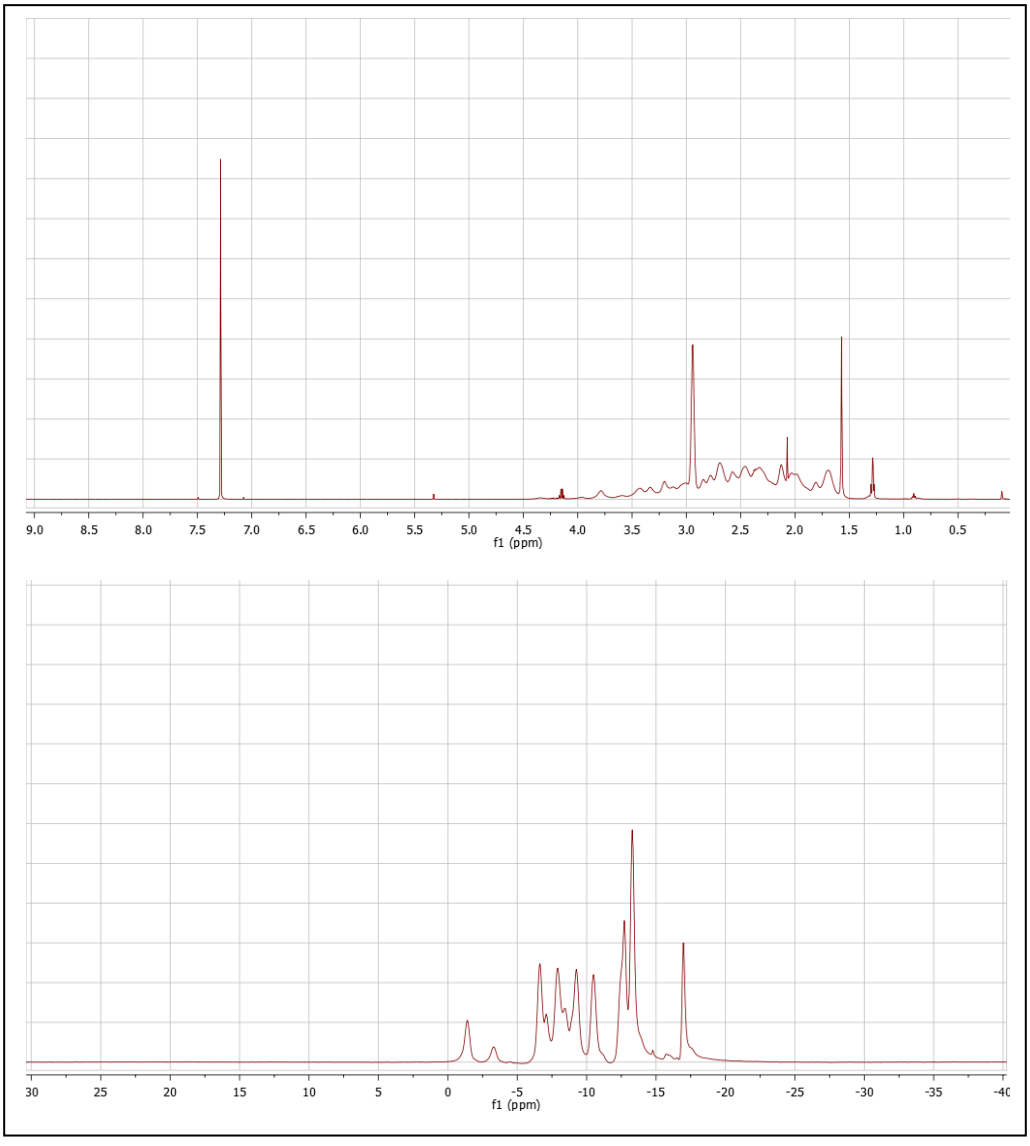

Compound Reference Number: 7.7

Name: 1-OTf-1, 7-dicarba-closo-dodecaborane
Molecular Formula: $C_3B_{10}H_{11}F_3O_3S$
Molecular Weight: 292.29